High Temperature Experiments in Chemistry and Materials Science

High Temperature Experiments in Chemistry and Materials Science

Ketil Motzfeldt
Department of Materials Science
Norwegian University of Science and Technology,
Norway

WILEY
A John Wiley & Sons, Ltd., Publication

This edition first published 2013

Registered office

John Wiley & Sons Ltd, The Atrium, Southern Gate, Chichester, West Sussex, PO19 8SQ, United Kingdom

Library of Congress Cataloging-in-Publication Data applied for.

A catalogue record for this book is available from the British Library.

HB ISBN: 9781118457696

Set in 10.5/13pt, Sabon by Thomson Digital, Noida, India.

Contents

Foreword

This book sets a standard for reliable high temperature experiments. It originates from the distinguished group in high temperature research at Institute of Inorganic Chemistry, The Technical University of Norway. The group was started shortly after 1945 by Professor Håkon Flood and his students, later Professors, Tormod Førland, Kai Grjotheim and the present author, and continued with their students.

The author, Ketil Motzfeldt, has a profound understanding of experimental techniques. He gives not only the theoretical background but also practical hints to avoid pitfalls. He is responsible for only a limited number of publications (about 40) but of correspondingly high quality. The reputation of the Institute of Inorganic Chemistry as a first rate experimental laboratory is to a large extent due to Motzfeldt's assistance to colleagues and students.

High temperature systems are usually characterized by thermodynamics. Temperature and pressure are the two essential parameters. The book describes equipment and materials needed to obtain a well characterized temperature and how temperature and pressure are measured reliably.

The book is full of practical examples: How do you establish a reliable vacuum system? What are the pitfalls to avoid in order to obtain the correct temperature? What materials should be chosen, and are two chosen materials compatible in contact at temperatures above 2000°C ?

Although the book mainly treats high temperature systems, many of the techniques are useful at lower temperatures as well. I have for instance used the boiling point method, described in detail in the book, at temperatures from 200 to 800°C. The advantage with this method is

that the experimental temperature range can be chosen so that the measurements are simple, and then you may extrapolate due to the fact that the logarithm of pressure is very nearly a linear function of 1/T.

In general, the book has a solid scientific base, but it is pedagogical with an easy-to-read style which makes it a pleasure to read.

Harald A. Øye

Preface

The present text is centred around some central topics within high-temperature chemistry. It concerns the control and measurement of the basic properties: temperature, pressure and mass.

The text is primarily written for the newcomer with limited experience in the field. The emphasis is on 'how to do it'. Hence the text deals with materials and methods, including detailed drawings of various equipment. A final chapter relates some previous experimental investigations to justify the main title.

It is assumed that the reader is versed in chemical thermodynamics, since this is an essential background which is not included in the present text. There is, however, a lot more that has not been included. An investigation in the area of high-temperature chemistry will most often include detailed characterization of the resulting materials. Identification by X-ray diffraction is standard, and a range of other modern methods are available, but this is all outside the scope of the present text. Thus the book has neither a beginning nor an end, but it is hoped that it fills a gap in-between.

Acknowledgements

A number of colleagues and friends should be thanked for their willing assistance, but only one is mentioned by name. The author wants to express his gratitude to his late friend, Professor Dr. techn. Terkel Rosenqvist (1921-2011). Thank you for encouragement, interesting discussions, and good friendship through more than fifty years.

Financial support from The Research Council of Norway is gratefully acknowledged.

1

Introduction to High Temperature Research

CONTENTS

High Temperature Experiments in Chemistry and Materials Science, First Edition.
Ketil Motzfeldt.

Preamble

This chapter, the first, starts with a brief introduction to our very existence on Earth, the chemistry of life, and the interaction between carbon and oxygen. Next follow some examples of industrial high temperature processes as an introduction to the main topics of the book: design of equipment for chemical research at high temperatures.

1.1 THE BASIS OF IT ALL

1.1.1 Photosynthesis

We live on the planet Earth, which appears to be just right for us. The water in the oceans, which cover about 70% of the surface, is for the most part liquid and suitably cool. Above us is an atmosphere containing roughly 20% oxygen plus a small fraction of carbon dioxide (the rest is nonreactive nitrogen and a little argon). Oxygen is a reactive, one might say aggressive, gas, but over millions of years, plants and animals have adapted to its presence.

This works in the way that carbon dioxide, plus water, in the presence of sunlight, reacts to produce organic materials plus free oxygen:

$$\underset{\text{carbon dioxide}}{6\,CO_2} + \underset{\text{water}}{6\,H_2O} \xrightarrow[\text{Enzyme System}]{\text{Light}} \underset{\text{glucose}}{C_6H_{12}O_6} + \underset{\text{oxygen}}{6O_2(g)}$$

The above is only a schematic description of how plant materials are produced by photosynthesis. Glucose is a form of sugar (carbohydrate) and is the building block for other carbohydrates in plants.

The plant materials are in turn eaten by animals, including man. During this process, the reaction goes the other way, with consumption of the nutrients and oxygen, production of carbon dioxide, and release of energy for the body. This, in short, is the life cycle on Earth.

This may seem a strange start for a book which eventually deals with equipment and methods within high temperature chemistry. But it encapsulates the idea that 'everything depends on everything else', a fact that is often underrated.

1.1.2 The Role of Carbon

In the above process, a long time ago, parts of the energy-rich plant materials were not converted all the way back to carbon dioxide, instead ending up halfway between as carbonaceous materials or impure carbon. This was buried underground for millions of years. Some of it has been recovered more recently in the form of coal. Other parts of the material were converted to oil or gas and similarly buried.

The present quest for oil and gas is less than 100 years old; the oil activity in the North Sea started only 50 years ago. Apart from the Sun itself, carbon, oil, and gas are today the major sources of energy for all the industrial activities of modern man, from steel plants to domestic heaters.

This is today's problem. The population on Earth has just about doubled every 50 years for the last 100 years. The anthropogenic fluxes of carbon dioxide in the atmosphere have similarly increased. The CO_2 content in the air has increased from about 0.03 to 0.04% during the last 100 years. That is a relative increase of 30%, and is generally considered to be the main reason for global warming.

1.2 HIGH TEMPERATURES

1.2.1 Chemistry at Ambient Temperatures

A major part of chemical research around the world is concerned with the chemistry of life, that is, organic chemistry and biochemistry. Naturally, the activities within organic chemistry take place mainly at temperatures between the freezing point and boiling point of water. A multitude of species live and prosper in the temperature range between ice and hot water. Literally millions of carbon compounds have been analysed and synthesized, and presumably life itself has some millions more in store.

1.2.2 Chemistry at High Temperatures

When heated to a few hundred degrees, any plant or animal material will decompose to simpler molecules. As a result, high temperature

chemistry is very simple in comparison to organic chemistry. What makes high temperature chemistry interesting is not the complexity of its compounds, but the utility of its products. High temperature chemistry plays an important, not to say dominant, role in the industrialized world.

1.2.3 The Nitrogen Industry

As an example we might take a look at the nitrogen, or fertilizer, industry. Without it, starvation would have been a likely outcome many decades ago. It started at Norsk Hydro in 1905, with the production of nitrogen fertilizer by means of the Birkeland–Eyde process. This process used an electric arc to unite nitrogen and oxygen in the air, producing nitrogen oxides as the first step. The process was later superseded by the Haber–Bosch method where ammonia, NH_3, is the primary product. Norsk Hydro is still one of the world's largest producers of fertilizers, with an annual production of 15–20 million tons, some 7–8% of a world production of about 200 million tons.

1.2.4 Iron and Steel

Another example is the reduction of iron ore to produce steel. It is definitely a high temperature process, noting that the melting point of pure iron is 1535 °C. Its origin can be traced back at least 2000 years. It is the largest of the metal producing industries, with a present world production of close to 1000 million tons annually, one-third of this from China alone.

1.3 CARBOTHERMAL SILICON AND ALUMINIUM

1.3.1 Ferrosilicon and Silicon Metal

Silicon is the most abundant element in the Earth's crust next to oxygen. It never occurs in its elemental form, but is bound to oxygen in a variety of minerals. As an element it is brittle, hard and a poor conductor of electricity. Silicon, often in alloys with iron as ferrosilicon, is produced from a mixture of quartz, coke and eventually iron or iron oxide.

The mixture is heated in an electric arc furnace to temperatures around 2000 °C. The furnace runs continuously; the charge is fed on top, and the molten silicon or ferrosilicon is tapped periodically from the bottom.

This metallurgical process has been operated in Norway since the early 1900s, primarily in the form of ferrosilicon for use as a deoxidant and an alloying element in the steel industry. Towards the middle of the century, the market for aluminium grew rapidly, and as a common alloying element the demand for pure silicon also increased.

It was known that, in the presence of sufficient iron, the melting (reduction) process went well. When melting high-silicon alloys, however, a lot of white smoke went up the chimney, and the yield in terms of silicon was poor. Such was the situation when I, as a young graduate, was called upon to elucidate the process.

1.3.2 The First Laboratory Furnace

A metallurgical melting furnace with a power of, for example, 10 000 kW, is not the proper place for experiments. Thus, part of my job was to duplicate the process on a laboratory scale. Fairly soon I realized that laboratory equipment for studies at 1800–2000 °C was not readily available, so we had to make our own.

To cut a long story short, a high temperature laboratory furnace was designed and built, see Chapter 7, 'Beljara'. It served well for experiments to above 2000 °C in inert atmospheres or a vacuum. Some results from our work on the silicon process are presented in Chapter 8.

1.3.3 Carbothermal Aluminium

After some years' work on the silicon process, I was transferred to work on a carbothermal process for aluminium. In this context, some words are necessary about the conventional aluminium process, which occurs by electrolysis.

Compared to iron and steel, aluminium is a recent metal. The commercial production through electrolysis started only a little more than 100 years ago. The process today is essentially the same that Charles Hall in USA and, independently, P. L. Héroult in France, patented in 1886. Aluminium oxide is dissolved in a bath of molten cryolite (Na_3AlF_6), with anode and cathode of carbon materials. The process and equipment are

radically improved since the first cells, but it is inherent that the electrolytic process is not particularly energy-efficient.

The alternative would be a direct carbothermal reduction, similar to that used for silicon. From about 1960 and for several decades, a number of the large international aluminium companies spent time and money in developing a carbothermal process for aluminium. As a consequence, a research group was formed in Trondheim for the same purpose.

1.3.4 More Laboratory Furnaces

With several coworkers we had a need for a second furnace. So I designed another one, 'Versatilie', see Chapter 7, Section 7.3.4. It was quite unlike the first one except for similar specifications: up to some 2300 °C in an inert atmosphere, or evacuated to 10^{-8} atm. Some of the research results are described in Chapter 8.

Altogether, four different laboratory furnaces were built during that period, actually four different designs. Several of them were also equipped with balances, thus constituting thermobalances.

These pieces of equipment were designed to serve a purpose; they were not an end in themselves. Not until I retired did I consider the idea that these pieces of equipment, and the ideas behind them, might be worth writing about.

1.3.5 A Note on Chemical Thermodynamics

The methods within high temperature chemistry are to a large extent based on chemical thermodynamics. The present text, however, contains only scant references to this basic theory, hence a separate chapter on it is not included. Chemical thermodynamics is better studied as a separate subject; some suitable textbooks are mentioned in the reference list.

1.4 SUMMARY OF CONTENTS

The present text is largely based on the idea of 'how to do it'. Chapter 2 describes the design principles for laboratory furnaces. Chapters 3 and 4 deal with temperature measurement by means of thermocouples and radiation pyrometry, respectively. In Chapter 5 a review of refractory

materials is given, while the rather important topic of vacuum technique is dealt with in Chapter 6. Finally, various designs of high temperature furnaces and thermobalances are described in Chapter 7.

Chapter 8, in a sense, is an 'extra' chapter, with descriptions of selected experimental results.

SELECT BIBLIOGRAPHY

Chemical Thermodynamics

Gaskell, D.R. (2008) *Introduction to the Thermodynamics of Materials*, 5th edn, Taylor & Francis, New York, 618 pp.
The title suggests 'just what we need', but it is a rather voluminous book.

Lee, H.-G. (1999) *Chemical Thermodynamics for Metals and Materials*, Imperial College Press, London, 309 pp.
Nearly the same title as that of Gaskell, but half the length. The text is accompanied by a CD-ROM for interactive learning.

Pitzer, K.S. (1995) *Thermodynamics*, 3rd edn, McGraw-Hill, New York, 626 pp.
The first edition of this book, G. N. Lewis and M. Randall, *Thermodynamics and the Free Energy of Chemical Substances* appeared in 1923, and laid the foundations for the present day use of thermodynamics in chemistry. The second edition, revised by K. S. Pitzer and L. Brewer, came out in 1961. This third edition is again revised, yet retains the clarity and exactness of its predecessors.

Reid, C.E. (1990) *Chemical Thermodynamics*, McGraw-Hill, New York, 313 pp.
A clear and comprehensive text within a moderate volume.

Smith, E.B. (2004) *Basic Chemical Thermodynamics*, 5th edn, Imperial College Press, London, 166 pp.
A simple and well written text for the beginner. A discussion of phase diagrams, however, is missing and must be sought elsewhere.

Stölen, S. and Grande, T. (2004) *Chemical Thermodynamics of Materials*, John Wiley & Sons, Chichester, 395 pp.
The title is almost the same as that of Gaskell's except for the 'Introduction to', which indicates that this book is not strictly for beginners.

In addition, at least another half dozen books with the title Chemical Thermodynamics may be found under the UDC No. 541.11.

Materials Science

Balducci, G., Ciccioli, A., de Maria, G., Hodaj, F., and Rosenblatt, G.M. (2009) *Pure Appl. Chem.*, **81**, 299–338: 'Teaching High-Temperature Materials Chemistry at University' (IUPAC Technical Report).
The report outlines various areas, with a wealth of literature references within each section.

Askeland, D.R. and Pulé, P.P. (2006) *The Science and Engineering of Materials*, Thomson/Nelson, 863 pp.

Callister, W.D. Jr. and Rethwisch, D.G. (2011) *Materials Science and Engineering*, 8th edn, John Wiley & Sons, 990 pp.

The last-mentioned two textbooks have nearly the same title. And they have more in common than that: Neither of them mentions chemical thermodynamics at all!

Experimental Methods

Bockris, J.O'M., White, J.L., and Mackenzie, J.D. (1959) *Physicochemical Measurements at High Temperatures*, Butterworths, London, 394 pp.

An old book by now, but still of interest. One of the few books that treats experimental methods in some detail.

Kubachewski, O., Alcock, C.B., and Spencer, P.J. (1993) *Materials Thermochemistry*, 6th edn, revised, Pergamon Press, Oxford, 363 pp.

This is the sixth edition of the well-regarded book *Metallurgical Thermochemistry* by Kubaschewski that originally appeared in 1951. It contains a useful summary of chemical thermodynamics, but also an interesting section on experimental methods. A final section gives examples from materials problems.

IUPAC Commission on High Temperatures and Refractories (1964) *High Temperature Technology*, Butterworths, London, 598 pp.

The book is not very detailed on experimental equipment, but it contains thorough discussions of high-temperature materials problems.

Margrave, J.L. and Hauge, R.H. (1980) 'High Temperature Techniques', Chap. VI (pp. 277–366) in *Chemical Experimentation under Extreme Conditions*, B. W. Rossiter, ed., Vol. **IX** in the series Techniques of Chemistry, Wiley, New York (14 vols).

A condensed survey of a large number of methods and equipment for experiments at temperatures to some 2500 °C and pressures to 10–50 000 bar, with 491 literature references.

Garland, C.W., Nibler, J.W., and Shoemaker, D.P. (2009) *Experiments in Physical Chemistry*, 8th edn, McGraw-Hill, 734 pp.

A very thorough book, contains almost everything except high-temperature techniques.

Thermochemical Data

Aylward, G.H. and Findlay, T.J.V. (2008) *SI Chemical Data*, 6th edn, John Wiley & Sons Australia Ltd., 212 pp.

This little book is used in basic chemistry and chemical thermodynamics courses. It is, however, very useful also for later work and thus strongly recommended.

Chase, M.W. Jr. (ed.) (1998) *NIST-JANAF Thermochemical Tables*, 4th edn, American Chemical Society/American Institute of Physics, New York, Part I + II 1950 pp.

This is generally the first choice when looking for thermochemical data. The first edition appeared in 1964. In addition to the tables, thorough documentation and

literature references are given for all data. NIST is the abbreviation for National Institute of Standards and Technology, USA. (JANAF means Joint Army, Navy, Air Force!).

Barin, I. (1995) *Thermochemical Data of Pure Substances*, 3rd edn, VCH Verlag, Weinheim, Part I + II, 1885 pp.

These tables contain data for many more substances than NIST-JANAF, but documentation and references are more limited.

The Barin tables contain the usual quantities ΔH^0f and ΔG^0f for the enthalpy and the Gibbs energy of formation of a compound at the temperature T from its elements at the same temperature. But Barin also gives the symbols H and G to mean the change in enthalpy and Gibbs energy of formation of the compound at temperature T from the elements at 298 K. A closer explanation is given in his Introduction.

Knacke, O., Kubaschewski, O., and Hesselmann, K. (1991) *Thermochemical Properties of Inorganic Substances*, 2nd edn, vol. **I + II**, Springer-Verlag, Berlin, 2412 pp.

These volumes give the data in the form of tables as well as in analytical form. The latter is advantageous when using the data in a computer.

Binnewies, M. and Milke, E. (2002) *Thermochemical Data of Elements and Compounds*, 2nd edn, Wiley – VCH Verlag, Weinheim, 928 pp.

A compact collection of data, giving $\Delta H^0{}_{298}$ and $\Delta G^0{}_{298}$ together with C_P as f(T) in analytical form, suitable for computer use. The format permits about 5000 substances and includes about 300 literature references.

Phase Diagrams, Metal Systems

Massalski, T.B. (ed.) (1990) *Binary Alloy Phase Diagrams*, 2nd edn, vol. **I–III**, ASM International, Materials Park, Ohio, 3542 pp.

This collection has its predecessors, connected to names like W. G. Moffat, F. A. Shunk, R. P. Elliott, and M. Hansen. It is the first choice with respect to binary metal systems, but this does not mean that all the diagrams are correct. For example, the diagrams for the systems Si-C and Al-C are grossly inaccurate, and the references should be consulted.

Effenberg, G., Petzow, G., and Petrova, L.A. (1990–1993) *Red Book. Constitutional Data and Phase Diagrams of Metallic Systems*, vol. **I–IX**, VINITY(Moscow)/MSI (Stuttgart).

The collection comprises some binary, but mostly ternary and quaternary alloys. Apparently it was intended to be updated every year, but we do not know whether any volume has appeared after 1993.

Phase Diagrams, non-metals

American Ceramic Society (1964–1990) *Phase Diagrams for Ceramists*, vol. **I–VIII;**

ACerS-NIST (1995–2001) *Phase Equilibria Diagrams*, vol. **IX–XIII**.

This is essentially one series of volumes with two slightly different titles, mostly covering oxide systems. The numbering of diagrams runs continually from Fig. 1

in 1964 to Fig. 10 840 in 2001. A Cumulative Index (1995, 213 pp.) covers Vol. **I** to **XI**, subsequent volumes have separate index. Vol. **I** (1964) starts with a useful 'General Introduction to Phase Diagrams.

Properties of Materials

This subheading could cover a number of texts, including Metals Handbooks, and so on but only one reference is given here:

Touloukian, Y.S. (1967) *Thermophysical Properties of High Temperature Solid Materials*, **6** vol.s, 9 parts, Macmillan, New York.

This is a useful reference for any property, for example, thermal conductivity, electrical conductivity, spectral transmissivity, and so on, given as functions of temperature in graphical form. (Note, however, that it is now almost 40 years old.)

2

Basic Design of Laboratory Furnaces

CONTENTS

High Temperature Experiments in Chemistry and Materials Science, First Edition.
Ketil Motzfeldt.

Preamble

A more general title for this chapter might have been 'Means of Attaining and Controlling Temperature' as in Bockris *et al.* (1959) pp. 47–86 (see p. 8 under *Experimental Methods*). However, the most common way to attain high temperatures for laboratory experiments is by use of some sort of apparatus, generally termed a furnace as in the present text. More esoteric techniques such as electron bombardment, image heating and impulse or flash methods are not covered, nor is combustion heating.

Furthermore, the present chapter covers only the more ordinary laboratory furnaces. Specialized furnaces for controlled atmospheres at 2000 °C and beyond will be dealt with in Chapter 7, after the necessary vacuum technique has been discussed in Chapter 6.

2.1 METHODS OF HEATING

For laboratory furnaces of moderate size, the cost of power is unimportant. The choice of the method of heating depends primarily on the maximum temperature to be attained, the desired atmosphere in the furnace, and the required precision of temperature control. Electric heating is preferred because it offers better possibilities for control than, for example, combustion heating.

Two different methods of electric heating are in general use in the laboratory. In **resistance heating**, a current I is passed through an electric

conductor or *resistor* with resistance R, generating the thermal power $W = RI^2$.[1] The resistor is connected at each end to a power supply through copper terminals. In **induction heating**, on the other hand, the conductor forms a closed loop with no terminals. Electric current in this body, the *susceptor*, is induced by high-frequency current through a surrounding copper coil.

A resistance furnace is well suited to precise temperature control with respect to temperature uniformity and constancy in time. Induction heating, on the other hand, permits a simple and versatile furnace; the crucible itself often serves as the 'heating element.' In both cases, however, the temperature limit and general behaviour are determined by the resistor material in combination with the surrounding atmosphere and eventually the supporting ceramics.

Several other methods of attaining high temperatures are available, such as the electric arc, plasma, image and solar furnaces, and shock heating. Motzfeldt (1959) presented a brief review. These methods, however, are not well suited when a uniform temperature in time and space is required, and they are not further considered here.

2.2 MATERIALS

2.2.1 Electric Conductors or Resistors

The majority of resistor materials are metals (or carbides or silicides) that are thermodynamically unstable in the presense of oxygen. A number of them may nevertheless be used to quite high temperatures in air, because a dense oxide film is formed on the surface which prevents (or slows down) further oxidation. The development of good high temperature resistor materials has thus been a question of developing materials which form dense, protective surface layers when oxidized.

A number of resistor materials are listed in Table 2.1. The materials that may be used in oxidizing atmospheres are listed first, in order of increasing temperature limit. Today, resistor materials are available

[1] The standard symbol for power in electrical engineering is P, but in chemistry this symbol is used for pressure. In the present text, W has been chosen for electrical power, while q is used for the equivalent 'thermal power' in the sense of heat flow.

Table 2.1 Maximum element temperature for resistor materials.

Material	Melting point °C	Maximum element temperature in °C for atmosphere; Oxi-dizing	Vacuum $<10^{-4}$ millibar	Reducing or inert	Notes
80 Ni-20 Cr	(1400)	1175	(1200?)	(1100)	Avoid contact with sulphur compounds
Kanthal A-1[a]	(1500)	1400	(1200?)	(1200)	Avoid contact with hydrocarbons, free SiO_2 or alkali
SiC resistors[b]	(subl.)	1600	x	(1300)	Avoid contact with hydrocarbons or excess $H_2O(g)$
Kanthal Super[c]	(subl.)	1900	x	(1500)	Avoid contact with dry H_2 or sulfur compounds
Pt	1770	1600	1700	x	Pt becomes soft above 1500 °C; Pt and Rh are volatile in O_2 above 1600 °C
60 Pt-40 Rh	1940	1800	1700	x	
Rh	1966	1800	1700	x	
Oxide semiconductor	—	~2200	x	xx	See text, p. 29
Mo	2620	xx	2100	2400	Sags above 1800 °C
Graphite	(subl.)	xx	2200	2800	Some reaction with H_2 and N_2
Ta	2997	xx	2700	2800	
W	3380	xx	2700	3200	Sags above ~2300 °C

Notes: The temperatures are not sharp limits; lower temperatures give longer service life. The temperature limits in vacuum refer to vapour pressures of about 10^{-4} millibar. Parentheses indicate estimated or uncertain values. x indicates not recommended for use, xx impossible for use.

[a]Kanthal alloys include Kanthal APM (max. 1425 °C), A-1 (max. 1400 °C), A (max. 1350 °C), AF and AE (max. 1300 °C element temperatures). The five alloys have approximately the same composition: 22 Cr, 5.3–5.8 Al, 0.6–1.0 Co, < 0.1 C, balance Fe.

[b]SiC resistors exist in various qualities with reported max. element temp. from 1550 to 1650 °C.

[c]Powder-metallurgical product, principally molybdenum disilicide. Three qualities, Kanthal Super 1700, 1800 and 1900, where the numbers indicate the maximum element temperature.

that may be used in oxidizing atmospheres up to some 1800 °C. Temperatures in excess of this may be attained by use of high-melting metals such as molybdenum or tungsten, or by graphite, but the use of these materials necessitates a neutral or reducing atmosphere, or a good vacuum. This is a subject in itself and is postponed to Chapters 6 and 7, while the present Chapter 2 primarily deals with furnaces using oxidation-resistant resistors.

The resistivity (ohm-cm) for a number of resistor materials is given in Figure 2.1 as a function of temperature, with the curve for copper included for comparison. It is noted that the resistivity of *pure metals* increases markedly with temperature, while the resistivity of the *base metal alloys* is less temperature dependent. The latter fact is an advantage when using these alloys for heating elements in furnaces. Some further comments regarding the various resistor materials are given in connection with furnace design, in the next section.

2.2.2 Insulating Materials

The term '*insulating*' includes at least two different properties, *electrical* insulation, and *thermal* insulation.

Electrical Insulators. The resistor of the most commonly used laboratory furnace consists of a wire wound round an electrically insulating tube. Commonly used materials for refractory tubes are various makes of refractory porcelain, that is, materials consisting essentially of mullite, $3Al_2O_3{\cdot}2SiO_2$, with less free silica than used in ordinary porcelain. These tubes are generally dense-sintered and gas tight, so that they may also be used as the working tube in a controlled atmosphere. The temperature limit is around 1500 °C.

An alternative is alumina (usually around 99.6% Al_2O_3). The melting point of alumina is 2054 °C, but tubes of dense-sintered alumina become mechanically weak above some 1800 °C. They are also more sensitive to thermal shock or steep temperature gradients, and their price is roughly ten times that of refractory porcelain. Thus the use of dense-sintered alumina tubes is not recommended unless the higher maximum temperature is required.

A tube of porous alumina is another alternative. It is less sensitive to thermal shock, and may be used when a controlled atmosphere is not

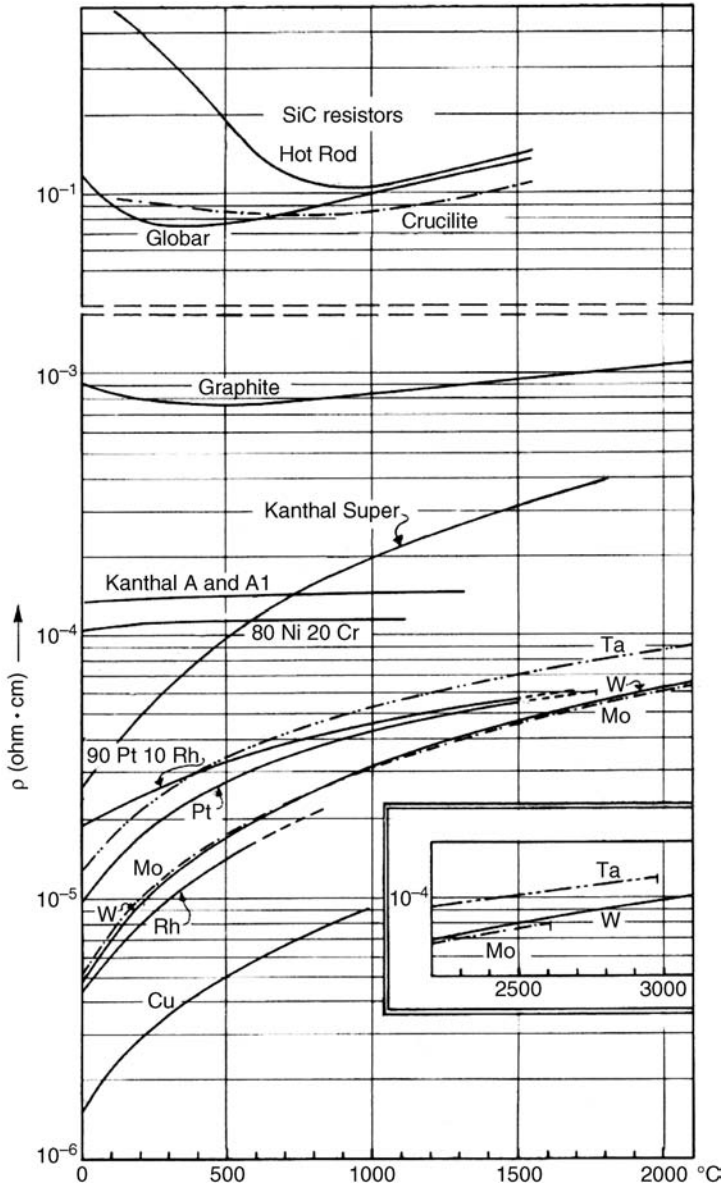

Figure 2.1 Resistivity (ohm cm) as a function of temperature (°C) for some resistor materials and for copper. *Note:* The curves for SiC are given primarily to indicate the spread in the data and do not indicate any preference for the quoted brands.

required. A further discussion of ceramic and refractory materials is given in Chapter 5.

Thermal Insulation. The temperature inside a laboratory furnace is attained as a balance between the power input and the thermal insulation, hence the insulating material has an important role. Obviously the insulating material next to the resistor has to withstand at least the same temperature as the resistor itself. In addition the two should be compatible, that is, they should not react chemically. Formerly, refractoriness and effective thermal insulation were hard to combine, but in recent years insulating fibre materials have been developed that withstand temperatures up to some 1800 °C. Some further discussion on thermal insulation is given in Section 2.5.2, pp. 37–40.

2.3 BASIC FURNACE DESIGN

2.3.1 Obtaining a Uniform Temperature

For a start, we consider a refractory tube heated by evenly spaced resistance wire and with no thermal insulation, as in Figure 2.2a. With a certain power input, the temperature inside the tube will not be very high, but it will be quite uniform along the tube. Now suppose the power is kept constant while a concentric layer of insulation is placed on the furnace as in Figure 2.2b. Near the ends of the furnace the heat loss occurs mainly to the open ends, and the temperature will increase only a little.

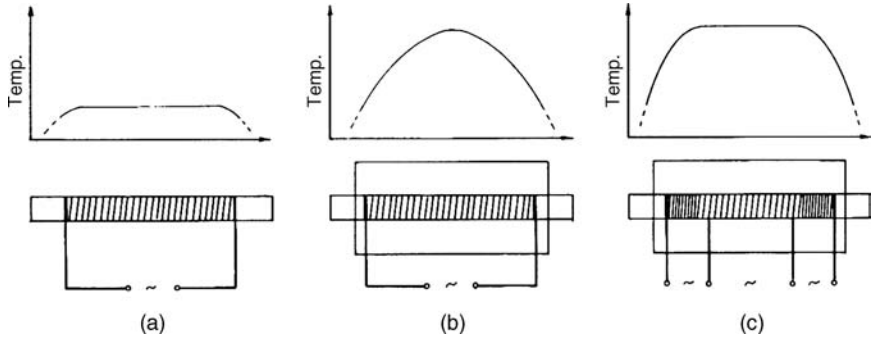

Figure 2.2 On the temperature distribution in a cylindrical furnace (see text).

In the middle part, however, the heat loss occurs mainly through the insulation, and the temperature increases substantially. The resulting temperature distribution shows a marked maximum in the central region. This is not at all desirable if the intention is to study the property of an object at a defined, uniform temperature. Thus, a poorly insulated furnace (Figure 2.2a) may have advantages as far as temperature distribution is concerned. (It also has the advantage of quick response, cf. Section 2.4.)

With increasing insulation, remedies for improving the temperature distribution are increasingly necessary. An obvious solution is to increase the heat input towards the ends; this may be done by spacing the resistance wire more closely at the ends as indicated in Figure 2.2c. The optimum magnitude of this compensation, however, is not easily foreseen and may vary with the furnace temperature. For this reason the end sections of the resistor should preferably be provided with taps to allow adjustment of the current in each section.

In the examples in Figure 2.2 the furnace was shown horizontally. In practice, tube furnaces more often are placed vertically for various practical reasons. An example of a general-purpose laboratory furnace is shown in Figure 2.3, with a total of four terminals as explained above. Note also that the furnace tube inside is provided with a set of horizontal 'radiation shields' to reduce heat loss toward the ends. This thermal insulation should hinder heat transfer axially, but at the same time should allow heat exchange crosswise. For this reason, thin radiation shields are better than, for example, a plug of porous firebrick. Another reason for choosing radiation shields is that porous firebrick internally would hamper the establishment of a controlled atmosphere in the furnace tube.

Other remedies to obtain a zone of uniform temperature have been tried, notably a cylindrical metal liner in the hot zone. Aluminium, silver and copper are candidates, but of limited use due to their low melting point (660, 961 and 1083 °C, respectively); the use of copper also demands a neutral or reducing atmosphere. Stainless steel may withstand higher temperatures and oxidizing atmospheres, but its thermal conductivity is much lower than that of the above metals and in fact comparable with ceramics; thus stainless steel is of little use for the said purpose (see also p. 41, Table 2.2).

The temperature distribution along the furnace tube may be scanned by means of an internal thermocouple. In the case that the furnace is

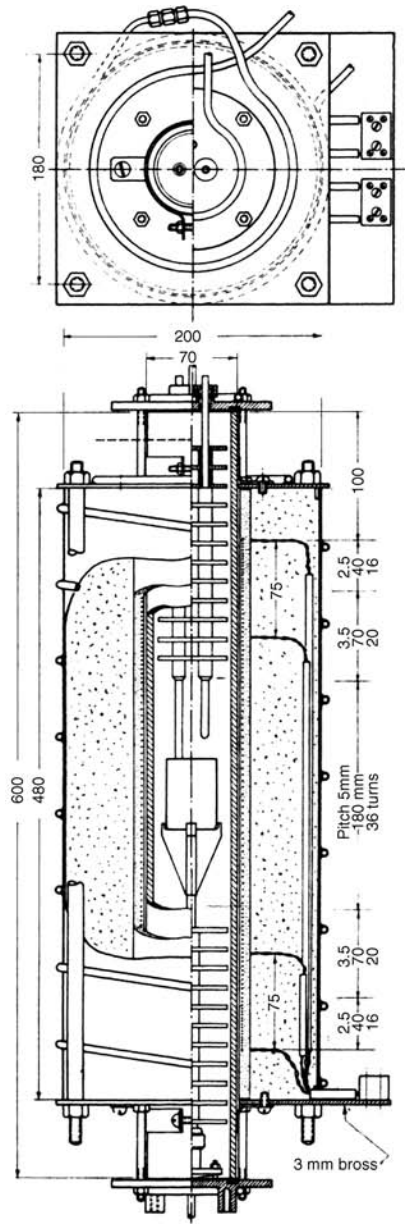

Figure 2.3 General purpose laboratory furnace. Cylindrical shell: 1.2 mm copper sheet, with soft-soldered 6 mm copper cooling tubes. Insulation: alumina-silica fibre. Windings: Kanthal A, 1.2 mm dia., about 27 m (plus terminals), about 35 ohm.

provided with taps for separate adjustment, as in Figure 2.3, the best distribution of heat input must be found by trial and error. Even in the absence of means for separate power adjustments, mapping of the temperature distribution in a furnace should be made as a preliminary to any serious work.

The vertical position of a tube furnace has an effect on the temperature distribution since hot gas tends to move upwards. Any 'chimney effect' should be avoided by keeping the furnace tube closed during use, in particular at the upper end. Even so, a furnace with evenly distributed power (resistor windings) will tend to have its hottest section somewhat above the middle. This may be compensated for by placing also the specimen (crucible, cell, - -) somewhat above the middle. Once again, the optimum position may be found by mapping the temperature distribution beforehand.

2.3.2 Base Metal Wire

There are two main types of oxidation-resistant electric resistance alloys. Nickel-chromium (e.g. 80 Ni, 20 Cr) was developed about 100 years ago and was soon used for heating elements in furnaces as well as household appliances. Around 1930 another resistance heating alloy, based on iron-chromium-aluminium, was developed by the company *Kanthal*. (The name was derived from the family name of the inventor, Hans von Kantzow, and the location of the factory, Hallstahammar in Sweden.) Kanthal alloys have better oxidation resistance, which means a higher maximum operating temperature or a longer life at corresponding temperatures. Nickel-chromium may have certain advantages with respect to good mechanical properties at elevated temperature, but in most respects the various types of Kanthal wire are superior. The company has come to dominate the market to the extent that resistance wire for heating elements is considered synonymous with Kanthal wire.

For laboratory furnaces where the cost of the wire itself is unimportant, the quality A1 has been the standard. More recently the quality APM has been developed which has even better form stability and less tendency to sagging at high temperatures.

On Furnace Temperature and Surface Load. Considering any kind of heating element in a furnace, it is realized that the heating element must

be at a higher temperature than the furnace in order that heat can be transported from the element to its surroundings. Given a maximum temperature for the heating element, the temperature difference between that and the furnace should be less as the furnace temperature is increased. As a consequence, the permissible maximum surface load goes down as the furnace temperature goes up. To be on the conservative side, the surface load should not be more than 2 watt per cm^2 of surface area of Kanthal A wire when the furnace is intended for use at 1300 °C. More detailed information on this point is given in the Kanthal Handbook.

A 'Homemade' Heating Element. The heating element in the furnace shown in Figure 2.3 is made from 1.2 mm dia. Kanthal wire. This thickness is suitable for winding a furnace without special skills. The wire may be placed directly on the ceramic tube, but it is advisable to put several turns of paper on the tube before the wire is put on. The position for the windings is marked on the tube (the paper) and the wire is put on, preferably by means of a lathe with adjustable pitch. The wire is then covered with a layer of alumina cement, an operation that may have to be repeated in order to obtain a sound layer.

Once the cement has dried, the tube with element may be put in place in the furnace casing, and the interspace filled with thermal insulation (cf. Section 2.5.2, pp. 37–40). The furnace may then be slowly heated, preferably in a hood. At some 200–300 °C the paper will begin to char. The refractory tube may eventually be removed and the remaining, partly charred, paper removed to avoid excessive smoke. With the tube back in place and secured by a clamp at the upper end, the furnace is ready for service.

The idea of the paper in the first place is that, when burnt away, it leaves sufficient free space that the furnace tube may be removed and exchanged without interfering with the heating element. The alumina cement will not be very sound even after heating to some 1000–1200 °C, and hence the heating element should be handled with care. It should also be noted that Kanthal A wire becomes brittle after use at high temperatures.

The furnace heating element described in Figure 2.3 has a total resistance of about 35 ohm, suitable for operation on 220 V mains through a variable autotransformer.

Factory Made Heating Elements. The life of the heating wire depends on its rate of oxidation. For a given rate of oxidation, a thicker wire will have a longer life. Thus thick wire is preferable, but wires thicker than some 1.5 mm dia. become unmanageable for the amateur.

Kanthal manufactures its standard heating elements from thicker wire. The company has also developed ceramic fibre materials that are sturdy yet lightweight and well insulating, marketed under the name *Fibrothal*. Various modules are available, with heating elements of 5 mm dia. (or rectangular cross-section) Kanthal wire embedded in an outer body of thermally insulating Fibrothal. An example is seen in Figure 2.4, showing a furnace similar to that in Figure 2.3 but with a standard heating element (Kanthal type RAC 100/500).

A difference between the two furnaces is that the one in Figure 2.4 does not have extra terminals for adjustment of current to the end sections. Heating elements with extra terminals are delivered only on special order. Another difference is that the furnace with the thicker wire runs on lower voltage and higher current, so that a separate transformer is required. An ordinary transformer for a few kW, however, does not cost very much and lasts forever. Altogether the factory made heating elements may have economic advantages in the long run.

Furnace Furniture. The term covers whatever is needed inside the furnace tube. Sets of horizontal radiation shields are shown in Figure 2.3, and the rationale explained above. The term 'radiation shield' stems from the fact that heat transfer by convection/conduction and by radiation are of roughly the same magnitude in air at 1 atm and room temperature; at elevated temperature the radiation always dominates. The shields may be produced like cookies from alumina cement, but for many purposes they may equally well be made from stainless steel which is less liable to break. As indicated in Figure 2.3 the shields are suspended from thin refractory tubes, with spacers cut from slightly larger tubing.

In Figure 2.3 a crucible is indicated, resting on a 'supporter' with the head made from alumina cement. This head is not a pear-shaped solid lump; looking from above it has the shape of a cross. The idea is that it provides stable support and at the same time provides, as far as possible, free access for radiation to the bottom part of the crucible.

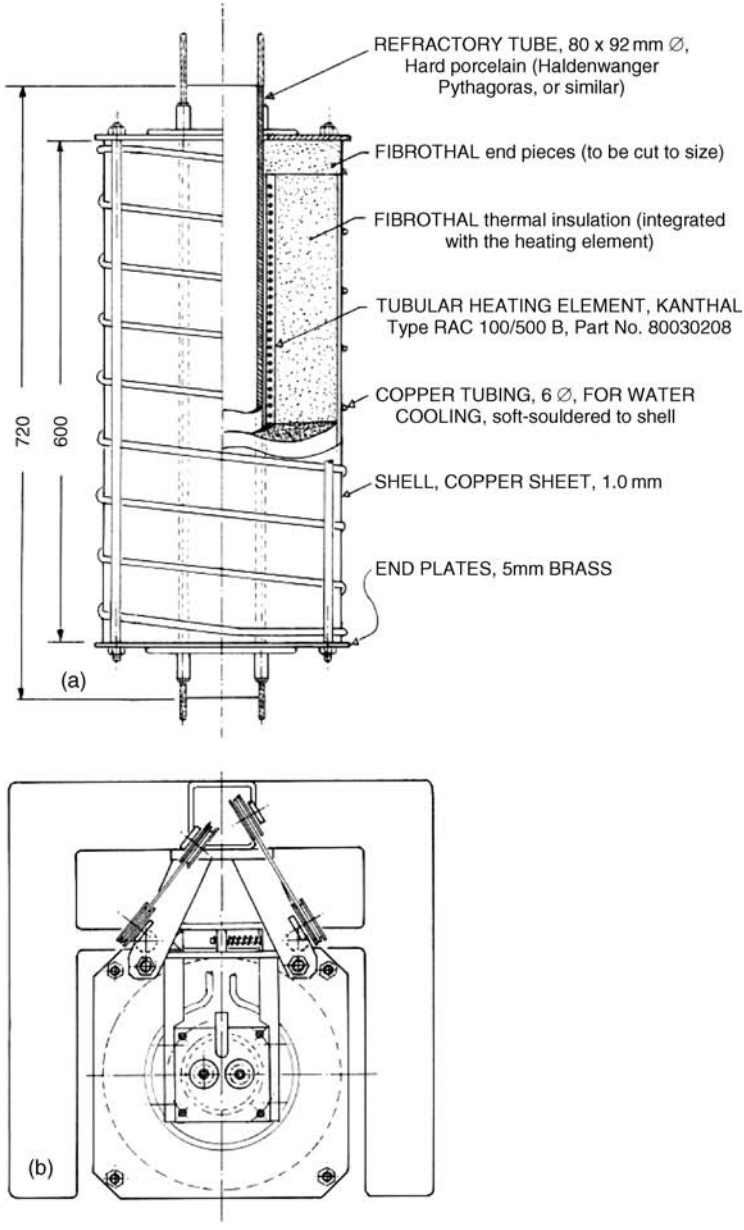

Figure 2.4 (a) General purpose laboratory furnace with factory-made heating element, Kanthal A, 5 mm dia., about 1.4 ohm, with Fibrothal insulation. Refractory tube about 80 × 92 mm. (b) Same furnace from above, mounted in the stand shown in Figure 2.6, p. 26.

2.3.3 The Stand and Auxiliaries

A laboratory furnace may be placed on a nearby table; an easy solution, but usually not the best. The placement in general should be decided from its purpose. Assuming that we have a vertical tube furnace, the specimen or crucible may be lowered into it by means of a pair of crucible tongs, the way it was done 100 years ago. More convenient handling is provided by some sort of supporter where the crucible may be lifted into the furnace from below. For this purpose, a stand of angle steel with counter-balanced sliding support was designed, as shown in Figure 2.5.

At a later date it was found convenient to have controlled movements of both the lower and the upper parts of the furnace furniture. This is useful, for example, when studying electrochemical cells where the cell body comes from below while the electrodes come from above. For this purpose another type of stand was designed, shown in Figure 2.6. It has a sturdy 'backbone' of 80×80 mm square hollow steel, while the sliding supports are mounted on pairs of 25 mm dia. stainless tubing above and below the furnace. The design permits swinging the supports to one side for easy access to the interior of the furnace when necessary.

It may take a bit of effort to design these sort of custom-made auxiliaries, to align them, and to maintain them in good condition. When in place and working, however, it is certainly worthwhile in terms of easier and more accurate work.

A further discussion of practical aspects regarding laboratory furnaces is postponed to Sections 2.5 and 2.6.

2.3.4 Silicon Carbide

Pure SiC is a semiconductor, characterized by high electrical resistivity at room temperature, decreasing as the temperature is raised. The silicon carbide materials used for heating elements are essentially ceramic materials, compounded to give a fair resistivity at ambient temperature. The resistivity at first falls off and then increases again with increasing temperature, see Figure 2.1 (p. 16). Various producers have different, patented ways of making their materials, resulting in somewhat different resistivity/temperature characteristics. There are various brands like Crucilite, Globar, Hot Rod, and Silit, but it appears that most of them are now marketed by the company Kanthal.

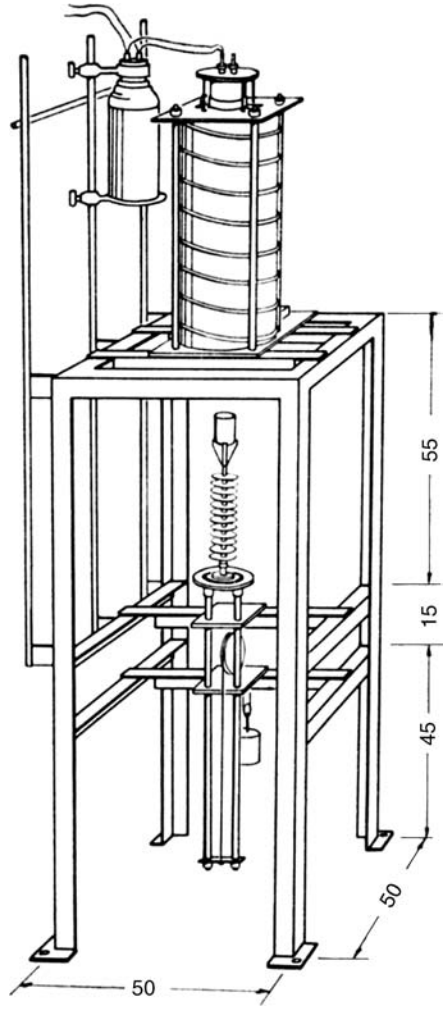

Figure 2.5 Furnace mounted on stand (40 mm angle iron) with counter-balanced sliding support for lower lid. (Dimensions in centimetres.)

Silicon carbide for heating elements was first made in the form of rods, and this is still the usual form for use in larger, industrial furnaces as well as smaller ceramic kilns in the laboratory. Rods may also be used for an extremely simple laboratory furnace as shown in Figure 2.7. More recently, other forms have become available for special purposes, such as a spiral form for heating in a tube furnace.

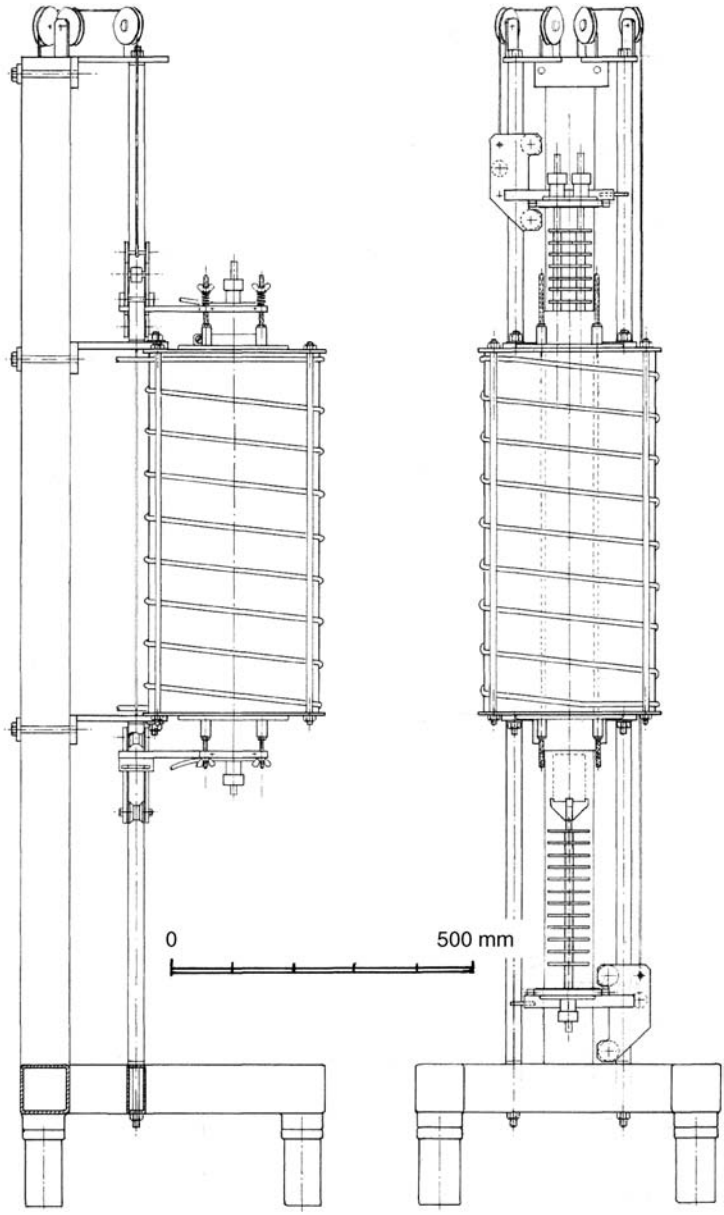

Figure 2.6 A more versatile furnace stand, built from 80 × 80 mm hollow steel, with pairs of 25 mm dia. tubular stainless steel to carry sliding supports for both upper and lower furnace lid. (See also a top view of the same stand, Figure 2.4, p. 31.) Note: This stand is drawn to scale. However, in future models the pairs of stainless steel tubes should preferably be increased to about 620 mm (lower) and 520 mm (upper tubes), increasing the total height (ex. pulleys) to at least 2 m.

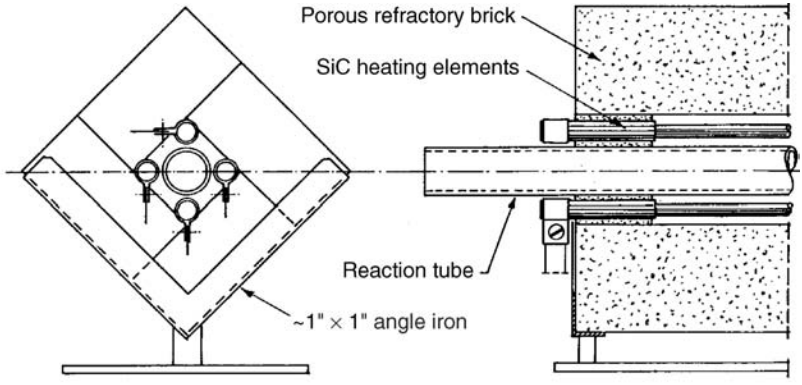

Figure 2.7 A simple assembly for a tube furnace, made from high-alumina porous firebrick with SiC rod resistors.

Silicon carbide is inherently unstable in air and, like the base metals, is always covered by a layer of oxide. In the case of SiC the oxide is SiO_2 (silica) which has a tendency to form a glassy phase. This may be a reason why silica is particularly efficient as protection against further oxidation. In dry air, silicon carbide heating rods may be used to a maximum element temperature of about 1650 °C. At a furnace temperature of 1500 °C, the maximum recommended surface load is about 4 W/cm^2.

In the presence of water vapour the temperature should be lower because the oxidation proceeds more rapidly. The reason is that molecules of H_2O penetrate the silica film more readily than O_2. Their use in reducing atmospheres is not recommended. Regarding oxidation of SiC, see also Chapter 5, pp. 139–146.

Silicon carbide differs from most other resistor materials in that it is subject to ageing; that is, the resistance of the heating rod increases with time under load. The resistance of a rod may increase to twice its original value while the rod is still serviceable. For this reason, the set of rods in a furnace should be connected in parallel; in this way the 'weakest' rod will carry less load, and the rods will age evenly. If connected in series, the weakest rod will carry most of the load and will quickly burn out.

A furnace with silicon carbide heating elements will normally need a transformer for its power supply. Because of the ageing effect, the transformer should have about twice the capacity needed for the furnace.

With new elements it is run on low voltage and high current, and with increasing ageing a shift to higher voltage and lower current is necessary.

2.3.5 Molybdenum Disilicide

This is a more recent development. Molybdenum disilicide for heating elements, like silicon carbide, is a brittle ceramic material. The main component is the silicide $MoSi_2$, with additions that aid in forming a dense protective layer of glass at working temperature. Three different qualities are available, named Kanthal Super 1700, 1800 and 1900 where the numbers indicate the maximum permissible element temperature. The furnace temperature must be lower as explained in Section 2.3.2; the Kanthal Super manual should be consulted for a graph showing the relation between furnace temperature, element temperature and surface load for each of the three top qualities.

In contrast to silicon carbide, Kanthal Super heating elements are not subject to 'ageing', that is, the resistance does not increase during use. On the other hand, they do have a tendency to sag at working temperature, and for this reason they are preferably made in the 'hairpin' or U shape, suspended with both terminals upwards. If mounted horizontally, the heating elements should be supported by a suitable refractory material. Even though the material cannot be made into wire, spiral-shaped heating elements are also available.

For use at slightly lower temperatures, *Superthal* heating modules are made with the heating element embedded in a lightweight insulation like the Fibrothal mentioned on p. 22. Cylindrical or half-cylinder modules are available for use up to a maximum of 1600 °C furnace temperature. Multi-zone Superthal muffle furnaces allow precise control of the temperature uniformity along the furnace, as previously discussed in Section 2.3.1.

2.3.6 Oxide Resistors

These comprise a group of electrically conducting oxide materials that may be used in oxidizing atmospheres. Examples are ceramic materials based on ZrO_2 or ThO_2 with addition of di- or trivalent oxides to enhance conductivity. These materials, however, are semiconductors

with a negative temperature coefficient of conductivity. At room temperature they are practically non-conducting and need some kind of preheating, for example, by a wire-wound heating element. Altogether, oxide resistor heating elements are troublesome to operate and have not gained much acceptance, particularly not after the temperature range of molybdenum disilicide elements was expanded to 1900 °C. The same is true for heating elements made from another class of semiconducting oxides, such as lanthanum chromite, $LaCrO_3$.

The use of semiconducting oxides as temperature sensors, solid-state electrolytes, semipermeable membranes, and in electronic applications is quite another story, and is outside the present scope.

2.3.7 Noble Metals

These are the last group of materials to be mentioned that may be used in oxidizing atmospheres. Platinum is probably the best known, with a melting point of 1768 °C. Pure platinum, however, is mechanically weak and not recommended as a construction material for any purpose. Alloying with only 10% rhodium greatly improves the mechanical properties and at the same time increases the melting temperature. Pure rhodium melts at 1970 °C, and the phase diagram Pt-Rh shows a continuous solid solution with a steep increase in the melting temperature for only a few percent rhodium (cf. Chapter 3, p. 73).

Because of the price, Pt-Rh alloys are of interest as heating element only for very small 'furnaces', for example, in high temperature x-ray diffraction equipment. When judging the practicality for laboratory use it should be borne in mind that more than half the value of the platinum may be retrieved when the equipment is scrapped.

2.3.8 Molybdenum Wire

We now turn to metals that cannot be used in oxidizing environments, with molybdenum and tungsten as the most prominent representatives. Both form oxides that are not only non-protective, they are *volatile* at elevated temperatures. Molybdenum wire is reasonably ductile at room temperature and is suitable for heater windings. Furnaces with molybdenum wire wound on an alumina tube have been commonly used in

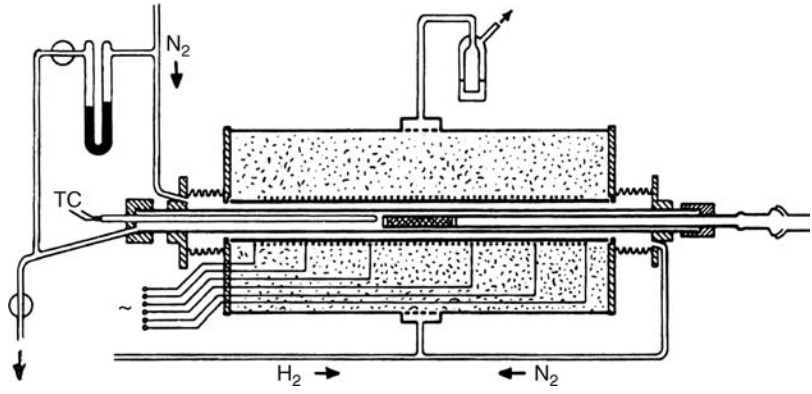

Figure 2.8 Simplified drawing of a tube furnace with molybdenum wire wound on an outer, porous alumina tube. The heater windings have five sections to control the temperature distribution. Note the gas-tight packing glands at both ends and the flexible bellows to avoid straining the inner alumina tube.

laboratories for temperatures to 1800 °C. The working tube has to be of a dense-sintered, gas-tight quality when the idea is to use the furnace with an oxidizing gas on the inside of the tube and a reducing gas on the outside. For this reason the design of a molybdenum-wound furnace should take into account the fact that the connection between alumina tube and furnace shell should be gas tight. Nitrogen with a moderate admixture of hydrogen has been commonly used as a protecting gas.

A simplified drawing of a molybdenum-wound furnace with four tappings is shown in Figure 2.8, designed for adjustment of the power to each section. Otherwise a furnace with silicon carbide or Kanthal Super heating elements is a simpler alternative for work in oxidizing atmospheres.

2.3.9 Graphite

Graphite belongs to the materials that cannot be used in an oxidizing atmosphere, and thus is left for a more thorough discussion in Chapter 7. However, it is mentioned here because of its versatility and availability. Furnaces with graphite heaters were built for various purposes more than 100 years ago. A rough furnace may be built with the heater as well as the insulation consisting of carbon, and with the shell only moderately gas tight. The carbon will be slowly oxidized by the

penetrating air, but so what? The carbon parts may be replaced at moderate cost. This works well if a variable and unknown partial pressure of carbon monoxide may be tolerated, but in almost any serious work it cannot. And so we leave the rest to Chapters 6 and 7.

2.4 INDUCTION HEATING

2.4.1 Elementary Principles

A high-frequency induction furnace consists generally of a water-cooled copper induction coil with a concentric, cylindrical load, also called the *susceptor*, as the main component, see Figure 2.9. Only non-magnetic loads will be considered here.

When an alternating current is fed through the coil, an alternating magnetic field running parallell to the centre line of the coil is generated. This magnetic field induces an alternating current in the load, running in closed loops perpendicular to the centre line of the coil and in such a direction as to oppose the original magnetic field. The current induced near the surface will largely neutralize the field in the interior of the load, hence the greater part of the current will be near the surface. This is known as the *skin effect*. The current density decreases exponentially from the surface inwards. The effective thickness (or penetration depth) δ is defined as the thickness which would carry the same amount of current if the current density at the surface was uniform to a depth δ instead of falling off exponentially. For δ much smaller than the diameter d of

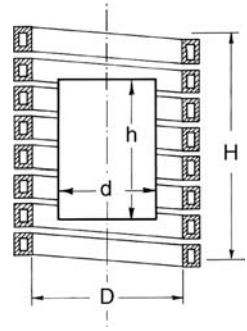

Figure 2.9 Basic arrangement for induction heating.

the susceptor, a conductor with resistivity ρ (ohm cm) for a current with frequency f (cycles/sec) has an effective thickness

$$\delta = \frac{1}{2\pi}\left(\frac{10^9\rho}{f}\right)^{1/2} = 5030\left(\frac{\rho}{f}\right)^{1/2} \tag{2.1}$$

In calculating the effective resistance of a conductor to high-frequency current, the cross-section used is obtained from this effective thickness, which is given as a function of resistivity for various frequencies in Figure 2.10. Note that the resistivity of the load may change markedly during heating, cf. Figure 2.1 (p. 16).

The arrangement in Figure 2.9 is analogous to a transformer with the secondary consisting of one closed loop of length πd and cross-section δh. One difference from the ordinary transformer is that the

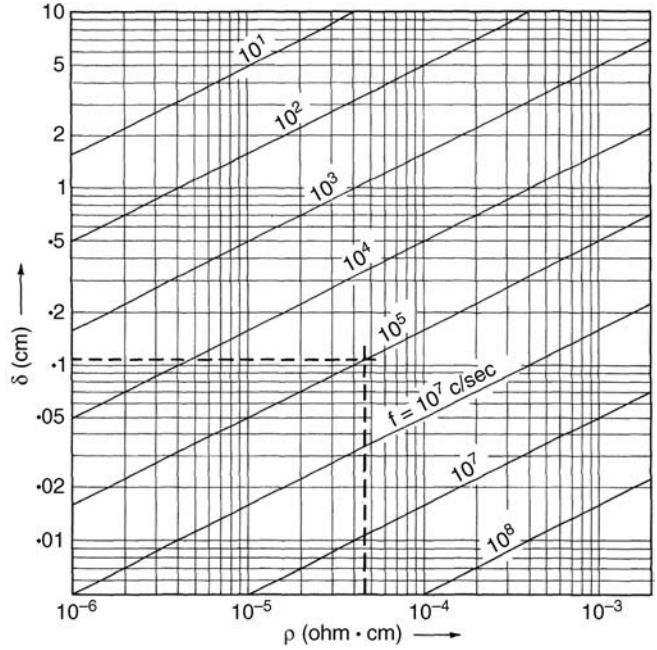

Figure 2.10 Effective thickness (penetration depth) δ as a function of resistivity for various frequencies.

power efficiency may be much less than unity. The problem is to design the coil and load assembly so as to obtain optimum efficiency. The solution to this problem is rather complex, and in practice a satisfactory design is often found by trial and error. Ribaud (1950) has given an equation for the power efficiency η that may be used as a guideline:

$$\eta = \frac{q_{load}}{q_{load} + q_{coil}} = \frac{1}{1 + \frac{D}{d}\frac{H}{h}\left(\frac{\rho'}{\rho}\right)^{1/2}} \tag{2.2}$$

Here, q is the power dissipated as heat, ρ' is the resistivity of the coil material (usually copper), ρ that of the susceptor material, and the other symbols appear from Figure 2.9. This equation is derived for $H > D$ and $h > d$, but it is approximately valid for heights about equal to the diameters. The frequency must be sufficiently high so that $\delta < 1/4\ d$; at lower frequencies efficient heating of a solid load is impossible.

In a high-frequency furnace a layer of thermal insulation is usually necessary between load and coil, so that d is considerably less than D. Equation (2.2) shows that this results in decreased power efficiency, hence a balance must be struck between insulation and efficiency.

A hollow load with wall thickness $\Delta d \gg \delta$ behaves like a solid load. However, if the wall thickness is decreased to be of the same order of magnitude as δ, the effective resistance of the load increases, and the power efficiency may increase above the value given by Eq. (2.2) before it drops to zero for $\Delta d = 0$.

2.4.2 High Frequency Generators

During the previous century, three main types of high-frequency generating equipment were in use, namely spark-gap converter, vacuum tube oscillator, and motor-generator. All three types today are considered outdated; the present generator is a product of solid-state electronics. The *Insulated Gate Bipolar Transistor* (IGBT) was developed at SINTEF/NTH in Trondheim at the end of the 1980s. An offspring of this development, the company *EFD Induction a/s*, at present has more than half the world market for induction equipment. The standard range includes equipment for 6 to 200 kW and frequencies of 10 to 25 kHz.

The main applications are for welding, brazing, or heating in industrial production processes, but the indicated frequency range should also be well suited for an induction furnace in the laboratory. The smaller units have built-in automatic impedance matching to give the optimum heat output for a given coil and load. The main problem from the experimentalist's viewpoint is that these high-frequency generators are quite expensive.

Generators based on IGBTs for 0.5 to 500 kHz may be built for special purposes. Generators based on vacuum tubes are only still of interest for frequencies in the MHz range. Very high frequencies may be applied in capacitive heating of electrically insulating materials.

2.4.3 Some Laboratory Applications

Induction heating has been widely applied in high temperature chemistry, with the load inside and the work coil outside a glass container. Figure 2.11 shows a design with a silica glass tube enclosed in a 'water jacket' made from a perspex tube. The coil is supported in grooves machined into the perspex. Alternatively, forced air cooling may be used instead of water. The silica glass tube is joined vacuum tight to brass flanges by means of flat rubber gaskets. The load, in this case a graphite crucible, is surrounded by a cylinder of thermally insulating material. If this cylinder is electrically conducting, it has to be split lengthwise to avoid induced current in the insulation.

Other designs, of course, are possible by using standard ground-glass joints. Borosilicate glass (Pyrex) may be used instead of silica when steep thermal gradients between load and coil can be avoided.

Many melts of interest to chemists and metallurgists are difficult to handle because, at the necessary high temperature, they will react with any conceivable container material. An approach to this problem is *levitation melting* which makes it possible to heat and melt small samples of metal or slag without any container. The coil is given a special shape so that, with the current turned on, the charge hovers within the coil. Harris and Jenkins (1959) show an example of the design. The technique cannot be considered simple, notably because the levitating force and the temperature of the specimen cannot be varied independently. Thus it is limited to the melting of small samples for experimental purposes, and apparently it has not found widespread use.

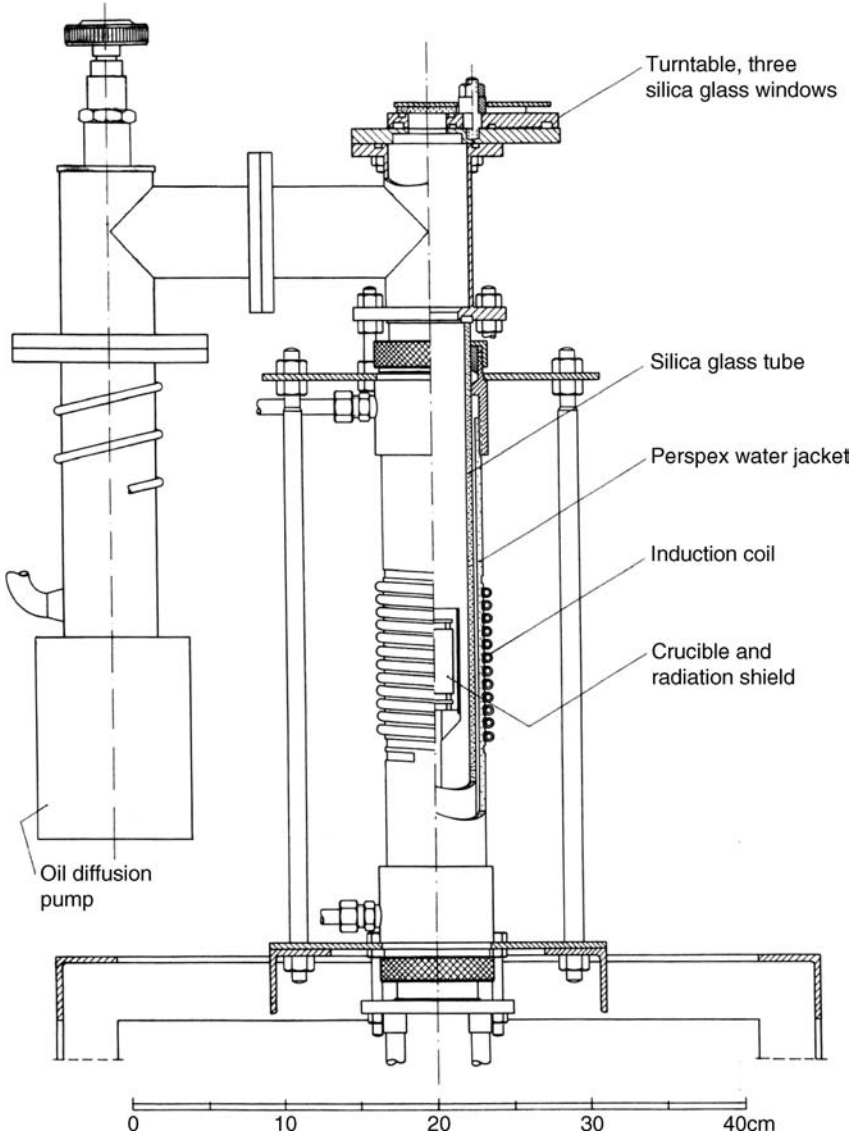

Figure 2.11 A laboratory furnace for high-frequency induction heating, with inner tube of silica glass and outer tube of Perspex for water cooling. Top and bottom parts are made of brass; top with window for optical pyrometry, and outlet to oil diffusion pump.

A more promising approach is that of the 'cold crucible', developed during recent years.[2] The central part is a water-cooled copper 'crucible', split vertically into a number of segments so that it does not form a closed loop for the induction current. Each segment has its own internal water cooling. During use, a thin layer of the frozen melt is formed on the internal copper surfaces, effectively acting as a container for the melt. Temperatures approaching 3000 °C have been attained. The steep temperature gradient between the melt and the water-cooled copper necessitates a generator of high capacity, for example, up to 75 kW for a 60 mm ID crucible.

2.5 POWER INPUT, INSULATION AND COOLING

2.5.1 Power and Temperature

Consider a laboratory furnace where the power is turned on at time zero and maintained at a constant level. The furnace temperature will at first increase rapidly, then more slowly, and finally the furnace comes to a *steady state* as shown in Figure 2.12 for the furnace shown in Figure 2.3. At steady state the power input is balanced by the heat loss to the surroundings, and the temperature remains constant. The diagram includes also a curve for the temperature at steady state versus the power input.

At a constant power input q, the rate of heating will be proportional to the difference between the temperature at steady state, t_{ss}, and the instantaneous temperature t. Thus, with time designated by θ:

$$\frac{dt}{d\theta} = \frac{t_{ss} - t}{\tau_F} \tag{2.3}$$

where τ_F is a constant, the *time constant*. Given an initial temperature t_0 at zero time, the integrated form of this equation is:

$$t - t_0 = (t_{ss} - t_0)(1 - e^{-\theta/\tau_F}) \tag{2.4}$$

[2] Developed by ANSTO, New Illawarra Road, Lucas Height, New South Wales, Australia.

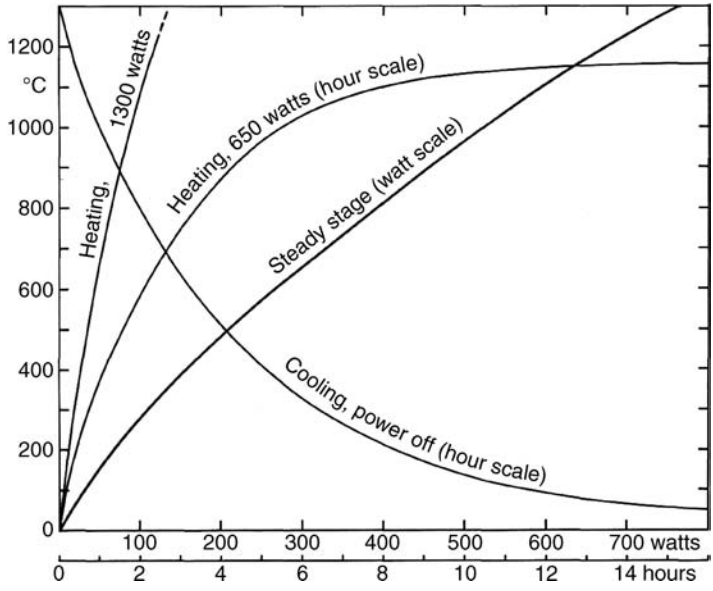

Figure 2.12 Heating and cooling curves for the furnace shown in Figure 2.3.

The time constant τ_F is a property of the furnace. For example, for the furnace in Figure 2.3 the heating curve in Figure 2.12 gives $\tau_F = 2.9$ hours. From Eq. (2.4) it is seen that the time constant is equal to the time it takes to heat a furnace at constant power from room temperature to 63% of the temperature at steady state; a useful rule of thumb.

Generally speaking, a large time constant results from a well insulated furnace with a correspondingly low power consumption at steady state. This sluggishness is no advantage in laboratory work, hence the furnace in Figure 2.3 (and eventually that in Figure 2.4) could to advantage be less well insulated. It would eventually mean a higher power consumption, but power cost is usually of secondary importance in a research laboratory.

2.5.2 Thermal Insulation

The rate of heat flow q through a solid with thermal conductivity k is given by:

$$q = -kA\frac{\mathrm{d}t}{\mathrm{d}x} \tag{2.5}$$

where $\mathrm{d}t/\mathrm{d}x$ is the temperature gradient in the direction x normal to the surface of area A. For the case of a long tube furnace with a concentric layer of insulation with an effective mean thermal conductivity k_m (watt $\mathrm{m}^{-1}\,\mathrm{K}^{-1}$), such as represented in cross-section in Figure 2.13, this equation may be integrated to give the heat loss for a length l (m) of the furnace:

$$\frac{q}{l} = \frac{2\pi k_m(t_1 - t_2)}{\ln(d_2/d_1)} = \frac{2.73k_m(t_1 - t_2)}{\log(d_2/d_1)} \tag{2.6}$$

For a laboratory furnace with no forced cooling, the surface temperature t_2 at steady state will be such that the heat transfer by convection and radiation to the surroundings equals the heat transfer through the insulation. This t_2 is essentially unknown, and difficult to derive explicitly. Motzfeldt (1959) devised a nomogram where the surface temperature, and hence the power requirement, could be determined from the given dimensions of the furnace, the intended furnace temperature, and the mean thermal conductivity k_m of the insulating material. The method was found to be quite useful for its time. For most purposes, however, we now prefer water cooling on the furnace shell. In this case the temperature t_2 is essentially known, the required power input for a given furnace may be estimated from Eq. (2.6), and the said nomogram is not reproduced here.

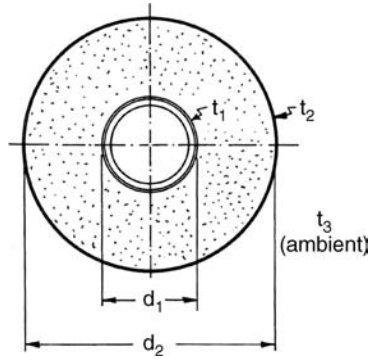

Figure 2.13 Cross-section of a resistance-heated electric tube furnace, schematic.

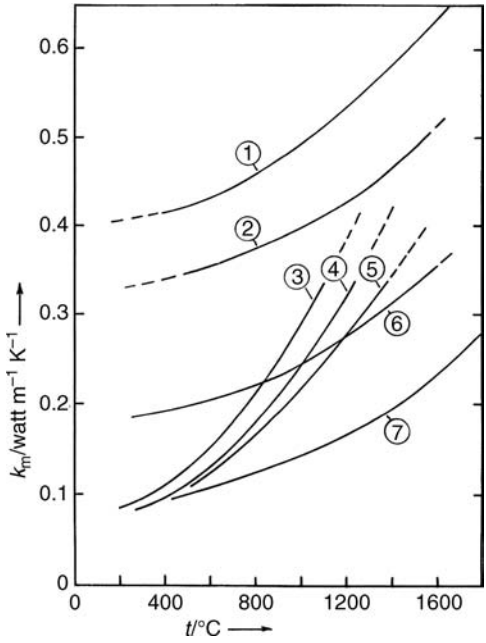

Figure 2.14 Mean thermal conductivity between room temperature and the temperature t, for various insulating refractory materials. (1) Alumina-silica firebrick from Dr. C. Otto Feuerfest GmbH, Germany; Qual. OFL 86, 67% Al_2O_3, 70% porosity. (2) Same, Qual. OFL 65, 62% Al_2O_3, 75% porosity. (3) Kaowool Bulk Fibre, Morgan Thermal Ceramics Ltd., England, Standard, 96 g/dm^3. (4) Same, Standard, 128 g/dm^3. (5) Same, 14% ZrO_2, 128 g/dm^3. (6) Fibrothal HT 1800 (90% Al_2O_3), Kanthal AB, Sweden. (7) ZrO_2 (8% Y_2O_3) Bulk Fibre 30, 830 g/dm^3; Zircar Products Inc., USA.

Curves are shown in Figure 2.14 for the mean thermal conductivity of a number of insulating materials as functions of temperature. (Only a few qualities are represented here amongst the large number of insulating materials now on the market.) The *mean* is taken to give the mean conductivity k_m between room temperature and the temperature t; suitable for use with Eq. (2.6). In a furnace with circular cross-section, however, the thermal conductivity at high temperature will be of dominant importance, and a calculation based on k_m will not be quite correct. For the present purpose, however, it is assumed that an accurate calculation would be a waste of time, and that an approximate estimation of the power consumption will suffice.

A difference between porous solid and fibre insulation is that a material of essentially loose fibres may vary markedly in packing density. It follows from the analogy with radiation shields that a loose packing is *not* favourable for good insulating properties. Denser packing gives lower thermal conductivity up to a certain point, see curves (3) and (4) (cf. also Seltveit, 1992, p. 331). If a loose fibre material is used to insulate a furnace shell like that in Figure 2.3; use a blunt wooden stick to pack the material solidly into the shell. By weighing the total amount of material beforehand and then the left-over, the bulk density of the insulating material in the furnace may be determined. From Seltveit (*loc. cit.*) it appears that the optimum bulk density for alumina-silica insulating fibres should be in the range 100–150 g/dm^3.

From curves (3) to (5) it appears that the thermal conductivity of fibre insulation increases steeply with temperature, probably due primarily to the radiation which increases as T^4. Porous solids appear better in this respect, compare curves (2) and (6). The nature of the solid is also of importance, compare curve (7) for densely packed fibres of zirconia, which is known to have a low thermal conductivity.

The volume stability of the insulating material is also a matter of some concern. Some lightweight fibre materials have shown a tendency to shrink or crumble when used at the highest temperature, and the manufacturer's advice should be noted.

Finally it should be noted that the gas within the insulating material also plays a part. A light gas like H_2 has a thermal conductivity roughly 7 times that of N_2 at 1 bar and room temperature. In consequence, the protective gas in a Mo-wound furnace should contain N_2 with only a small and constant admixture of H_2, not only for fear of explosion but also to maintain the thermal characteristics of the furnace.

2.5.3 Water Cooling

A closed furnace must be so constructed that the power supplied to the furnace may escape as heat through the furnace enclosure without damaging it. Particularly for vacuum furnaces, this may necessitate water cooling. But water cooling is recommended also in cases where it is not strictly necessary. For one thing, a room with furnaces without cooling (or with forced-air cooling) tends to become hot and uncomfortable. It

may be argued that external water cooling leads to increased power consumption, but most of the temperature drop occurs in the thermal insulation anyhow, so the difference is insignificant.

Water cooling on a metal enclosure is most simply effected by copper tubing, soft-soldered to the metal wall. Two points must be considered in the design of cooling tubes, viz. the maximum allowable temperature rise of the water, and the maximum permissible temperature of the furnace wall between each turn of copper tubing. We will consider the latter point first, because it relates to the material of the casing.

The Chamber Wall. A number of metallic materials are given in Table 2.2 with approximate values of their thermal conductivities at room temperature. Soft steel is usually ruled out because of the inevitable corrosion. Stainless steel causes problems because of its very low thermal conductivity; the use of stainless steel may necessitate a complete water jacket which makes for costly fabrication. In addition, soft soldering on stainless steel is difficult. Looking at the thermal conductivity, aluminium would be an ideal material, but soft soldering is difficult on aluminium. Until this problem is solved, copper and brass are still the most suitable materials for the casing of furnaces like those in Figures 2.3 and 2.4.

The relation between spacing of cooling tubes and maximum wall temperature will be considered in connection with the schematic section of a furnace wall shown in Figure 2.15. The incident power q' per unit height of the wall is estimated from the total power input and the height of the chamber (disregarding any 'end effects'). The chamber wall has a thermal conductivity λ, and the wall cross-section A is the circumference times the wall thickness. The distance between cooling turns is set equal to x. The temperature at a turn is t_0 and mid-way between turns it is $t_{x/2}$. To find this latter temperature we consider

Table 2.2 Some metallic materials, with their thermal conductivity at room temperature, in watt $cm^{-1}K^{-1}$.

Copper (pure)	3.9
Copper (alloy)	2.0–3.0
Aluminium (pure)	2.4
Aluminium alloys	1.6–2.1
Brass	1.2
Soft steel	0.6
Stainless steel	0.15

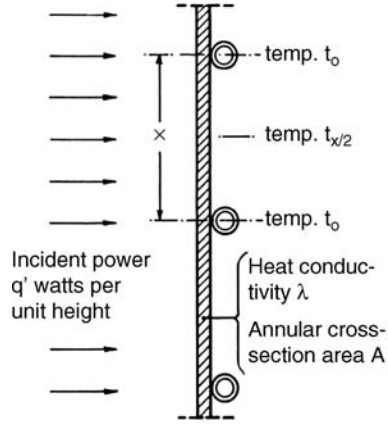

Figure 2.15 On the spacing of water-cooling tubes on a furnace shell (see text).

that the heat arriving at the furnace shell at any arbitrary height x with temperature t must be conducted to the cooling coil. This gives $\lambda A \mathrm{d}t/\mathrm{d}x = q/x$. Integrated from $x/2$ to $x = 0$:

$$t_{x/2} - t_0 = \frac{q'x^2}{8\lambda A} \tag{2.7}$$

The maximum allowable temperature $t_{x/2}$ will be a matter of judgement. For instance the tensile strength of brass at 200 °C is still about 80% of that at room temperature, while a lower temperature may be desirable for other technical reasons or simply for comfort.

The Rate of Water Flow. The temperature rise of the water depends upon the power input and the water flow. The necessary background may be found in any textbook of chemical engineering. Consider the water flow F (litre/sec) flowing through a tube of inside diameter D (cm) and length L (cm) connected to a water pressure P (bar). For a smooth copper tube of small diameter we may assume the Fanning friction factor $f = 1/160$ or $4f = 0.025$. The flow rate is then given approximately by the equation

$$F = 1.0D^2\left(\frac{P}{1 + 0.025(L/D)}\right)^{1/2} \tag{2.8}$$

The professional engineer prefers the consistent use of SI units, that is, F' in $m^3\ s^{-1}$, D' and L' in metres, and P' in Pascal. This gives the flow rate

$$F' = 0.035D'^2\left(\frac{P'}{1 + 0.025(L'/D')}\right)^{1/2} \tag{2.8a}$$

The temperature rise of the water is found as the power input divided by the heat capacity of the water flow, that is, $\Delta t = W/4184F$. Approximately, water flowing at full rate in a copper cooling tube of several metres' length under average tap pressure will acquire a temperature rise pr. kW power input of about 5 °C for a 6 mm tube and 2 °C for a 8 mm tube (0.8 mm wall thickness).

The above figures indicate that cooling tubes of moderate size are adequate for most laboratory furnaces. Note also that running water has a price per cubic metre. A throttle valve should be mounted next to the stopcock, so that the flow rate may be adjusted to the optimum level, considering a suitable temperature rise of the water with the furnace at full load. In the same context, remember that any rubber hose between the copper tube and the water tap should be of the reinforced type intended for pressure use, and secured at both ends with hose clamps.

Sometimes it is necessary to provide particularly efficient cooling in places of high thermal load, such as, for example, by an internal water channel in an exposed copper part. It should then be observed that the heat transport from a heated object to the cooling water takes place through a surface film that represents a certain resistance to the heat transport. The 'film coefficient' representing this resistance is decreased by increasing the linear flow velocity. Efficient cooling of a critical part is thus effected by making a flat, narrow passage for the water through that area, thus speeding up the water velocity without reducing the area of contact. Some examples will be shown in Chapter 7.

Fail-Safe Circuits. A water-cooled furnace may be ruined if left under load when the water fails (or if the operator forgets to turn it on!). For this reason, an automatic switch operated by the water pressure should be built into the power circuit and arranged to go off if the water fails, and does *not* automatically start when the water pressure returns. More about this in Section 2.7.3 (p. 52).

2.6 TEMPERATURE CONTROL

This section discusses control of temperature as a function of *time*, while control of temperature with respect to position in *space* was discussed at the start of Section 2.3 (pp. 17–20). Temperature control is but a part of the extensive area of automatic control, rendering a vast and sophisticated literature. This text does not give any treatment of control theory, it only aims at providing a qualitative understanding of some basic features.

2.6.1 Elementary Principles and Two-Position Control

The equations for heating-up and the concepts of *time constant* and *steady state* were presented in Section 2.5.1 (p. 36). Obviously it is not very efficient to maintain a constant temperature merely by manual control and steady state, although it may well be done. Some sort of automatic control is better. The simplest sort of control circuit is shown schematically in Figure 2.16 where the shaded area represents the furnace. The sensing element (usually a thermocouple) is represented by **S**. The output from **S** is fed to the controller **C**, which compares it with the pre-set value and acts on the power regulator **P** to alter the power input to the heating element **R** accordingly.

In its simplest form, **P** is an on/off switch or contactor. In addition, a suitable resistance may be connected in parallell, so that **P** works between a higher and a lower value rather than straight on/off. Let us

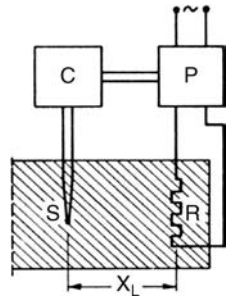

Figure 2.16 Schematic diagram of automatic temperature control system. **C**: Controller. **P**: Power regulator. **S**: Sensing element. **R**: Heating element in furnace.

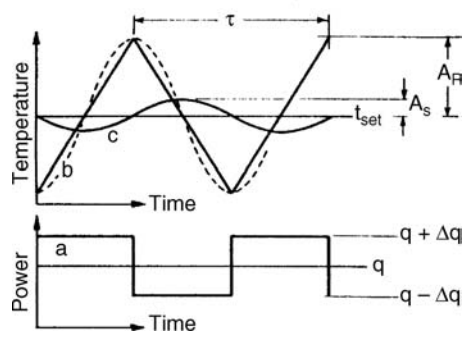

Figure 2.17 Cycles in two-position control. Curve **a**: Power input to heating element **R**. Curve **b**: Power input to heating element **R**. Curve **c**: Temperature on sensing element **S**.

assume that at a certain point of time, the temperature is somewhat lower than the desired t_{set} and the switch **P** is on. Let us see what happens, as illustrated in Figure 2.17.

We start at time zero. The power is on 'high' (curve **a**), and the temperature on **R** increases (curve **b**). Owing to the separation of **R** and **S**, a change in temperature at **R** will not be sensed at **S** until a finite time has passed. And by the time **S** has reached the pre-set temperature and **P** is switched to 'low', the temperature on **R** has gone a bit above t_{set}. Then the same sequence is repeated in reverse. The result is a cyclic event. In Figure 2.17 the temperature variation on the heating element (curve **b**) has been depicted as a zigzag curve, but in reality it will be more rounded (dashed curve). The course of the temperature on **R** may be described by a sinus wave with amplitude A_R, while the temperature on **S** gives another sinus wave (curve **c**), 90° delayed with respect to curve **b** and with the smaller amplitude A_S.

In Figure 2.17 it has been arbitrarily assumed that the rates of heating and cooling, and hence the duration of *on* and *off* periods, are approximately equal. The course of events may then be handled mathematically as a harmonic oscillation, but we will be content with only the qualitative picture. The point is that control systems do have a tendency to oscillate, and it may be useful to understand why. The length of the periods and the amplitude of the oscillations are dependent upon the thermal inertia of the furnace, but they are even more dependent on the physical distance between the sensing element **S** and the heating element **R**. Close proximity favours short periods and small deviations from the set value, but some time lag is unavoidable.

2.6.2 PID Control

The three letters stand for *proportional, integral* and *derivative* control. All three modes of action are built into a modern controller. We will take each in turn, but only to give a qualitative understanding.

Proportional Control. A controller with proportional action adjusts the power input in proportion to the deviation from the set temperature. If the power input is exactly correct to keep the furnace on the desired temperature, then the 'proportional signal' is essentially zero; everything is fine.

Now suppose that conditions have changed slightly. Temperature has fallen for some reason (for instance the trivial case that the voltage on the mains has dropped). The deviation in temperature causes a 'proportional signal' to restore the original temperature. But since conditions have changed, this signal has to remain there, but it does so only by having a slight permanent offset from the desired temperature.

The 'proportional band' of the controller tells us something about the magnitude of the action for a given off-set. A narrow proportional band means a lot of action for a small deviation in temperature. It might mean accurate control, but more likely it leads to oscillations in the whole system. Hence some deviation must be tolerated, and a proportional control alone cannot maintain exactly the set temperature when conditions change.

Integral Control. The controller is designed to realize that a permanent off-set remains after purely proportional action. The integral action acts to 'repeat' the contribution from the proportional action within a certain time, so that the deviation finally disappears.

Derivative Control. This third mode is designed to anticipate what is going to happen in the near future. Assume that a furnace is under full power to achieve rapid heating-up. If the power is left fully on until the set point is reached, a considerable overshoot will result, followed by oscillations that are gradually damped. The derivative action is designed to reduce the rate of change *before* the set point is reached, so that overshoot and oscillations are avoided.

Adjustment of Parameters. The same electronic controller may be used to control the temperature for furnaces of widely different sizes and shapes, but the parameters of the controller have to be adjusted to fit the

furnace in question. The parameters may have the designations 'proportional band', 'reset time' and 'rate' or some equivalent terms. More recent models have built-in self-adjustments, that is, the instrument finds its own best parameter values by trial. But in any case the user has to read and follow the directions given with the instrument.

Program Control. A few decades ago, a controller was designed to take care of only one set of temperatures. Today an electronic controller may govern a furnace through a varied temperature program. Usually the program consists of periods of increasing or decreasing periods (ramps) and periods of constant temperature (dwells). The only limitations are that the ramps cannot exceed the maximum possible rate of heating or cooling for the furnace in question.

2.6.3 Power Regulators

Figure 2.16 shows schematically a controller **C** and a power control unit **P**. The latter acts as an adjustable valve for the current. Nowadays it is nearly always a *thyristor*, or rather a unit containing two thyristors.

A thyristor is a silicon controlled rectifier (SCR) with an anode, cathode and gate. A trigger pulse (positive voltage) applied to the gate opens the passage of current. In order to utilize both half-periods of AC current, two rectifiers plus associated electronics are combined to a unit. By adjustment of the time for the trigger pulse in each half-period, the effective current through the thyristor unit may be adjusted from null to full power.

The mode of operation is illustrated in Figure 2.18a. This mode is called 'phase angle firing'. Alternatively the unit may be arranged for 'burst firing', where the valve is open for a number of cycles, and then closed for another number of cycles, as illustrated in Figure 2.18b. The duration of each burst may be from a fraction of a second up to several seconds or even minutes.

Phase angle firing distorts the shape of the AC current on the mains grid and, when heavy currents are involved, may be harmful to nearby electronic equipment. Another point to be observed is that ordinary electronic instruments (multimeters) do not give correct readings of effective current when used on a thyristor controlled circuit. The more old-fashioned moving-iron instruments are more reliable for this purpose.

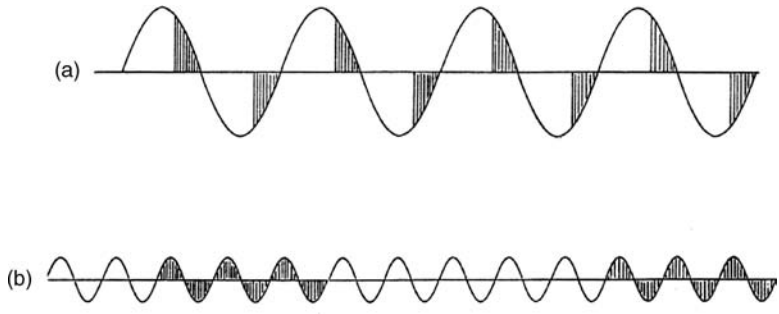

Figure 2.18 Mode of operation of a Thyristor unit: (a) Phase angle firing. (b) Burst firing.

2.6.4 Sensing Elements for Control

In Section 2.6.1 it was mentioned that the sensing element **S** most commonly is a thermocouple. The principles and use of thermocouples will be further discussed in Chapter 3: Temperature Measurement.[3]

Thermocouples for temperature control may be base metal (Type K, Nickel-Chromium/Nickel-Aluminium) up to some 1150 °C, or noble metal (Type S, Pt10Rh/Pt) up to 1600 °C. For control purposes it is not really necessary that the control element is located at the point of highest temperature. Thus it may be displaced to a location of lower temperature if the maximum is higher than the thermocouple will stand. It is important, however, that it is located close to *some* part of the heating element, in order to give rapid response.

For very high temperatures, or where thermocouples for some reason are impracticable, radiation pyrometry may be used. The use of radiation pyrometry for continuous service, however, has its disadvantages. Smoke from an open furnace, or coating of the window in a vacuum furnace, will decrease the signal to the pyrometer, and the response from the controller is to increase the power input. This in turn will increase the fogging; the system is self-amplifying, and a breakdown of the furnace may result.

[3] The purpose of temperature *control* is to maintain a steady temperature, or a pre-set temperature program, while temperature *measurement* aims at determining a *correct* temperature, which is a different thing.

A quite different approach is to omit the temperature-sensing element altogether, and to use the output from an accurate RMS (root-mean-square) amperemeter, converted to a DC signal, directly as input to the controller. The method has been used successfully with a standard electronic controller, with a deviation within $\pm 0.1\%$ of the current at steady state. Running heating and cooling programs has been equally successful.

Once again, this solution requires that the true temperature is determined by other means, see the next two chapters.

2.7 ELECTRIC CONNECTIONS AND CIRCUITS

The first two paragraphs of this section are intended to give the inexperienced student some hints regarding the handling of electrical equipment. It is clear that only the most basic advice may be included here. A recent edition of the *Norwegian* regulations for electrical installations, *Elektriskelavspenningsinstallasjoner* (Electrical low voltage installations), NEK 400:2010, is a book of 506 pages, and too complicated for the layman. The table of current-carrying capacity (below) and a few other hints are taken from the simpler 1979 edition.

2.7.1 General Rules

The fixed installations in a building or a laboratory should be made by a certified electrician. On the other hand, the connections from the mains wall outlet to the furnace and associated equipment is quite often left to the user. It is then an important point that this (more or less temporary) installation should be done with essentially the same professional quality. More specifically, the electrical installation

- must work properly in accordance with its purpose,
- must not overheat, fail or burn the fuses,
- must not invite electric shock for the user or for any other person.

A first rule in this context is that, when making contact by means of plugs and sockets, the voltage must always be in the socket, never on the plug. Stated differently, the *voltage is to be in a hole*, not on a pin. Live wires with naked copper ends are unacceptable.

In order to protect against electric shock, any switch in the mains supply should be bipolar (at least), so that both leads are disconnected when the switch is turned off. More on that in Section 2.7.3 below.

The regulations for electrical installations in a laboratory prescribe that all mains outlets should be grounded (as for basements and wet-rooms). This means that the plugs also have to be of that type, and that the cables used should have three wires. The colours of the two live wires may vary, red and blue, or grey and black, but *the grounded wire is striped green and yellow*. This third wire *should be used* to connect external metal parts, like the casing of a furnace, to earth.

The connection between a cable and a socket should be made by securing the de-insulated wire by means of the intended screws. Soft solder on the wire ends is not recommended. The wire is relieved of stress by clamping the cable to the body of the plug. More generally, an electric wire connection should not be exposed to any mechanical stress.

The rated capacity stated on plugs, sockets and other fittings should correspond to, or exceed, the expected load on the wires.

2.7.2 Current-Carrying Capacity of Insulated Copper Wire

The values given in Table 2.3 are for plastic insulated cables with a maximum of three wires to one cable, and mounted in a relatively open environment (i.e. not as a bundle of cables in a common tube). The 'maximum load' in practice is set by the heating of the

Table 2.3 Fuse and maximum load values for plastic insulated electric cable.

Cross-section mm^2	Fuse A	Max load A	Cross-section mm^2	Fuse A	Max load A
0.75	(10)[a]	5	16	63	65
1.0	(10)	8	25	80	90
1.5	10	14	35	100	120
2.5	16	20	50	125	150
4	20	25	70	160	200
6	25	31	95	200	240
10	35	43	120	225	280

[a]Fuses for less than 10 A are not used in permanent installations, but portable electronic equipment usually have built-in fuse holders and fuses with lower nominal values.

cable, and is thus to some extent dependent upon the type of insulation. For the same reason a thick wire has a lower carrying capacity than a thin one, counted per mm^2 cross-section. The reason, of course, is that the cross-section goes up with the square of the diameter, while the surface area available for air cooling only increases linearly.

From the curve for copper in Figure 2.1 (p. 16) it is seen that the resistivity increases markedly with temperature. Once a copper wire starts getting hot, a slight increase in current may make it *very* hot. Generally, when the current through a given cable comes close to the limit, it is a good idea to estimate the temperature by touch. An immediate crisis may be avoided by a fan or an air blower; more permanently it may be remedied by, for example, another cable in parallel.

Very high currents, some 1000 A or more, are encountered in the laboratory only in combination with low voltages, some 10 to 20 volts, where electric shock is not a problem. For these currents, bare copper rails are used instead of cables. In order to avoid unduly large dimensions, the rails may be water cooled by a copper tube (6 mm dia.) soft soldered to the rail. More on this in Chapter 7.

2.7.3 Fail-Safe Protection Devices

There are three main causes for failure: The cooling water may fail, the mains current may fall out, or the temperature sensor (the thermocouple) may be disrupted.

The cooling water protection was mentioned already in Section 2.5.3, p. 44. A suitable circuit to this end is shown in Figure 2.19. Starting from the upper left corner, fuses for XX amp are indicated, where the actual size is determined by the maximum power needed for the furnace. These fuses are quite often part of the mains installation so that extra fuses are unnecessary, but it is advisable to get acquainted with the location of these main fuses.

To the right of the mains fuses is shown another set marked 10A – it may be an ordinary mains wall outlet. Next comes a *water-pressure relay* or, in the present case, two of them, in case two different water cooling circuits are to be protected. These are devices that act on static water pressure by connection to 6 mm copper tubing branched from the

water cooling circuits.[4] Once the water is turned on, the white lamp lights up to indicate 'water on'.

Next the main switch is turned on, but nothing happens until the *start button* is pressed. This activates the *contactor*, and the transformer is under voltage as indicated by the red lamp. It is recommended, before pushing the start button, to check that the *thyristor unit* or its associated *controller* is turned down to a minimum, to avoid a sudden burst of high current. And then controlled heating may proceed. As an alternative to the controller, *manual control* is indicated; this is simply a potentiometer connected to the thyristor unit in the proper place.

To the upper right, another set of 10 A fuses (another mains outlet) is shown because both the thyristor unit and the controller need mains voltage for their electronics.

The transformer (lower left) is indicated as one with low voltage and high current on the secondary side. The amperemeter is indicated with a *current transformer*, that is a special sort of transformer that gives a low output proportional to the current in the main lead. For instance, a current transformer marked 1500/5 means that the associated ammeter takes 5 A when the main current is 1500 A. (The *scale* on the ammeter shows 1500 A if it is designed to work with that current transformer.)

The intention of the circuit in Figure 2.19 is as follows. If the water fails, the contactor falls out, and the current to the furnace is interrupted. In case the water pressure returns, the current to the furnace does *not* go on again. The thought behind this is that the user does not know what happened to the experiment in the meantime, so it is better to leave it off. The same applies to a failure in the mains.

In cases where the furnace is designed to operate at voltages similar to those of the mains, the transformer may of course be omitted. The rest of the circuit remains largely the same, with some exceptions. For small furnaces (and other devices that need water cooling) the current through the relay may be used directly on the furnace (up to some 10 A, as specified on the relay). However, some of the other safety characteristics are lost by only using a switch, and a contactor is generally recommended.

[4] The proper means for controlling the cooling water would be some sort of *flow* metre directly in the water line, but this would be more expensive. The control by means of water *pressure* in a side branch is considered safe enough. The device used does not have to be designed for water; pressure relays made to control the pressure in industrial refrigeration units have been used with success.

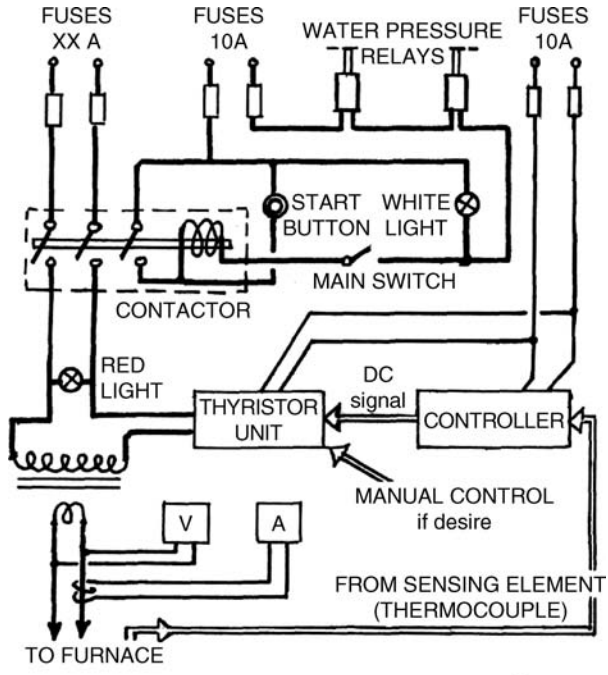

Figure 2.19 A suitable circuit for the power supply, control unit and fail-safe protection of a water cooled laboratory furnace.

In any case, the switch should be bipolar to avoid any accidental shock when the current is off.

Thermocouple failure is not included in the safety measures of the above circuit. It is, however, quite often built into the controller itself, so that the current is turned down if the thermocouple breaks.

A final precaution: whenever there is a risk of electric shock, use one hand only, to avoid possible electric shock through the chest region.

REFERENCES

Bockris, J.O'M., White, J.L., and Mackenzie, J.D. (1959) *Physicochemical Measurements at High-Temperatures*, Butterworths, London, 394 pp.

Harris, B. and Jenkins, A.E. (1959) Controlled atmosphere levitation system. *J. Sci. Instr.*, **36**, 238–240.

Motzfeldt, K. (1959) Means of attaining and controlling temperature, in *Physico-chemical Measurement at High-Temperatures*, (eds J.O'M. Bockris, J.L. White, and J.D. Mackenzie), Butterworths, London, pp. 47–86.

Ribaud, G. (1950) in *Les Hautes Temperatures et Leurs Utilisations en Chimie*, vol. **I**+**II** (eds P. Lebeau and F. Trombe), Masson et Cie, Paris, 1398 pp., Chap. IX.

Seltveit, A. (1992) *Ildfaste Materialer*, Tapir Forlag, Trondheim, 496 pp.

3

Temperature Measurements

CONTENTS

High Temperature Experiments in Chemistry and Materials Science, First Edition.
Ketil Motzfeldt.

Preamble

This chapter deals with an important subject. To quote from the preface in the textbook of McGee (1988):

> During a scientific career as an engineering professor I have observed that the most common mistake a scientist makes is to accept a temperature reading without question. The scientific literature is full of papers about otherwise fine research that is based on temperature measurements of uncertain quality.

In the years since McGee wrote this, his own book, and a number of other textbooks that have appeared, have hopefully led to an improved situation. Some of the books are mentioned specifically at the end of this chapter, otherwise they are included in the general list of references. The present text represents an attempt to cover part of the same material within a more limited frame and restricted to high temperature measurements.

For practical reasons, Chapter 3 covers only methods using a solid sensor in contact with the hot object (in particular thermocouples) while radiation pyrometry is treated in Chapter 4.

3.1 FUNDAMENTALS OF TEMPERATURE MEASUREMENT

3.1.1 The Concept of Temperature

From early childhood we experience the difference between hot and cold, or in other words, differences in temperature. The concept is familiar, and yet it is not easy to define.

What is Temperature? A partial answer is given by Zemansky (1964): *Temperature is a property of matter*. Other partial definitions have been tried. For instance, if two bodies A and B are in thermal contact with no heat flux between them, the two are at the same temperature. This is sometimes referred to as the zeroth law of thermodynamics, but it is not very informative.

We will attempt another approach, considering the concept of *energy*.

Generally, energy is equivalent to work or anything that may be converted into work. We note that each form of energy may be written as the product of an *intensive* factor and an *extensive* factor. For instance, electrical energy may be expressed as the product of voltage and charge; potential energy is the product of height and mass, and so forth. But what about thermal energy? The final product is familiar, it is expressed in joules (formerly in calories). But how is thermal energy expressed in terms of the above two factors?

The answer regarding the intensity is obvious: the intensive factor of thermal energy is *temperature*. The extensive factor of thermal energy is less familiar; it is termed *entropy*. Thus, a small amount of heat added to a system at constant volume results in an increase in its internal energy, $dU = T dS$, where T is the temperature and S is the entropy of the system. It is written in differential form since the absolute magnitude of the internal energy U of a body is unknown. Turned around and written as a partial differential, we have $T = (\partial U/\partial S)_V$ (although this is not the most convenient definition of temperature).

More could be said about energy and entropy, but that belongs in textbooks of thermodynamics. Here it is pointed out only that thermal energy is not quite like any other form of energy. In particular, other forms of energy, like mechanical or electrical, may be converted 100% to thermal energy, while complete conversion of thermal energy to mechanical or electrical work is impossible. For more on this in connection with the efficiency of steam engines, compare below.

The First Temperature Measurements. It was an early observation that objects expand upon heating. This is particularly so for a fixed volume of a gas. The first temperature-sensing device appears to have been invented by Galileo Galilei around 1592. His 'thermoscope' consisted of an inverted glass bulb with a long stem immersed in a liquid, see Figure 3.1. The liquid column rose or fell as a function of the ambient

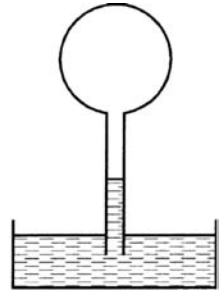

Figure 3.1 The 'thermoscope' of Galileo. (Reprinted with permission from Michalski *et al*. Copyright (2001) John Wiley & Sons, Ltd.)

temperature. Unfortunately it would also vary with the barometric pressure, and it was found favourable to replace the gas with a liquid. G. D. Fahrenheit, working as a glass blower in Amsterdam, designed the first mercury-in-glass thermometer in 1714. In order to develop a temperature scale he chose for his zero the lowest temperature he could achieve, that of a mixture of ice and rock salt, in order to avoid negative temperatures as far as possible. At the other end he chose the temperature of the human body, which he set at 100. In 1742, the Swedish astronomer A. Celsius developed the mercury thermometer with a different scale. His fixed points were the melting of ice and the boiling of water, now fixed at 0 and 100 °C respectively. This gave the Celsius temperature scale, now in worldwide use. (The Fahrenheit scale, still in use in the US, gives 32 °F for melting ice and 212 °F for boiling water.)

3.1.2 The Thermodynamic Temperature Scale

The mercury-in-glass thermometer serves its purpose excellently in a number of areas, and it may be designed to yield a high sensitivity. And yet it is a purely empirical device; the two fixed points are chosen arbitrarily, and the exact readings between these points depend on the properties of both the mercury and the selected glass. A fundamental temperature scale, on the other hand, should be independent of the properties of any particular substance. This leads us to a consideration of the early development of thermodynamics, and in particular the work of Sadi Carnot.

Towards the end of the eighteenth century the steam engine was developed in England, based on James Watt's patent from 1769. The young French military engineer, Sadi Carnot, was aware of the importance of these engines, and decided to find out something about their efficiency. He published his results in a small book entitled 'Reflexions sur la Puissance Motrice du Feu' which appeared in Paris 1824. In this he pointed out that a heat engine in general has to work by an input of heat at high temperature, while a part of this heat is given off again at a lower temperature. He showed also that, for given temperatures, a maximum of mechanical work is obtained from the machine when it is operated in such a way that no temperature difference appears between bodies in contact. That is, each step in the process shall take place *reversibly* (which is impossible in practice, but conceivable as a theoretical limit). He furthermore pointed out that the amount of work obtained for a given heat input will be larger for a larger difference between the high and the low temperature.

Carnot compared this to the action of a mill in a waterfall, where a longer fall gives more work, while the amount of water remains the same through the process. He compared this with a stream of 'calorique', considering the heat as a sort of fluid.

Carnot's work is largely descriptive and without mathematics. His ideas, however, were put into a more analytical form by Émile Clapeyron in 1834. Subsequently, the Scot William Thomson (Lord Kelvin) in his work 'On the Dynamical Theory of Heat' in 1851 gave the first full account of the ideas of Carnot, Clapeyron and Joule. It was left for the German physicist Rudolf Clausius, however, to introduce the concept of *entropy* in 1865.

Carnot's results may be summarized in modern terms. Assume that an engine works with an amount of heat input Q_2 at the high temperature T_2, while the exit heat Q_1 comes out at the lower temperature T_1. With the engine working reversibly, it is found that the two heats are in the same ratio as the two temperatures:

$$\frac{Q_1}{Q_2} = \frac{T_1}{T_2} \quad \text{or} \quad \frac{Q_1}{T_1} = \frac{Q_2}{T_2} \tag{3.1}$$

From the general definition of entropy it is seen that the right-hand formulation of Carnot's result corresponds to the statement that *the entropy change in a completely reversible process is zero*. In other

words, Carnot's 'calorique' is analogous to our 'entropy' in the sense that it remains unaltered throughout the process.

The same relations may be put in another form:

$$\eta = \frac{Q_2 - Q_1}{Q_2} = \frac{T_2 - T_1}{T_2} = 1 - \frac{T_1}{T_2} \tag{3.2}$$

The difference $Q_2 - Q_1$ represents that part of the input heat which is converted to work; that is, the equation gives the efficiency η of the engine. The right-hand expression shows that the efficiency will approach unity when the lower temperature T_1 approaches zero. An efficiency larger than unity is theoretically impossible according to the First Law of Thermodynamics. This proves that an absolute zero of temperature exists, and Eq. (3.2) may be used to define the thermodynamic temperature scale.

3.1.3 The Gas Thermometer and the Practical Temperature Scale

In principle the ratio of any two temperatures may be determined by measuring the efficiency of a reversibly working heat engine. In practice this would be exceedingly difficult, not to say impossible.

Fortunately, a simpler solution exists. It was found by Robert Boyle in England in 1660, and independently by Edmé Mariotte in France 1676, that the volume of a fixed amount of a gas is inversely proportional to its pressure. Hence this discovery is called Boyle's law in Great Britain, and Mariotte's law in France. It was left for J.-L. Gay-Lussac in France in 1802 to show that the product PV also varies in direct proportion to the temperature of the gas. He carried out accurate experiments of the expansion of a gas between 0 and 100 °C, and by extrapolation to lower temperatures he laid the basis for the idea of an absolute zero of temperature. In modern terms, the combined laws may be written

$$T = PV/\text{constant(for a given amount of gas)} \tag{3.3}$$

Thus, a temperature scale may be established, for example, by studying the variation of pressure with temperature at constant volume.

Equation (3.3), however, is exact only in the limiting case of an ideal gas. The behaviour of real gases deviates from Eq. (3.3), particularly at the lower temperatures. (It is obvious why this must be so; an extrapolation of Eq. (3.3) to $T = 0$ would indicate zero volume at a finite pressure, while real atoms do have volume. The attraction between gas atoms also contributes to the deviations.) Real gases approach ideal behaviour more closely as the pressure is lowered, hence precision measurements for a gas thermometer should be done for different pressures, and the result extrapolated to zero pressure. In addition, corrections have to be applied for the thermal expansion of the material in the gas bulb and a number of other effects. In short, establishment of the temperature scale by accurate gas thermometry has by no means been a simple process, and we should honour the men and women who did the early work. The work of Holborn and Day (1899, 1900) may be mentioned as an example: they extended the gas thermometric measurements to 1150 °C with the use of a bulb of platin-iridium, including accurate determinations of the thermal expansion of the alloy. An account of modern gas thermometry has been given by Quinn (1990, pp. 74–99).

The temperature scale of Celsius has been maintained, but some changes have been made regarding the fixed points. Recall that Celsius based his scale on two arbitrary fixed points; the melting point of ice and the normal boiling point of water. However, it had already been suggested by Thomson in 1848 that one defined fixed point would suffice; absolute zero would serve as the other. This proposition was renewed by Giauque (1939) and finally adopted in 1948, 100 years after its first proposal.

The zero of Celsius was fixed at the temperature of melting ice, with the system open to influence from the ambient atmosphere. A more precise fixed point is afforded by the triple point of water; that is, the equilibrium between ice, water and water vapour in a closed system. The temperature of this system is determined to 0.01 °C, or 273.16 K. This gives the conversion from Kelvin to degree Celsius: $T/\mathrm{K} = t/^{\circ}\mathrm{C} + 273.15$.

3.1.4 History of the International Temperature Scales

The international cooperation on weights and measures dates back to 1875, when a *Bureau International des Poids et Mesures* (BIPM) was established in Paris. This bureau makes recommendations to the

subsequently established, periodic *Conferences Générales des Poids et Mesures* (CGPM). The first task of these organizations was to reach agreement on the metre and the kilogramme, but it was foreseen that thermometry would soon be one of its essential areas.

The International Temperature Scale of 1927 (ITS-27) was adopted by the seventh CGPM, or General Conference of Weight and Measures, as an acceptable replacement for differing national temperature scales. It was formulated to allow measurements of temperature with as close an approximation to thermodynamic temperatures as could be determined at that time. Between the boiling point of oxygen and the freezing point of gold it was based on a number of reproducible fixed points to which numerical values were given. Up to 660 °C a platinum resistance thermometer was used for interpolation between the fixed points, and from 660 °C to the melting point of gold a platinum – 10% rhodium/platinum – thermocouple was used. For the region above the gold point, temperatures were defined in terms of the Wien radiation law, with an optical pyrometer as the instrument used.

The International Temperature Scale of 1948 (ITS-48) essentially followed the decisions from the previous conference, with a number of minor changes in numerical values. Also, the Planck radiation law replaced the Wien law.

An amended version was adopted in 1960. Notable changes were that the triple point of water, defined at 0.01 °C, was finally adopted as the sole point defining the Kelvin scale, and also that the word *Practical* was added to the title.

The International Practical Temperature Scale of 1968 (IPTS-68) incorporated extensive changes from IPTS-48 as regards the numerical values of the fixed points. Of particular interest to the high temperature experimentalist is that the melting point of gold, on which the scale beyond gold depends, was changed from 1063 to 1064.43 °C.

Amended versions of IPTS-68 appeared in 1975 and then again in 1976, mostly to correct and clarify the accompanying text.

3.1.5 The International Temperature Scale of 1990 (ITS-90)

This is the most recent version of the International Temperature Scale. The word 'Practical' has once again been omitted; it is now considered *the* temperature scale. The original text is published in French by the

CIPM, with an authorized translation by Preston-Thomas (1990); see also Preston-Thomas and Quinn (1992).

In analogy with the previous editions, the ITS-90 gives a list of defining fixed points, starting at −270 °C. For the purpose of high temperature work, however, temperatures below 0 °C are not considered in the present text. The fixed points above 0 °C are melting points of pure metals or, more correctly, freezing points. Freezing is specified in the ITS-90 because, experimentally, it may yield better reproducibility than melting.

While the IPTS-68 also included a list of secondary reference points, the ITS-90 has no such list. However, secondary reference points on the ITS-90 are given by Bedford *et al.* (1996). In Table 3.1, both the defined or primary points (P) and the secondary points (S) are given, in order of increasing temperature. One point in Table 3.1, that of nickel, is not found in any of the two references above, but it is a convenient and reproducible point which ought to be included in the future (Kim, Gam and Kang, 2001).

Many of the temperature values in the ITS-90 are given to three or even four decimals. In Table 3.1, however, values are given to two decimals only. Even this may be overdoing it; in practice high temperature determinations to the nearest whole degree is demanding in itself.

In previous editions, two different instruments were specified for interpolation, *viz.*, the resistance thermometer and a thermocouple (cf. above, IPTS-27). In contrast, the ITS-90 employs the standard platinum resistance thermometer as the only interpolating instrument; it is

Table 3.1 Defining or primary fixed points (P) and secondary fixed points (S) on the International Temperature Scale of 1990. Degrees Celsius.

H_2O triple point	0.01 P	Silver, Ag	961.78 P
Gallium, Ga	29.76 P	Gold, Au	1064.18 P
Indium, In	156.60 P	Copper, Cu	1084.62 P
Tin, Sn	231.93 P	Nickel, Ni	1455 -
Zink, Zn	419.53 P	Palladium, Pd	1554.8 S
Bismuth, Bi	544.55 S	Platinum, Pt	1768.2 S
Cadmium, Cd	594.22 S	Rhodium, Rh	1963 S
Lead, Pb	600.61 S	Iridium, Ir	2446 S
Antimony, Sb	630.63 S	Molybden., Mo	2622 S
Aluminium, Al	660.32 P	Tungsten, W	3414 S

P: Preston-Thomas (1990). S: Bedford *et al.* (1996). Ni: Kim, Gam and Kang (2001).

considered a more sensitive and accurate instrument than a 90Pt10Rh/Pt thermocouple. On the other hand, a thermocouple is more rugged, more easily installed, and accurate enough for almost any purpose, so in practice it remains the preferred means for measurements at elevated temperatures, cf. Section 3.3.

Above the gold point, temperatures are defined by the Planck equation.

For the purpose of temperature measurements, only *relative* intensities are considered, and the equation may take the form:

$$\frac{L_\lambda(T_x)}{L_\lambda(T_{\mathrm{Au}})} = \frac{\exp(c_2/\lambda T_{\mathrm{Au}}) - 1}{\exp(c_2/\lambda T_x) - 1} \tag{3.4}$$

In this equation, the constant $c_2 = 0.014388\,\mathrm{m\,K}$, λ is the wavelength of the radiation, T_x is the temperature to be determined, and T_{Au} is the temperature at the gold point. As given here, the equation corresponds to IPTS-68 where the gold point was preferred. In the ITS-90, the freezing points of silver (961.78 °C), gold (1064.18 °C) and copper (1084.62 °C) are considered equivalent for the purpose. Radiation pyrometry will be further dealt with in Chapter 4.

3.2 'LOW-TEMPERATURE' THERMOMETERS

This section is included mainly for completeness. 'Low temperatures' in the present context indicate temperatures below some 500 °C. Only a brief mention of the various types will be given.

3.2.1 Liquid-in-Glass Thermometers

Mercury-in-glass thermometers are the best-known, and laid the foundation for the whole area of temperature measurement. Since mercury freezes at −39 °C and the normal boiling point is 357 °C, their use is restricted to temperatures in this interval (or slightly higher, when an overpressure may be tolerated).

One single thermometer for the whole range results in low sensitivity. The sensitivity is increased by an adequate amount of mercury in the

bulb and a small internal cross-section of the stem. Made to be used over a short range of temperatures it may have divisions of 1/10° as in the ordinary fever thermometer. For temperatures below −39 °C, low-melting liquids like ethanol, toluene or pentane are used.

3.2.2 Bimetallic Thermometers and Thermostats

Two metal strips of different coefficients of linear expansion, welded or hot-rolled together, form a bimetallic strip. At a neutral temperature, most often 20 °C, the strip is flat. As the temperature is increased, the strip will bend towards the metal with the lower thermal expansion. The principle may be used to make rugged industrial thermometers of moderate sensitivity. More often it is used as the central element in simple thermostats.

3.2.3 Semiconductor-Based Thermometers

A *semi-conductor* is a piece of solid material characterized by a strongly positive coefficient of electric conductivity. Thus its electric resistance decreases at increasing temperature, in contrast to pure metals as in Figure 2.1 (p. 16). The whole field of solid-state electronics took off when Bardeen, Brattain and Shockley at the Bell Telephone Laboratories clarified the physics of semiconductors and came up with the first transistor in 1948.

The field of electronics is definitely outside the scope of the present text. It may only be mentioned that a *thermistor* is a semi-conducting two-terminal component which in principle acts as a temperature-dependent resistor. Today thermistors may be made from a variety of metallic or ceramic materials to almost any specification. In order to be used as a thermometer or a thermostat it needs a power supply (in contrast to a thermocouple).

Temperature measuring devices based on thermistors and transistors usually have operating ranges to a maximum of some 350 °C. Hence they are strictly not of interest for high temperature measurements, but definitely useful in auxiliary equipment. The technology is discussed by Meijer and van Herwaarden (1994).

3.2.4 Resistance Thermometers

The semiconductor-based temperature sensors of the preceding paragraph are based on the variation of electric resistance with temperature, and thus could be classified as resistance thermometers. Traditionally, however, the term is restricted to wire-wound resistors, usually of pure platinum, as originally developed by Callendar (1899) and others for precision measurements. A suitable length of fine platinum wire is wound on an insulating support of silica glass or ceramics, and held in place by a thin coating of the same material. The quality and purity of the platinum itself was a crucial point in early development and still is. As mentioned above, the platinum resistance thermometer is now the preferred reference standard in the ITS-90 all the way from the triple point of hydrogen to the freezing point of silver. The ITS-90 gives detailed relations between the resistivity of the Pt wire and the relevant temperature, in order to achieve a maximum accuracy. In most high temperature work, however, this extreme accuracy is not needed, and a thermocouple is more expedient.

3.3 THERMOCOUPLES

3.3.1 Principles of Thermoelectricity

The simplest thermoelectric circuit in principle consists of wires of two different metals, joined at both ends, compare Figure 3.2a. When the two junctions are held at different temperatures, a current will flow through the circuit. In Figure 3.2b a measuring instrument is inserted in the circuit for observation.

In the present case we are not interested in the current, but rather in the potential, or the *electromotive force* (e.m.f.) observed at zero current. It is found that this e.m.f. is dependent on the materials of the two wires and the temperatures T_1 and T_2 of the two junctions, while it is independent of the temperature along the wires. This thermoelectric effect was first observed by T. Seebeck in 1821, and the *Seebeck effect* forms the basis for the use of thermocouples in temperature measurement.

The effect may be explained in an elementary way. A metal is considered to be made up of a rigid lattice of atoms, with the conduction

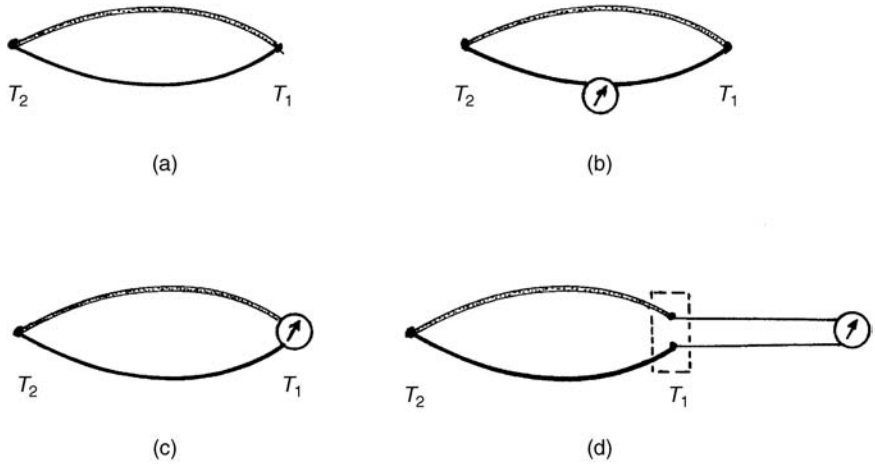

Figure 3.2 Thermoelectric circuits, schematic. (a) Closed circuit between two dissimilar metals, with junctions at temperatures T_2 and T_1. (b) The same with an instrument interspersed in one leg for observing the potential. (c) The instrument is placed between the two legs, thus at the same time representing the junction T_1. (d) A more realistic configuration; both thermocouple legs joined to copper at one end, both junctions held at the same temperature T_1. The measuring instrument may be at some arbitrary temperature.

electrons free to move in the lattice. With a temperature gradient along this conductor, the electrons at the hot end will have higher energy and thus diffuse towards the colder end, giving up, as they do so, some of their energy to the lattice. This is the familiar process of thermal conduction. The excess of electrons at the cold end gives rise to a potential gradient, and the negative charge builds up until a state of dynamic equilibrium is established: the number of electrons with a relatively high velocity, driven towards the cold end because of the temperature gradient, equals the number of electrons with lower velocity, driven towards the hot end of the conductor because of the electric potential gradient. Different metals show different electronic behaviour, and thus the potential resulting from a temperature gradient will vary for different metals. This is the basis for the use of thermocouples.

A thermocouple in a temperature gradient also shows other interesting features; the *Peltier* effect and the *Thomson* effect; briefly discussed towards the end of this chapter. For the present we will focus on the use of thermocouples for temperature measurement.

It is common practice to summarize the Seebeck effect in three 'laws'.

1. **The law of homogeneous metal**: A thermoelectric current cannot be maintained in a circuit consisting of one homogeneous metal.

   A practical consequence of this law is that the homogeneity of a thermocouple wire may be tested by connecting both ends of the wire to a sensitive metre and moving a heat source along the wire; any electromotive force (e.m.f.) shows that the wire is inhomogeneous.
2. **The law of intermediate metal**: The introduction of a third metal C in the circuit of the two metals A and B does not alter the resulting e.m.f., provided that both ends of the third metal C are at the same temperature.

   This law is used in practice in the circuit of Figure 3.2(d) where both terminals of the thermocouple are connected to copper wire; the e.m.f. remains the same provided the two 'cold junctions' are at the same temperature. (It is implicit also in the circuits Figure 3.2b and c since the measuring instrument would normally introduce a third metal.)
3. **The law of consecutive temperatures**: If a thermocouple shows the e.m.f. $E_{1,2}$ when the two junctions are at temperatures T_1 and T_2,

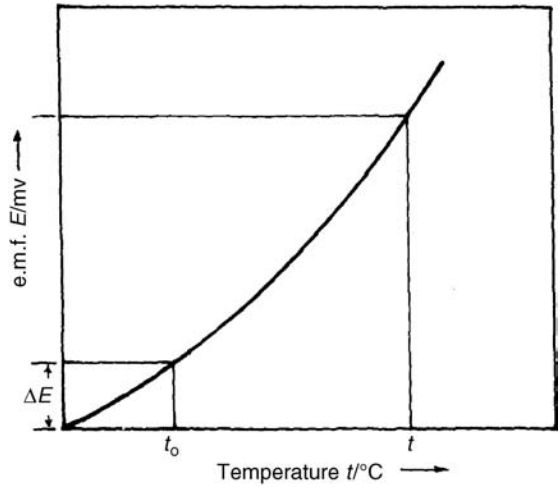

Figure 3.3 Schematic diagram of the e.m.f. of a thermocouple versus temperature.

and the e.m.f. $E_{2,3}$ when the temperatures are T_2 and T_3, then the e.m.f. with the junctions at T_1 and T_3 will be: $E_{1,3} = E_{1,2} + E_{2,3}$.

This law also has a practical consequence. Suppose you are using a thermocouple with the cold junction at, for example, 20 °C while the tabulated e.m.f. values refer to 0 °C (which is usually the case). Then you correct the observed e.m.f. value by adding the tabulated value for 20 °C. The important point is that the *e.m.f.* values are additive, while the *temperature* values are not. This is illustrated schematically in Figure 3.3, indicating also that the e.m.f. of a thermocouple is generally not a linear function of the temperature.

3.3.2 Thermocouple Materials

The most commonly used thermocouple materials are metals, available in wire form. A number of thermocouple types are standardized and given letter designation (International Electrotechnical Commission (IEC) 1995). When identified by their alloy name, the positive leg is listed first:

Letter	**Thermocouple type**
R	Platinum–13% rhodium/platinum
S	Platinum–10% rhodium/platinum
B	Platinum–30% rhodium/platinum–6% rhodium
J	Iron/copper–nickel
T	Copper/copper–nickel
E	Nickel–chromium/copper–nickel
K	Nickel–chromium/nickel–aluminium
N	Nickel–chromium–silicon/nickel–silicon

Type R, with 13% Pt, may have been the oldest of the noble-metal thermocouples, but it must now be considered obsolete. Types J, T and E with alloys containing copper are intended for lower temperatures. Thus, only the base-metal types K and N, and the two noble-metal types S and B, are in common use in the high temperature laboratory and will be discussed in some detail.

Reference tables giving the e.m.f. in microvolt as a function of the temperature in °C are available from the International Electrotechnical Commission (IEC 584-1 (1995) 155 pp.). The tables are given for each degree throughout the ranges and thus are too voluminous for inclusion in the present text, but the user of a given type of thermocouple should preferably have available a copy of the relevant table. Corresponding tables for every ten degrees (that is, shortened versions of the IEC tables) are available in a number of textbooks and in manufacturer's brochures, and may be used by interpolation. Another alternative is the use of a computer together with the detailed polynomials given for each type. A simple graph of the temperature against e.m.f. is presented in Figure 3.4 as a first guide, but it has too low resolution for scientific use.

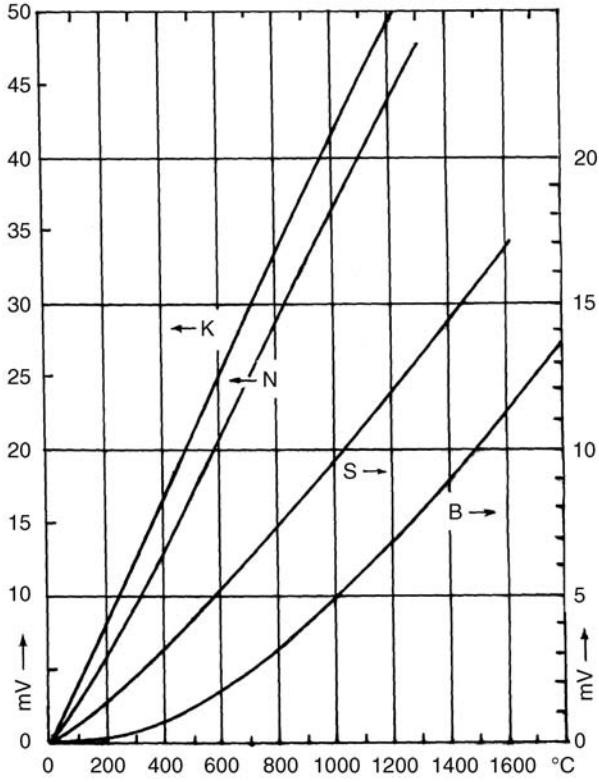

Figure 3.4 e.m.f. versus temperature for thermocouple types **K** and **N** (left-hand ordinate) and for types **S** and **B** (right-hand ordinate).

A significant difference between base-metal and noble-metal thermocouples is that the noble metals are much more expensive. For this reason, base-metal thermocouples should normally be preferred for work up to at least 1000 °C if cost is of any significance.

3.3.3 Base-Metal Thermocouples

The two types of base-metal thermocouples of interest in high temperature applications, types K and N, have nickel as the main constituent in both legs. High-nickel alloys are generally oxidation resistant, and these thermocouples are intended for use in oxidizing atmospheres. Apart from that, the two types have somewhat different temperature characteristics, and they should not be interchanged.

Type K is the oldest of the two, and well established. The nominal composition of the positive and the negative leg will be designated KP and KN, respectively (Quinn, 1990, p. 296).

KP: 90 Ni, 10 Cr. Trade names: Chromel, Tophel, ThermoKanthal KP.
KN: 95 Ni, 2 Al, 2 Mn, 1 Si. Trade names: Alumel, Nial, ThermoKanthal KN.

The agreement between a given type K thermocouple and the corresponding IEC reference table depends, of course, upon the accuracy and purity of the alloys concerned, or in other words, upon the dependability of the producer. Numerical data in this context are hard to find. A deviation of a few degrees must be expected for a new couple.

The effects of ageing, oxidation and interdiffusion come in addition, so that any thermocouple, new or old, should be checked or calibrated from time to time, see Section 3.3.10.

Type K thermocouples are subject to deterioration by oxidation, and it is clear that the effect is more severe for thin wires. The ASTM Manual (1981) gives a graph of recommended upper temperature limit as a function of wire diameter for various base-metal thermocouples. For type K the limit is about 900 °C for 0.5 mm dia., increasing to 1200 °C for 3.0 mm. These figures apply to long-term use under industrial condition; for short-term use in the laboratory, 0.5 mm dia. wire should be adequate at least to 1100 °C.

Type K thermocouples are not recommended for use in reducing or in alternately reducing and oxidizing atmospheres. In atmospheres with a

low content of oxygen, preferential oxidation of chromium may take place in the positive leg. The effect is known as 'green rot' with significant negative deviation of the e.m.f. In short, a type K thermocouple should preferably be mounted in a way that permits access of oxygen to the wires.

Type N is a more recent development. Type K, although widely used in industry, has been found to suffer from e.m.f. instability after extended exposure, primarily caused by internal oxidation and by structural changes in the metals. Considerable improvements in stability at elevated temperatures were obtained by increasing the chromium content of the positive leg, and introducing some silicon in both legs (Burley, Hess and Howie, 1980; Burley, 1986). The nominal compositions of these improved alloys are:

NP: 14.2 Cr, 1.4 Si, 84 Ni (Nicrosil).
NN: 4.4 Si, 0.15 Mg, 95 Ni (Nisil).

This thermocouple remains stable in an oxidizing atmosphere up to about 1250 °C. As stated by Montgomery (1992): '*It should be accepted by now that the type N thermocouple has a much higher thermoelectric stability than the type K - - -*'. A particular advantage is obtained by the use of Nicrosil as the sheath material in mineral-insulated, metal-sheathed (MIMS) thermocouples, see Section 3.3.6 (p. 77).

3.3.4 Noble-Metal Thermocouples

These are usually based on platinum as the main constituent.

Type S is the most common of the noble-metal thermocouple types.

SP: 90 Pt, 10 Rh. SN: 100 Pt.

It was also used in the establishment of the International Practical Temperature Scale (IPTS-68 and previous). It is considered useful to about 1600 °C; see also the discussion of properties below.

Type B is of more recent origin, originally introduced to extend the use of platinum-based thermocouples to higher temperatures.

BP: 70 Pt 30 Rh. BN: 94 Pt 6 Rh.

It was given the name 'PtRh18' indicating that it could be used to 1800 °C, which is beyond the melting point of pure Pt. It is seen from Figure 3.4 that the e.m.f. for type B is lower than for type S at the same temperature, but it should be noted also that the *slopes* of the two curves are almost equal in the temperature range around 1000 °C and above, hence the sensitivity (μV/°C, the Seebeck coefficient) is comparable for the two types at the measuring temperatures. At the same time it is seen that the Seebeck coefficient for type B around room temperature is practically nil, this represents an advantage in that the user may ignore the temperature of the cold junction (cf. also Section 3.3.8, p. 78).

The phase diagram for the system Pt-Rh is of interest in this context, see Figure 3.5. It can be seen that this is a rather unusual system, showing continuous solid solution, hardly any distance between liquidus and solidus, and positive deviation throughout. Already a few percent addition of Rh results in a marked increase in the melting point.

It is important to note that small additions of Rh also markedly improve the mechanical strength compared to pure platinum (Bennett, 1959). For this reason, when a type S thermocouple fails it is nearly always the pure platinum leg which is broken. Thus it may be advantageous to use type B instead of type S already well below the limit of 1600 °C.

The chemical behaviour of platinum and its alloys should also be taken into account. Noble-metal thermocouples are normally used under

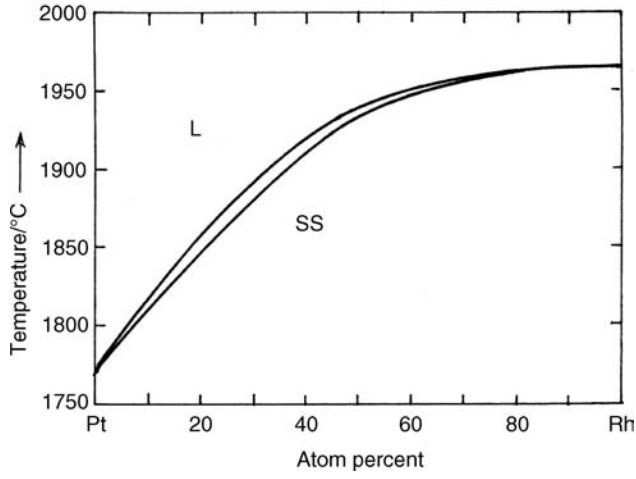

Figure 3.5 Phase diagram for the system platinum–rhodium.

oxidizing conditions. Platinum and rhodium do not form any solid oxide in oxygen. However, the volatile oxides $PtO_2(g)$ and $RhO_2(g)$ have been reported. The partial pressures are too low to cause any significant loss of metal value, but transfer of Rh through the gas phase to the pure Pt leg may be one reason for the drop of e.m.f. with time (Quinn, 1990, p. 307). Nevertheless, type S thermocouples may be considered quite stable in oxidizing atmospheres at least to 1400 °C. The transfer of rhodium should be of little consequence for type B where both legs contain Rh from the origin.

The behaviour under *reducing conditions*, on the other hand, may cause trouble. Older textbooks of chemical analysis state that platinum crucibles should not be heated in a reducing flame 'because of the possible formation of platinum carbides'. In fact, carbon is one of the few elements that do *not* react with platinum. The detrimental effect of a reducing flame, on the other hand, may be caused by reduction of almost any other element into platinum.

To take one example; silica at high temperatures in the presence of carbon may react according to the equation $SiO_2 + C = SiO(g) + CO(g)$.

And then: $Pt + SiO(g) \rightarrow Pt(Si) + SiO_2$. The reaction, schematically indicated here, may lead to formation of the silicide Pt_3Si and crumbling of the wire. Similar behaviour is expected for other refractory oxides in contact with carbon. Sulfur, phosphorus and a multitude of other elements are also detrimental to platinum.

The behaviour of alumina is of special interest since it is the most commonly used insulating material for thermocouples. In a reducing environment, reactions similar to those described above are likely to occur, with formation of $Al_2O(g)$ and finally destruction of the thermocouple. But even under 'neutral' conditions, a slow reduction may take place, resulting in a decreasing thermal e.m.f. Thus, when a noble-metal thermocouple is intended for use at the highest temperatures, it should preferably be assembled in a way that permits access of air to the wires (Quinn, 1990, p. 306).

Turning back to the system Pt-C, the phase diagram in Massalski (1990) is based on the work of Siller *et al.* from 1968. They reported solubilities ranging from 0.05 to 0.1 wt% C at temperatures from 875 to 1245 °C. Their experiments, however, were conducted in silica containers, compare above. In the careful work of Selman, Ellingson and Darling (1970), the authors conclude that the solubility appears to be less than 0.02 wt% C at 1700 °C.

3.3.5 Insulating Materials and Installation

Generally the thermocouple wires are electrically insulated by a twin-bore ceramic tube, and the assembly protected by a larger, closed-end tube, see Figure 3.6. In the case of *base-metal thermocouples,* ceramic parts of "hard porcelain" (main component mullite, $3Al_2O_3{\cdot}2SiO_2$) are adequate. For *noble-metal thermocouples*, dense-fired alumina ($\sim$99.7% Al_2O_3) should be used, considering the possible contamination from the silica in the porcelain as indicated above.

The *hot junction* should be welded, avoiding any third metal which might lower the melting point. The welding may be done by means of a small propane/oxygen torch (as used for glass blowing). In the case of base metals, some flux is necessary to remove the oxide scale; borax ($Na_2B_4O_7$) is suitable for the purpose. A practical method is to heat the wire ends to a red heat and quickly immerse them in powdered borax. A suitable amount of the powdered flux will then adhere to the wire ends, and welding may follow. A glass-blower's spectacles (didymium glass, removing the yellow sodium glare) or welding glasses should be used to

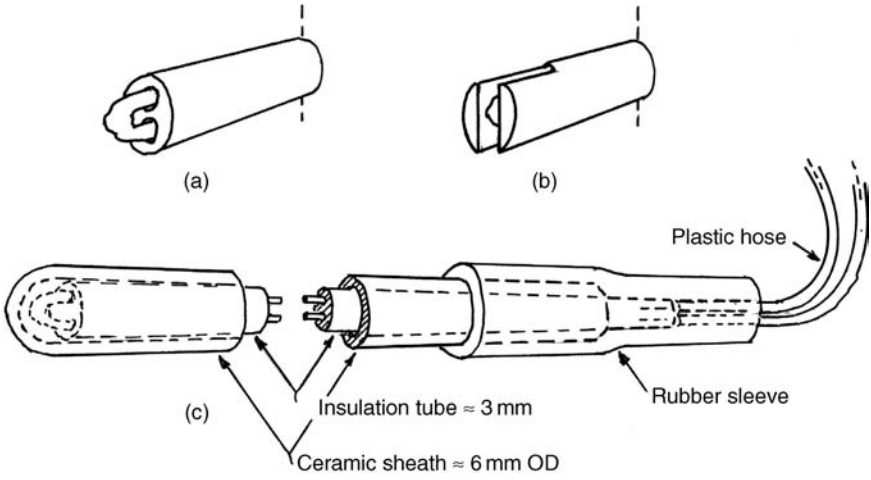

Figure 3.6 Various details of thermocouple design. (a) Twin-bore ceramic insulation and thermocouple wires with welded hot junction. (b) Twin-bore insulation tube with slot (cut on diamond saw) for better protection of the hot junction. (c) Thermocouple complete with ceramic sheath (cutaway). At the cold end the free wires are protected by thin plastic hose, and a short length of rubber tubing is slipped over the ceramic sheath to prevent undue bending. *Note:* For noble metal thermocouples, the ceramic insulation and sheath should be of recrystallized alumina.

observe exactly what happens during the fusion of the two metals. After welding, the remnant flux (borax) should be carefully removed by light hammering to make the glass-like flux bead crack, followed by washing in hot water.

Noble-metal wires are welded without a flux since the metals do not form any condensed oxide. A torch with oxidizing flame should be used. The use of dark glasses is important in the case of noble metals because of the higher temperature. Note also that the two metals of a thermocouple have different melting points, so that it may take some care to produce a neat junction.

In some applications the extra thickness of the protective sheath is unwanted. In this case protection of the hot junction may be provided by cutting a slot in the two-bore insulation tube as seen in Figure 3.6b. The junction is pulled into the slot, which is eventually covered with a suitable alumina cement.

The use of a noble-metal thermocouple under reducing conditions requires some extra measures. A protective sheath of sintered alumina may be gas tight, and yet it is not impervious to diffusing gas species at elevated temperatures. An extra protection outside the alumina sheath, made from platinum foil, may solve the problem as shown by Blegen (1976, p. 70). The diffusing species, in this case SiO(g), reacted with and was dissolved in the outside Pt sheath, while the thermocouple remained intact.

A thermocouple for laboratory use should be considered a delicate precision instrument and treated accordingly. This applies also to the "back end". The wire ends protruding from the ceramic insulation should be protected from inadvertent kinks or breaks. This may be achieved by a thin plastic hose on the wires, with a short piece of larger rubber hose slipped over the end of the sheath to provide a flexible transition, compare Figure 3.6c.

What has been said above applies primarily to thermocouples for laboratory use. In this sense it follows the excellent treatise by Quinn (1990), where industrial practice is hardly mentioned. On the other hand, books like that of Michalski *et al.* (2001) also give detailed drawings of various industrial thermocouples. A main difference from the laboratory practice is linked to the difference in dimensions; industrial installations often have the look of standard plumbing. The difference, however, has become less marked with the development of metal-sheathed thermocouples, see the next section.

3.3.6 MIMS Thermocouples

The abbreviation stands for 'Mineral Insulated, Metal Sheathed'. The design is illustrated in Figure 3.7. The thermocouple wires are placed inside a metal tube filled with an electrically insulating oxide powder, usually magnesia. By rolling, drawing or swaging, the tube is reduced in diameter, at the same time compressing the oxide.

The thermocouple wire pair may be of any type, although type K and, more recently, type N are commonly used. The sheath may be some sort of heat-resistant stainless steel, while Nicrosil has been particularly recommended. The combination has been denoted 'N-clad-N' by Burley (1992). Bentley (1992, 1998) uses the more general term 'ID-MIMS' where ID stands for 'Integrated Design', that is, compatibility between thermocouple and sheath alloys. MIMS thermocouples are now available in a variety of sizes, from 0.1 mm wire and outside diameter of 0.5 mm, to thick-walled thermocouples of some 20 mm O. D. for rough industrial use (Walker and Cassidy, 2003).

Pt-based thermocouples are also available in the MIMS configuration. With a base-metal sheath, however, the combination is unstable. The use of PtRh as a sheathing alloy gives some improvement, but the success then depends upon the porous MgO ceramics. Altogether it appears that Pt-based MIMS thermocouples may be of doubtful use at temperatures above some 1200 °C (Bentley, 1998, p. 41).

The MIMS thermocouples, regardless of type, cannot be used to the same high temperature as the corresponding thermocouple with ceramic

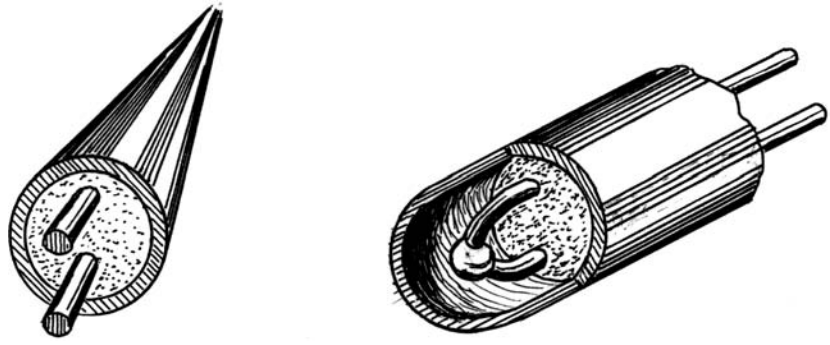

Figure 3.7 (a) Section of a MIMS thermocouple, showing the two wires, the oxide insulation and the metal sheath. (b) The junction and the closed end of the sheath.

sheath. On the other hand, within their range of use this type of thermocouple appears very practical. The smaller sizes may be bent like ordinary wire, and their small thermal mass make them well suited for laboratory applications. There is one difference, however: an amateur production of a hot junction like that shown in Figure 3.7b appears difficult. The initial manufacturer delivers MIMS wire on a roll, but the subsequent cutting to size, the hot junction and the closed end of the sheath should be left to a professional company.

3.3.7 Thermocouples for Very High Temperatures

Thermocouple type B is said to be useful to 1800 °C, although the practical limit may be lower. For the higher temperatures, metals like molybdenum and tungsten are available. Thermocouples of Mo-W or its alloys give low and unstable e.m.f., while tungsten in its combinations with rhenium has found considerable use in thermocouples. Common combinations are W 3 Re/W 25 Re and W 5 Re/W 26 Re. These are mostly used in the form of MIMS thermocouples, with sheaths of molybdenum or tantalum which are more malleable than tungsten. Other combinations like iridium–tungsten and graphite–silicon carbide are described in the literature.

The use of these thermocouples is limited by the fact that the metals are rapidly oxidized in air, with formation of volatile oxides. In contact with carbon they form carbides, so that the use is generally restricted to inert atmospheres, hydrogen and vacuum. The main use of this type of thermocouple is found in the nuclear power industry. As regards high temperature chemistry, optical pyrometry appears a better option.

3.3.8 The Cold Junction

The circuits actually used are not quite like any of those shown in principle in Figure 3.2 (p. 67). Assuming for illustration purposes that we deal with a vertical tube furnace, a more realistic diagram of the thermocouple assembly may look like Figure 3.8. In this diagram, both of the thermocouple leads are connected at the cold end to the same 'third metal', usually copper wire. The cold junctions are kept at constant temperature T_1 within a vessel, quite often a vacuum bottle filled with a mixture of ice and water so that $T_1 = 0.0\,^{\circ}\mathrm{C}$.

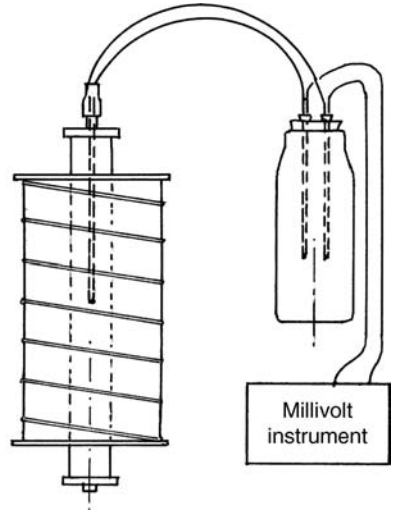

Figure 3.8 Schematic diagram of thermocouple installed in a vertical tube furnace, with cold junctions immersed in a suitable container to keep constant temperature.

A more detailed drawing of a suitable vacuum bottle is shown in Figure 3.9. The size should be sufficient to keep the mixture of ice and water for at least 24 hours. Remember that water has a maximum of density at about 4 °C, hence with very little ice left floating on top, the real temperature towards the bottom may be well above zero.

The two pairs of wire are enclosed in narrow glass tubes with sealed bottoms, as indicated in Figure 3.9. The copper wires should be plastic-insulated except for the soft-soldering at the junctions. As an alternative to soldering, a small amount of mercury may be placed in each of the closed-end glass tubes, as recommended in the ASTM Manual (1981, p. 105). This facilitates the removal of the thermocouple leads if necessary, without moving the rest of the assembly.

As regards the dimensions of the cold-junction assembly shown in Figure 3.9, the height of immersion of the wires (or the glass tubing) should be at least 100 mm; sufficient to nullify the effect of heat conduction from the ambient temperature to the point of the junctions. The points of junction should be about halfway to the bottom of the vacuum bottle to avoid the possible temperature rise of the water next to the bottom.

There are several alternatives to the depicted design. 'Ice point' electronic devices are available; small refrigerators based on the Peltier effect (cf. Section 3.3.12), although they may not be worth the cost. A simpler

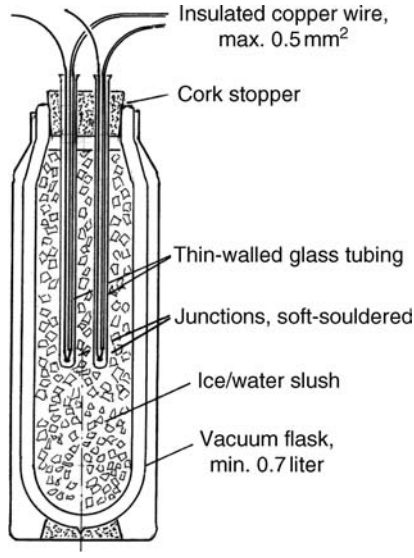

Figure 3.9 Dewar flask ('Thermos') with a mixture of ice and water, to keep cold junctions at the ice point.

solution is to use a vacuum bottle as shown above to keep the temperature constant, but leave the ice out and read the junction temperature with a thermometer. This temperature, translated to microvolts, is then added to the thermocouple reading. Another option is to use compensating wires in combination with a modern temperature control units, see the next section.

3.3.9 Extension and Compensating Wires

Referring again to Figure 3.2(d), the two junctions within the dashed square may not necessarily represent the cold junction. In the case of noble-metal thermocouples the wires are expensive, and outside the hot region they may be extended by base-metal *extension leads* that have the same e.m.f. characteristics as the thermocouple wires at moderate temperatures. Normally, however, each of the two junctions give rise to an e.m.f., and the two wires are then chosen so that the separate potentials cancel. In this case it is required that the two junctions are at the same temperature. The two connecting wires are then called *compensating*

cables. The result is the same as far as the terminal e.m.f. is concerned, and the two terms are used interchangeably.

Next, the expression 'compensating cable' also points to another feature. The lead from the thermocouple via the extension or compensating cable is often brought all the way to the terminals of a temperature regulator. The regulator includes an electronic unit which senses the ambient temperature (that is, the temperature of the regulator itself) and corrects the output signal from the thermocouple accordingly, so that the resulting output appears *as if* there had been a cold junction at 0 °C.

It is important to understand which type of control and readout instrument you are using. If it is a simple millivolt-type instrument you should use some sort of cold junction as shown in Figures 3.8 and 3.9. If it is a regulator with built-in room-temperature compensation, you should use compensating cable and *not* a separate cold junction. Mixing up the two types either way may lead to serious errors in the temperature reading.

Compensating cables have different colours for the + and – leads, and different colours for the different thermocouple types. Unfortunately the colour codes vary from one country to another, cf. Michalski *et al.* (2001, p. 466). An international colour code has been adopted by IEC 584-3 (1989). According to this the negative conductor is always *white*, while the positive leg is as follows: thermocouple type K *green*, N *pink*, S *orange* and B *grey*. It is probably wise, however, in all use of compensating cables to stick closely to the information given by the manufacturer of that specific cable.

3.3.10 Control and Calibration

The two terms as used here are almost synonymous. A thermocouple may be controlled by comparing with another, certified one, or it may be calibrated by means of known melting points.

Preliminary treatment. Noble-metal wires are expensive, and an expended thermocouple may well be reconditioned as indicated in Figure 3.10. It may be wise to first remove a short length of wire next to the hot junction, and then re-do the junction. Next, the wires (the naked thermocouple) should be cleaned by annealing in air at some 1400 °C for, for example, an hour. To this end it may be suspended from a set of terminals, and connected to the mains via a low-voltage transformer as

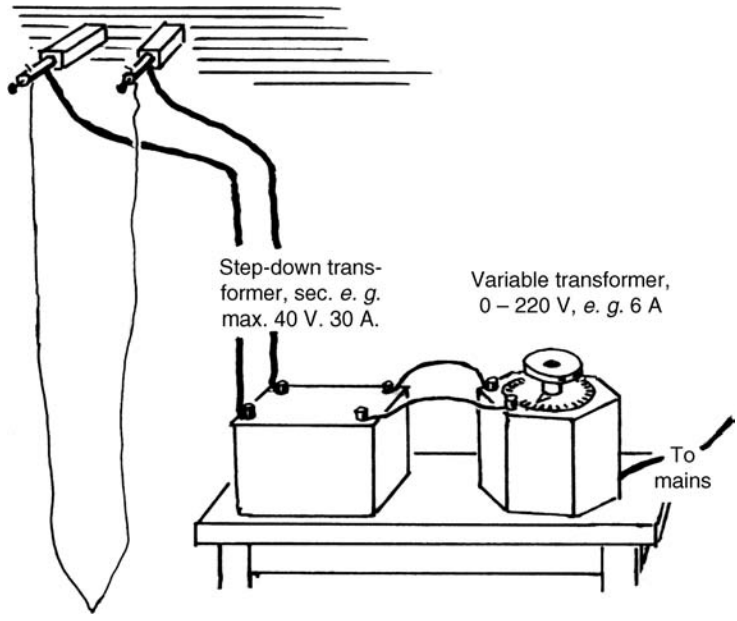

Figure 3.10 Arrangement for annealing of noble-metal thermocouples.

shown in Figure 3.10. The current is slowly raised to a bright glow. A current around 20 A may be suitable for a 0.5 mm. dia. platinum wire. The maximum allowable temperature is reached when the noble-metal wire starts to sag and straighten by its own weight. A simultaneous cloud of smoke indicates that impurities have been burnt off or have evaporated. Subsequently, the homogeneity of each wire may be checked by spot heating as already mentioned in Section 3.3.1, 'the law of homogeneous metal' (p. 68).

Comparison with a certified thermoelement may be done in a suitable furnace. A copper block fitted into the furnace, with suitably drilled holes at least 150 mm deep, will ensure equality of temperature. Copper, however, can only be used in a neutral or reducing atmosphere. Stainless steel might appear favourable but is useless for this specific purpose; the thermal conductivity of stainless steel is less than 1/10 of that for copper. An alternative is just to use a well-designed tube furnace with a central, free space of homogeneous temperature, and tie the thermocouples together with a piece of thermocouple wire.

Calibration against a known melting point is similar to ordinary thermal analysis. The sample is slowly heated, and the halt during melting is

observed. After complete melting, the heat input to the furnace is reduced, and the halt during freezing is observed. The two should preferably coincide, but the halt during freezing is often the sharper of the two.

For calibration, the substance must be pure. One may ask: *how* pure? Instead of heading for the purest sample on the market, some thermodynamic reasoning may be used. We consider a metal with melting point T_m and enthalpy of melting ΔH_m. The impurity is present with a mol fraction X. The observed melting occurs at T. Assuming for simplicity that the solubility of the impurity is zero in the solid state, we may write for the mol fraction of the main component in the liquid state:

$$\ln (1 - X) = -\frac{\Delta H_m (T_m - T)}{R T T_m} \cong -\frac{\Delta H_m (T_m - T)}{R T^2} \tag{3.5}$$

For small values of X we may write $\ln(1 - X) = -X$. Rearranging, we have the freezing point depression

$$\Delta T = \frac{R T^2}{\Delta H_m} X \tag{3.6}$$

We may use copper as an example, with $T_m = 1085\,^\circ\mathrm{C} = 1358\,\mathrm{K}$ and $\Delta H_m = 13\,\mathrm{kJ}$. This gives $\Delta T = 1180\,X$. That is, 0.1 mol% impurity would give a freezing point depression of about 1.2 °C, 0.01 mol%, 0.12 °C. And this is the 'worst case'; any solubility of the impurity in the solid state results in a smaller freezing point depression. Assuming that we may regard mol percent as roughly equivalent to weight percent, the example shows that a purity of some 99.9% is generally satisfactory.

During heating and cooling there will always be a temperature difference between the sample and the thermocouple, but it is the aim of the experimental arrangement to minimize this difference. To this end the thermocouple well should be narrow, the depth of immersion adequate, and the furnace should have a zone of homogeneous temperature as already discussed in Chapter 2. In addition, the rate of heating or cooling should be low.

Figure 3.11 shows a graphite cell for calibration by means of melting points of metals, similar to the classic arrangement of Roeser and Wensel (1941). The dimensions of the cell will vary with the thickness of the thermocouple; a coarse-calibre thermocouple needs a larger depth of immersion and hence a larger cell (and eventually a larger furnace).

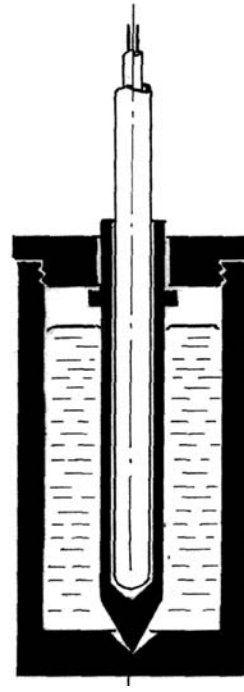

Figure 3.11 Graphite cell for calibration of a thermocouple by use of the known melting point of a metal. Graphite, used with inert atmosphere in the furnace, is suitable for aluminium (660.3 °C), silver (961.8 °C) and copper (1084.6 °C).

The general design deserves some comment. The inside protection tube of graphite is sharpened to a point at the lower end, to avoid thermal contact with the crucible bottom. At the upper end the tube is provided with a collar below the lid, to prevent the tube floating up. Threads or other means may be used to keep the lid in place.

Graphite is a suitable material for melting various metals including aluminium and copper; the solubility of carbon in these liquid metals at their melting points is essentially nil. Silver is also suitable for use with graphite. Gold, on the other hand, apart from being too expensive, dissolves substantial amounts of carbon. Nickel likewise dissolves carbon and must be used in an oxide crucible, preferably of alumina (Kim, Gam, and Kang, 2001).

There is another alternative; instead of the melting point of the metal, the temperature for the eutectic Me-C may be used as a fixed point. Nickel may again serve as an example; with about 8 atom percent C the

melting point is lowered from 1455 °C for pure nickel to 1326.5 °C for the eutectic (Massalski, 1990). The latter temperature is equally reproducible and may be observed with a graphite cell, which is more convenient and less liable to cracking than an oxide crucible.

The idea of metal-carbon eutectica as fixed points was introduced by Yamada *et al.* (1999), and shortly afterwards a series of papers on the subject appeared. This method, however, is particularly well suited in connection to radiation pyrometry and hence will be further discussed in Chapter 4.

The use of pure salts is yet another possibility. A number of fluorides and chlorides may be molten in graphite cells. Sodium chloride (802 °C) has been particularly studied by Zhu and Walker (1992). For oxy-salts like sulfates and carbonates, platinum crucibles and oxidizing atmosphere should be used. Good contact with the melt may be obtained by immersing the bare thermocouple wires, as indicated in Figure 3.12.

In situ calibration is generally recommended wherever possible. It means that the thermocouple is calibrated in the same place, the same furnace, where it is afterwards to be used. Therefore, any deviation along the line from the thermocouple to the extension cables and the measuring instrument is taken care of in one run.

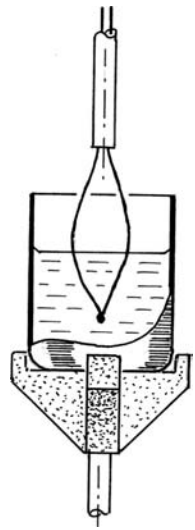

Figure 3.12 Platinum crucible used in oxidizing atmosphere for molten salts, with a naked noble-metal thermocouple dipping into the melt.

The proper application of corrections may be a matter of some concern. Assuming that the signal from the thermocouple is read on a millivolt instrument and the cold junction is kept at 0 °C, the transfer to temperature is straightforward by means of the IEC table for that type of thermoelement. The difference between 'correct' and observed temperature is noted.

On the other hand, if the signal is read on an instrument giving the temperature directly in °C, the connection between e.m.f. and temperature is built into the instrument. In this case the experimenter should check beforehand whether the instrument is made for that specific type of thermocouple, and secondly whether an automatic room temperature compensation is built into the instrument. In the latter case, compensating cables and no cold junction should be used, as noted above.

Next comes the question of how to treat the deviation as a function of temperature, in particular if the thermocouple has been checked or calibrated for one temperature only. There is really no theoretical basis for assuming that the deviation is a linear function of the temperature, but it is certainly the simplest assumption, and the observed temperatures may be corrected accordingly.

3.3.11 The Measurement of Small e.m.f.'s

The output from a thermocouple is a d.c. voltage of a few millivolts. It is desirable to measure it with an accuracy better than one part in a thousand.

Formerly, d.c. voltages were measured with a sensitive moving-coil instrument. A dial instrument, however, hardly ever obtained this level of accuracy. In addition, the instrument had a finite internal resistance, say, 100 ohm. The thermocouple itself had a comparable resistance, say, 5 ohms. In that case the reading would be lower by roughly 5%, unless the instrument was calibrated for use with a load resistance of just 5 ohms.

This should be sufficient to show why the accurate determination of low d. c. voltages had to be done in a different way, that is, by means of a resistance bridge. When used for the measurement of voltages, it is called a ***potensiometer***. The measurement is done by 'compensation', that is, the e.m.f. to be measured is compared to a known potential of opposite polarity, and the latter is adjusted until balance is obtained.

Precision potentiometers were elaborate, but the principle is simple and may deserve revival. Figure 3.13 shows the simplest form of a potentiometer. A voltage source at A is connected to a bridge of resistance $R = R_1 + R_2$.

Across this resistance exists the same voltage as given by the source, for example, 2.0 volt. Now suppose that the resistance R_1 is 95 ohm, while R_2 is 5 ohm. Then the voltage existing across R_2 would be $2.0 \times 5/100 = 0.1\,\text{V} = 100\,\text{mV}$; a suitable range to measure the voltage from a thermocouple. The thermocouple e.m.f. is indicated by TC, connected to R_2 by one fixed and one moving contact. A measurement is taken by moving the contact until balance is obtained, as shown on a sensitive null galvanometer G.

Simpler versions, used in freshman physics courses, simply had the resistor R_2 in the form of a resistance wire stretched out on a metre stick, measuring the unknown e.mf. by the position of a knife-edge contact. In potentiometers for scientific measurements the resistor R_2 is divided into decades, with contacts from 0 to 9 for each decade. Potentiometers for thermoelectric measurements were developed into precision instruments, see, for example, White (1941).

During the last half century, electronic instruments based on digital technology have made potentiometers obsolete. It may still be useful, however, to bear in mind the basic principle of the resistance bridge. For instance, if you want an initial check on the function of a temperature regulator, you need a suitable low-voltage source. You can make it from the principles of Figure 3.13, using a standard 1.5 V cell, a suitable resistor from the electronics storeroom, and a piece of resistor wire.

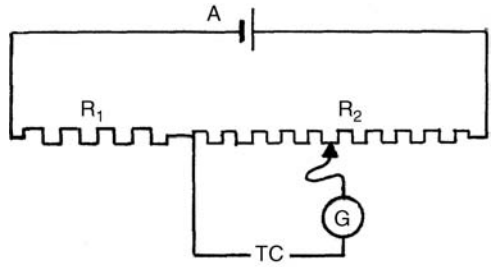

Figure 3.13 The simplest diagram for a potentiometer. **A**: DC source. $\mathbf{R_1}$ and $\mathbf{R_2}$: Resistors. **TC**: Thermocouple e.m.f. **G**: Null-point galvanometer.

Returning to the present-day digital precision instruments, the internal resistance of an electronic voltmeter is essentially infinite, thus within wide limits the measurement is independent of the internal resistance of the source. The sensitivity may be, for example, ± 1 μV, far beyond that required for temperature measurements. The absolute accuracy may not be that good, thus an instrument in active use should be checked at intervals by another one with certified accuracy.

3.3.12 More about Thermoelectricity

The thermoelectric effect discovered by T. J. Seebeck (1770–1831) and discussed in the preceding chapters concerns the electromotive force produced with zero current in the circuit. In contrast, the two other effects to be mentioned occur under the flow of current. These other effects have no bearing upon the use of a thermocouple for temperature measurement, but they are mentioned here for completeness.

When a current flows through a junction between two dissimilar materials, heat is absorbed or released in the junction (depending upon the direction of the current). This effect was discovered by J. C. A. Peltier (1785–1845).

When a current flows through a single conductor in the presence of a temperature gradient, heat is released or absorbed in the conductor. This 'Thomson heat' was first predicted by W. Thomson (1824–1907) from thermodynamic argument, and later found experimentally. It is to be noted that both the Peltier and the Thomson heats come *in addition to* the Joule heat ri^2 evolved in any conductor by the passage of current. This makes it experimentally demanding to observe the Thomson heat separately.

The Peltier heat at a junction of two metals is also small, smaller than the corresponding Joule heating. Semi-conductors, on the other hand, have large Peltier coefficients, and the effect may be used in practice for cooling purposes such as 'artificial ice points' in thermometry.

Thomson, the later Baron Kelvin, elucidated the relationship between the Seebeck, Peltier and Thomson effects on the basis of equilibrium thermodynamics. He was fully aware that the flows of heat or current in a temperature gradient are not equilibrium phenomena, but he applied the second law to those effects which *are* reversible, and arrived at the correct relations. The problem is adequately treated by irreversible

thermodynamics, or *thermodynamics of the steady state*, the term used by Denbigh (1951). A concise summary is given by Bentley (1998, pp. 207–217). For further discussion, see for example, Förland, Förland and Kjelstrup (2001). Discussions on irreversible processes and thermoelectricity are also given in a number of standard textbooks on thermodynamics, including that of Pitzer (1995, pp. 435–456).

3.4 LITERATURE

As mentioned at the beginning of this chapter, a number of excellent textbooks on temperature and its measurement have appeared in the later years. Only the authors and years (and in some cases the titles) are given in this section, while the full references are to be found in the alphabetical list below.

First should be mentioned the authoritative monograph *Temperature* by T. J. Quinn (1990). His book is particularly strong on the fundamentals, with a wealth of references.

A number of other books represent more of a balance between theoretical and practical aspects, such as those of McGee (1988), Childs (2001), and Michalski *et al.* (2001). A somewhat different approach is represented by *Traceable Temperatures* by Nicholas and White (2001), discussing heat flow, sources of error and evaluation of the measurements. The book *Thermal Sensors* by Meijer and van Herwaarden (1994) leans more towards the electronics side of temperature measuring devices.

Concerning the use of thermocouples, the ASTM Manual (1981, 1993) as well as the handbook by Bentley (1998) are both thorough and dependable.

A different type of book is represented by the proceedings from the international symposia on temperature measurements. A meeting was held in New York City in 1939, and the proceedings appeared in 1941 under the heading *TEMPERATURE. Its Measurement and Control in Science and Industry*. It was later counted as the first of a series of symposia proceedings maintaining the same lengthy title; for brevity it is shortened to *TMCSI* in the reference list. Since 1952 these symposium proceedings have appeared every tenth year, mostly in two parts for practical reasons. Thus Vol. 5 appeared in 1982 with a total of 1395 pages; Vol. 6 (1992) 1269 pp., Vol. 7 (2003) 1132 pp., plus author and subject indexes. The proceedings have generally been published by

American Institute of Physics in cooperation with other scientific institutes. These symposium proceedings represent tremendous sources of information on all aspects of temperature measurement.

REFERENCES

ASTM Spec. Tech. Publ. 470 B: (1981) *ASTM Manual on the Use of Thermocouples*, American Society for Testing and Materials, Philadelphia, 258 pp. 4th Revised Ed. (1993), 290 pp.

Bedford, R.E., Bonnier, G., Maas, H., and Pavese, F. (1996) Recommended values of temperature on the International Temperature Scale of 1990 for a selected set of secondary reference points. *Metrologia*, **33**, 133–154.

Bennett, H.E. (1959) The care of platinum thermocouples. *Glass Industry*, **40**, 190–91, 210.

Bentley, R.E. (1992) Thermoelectric behaviour of Ni-based ID-MIMS thermocouples using the Nicrosil-Plus sheathing alloy. *TMCSI*, **6**, 585–590.

Bentley, R.E. (1998) *Theory and Practice of Thermoelectric Thermometry (Handbook of Temperature Measurement, Vol. 3)*, Springer, Singapore, 245 pp.

Blegen, K. (1976) *Equilibria and Kinetics in the Systems Si-N, Si-O-N, and Si-C-O-N*. Dr.-Ing. Thesis, NTH (now NTNU), Trondheim, 259 pp.

Burley, N.A., Hess, R.M., and Howie, C.F. (1980) Nicrosil and Nisil: New nickel-based thermocouple alloys of ultra-high thermoelectric stability. *High Temp. High Press.*, **12**, 403–410.

Burley, N.A. (1986) N-CLAD-N: A novel advanced type N integrally-sheathed thermocouple of ultra-high stability. *High Temp. High Press.*, **18**, 609–616.

Burley, N.A. (1992) A novel integrally sheathed thermocouple: Optimum design rationale for ultra-high thermoelectric stability. *TMCSI*, **6**, 579–584.

Callendar, H.L. (1899) On a practical thermometric standard. *Phil. Mag.*, **48**, 519–547.

Childs, P.R.N. (2001) *Practical Temperature Measurement*, Butterworth-Heineman, Oxford, 372 pp.

Denbigh, K.G. (1951) *The Thermodynamics of the Steady State*, Methuen & Co., London, 103 pp.

Førland, K.S., Førland, T., and Kjelstrup, S. (2001) *Irreversible Thermodynamics*, 3rd edn, Tapir Academic Press, Trondheim, 281 pp.

Giauque, W.F. (1939) A proposal to redefine the thermodynamic temperature scale. *Nature*, **143**, 623–626.

Holborn, L. und Day, A. (1899) Über das Luftthermometer bei hohen Temperaturen. *Annalen der Physik und Chemie NF*, **68**, 817–852.

Holborn, L. and Day, A. (1900) Über das Luftthermometer bei hohen Temperaturen. Zweite Abhandlung. *Annalen der Physik, Vierte Folge*, **2**, 505–545.

International Electrotechnical Commission (IEC), Bureau Central de la Commision Electrotechnique Internationale, Geneve, Suisse. IEC 584-2 (1982) "Thermocouples, Part 2: Tolerances", 7 pp.

IEC 584-3 (1989) "Thermocouples, Part 3: Extension and compensating cables. Tolerances and identification system", 9 pp.
IEC 584-1 (1995) "Thermocouples, Part 1: Reference tables", 155 pp.
Kim, Y.-G., Gam, K.S., and Kang, K.H. (2001) A nickel freezing point cell for thermocouple calibration. *Metrologia*, **38**, 319–323.
Massalski, T.B. (ed.) (1990) *Binary Alloy Phase Diagrams*, Vol. **I**, ASM International, Materials Park, Ohio, pp. 130–131.
McGee, T.D. (1988) *Principles and Methods of Temperature Measurement*, John Wiley & Sons, New York, 581 pp.
Meijer, G.C.M. and van Herwaarden, A.W. (1994) *Thermal Sensors*, Inst. of Physics Publishing, London, 304 pp.
Michalski, L., Eckersdorf, K., Kucharski, J., and McGhee, J. (2001) *Temperature Measurement*, 2nd edn, John Wiley & Sons, Chichester, 501 pp.
Montgomery, K.K. (1992) Type N versus type K thermocouple comparison in a brick kiln. *TMCSI*, **6**, 601–605.
Nicholas, J.V. and White, D.R. (2001) *Traceable Temperatures. An Introduction to Temperature Measurement and Calibration*, 2nd edn, John Wiley & Sons, 421 pp.
Pitzer, K.S. (1995) *Thermodynamics*, 3rd edn, McGraw-Hill, Inc., 626 pp.
Preston-Thomas, H. (1990) The international temperature scale of 1990. *Metrologia*, **27**, 3–10 and 107.
Preston-Thomas, H. and Quinn, T.J. (1992) The international temperature scale of 1990: Part I. *TMCSI*, **6**, 63–67.
Quinn, T.J. (1990) *Temperature*, 2nd edn, Academic Press, London, 495 pp.
Roeser, W.F. and Wensel, H.T. (1941) Methods of testing thermocouples and thermocouple materials. *TMCSI*, **1**, 284–314.
Selman, G.S., Ellingson, P.J., and Darling, A.S. (1970) Carbon in platinum and palladium: solubility determination and diffusion at high temperature. *Platin. Met. Rev.*, **14**, 14–20.
Walker, J. and Cassidy, G. (2003) Development of a new thermocouple for harsh environments. *TMCSI*, **7**, 457–461.
White, W.P. (1941) Potentiometers for thermoelectric measurements. *TMCSI*, **1**, 265–278.
Yamada, Y., Sakate, H., Sakuma, F., and Ono, A. (1999) Radiometric observations of melting and freezing plateaus for a series of metal-carbon eutectic points in the range 1330 °C to 1950 °C. *Metrologia*, **36**, 207–209.
Zemansky, M.W. (1964) *Temperatures Very Low and Very High*, Dover Publications, New York, 127 pp.
Zhu, Q. and Walker, J.H. (1992) A determination of the freezing point of sodium chloride. *TMCSI*, **6**, 363–368. ibid 369–372: Design and preparation of a sodium chloride blackbody.

4

Radiation Pyrometry

CONTENTS

High Temperature Experiments in Chemistry and Materials Science, First Edition.
Ketil Motzfeldt.

Preamble

Pyrometry is just another name for temperature measurement, primarily used for elevated temperatures. A thermocouple assembly may be called a pyrometer, but more usually the term is reserved for devices based on radiation.

Radiation, as used in the present context, covers the range from visible light to far infrared. (Since 1945 the word is increasingly associated with *radioactive* radiation, which is not part of the present topic.) The nature of light and heat radiation as electromagnetic waves was first established through the theoretical work of James Clerk Maxwell around 1860. His work laid the foundation for the subsequent work of Max Planck on the distribution of energy in the wavelength spectrum, which in turn led to a complete revolution in the physical sciences. A summary of the thoughts that led to this revolution is included for its historical interest.

The radiation pyrometer and the thermocouple serve the same purpose, and their temperature ranges overlap to some extent. The basic principles and the techniques, however, are entirely different. Thus it appeared expedient to treat the two topics in separate chapters.

4.1 BASIC PRINCIPLES

4.1.1 The Nature of Heat and Radiation

Heat is generally considered as the stored, disordered kinetic energy of the atoms or molecules in matter. But heat may be transferred through a

medium by two entirely different processes, conduction and radiation. Thermal conduction is dependent upon the temperature in the material and gradients in temperature. Thermal radiation, on the other hand, travels through empty space, or through condensed media independently of their temperature. For example, the rays from the sun may be focused through a lens of ice at 0 °C, in order to ignite a fire. All kinds of thermal radiation are essentially electromagnetic waves, travelling through empty space with a velocity of 300×10^6 m/s.

Some symbols and definitions may be useful. We consider a source of radiation, most easily conceived as a source of limited area A and uniform radiation density.

- Radiant *flux* Φ (watt) is the total radiant power emitted from the source.
- Radiant *intensity* $I = d\Phi/d\omega$ (watt/steradian) is the part of the flux emitted per unit solid angle (in a specified direction).
- Radiant *exitance* $M = d\Phi/dA$ (watt/m^2) is the radiant power per unit area of the source (formerly called *emittance*.)
- The *radiance* $L = dM/d\omega = d^2\Phi/dAd\omega$ (watt/(m^{2}sr)) is the exitance within a specified solid angle.

So far we have considered only radiation *originating from* a surface. We may add one term related to radiation *incident upon* a surface:

- The *irradiance* E (watt/m^2) is the radiant power incident on a surface, per unit area of the surface. (The term as defined here relates to the total radiation, while the term *illuminance* refers to visible light only and is measured in lumen per square metre)

If this seems cumbersome, don't worry. It may be useful only to get acquainted with the terminology used in various textbooks. Discussion on radiation pyrometry is included in a number of texts on temperature measurement referred to in Chapter 3, while it is treated at length by DeWitt and Nutter (1988).

4.1.2 Formation and Propagation

Any object at temperatures above zero Kelvin emits thermal radiation. In colloquial speech we say that heat and light radiate from the surface, but this is not strictly correct; a surface as such cannot produce electromagnetic radiation. The heat is transported from the inside of the

material to the surface; exactly at which depth this heat transport is converted from thermal conduction to radiation remains in doubt. It is clear, however, that some of the radiation produced within the solid is reflected at the surface, so that only a part is emitted (Planck, 1913, p. 4). The reflection is different for different materials and also depends on the surface structure. This is one reason why different materials at the same temperature show marked differences in their ability to emit thermal radiation.

The Spatial Distribution. The radiation emitted from a source spreads in all directions. But the apparent distribution of intensity may depend upon the way we observe it. Consider a small, planar source with intensity I_o in the direction normal to the plane, compare Figure 4.1a. Assume that our means for observing the light has a field of vision considerably larger than the source. Looking at the source from an angle, the radiant intensity arriving at our pyrometer would be $I_o \cos \theta$. This relationship is known as Lambert's cosine law and is valid as a limiting law for an ideal source with no directional effect.

On the other hand, if the field of vision is much smaller than the planar source, the pyrometer would see the projection of the source normal to the line of observation, the resulting equation contains $\cos \theta / \cos \theta = 1$, and in the limit the intensity appears independent of the direction, Figure 4.1b.

The latter would be the normal case in pyrometry (within certain limits). A corresponding effect is observed in reflected light, for example, when looking at the moon. We know it is spherical, and yet the full moon looks like an evenly illuminated planar disc.

Reflection, Absorbtion, Transmission. Consider a light ray of intensity I_o which falls on a solid object. There are three possibilities: it may be reflected, absorbed or transmitted. Generally all three processes occur

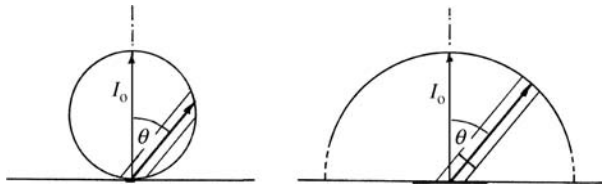

Figure 4.1 Spatial distribution of radiation (idealized curves): (a) From a 'point source'. (b) From a plane.

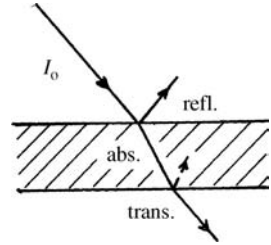

Figure 4.2 Reflection, absorbtion and transmission, with a glass disc as an example.

simultaneously, although to very different degrees for different materials. In the case of ice or a glass disc, most of the light is transmitted, with a small part reflected at the entrance and exit interfaces and hardly any absorbed, see Figure 4.2. In the case of an opaque (optically dense) material such as a metal, most of the light will be reflected if the surface is shiny, otherwise a larger part of it will be absorbed and thus converted to heat in the material.

Because of the conservation of energy we may write the sum of reflected, absorbed and transmitted energy as

$$I_r + I_a + I_t = I_o \tag{4.1a}$$

Dividing through with I_o we have

$$\rho + \alpha + \tau = 1 \tag{4.1b}$$

where the Greek letters represent *reflectance*, *absorbtance* and *transmittance*, respectively.

Reflectance may be specular as in a mirror, or diffuse as from a sheet of white paper, or something inbetween, but this need not concern us for the time being.

4.1.3 The Concept of the Black Body

Different substances at the same temperature show different exitance. A 'perfect radiator' is needed, one that exites a maximum of radiation for a given temperature.

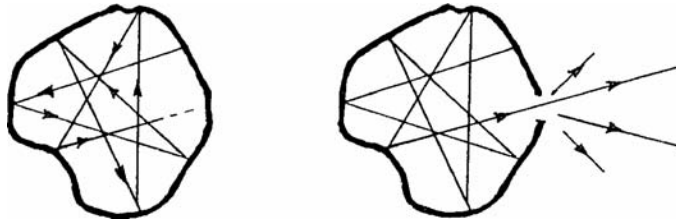

Figure 4.3 (a) Radiation within an isothermal cavity (schematic); equilibrium radiation. (b): The same cavity with an orifice. A small part of the radiation escapes, but the radiation in the cavity is still close to equilibrium.

Consider a cavity in an optically dense material, of arbitrary inside shape and at a uniform and constant temperature, see Figure 4.3a. The inside surfaces emit radiation which strikes other parts of the inside surface, where it is in part reflected, in part absorbed. Since no part of the radiation escapes, the space within the cavity must in time come to thermal equilibrium.

Next we make a small hole in the cavity, Figure 4.3b. Some of the radiation will escape through the hole. But if the cross-section of the hole is small compared to the total interior surface, we may assume that the cavity is still very close to equilibrium, and hence that the radiation emitted through the hole is a good approximation to *equilibrium* radiation, or *black-body radiation*.

The term 'black body' may be understood by looking at a cavity or a hollow body illuminated from the outside. The hole in the body appears completely dark, because any light entering into the hole will 'get lost' inside. Another interesting approach to a black body is a stack of sewing needles tied to a bundle and observed from the sharp ends. Try it!

4.1.4 Emission, Absorbtion and Kirchhoff's Law

The *emissivity* ε is defined as the ratio between the radiant energy emitted per unit area from a real surface, and the energy emitted from a black body at the same temperature. The emissivity of a real surface is always less than unity. It may be added that the emissivity ε of a given material is not a specific property of the material, it will vary with the texture and surface treatment. As a consequence, direct observation on a hot surface cannot give a true temperature.

Returning to the cavity, Figure 4.3a, any part of the inside surface will emit radiation. The radiation emitted from one area will strike another area as mentioned above; it is in part reflected, in part absorbed. Simultaneously this other area also emits radiation.

Now suppose that the ratio between absorbtance and emissivity, α/ε, is larger in one area than in another inside the cavity. This would mean that the first area would absorb more of the radiant energy and thus get hotter. But a spontaneous creation of temperature differences is counter to the Second Law of Thermodynamics. Hence the ratio between absorbtance and emissivity must be the same at all parts of the cavity. But different areas of the cavity may differ in texture, they may even be made from different materials. The only answer to the problem is that $\alpha/\varepsilon = 1$, or that *emissivity is equal to absorbtance* for any material. In writing:

$$\alpha = \varepsilon \tag{4.2}$$

This, essentially, is Kirchhoff's law (1860). The above reasoning is based on a system in equilibrium, but it is generally accepted that Kirchhoff's law is valid also for non-equilibrium systems such as, for example, the surface of a hot object located in a colder environment.

We may note that a perfectly black substance, one that absorbs all incident radiation, would simultaneously be the perfect emitter with $\varepsilon = 1$. Such a substance is an abstraction, but it provides a more precise explanation for the term *black body*.

It is noted also that the reflectance does not enter into the above reasoning. But it follows from Eq. (4.1b) with $\tau = 0$ that a body with high reflectance must have low absorbance and hence low emissivity. As a consequence, a polished silver teapot keeps its temperature better than a dull one.

Transmittance does not enter into the reasoning since the cavity was assumed to be of opaque material. But Eq. (4.1a) applies equally well to transparent materials like glass. Most of the incident visible light passes through glass, very little is absorbed. Correspondingly, very little visible light is emitted from a hot piece of glass; a common experience for anyone who has worked with hot glass in the lab.

So far we have considered total radiation (and visible radiation), but Kirchhoff's law must be valid for the radiation within *any* range of wavelengths, that is: $\alpha_\lambda = \varepsilon_\lambda$. This is also a consequence of the Second

Law. It goes without saying that absorbtance and emissivity are strongly dependent upon the wavelength.

4.1.5 Total Radiation, Stefan and Boltzmann

The next question concerns the total energy emitted by a black body as a function of its temperature. In 1879 Josef Stefan in Vienna studied the problem experimentally by means of a glowing platinum wire, and he concluded that the emitted energy was proportional to the fourth power of the absolute temperature. Subsequently one of his students, Ludwig Boltzmann (1884) considered the same problem on the basis of the electromagnetic theory of Maxwell, which shows that radiation in a confined volume contains a certain amount of energy and exerts a pressure on the walls, analogous to a gas. Boltzmann imagined various thermodynamic cycles with radiation as the working medium, and thus was able to provide a theoretical proof to Stefan's observations.

The Stefan–Boltzmann law may be written

$$M_b = \sigma T^4 \tag{4.3}$$

where M is the exitance, subscript b stands for black body, and the more recent value of the constant $\sigma = 5.670 \times 10^{-8}\ \mathrm{W\,m^{-2}\,K^{-4}}$.

The Stefan–Boltzmann law may be used for temperature measurement, although it is not the best method. It is useful, however, for calculations of energy requirement, for example, in high temperature furnaces where a major part of the heat loss is due to radiation. In real cases, some suitable value of the emissivity $\varepsilon < 1$ should be inserted.

4.1.6 Spectral Distribution, Wien and Planck

The radiation from a black body consists of a range of wavelengths. In order to investigate the radiant energy as a function of wavelength, the radiation may be focused on the slit of a spectrometer and then dispersed into a spectrum. (This cannot be done with a prism of ordinary glass which absorbs strongly above some 2 μm, but it may be done with, let us say, a rock salt prism.) The spectrum may be investigated by placing the thin junction of a thermocouple

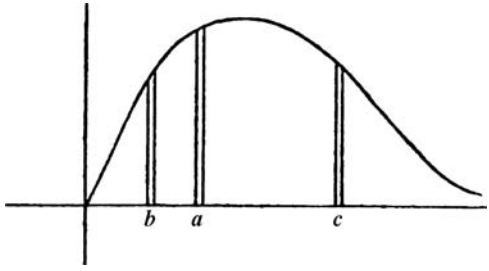

Figure 4.4 Spectral distribution in principle: Energy density on the ordinate, wavelength on the abscissa. (Reprinted from Wien Copyright (1894).)

at various places, corresponding to various wavelengths. At any particular spot in the spectrum, the thermojunction intercepts a wavelength interval between λ and $\lambda + \Delta\lambda$. The thermocouple therefore indicates the energy within a wavelength band. If this energy is divided by $\Delta\lambda$, the quotient is the energy per unit wavelength band. If we now measure the rate of emission and the area of the emitting surface, we will have finally *the radiant exitance per unit wavelength band*, with the symbol M_λ.

Measurements like these were done already towards the end of the nineteenth century, yielding curves like the one shown in Figure 4.4. The next problem was to provide an explanation for these curves.

Wien's Law. It was clear to the authors of the time that this was related to the *most probable* distribution, or in other words, to the *entropy* of the radiation. Willy Wien (1896) chose to consider the radiation from a gas. In his own words (in translation from German): '*We now make the hypothesis that each molecule radiates with a wavelength that depends only on the speed of that molecule, and with an intensity which is a function of this speed.*' He then used Maxwell–Boltzmann statistics on the molecules of the gas, in combination with the known T^4 relationship for the temperature. In this way he arrived at an equation which, with our symbols, reads

$$M_\lambda = \frac{C_1}{\lambda^5 \exp\left(\dfrac{C_2}{\lambda T}\right)} \tag{4.4}$$

With suitable values for the two constants C_1 and C_2, this equation gave a close fit to the experimental data for moderate values of the

product λT. For the longer wavelengths and higher temperatures, however, increasing deviations were found.

Planck's Law. The above equation, after all, was founded on a rather loose hypothesis. Max Planck (1900) went more deeply into the matter. While most previous authors had considered the temperature of the emitting substance only, Planck ascribed a temperature to the radiation itself. Considering radiation as an independent entity with a temperature and a certain energy per unit volume, it must also have an entropy. Now, entropy is related to statistics. If radiation occurs as a continuous process, the number of possible states and hence the entropy would be infinite, while Planck believed it to be finite. In his own words (English translation 1913, p. 153):

> That is to say, we shall assume that the emission does not take place continuously, . . . but that it occurs only at certain definite times, suddenly, in pulses, and in particular we assume that an oscillator can emit energy only at the moment when its energy of vibration, U, is an integral multiple n of the quantum of energy, $\varepsilon = h\nu$.

Planck's mathematical deduction must be left for the trained physicist; we give only the end result, noting also that $\nu = c/\lambda$ where ν is the frequency and c is the velocity of light:

$$M_\lambda = \frac{c_1}{\lambda^5\left[\left(\exp\frac{c_2}{\lambda T}\right) - 1\right]} \tag{4.5}$$

$$c_1 = 2\pi hc^2 \approx 3.742 \times 10^{-16}\text{W m}^2; c_2 = hc/k \approx 1.439 \times 10^{-2}\text{m K}.$$

Planck constant $h = 6.626 \times 10^{-34}$ J s
Boltzmann constant $k = 1.380 \times 10^{-23}$ J K^{-1}.

Integration of the expression for M_λ in Eq. (4.5) over all wavelengths results in M_b from Eq. (4.3), Stefan–Boltzmann's law.

The above notation for Eq. (4.5) and the constants is in accord with the recommendations of ISO Quantities and Units (1993). The first radiation constant c_1 is alternatively given the value hc^2, in connection with the expression for spectral radiance $L_\lambda = M_\lambda/\pi$, remembering also that the solid angle of a hemisphere is 2π.

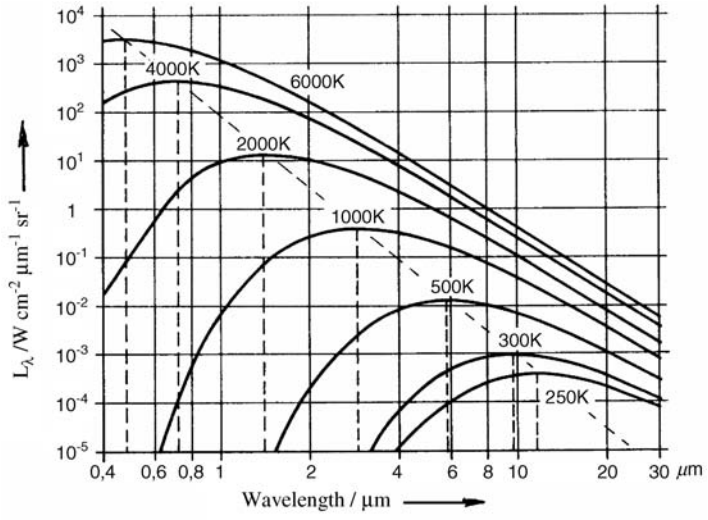

Figure 4.5 Radiance for a black body according to Planck's law, plotted as a function of wavelength for various temperatures. The dashed straight line indicates Wien's displacement law. (The diagram is mainly restricted to wavelengths of interest in optical pyrometry.)

The spectral radiance L_λ as a function of wavelength is shown graphically in Figure 4.5. Since the numbers on both axes cover several powers of ten, the results are presented on a log-log plot. The graph is mainly limited to the wavelength region of interest in radiation pyrometry.

It is noted from Eq. (4.5) that the exponential is a function of the product λT. This has as a consequence that the wavelength for maximum exitance is inversely proportional to the temperature, or that $\lambda_{\max} T = \text{const}$. This was noted already by Wien and is known as *Wien's displacement law*.

A striking similarity is noted between equations (4.4) and (4.5). The only apparent difference is the number 1 after the exponential. For moderate values of the product λT, the value of the exponential is large and the subtraction of 1 makes little difference. In fact, for wavelengths around 1 μm, as used in optical pyrometry, the deviations between Wien's and Planck's equations are negligible at least to 2500 K. However, the difference *in principle* between the two equations is great.

Planck's introduction of the 'elementary quantum of action' hc/λ led to a complete revolution within natural sciences, and what is now known as quantum mechanics, quantum physics and quantum chemistry. The concept of light as a stream of photons, and the dualism between waves and particles, are but a small part of it. The translator of Planck's book wrote in his preface:

> Probably no single book since the appearance of Clerk Maxwell's Electricity and Magnetism has had a deeper influence on the development of physical theories.

This was written in 1914. Nearly 100 years later it is still true. Hence it was felt proper in the present text to include an attempt at a summary of the background.

> Max Planck (1858–1947) in spite of his professional success, did not have a happy old age. During World War I his elder son Karl died from wounds suffered in action. His twin daughters both died during childbirth in 1917 and 1919, respectively. In 1933 he protested to Hitler himself against the racial laws and the harassment of Jews, but without success. His home was destroyed by allied bombing in 1944. His one surviving child, Erwin, was executed in 1945 for complicity in the 1944 attempt to assassinate Hitler.
>
> (Abstracted from "A Dictionary of Scientists", Oxford University Press 1999.)

4.1.7 The Radiation Law as Used in Pyrometry

Measurements of the radiant energy within a wavelength interval between L_λ and $L_{\lambda+\mathrm{d}\lambda}$ would be a tedious way of measuring temperatures. In practice, only *relative* radiance temperatures are measured. Let us say that the radiance (or something proportional to the radiance) is measured at the gold point T_{Au}. The unknown temperature T_{x} is then measured by means of the equation

$$\frac{L_\lambda(T_x)}{L_\lambda(T_{Au})} = \frac{\exp\left(\dfrac{c_2}{\lambda T_{Au}}\right) - 1}{\exp\left(\dfrac{c_2}{\lambda T_x}\right) - 1} \tag{4.6}$$

(The same equation was given in Chapter 3 (p. 64) in connection with the International Temperature Scale.)

It was mentioned above that Wien's and Planck's laws give nearly identical results within the range of wavelengths and temperatures encountered in radiation pyrometry. For this reason, Eq. (4.6) may be simplified by omitting the number 1 in both numerator and denominator. At the same time we generalize by denoting the temperatures T_0 and T_1, and we take the logarithm on both sides. This gives a useful form of Wien's law:

$$\ln \frac{L_\lambda(T_1)}{L_\lambda(T_0)} = \frac{c_2}{\lambda}\left(\frac{1}{T_0} - \frac{1}{T_1}\right) \tag{4.7}$$

So far we have considered the radiation from a black body only. Equation (4.7) may be used to check the influence of an emissivity less than unity. Assume that T_o is the true temperature of an object, and T_1 is the temperature observed with an emissivity ε. We then have

$$\frac{\lambda}{c_2} \ln \frac{1}{\varepsilon} = \frac{1}{T_1} - \frac{1}{T_0} \tag{4.8}$$

For illustration, assume $\lambda = 1\,\mu\text{m}$ and $T_0 = 2000\,\text{K}$. A quick calculation shows that with, for example, emissivity $\varepsilon = 0.8$, we have $T_1 = 1940\,\text{K}$, that is, an error of 60 K. With an emissivity of 0.5 the error would be around 175 K. Most materials have reported emissivities even lower, indicating (once again) that indiscriminate use of any radiation pyrometer may lead to serious errors.

The user of a commercial pyrometer does not need to know *how* the pyrometer was calibrated, but the basic principle may be of interest. Assume that we have a black body containing a mixture of solid and liquid gold, that is, at the temperature T_{Au}. The signal from the pyrometer at this temperature is carefully noted. Next we have the black body at some higher temperature (e.g. the melting point of nickel, cf. p. 63). The signal from the pyrometer is brighter. The brightness may be reduced by means of a rotating sector in the path of the pyrometer, with a speed of rotation sufficient to avoid flicker. It cuts off a certain fraction of the intensity during each revolution, acting like a grey filter. The position of the rotating sector is varied until the signal from the pyrometer exactly matches that from the gold point. With a known geometry of the sector, the difference in intensity and hence the unknown temperature T_x may be determined.

This is just a sketch of the method by which the temperature scale at high temperatures was first established. It might appear simple, but it was a lengthy pioneering job. Nowadays a pyrometer is calibrated or checked by means of a specially calibrated lamp or by known melting points, as further related in Section 4.6 (pp. 121–125).

What follows is a discussion of different types of radiation pyrometers, with some comments on their respective advantages and limitations. It may be helpful as a guide for choosing the best pyrometer for a given task. But the reader is warned that these notes do not represent the ultimate truth about any one type. Instruments are continuously improved, and the development of digital electronics continues at an impressive rate. Thus the best advice to the user of any one pyrometer is this: read the manufacturer's instructions!

4.2 TOTAL RADIATION PYROMETRY?

The total radiation given off from a black body at temperature T is expressed by Eq. (4.3): $M_b = \sigma T^4$, and this might seem suitable for temperature measurement. Adhering to this equation, however, would require a sensor that could detect *all* of the radiation within a given solid angle; furthermore any lens system would spoil the measurement because of selective absorbtion in the glass. Hence the term 'total radiation' is usually misleading; practical instrument are at most broad-band pyrometers. Instruments of this sort have been widely used in industry over the years, generally with a thermopile as the sensor. They have served their purpose, but for accurate temperature determination, a pyrometer using only a narrow band is generally better. Wide-band pyrometers and the so-called total radiation pyrometers are described in a number of textbooks and will not be further discussed here.

4.3 DISAPPEARING-FILAMENT OPTICAL PYROMETER

4.3.1 The Classical Optical Pyrometer

Generally, the classical pyrometer is based on the human eye, Figure 4.6. With some experience a man may estimate the temperature of a glowing

Figure 4.6 'The first optical pyrometer'. (Reprinted from Forsythe Copyright (1941) Reinhold Publishing Company.)

object at temperatures from dark red heat (about 600 °C) until it becomes too bright for direct observation (about 1400 °C).

Given some standard for comparison, however, the situation is greatly improved. The filament of an incandescent lamp is a particularly convenient object for comparison. A pyrometer based on this idea was patented by Mr. E. F. Morse in 1902 (cf. Forsythe and Adams, 1945). The operator sighted directly through the lamp onto the target, adjusting the current through the lamp filament until the filament and the target appeared of equal brightness. The current was then taken as a measure of the temperature. Subsequent and essential improvements were the introduction of a telescope, and that the pyrometer lamp was put inside the telescope.

The use of the eye limits the waveband to the range of visible light, about 0.4 to 0.8 μm, and instruments operating in this range are generally denoted *optical* pyrometers. The importance of this type of instrument in the development of pyrometry may be illustrated by a quotation from Quinn (1990, p. 391): '*The disappearing-filament optical pyrometer, [was] at one time universally used in standard*

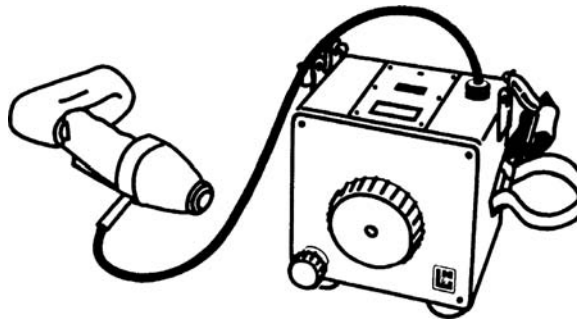

Figure 4.7 A disappearing-filament optical pyrometer: The telescope, and the instrument case. (Model 8622-C from Leeds & Northrup Co., Philadelphia, USA.) (Reprinted from Heraeus Holding GmbH Copyright (2012) Heraeus Holding GmbH.)

laboratories for the realization of the International Temperature Scale, and widely used in science and industry for practical thermometry . . . '. Quinn goes on to say that the disappearing-filament pyrometer has now largely been superseded by photoelectric pyrometers of one sort or another. This is generally true, but the disappearing-filament pyrometer still has specific advantages for use in laboratory experiments. For this reason we will go through it in some detail.

The following discussion is tied to one particular model. Figure 4.7 shows a drawing of the instrument, consisting of the telescope and a separate battery and instrument case, connected by a short flex.

The telescope part is shown in longitudinal section in Figure 4.8. Several details may be pointed out, reading from left to right on the drawing:

- The **objective** is provided with threads to permit adjustment to sharpness of targets at different distances.
- The **range-changing screen** has three windows: one open for the low range (775–1225 °C), one with a medium-grey glass for the high range (1075–1750 °C) and one dark-grey for the X-high range (1500–2850 °C). Correspondingly the instrument scale (located in the instrument case) has three parallell graduations, one for each range.
- The **lamp** is an essential part; the quality of the lamp is decisive for the quality of the instrument. In Figure 4.8 it is shown with the filament in a vertical position, in reality the lamp is mounted horizontally. The lamp has *flat windows* on both sides to give a sharp image. Furthermore the two windows are slightly offset from the normal (slightly wedge-shaped) to avoid multiple reflections.

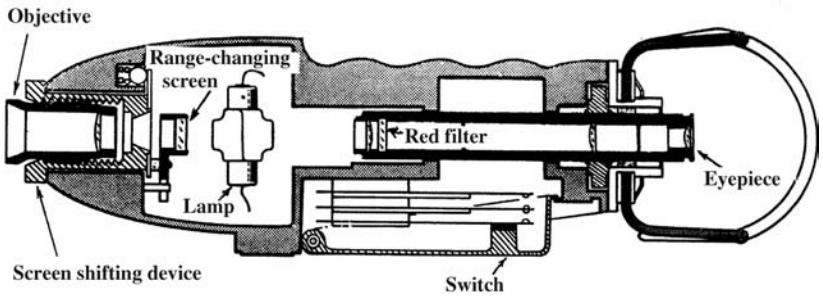

Figure 4.8 Longitudinal section through the telescope of a disappearing-filament optical pyrometer. (Note that for the purpose of illustration the lamp is shown in a vertical position, while in reality the filament appears horizontally in the field of vision.) (Reprinted from Heraeus Holding GmbH Copyright (2012) Heraeus Holding GmbH.)

- The **red filter** has a dual purpose. The human eye is sensitive to light only in the range about 0.4 to 0.8 μm. The red filter limits this range even further, leaving only the red part of the spectrum which is more comfortable to the eye. The particular red glass used has a fairly sharp cut-off for wavelengths shorter than some 0.6 μm. On the other hand, the human eye loses its sensitivity gradually for wavelengths above some 0.7 μm. As a result, the instrument acts as a narrow-band pyrometer with an effective wavelength of 0.65 μm. This is still a standard wavelength for accurate pyrometry.
- The **eyepiece** is provided with an adjustment wheel, visible on the right-hand side of the telescope. The idea is that people who normally wear corrective glasses have to remove them when using the pyrometer. Then the adjustment is used to obtain a sharp image of the filament; this is essential for accurate reading.
- The **switch** operates the current to the pyrometer lamp; it is activated by pressing the handle at the underside of the telescope. A normal right-handed person will use the left hand to keep the switch depressed, while the right hand is used to turn the **large circular handle** on the instrument case (cf. Figure 4.7), thereby adjusting the current in the filament until a brightness match is obtained. Sketches of the view in the telescope are shown in Figure 4.9 for different settings of the lamp current; explanations are given in the figure text.
- The temperature reading is not yet complete, however. Once a satisfactory brightness match is obtained, the corresponding current should be accurately determined. Pressing **the lower left button** on the instrument case (Figure 4.7) changes the mode from *varying* the

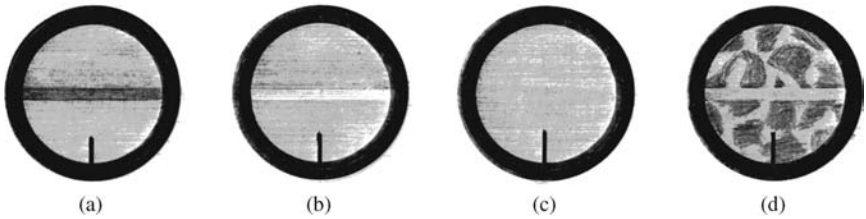

Figure 4.9 Schematic drawings of the view in the pyrometer telescope for different settings of the lamp current. (a): Too low. (b): Too high. (c): Correct setting; the filament 'disappears'. (d): A possible view when sighting on, for example, the top of a crucible containing a coarse-grained charge. The interspaces between grains appear brighter than the surfaces; the interspaces represent fair approximations to 'black bodies' and thus are closest to the 'true temperature' of the crucible. (Note: The working space of a laboratory furnace should ideally approximate a black body in itself. In this case all contours and details like those shown in drawing (d) should disappear when the furnace has come to constant temperature.)

> current in the filament to *measuring* it. Keeping the switch on the telescope pressed with one hand, the lower left button is pressed with the other hand, and turned until the galvanometer in the window on top of the instrument case indicates balance. And *then* the temperature in question may be read on the drum-shaped scale, as seen through the large window.

These rather detailed 'directions for use' are given here for two reasons. Firstly, pyrometers of this kind are still available in various laboratories and may be useful, while the directions for use are often lost. And secondly, the directions indicate what really happens, even though modern versions do part of it automatically.

The mode of operation may be further explained along with the diagram Figure 4.10. **B** is a battery (4 dry-cells of 1.5 V). **R** is a variable resistor; in reality a circular slidewire operated to adjust the lamp current. Once the point of 'disappearing filament' has been reached, the corresponding current has to be determined as noted above (notwithstanding the fact that the scale reads temperature).

In 'the old days' before the development of modern electronics, the accurate measurement of either current or voltage had to be done by compensation, as discussed in Chapter 3 (p. 87) and shown in principle in Figure 3.13. In the present case, measurement of the current in the pyrometer lamp is made by a separate potentiometer located on the same drum as the one used to regulate the current. Changing from one to

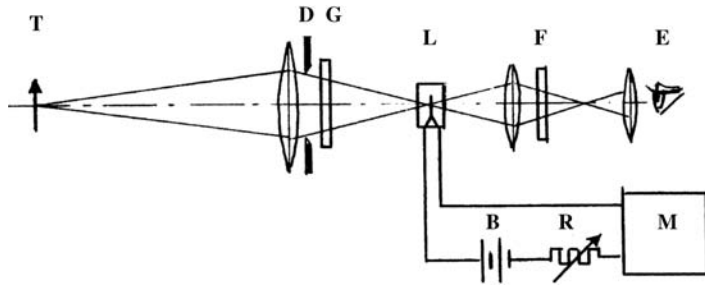

Figure 4.10 Principles of an optical pyrometer (cf. Figures 4.7 and 4.8): **T:** Target. **D:** Entrance cone diaphragm. **G:** Grey filter. **L:** Pyrometer lamp. **F:** Red filter. **E:** Observer's eye. **B:** DC power source (4×1.5 V). **R:** Variable resistor. **M:** Measuring device.

the other potentiometer is done by pressing the lower left-hand knob as indicated above. For simplicity in Figure 4.10, this second potentiometer with associated standard Weston cell and galvanometer is only marked **M** (for Measuring).

The need for this separate measurement stems from the fact that the voltage of the dry cells may differ somewhat from the value for which the pyrometer is calibrated. With the invention of the transistor and the subsequent development of digital electronics, the situation was fundamentally changed. Still the disappearing-filament pyrometer has its place.

4.3.2 The Automated Version

Around 1965 an automatic version based on essentially the same principles (and the same pyrometer lamp) was brought on the market (L&N 8641 High Precision Automatic Optical Pyrometer), see Nutter (1972, 1988). The comparison between the brightness of the filament and that of the target was effected by a rapid shifting between the two images. Any difference in brightness would create an alternating current which activated a servo system to minimize and eventually nullify the difference. The temperature was shown on a digital display or a strip-chart recorder.

The instrument was very sensitive; a difference of 1 °C at 2000 °C could be easily detected. It was very advanced (for its time), but it was also rather bulky and very expensive. In addition, the extreme sensitivity was not usually met by a corresponding accuracy due to errors from other sources. Thus it appears that there was not a sufficient market for this type of instrument, and the production was discontinued.

4.3.3 The Modern Manual

In the introduction above, it was quoted from Quinn (1990) that the diappearing-filament pyrometer is now generally superseded by photoelectric pyrometers of one kind or another. So why another edition of the disappearing filament?

Forsythe and Adams (1945) gave some good reasons:

> This type of pyrometer possesses several advantages over other forms. In the first place, the observer is able to see the object whose temperature is measured directly through the pyrometer . . . It is hard to overestimate this advantage . . .

The quotation given above was written some 60 years ago; today automatic pyrometers generally are equipped to give a view of the target area. The sighting, however, is of necessity 'done with mirrors' and the sight is generally less precise than the direct view through a telescope.

Hence it is interesting that a modernized version of the disappearing-filament pyrometer appeared on the market a few years ago.[1] It is based on essential parts of the old technology in combination with modern electronics. It now appears as a one-piece instrument, hand-held or mounted on a stand. It is said about the disappearing-filament pyrometer that 'as long as you can *see* the target you can also measure its temperature'. Automatic pyrometers, on the other hand, require a certain minimum target size, as related in Section 4.4.3.

4.4 PHOTOELECTRIC PYROMETERS

4.4.1 Basic Prinsiple

Sensors in photoelectric pyrometers may be of various kinds, but the majority is based on the photovoltaic effect, the same as utilized in a solar cell. Explained in simple terms, a quantum of light striking the surface of a semiconductor may excite an electron in the material from the valence band to the conduction band. Normally the excited electron and the positive hole will recombine within a very short time, and the energy

[1] Model DFP 2000 from Spectrodyne, Inc., Quakertown, Philadelphia, USA.

comes out as heat. However, by a suitable configuration, the electron may be captured on an adjacent metallic electrode, while the positive hole ends up at the other electrode. The two may then recombine only through an external circuit.

A requirement is that the light quantum has sufficient energy $h\nu$ (which means sufficiently short wavelength λ) to overcome the band gap of the material. Silicon is universally used for the production of solar cells, and it is also the dominating material for sensors in photovoltaic pyrometers. Pure silicon has a band gap of 1.12 eV (Ibach and Lüth, 2003), corresponding to a maximum efficiency in the near infrared with wavelengths around 1 μm.

In order to be useful, either for solar cells or for sensors in pyrometry, pure silicon has to be doped to form what is termed a p-n junction (or several junctions). The specific technologies, however, are way out of the scope of the present text. It may be noted only that the photovoltaic cell yields a *current* which is proportional to the intensity of the radiation, while the voltage remains nearly constant within reasonable values of the internal resistance of the circuit. Present-day photovoltaic pyrometers have achieved a very high level of sensitivity, stability and (when properly used) accuracy. Some questions remain, however.

4.4.2 The Choice of Wavelength

As noted above, Si is a suitable material for wavelengths around 1 μm. Farther into the infrared, other materials may be used, such as Ge, InAs or InSb, with maximum efficiencies around 1.5, 3 and 5 μm, respectively. Still further into the range of 'heat radiation', thermal detectors are used. We may ask, which part of the spectrum is the best for a given application?

We recall the expression for spectral radiance, in terms of Wien's law:

$$L_\lambda = \frac{c_1}{\lambda^5 \exp \frac{c_2}{\lambda T}} \tag{4.9a}$$

$$\text{By differentiation}: \frac{dL_\lambda}{L_\lambda} = \frac{c_2}{\lambda T^2} dT \tag{4.9b}$$

The term $\Delta L_\lambda / L_\lambda$ shows the relative change in the radiance in response to a change ΔT in the temperature. It is seen from Eq. (4.9b) that the relative change, or the sensitivity, decreases for increasing temperature,

this cannot be avoided. But it is also seen that the temperature error ΔT caused by a given change in radiance is directly proportional to the wavelength. Hence shorter wavelengths give better accuracy.

On the other hand, it is seen from Figure 4.5 (p. 103) that the absolute magnitude of the radiance almost vanishes at short wavelengths in combination with moderate temperature. For this reason, infrared pyrometers for moderate temperatures use wavelengths in the range of about 3 to 10 μm or more. For elevated temperatures, shorter wavelengths are preferred. Pyrometers with silicon detectors, with effective wavelength around 1 μm, are preferred for high temperature use. The disadvantage, of course, is that the pyrometer shows nothing until a temperature of, for example, 1000 °C is reached.

For comparison, the disappearing-filament pyrometer with an effective wavelength of 0.65 μm comes out favourably in this respect. At the same time it may read temperatures down to dark red heat, about 760 °C, due to the flexibility of the human eye.

4.4.3 Target Size and Free Sight

It has already been mentioned above that a photoelectric pyrometer requires a certain minimum target size, and free sight between the target and the pyrometer lens. This is illustrated schematically in Figure 4.11. Two aspects of the figure are noted. The first is that the required minimum target diameter increases in proportion to the distance from the pyrometer (within certain limits; the pyrometer optics require a certain minimum distance). The second aspect is the requirement of free sight between the target and the pyrometer. As seen by dashed lines in Figure 4.11, this goes from a diminishing cone at short distances to a

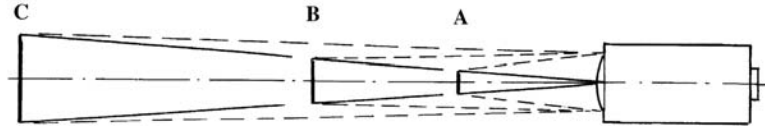

Figure 4.11 Schematic demonstration of the path of light for an automatic optical pyrometer. At a given distance **A** the required minimum target size is moderate (e.g., 5 mm dia.) and the cone of free sight (dashed lines) widens towards the lens opening. At the distance **B** the required target diameter is doubled, and at **C** it is quadrupled, with a correspondingly large required cone of free sight.

widening cone at long distances. For large industrial furnaces these requirements may not pose any problem.

For laboratory furnaces, on the other hand, it is usually desirable with radiation shields towards the ends to approach black-body conditions within the working space. Large openings in these shields are unwelcome. Thus the path of free sight is made as narrow as compatible with the requirements of the pyrometer. And then, *if* some part of the apparatus has inadvertently come into the sighting path, it may not be observed when looking into the sighting device. It merely causes a wrong temperature reading, maybe entirely wrong.

It follows that, when using a photoelectric pyrometer through a narrow sighting path, it should be stationary; preferably on a sturdy mount that at the same time permits small, controlled changes of position. A very slight change of direction either way without noticeable change of the temperature reading will show that the positioning is OK. Still a number of points have to be satisfied in order to give the true temperature, as discussed in subsequent sections.

4.4.4 Two-Colour Pyrometers

So far, pyrometers working at one effective wavelength or a limited wavelength band have been discussed. These pyrometers will give too low temperatures for any obstruction in the radiation path, and in particular for low emissivity, unless accounted for. It is also well known that it is difficult to estimate an effective emissivity within reasonable limits. In such cases the problem may in part be circumvented by noting that, while the total intensity of radiation is lowered because of a low emissivity, the *ratio* between intensities at two different wavelengths remains constant (or nearly constant, see below). The two-colour pyrometer may be designed with one photocell and two monochromatic filters, or with two photocells with accompanying filters. Multi-wavelength pyrometers have also been used.

The two-colour pyrometer will in principle give the correct temperature, provided that the emissivity is the same at the two wavelengths, or the target behaves as a 'grey body'. This condition, however, may not be fulfilled; the emissivity of a surface in general varies with the wavelength. To take but one example, the normal spectral emissivity of tungsten is $\varepsilon \cong 0.4$ at $\lambda = 0.8$ μm, decreasing to 0.3 at 1.5 μm.

In order to approach the requirement of a 'grey body', the two wavelengths chosen should not be very different. It is difficult, however, to determine the ratio of intensities for closely spaced wavelengths with sufficient accuracy to obtain a reliable result for the temperature. Quinn (1990, p. 418) concludes that ratio pyrometry is not a suitable method for making high-precision temperature measurements. He points out, however, that two-colour pyrometry may be useful under certain conditions, for example, in the temperature measurement on very small objects. Furthermore, steady improvements in digital electronics as well as sensor materials may increase the importance of two-colour and multi-wavelength pyrometers as time goes on.

4.5 CORRECTIONS FOR WINDOW AND MIRROR

4.5.1 Reflection and Absorbtion in a Window

Experiments in high temperature chemistry generally involve work in controlled atmospheres or vacuum, which in turn requires a window between the hot zone inside and the pyrometer outside the furnace. The concepts of reflection, absorbtion and transmission were introduced on p. 96. Here we will look more closely at the loss of intensity caused by passage through a glass window, and how it may be accounted for in terms of temperature.

From p. 105 we have a form of Wien's law:

$$\ln \frac{L_\lambda(T_1)}{L_\lambda(T_0)} = \frac{c_2}{\lambda}\left(\frac{1}{T_0} - \frac{1}{T_1}\right) \tag{4.7}$$

The left-hand expression gives the ratio between radiances at two different temperatures T_0 and T_1, and in principle it is equivalent to the ratio between intensities before and after passage of a window. The equation may thus be rewritten

$$\frac{\lambda}{c_2} \ln \frac{I_0}{I_1} = \left(\frac{1}{T_1} - \frac{1}{T_0}\right) \tag{4.10}$$

The ratio I_1/I_0 is a constant for a given window, independent of the absolute intensities. Thus the equation may be rewritten in a simpler form:

$$A = \left(\frac{1}{T_1} - \frac{1}{T_0}\right) \tag{4.11}$$

The quantity A is a characteristic constant for that window, when used at the effective wavelength λ.

The value of A may be determined experimentally by measuring the temperature of any arbitrary hot object at a constant temperature, with and without the window in the path of light. An ordinary incandescent lamp may be suitable for the purpose, when care is taken to reproduce the conditions for each reading. It should be noted also that, for the same window but another pyrometer with a different effective wavelength, the value of A will be different, while Eq. (4.11) remains valid.

In exacting laboratory work, silica glass is almost the only choice of material for windows. This is not only because fused silica is very resistant to thermal shock, but also because pure fused silica has a very high transmittance in the wavelength range of interest. This is shown in Figure 4.12. It is noted that the absorbtance is essentially nil within the range of interest for high temperature pyrometry.

In spite of this near-zero absorbtance, it is found that the intensity is measurably reduced by passing through a silica window. This is explained by the fact that the effect is caused, not by absorbtion in the window, but by reflection from its surfaces. The extent of the reflections is determined by the properties of the material, in this case silica. Thus any special cleaning or polishing of a silica window is not expected to have much effect on its A-value.

For normal incidence, theoretical optics yields the reflectance

$$\rho = \left(\frac{n-1}{n+1}\right)^2 \tag{4.12}$$

where n is the index of refraction for silica. At a wavelength around 0.65 μm, $n = 1.456$. Inserted in Eq. (4.12) this yields $\rho = 0.0345$. A window has two surfaces, so we assume a total reflectance of 0.0690. (This is not quite correct because of multiple reflections, but adequate for our purpose). Assuming no absorbtance, we have $I_1/I_o = 0.931$. Inserted in Eq. (4.10) with c_2 from p. 95, this yields $A = 0.32 \times 10^{-5}$. At, for

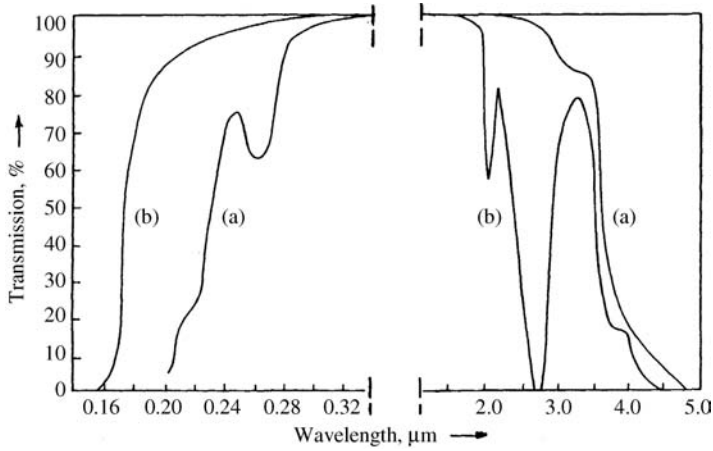

Figure 4.12 Optical transmission of vitreous silica, two different qualities denoted by their trade names. (a): *Vitreosil*, made by fusion of quartz crystal. (b): *Spectrosil*, made by hydrolysis of $SiCl_4$. The former shows absorbtion in the low-wavelength region due to impurity of Al_2O_3, while the latter has a characteristic absorbtion band around 2.7 μm due to OH^--groups (impurity of H_2O). It is noted, however, that both have 100% transmission (within the accuracy of the diagram) in the wavelength range of interest in high temperature pyrometry. Note also that fused silica, in common with other silicate glasses, is optically dense and behaves almost like a black body at wavelengths above some 5 μm. (Reprinted with permission from Bansal and Doremus Copyright (1986) Academic Press.)

example, observed temperature $t_1 = 1500\,^\circ\text{C}$ or $T_1 = 1773\,\text{K}$, this would give a correction of 10 K, that is, $t_o = 1510\,^\circ\text{C}$.

The mentioned A-value represents the theoretical minimum for a silica window. Experience shows that the experimentally determined A-values for clean silica windows generally come out somewhat higher, possibly due to a small contribution from absorbtion. Still the experimental observations are in general accord with the theoretical prediction.

4.5.2 The Use of a Mirror

High temperature furnaces made explicitly for precision measurements of temperature are usually placed horizontally to permit direct, horizontal observation, and the use of inert purge gas obviates the corrections

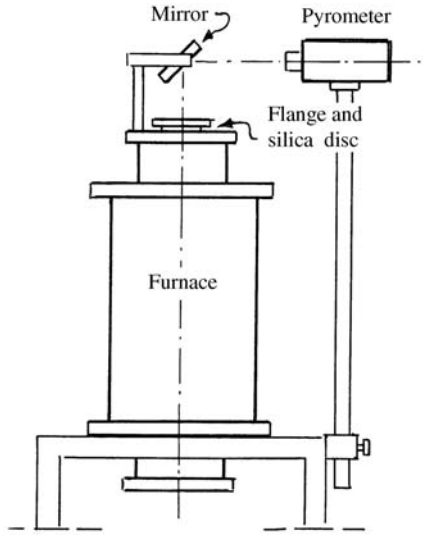

Figure 4.13 Schematic representation of a high temperature laboratory furnace with window, mirror and pyrometer.

associated with a window (see, e.g. Yamada *et al.*, 2003). On the other hand, laboratory furnaces intended for varied experiments are more often placed vertically, with a window on top for observation. For convenience a 45° mirror is introduced, as shown schematically in Figure 4.13. This mirror causes a reduction of intensity, much the same as a window. The effect may be accounted for in the same manner, by determining the *A*-value of the mirror. *A*-values in series are addditive, thus the combined effect of a window and a mirror gives $A_{\text{tot}} = A_{\text{win.}} + A_{\text{mir.}}$.

There are also certain differences. The first is one of convenience. It is quite simple to introduce or remove a window in the path between the source and the pyrometer. Checking the *A*-value of a mirror is another matter. For each change from 'with' to 'without' the mirror, the line of sight has to be changed by 90° by moving either the pyrometer or the source. In order to reduce spurious error, each reading should be repeated several times, so the procedure may be time-consuming. For this reason it is important that the window does not change with time. That is, its *A*-value, once determined, should remain constant.

Next we will look at various types of mirrors. An ordinary ***pocket mirror*** (such as found in a lady's handbag) is made from ordinary glass with a layer of reflecting metal (aluminium) on the back (or between two layers of glass). Some reflection from the front layer of the glass gives a tendency to 'double images', furthermore the absorbtance of the glass may be higher than that of fused silica. Experience has shown, however, that this simple sort of mirror is adequate for the purpose, with *A*-values only slightly higher than for silica windows.

A ***first-surface mirror*** was used by the author at one time to avoid the effect of the 'double image'. This mirror had the reflecting aluminium layer plated on the front surface of the glass. It turned out, however, that the *A*-value slowly increased with time, so it was abandoned.

A ***total-reflection prism*** is a good alternative. An optical prism of good quality is more expensive than a pocket mirror, but probably also better for the purpose. The *A*-value of such a prism has been found to be not much higher than for a window, indicating that the absorbtion through the increased optical path makes little difference.

In order to avoid having *two* correction terms, the prism may be put directly on the observation port, serving simultaneously as a window. This, however, is a poor idea. In particular when doing high temperature experiments in a vacuum, the side facing the vacuum will to some extent be coated, and its *A*-value has to be determined after each experiment. This is much more tedious for a prism than for at flat window, as explained above.

The problem of coating, or darkening of the window, is a common one in high temperature work. It may in part be solved by having several windows mounted on a revolving disc, with one window at a time exposed to the hot furnace, as further described in Chapter 7, pp. 256–259.

4.5.3 Graphical Representation of A-Values

Commercial pyrometers give the temperatures in degrees Celsius (°C), while equation Eq. (4.11) is given in terms of absolute temperature (K). Thus the use of the equation for computing an *A*-value involves converting from °C to K, taking the inverse, subtracting, and back again; a tedious job if done often. Today the operator would apply a simple program

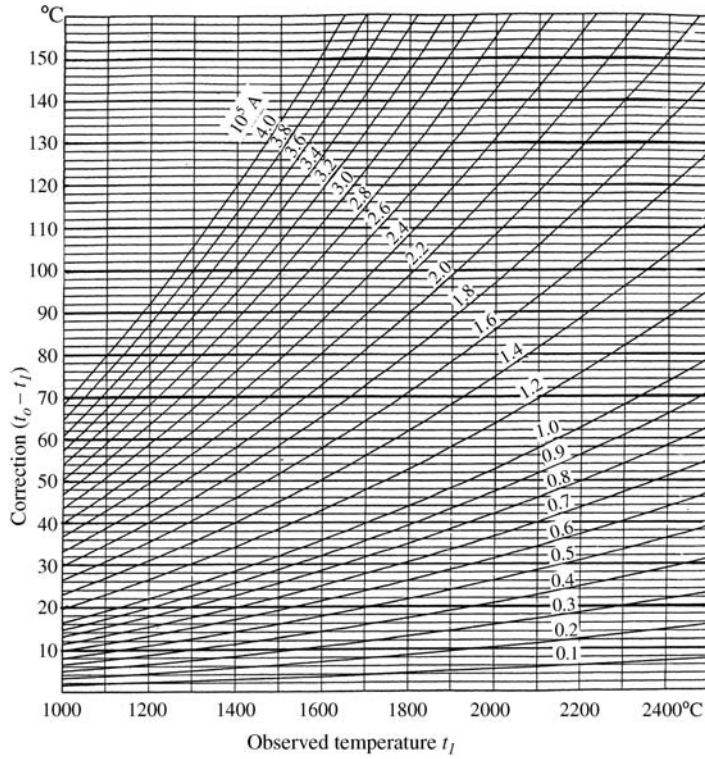

Figure 4.14 The diagram gives the correction $(t_0 - t_{1)}$ as a function of the temperature t_1 observed through a window/prism/mirror. Curves are given for a number of different values of $10^5 A$, where $A = (1/T_1 - 1/T_0)$, cf. Eq. (4.11), p. 114.

on his pocket computer; still, the graphical representation in Figure 4.14 may be useful.

4.6 CONTROL AND CALIBRATION

4.6.1 Tungsten Ribbon Lamps

The purpose of a tungsten ribbon lamp is to provide a portable source of temperature that may be calibrated at a standard laboratory. Tungsten is used for the filament because it has the highest melting point and the lowest vapour pressure of available metals. The word 'filament' is slightly misleading, since it is used in the form of a flat

ribbon to provide a suitable target for pyrometry. Tungsten is easily oxidized, hence the lamp is carefully evacuated and eventually filled with an inert gas, like any other incandescent lamp. The lamps used for pyrometric standards, however, are of very special design. Two different shapes have been in common use, both with tungsten ribbons some 1.5 to 3 mm wide and 30 to 50 mm long, mounted in a vertical position. One design uses a cylindrical bulb, with a distinct mark on the back of the bulb to distinguish the sighting direction. The other, high-precision lamp is provided with flat windows at entrance and exit, both windows placed slightly off 90° to the normal to avoid multiple reflections. (The design is similar to that used in the disappearing-filament pyrometer, cf. Figure 4.8, p. 109, but some ten times the size.) A tungsten ribbon lamp for pyrometric standard requires great care in design and production, as further discussed by Quinn (1990, pp. 377–388). When properly produced and handled, however, it represents a standard of temperature that will remain unchanged for many decades.

It should be noted that this sort of lamp is a purely empirical device. The emissivity of tungsten is rather low (less than 0.5), thus the true temperature of the tungsten ribbon during use is higher than that observed by the pyrometer. For example, at a colour temperature of 2000 °C, measured at 0.65 μm, the true temperature of the tungsten is about 2285 °C, see Nutter (1988, p. 393). The calibration of the lamp consists in measuring the apparent temperature for a given value of the current, measured at a specified effective wavelength. The results from the standards laboratory are given in the form of a list of temperatures and the corresponding currents; the user may then reproduce the temperature by adhering to exactly the same lamp current and other conditions. It was pointed out by Matveyev, Pokhodun and Sild (2003) that slight differences in the effective wavelength will result in deviations, hence comparisons between different standard laboratories are now made by transfer of complete black-body furnaces and/or radiation instruments.

For ordinary use it is important to note again that the calibration is valid only for the specified wavelength; recalculation to a different wavelength does not appear possible. This is a difficulty with lamps calibrated for 0.65 μm, in combination with commercial photovoltaic pyrometers that often have effective wavelengths around 1 μm or higher. Returning the lamp to the standards laboratory for complete recalibration may seem unwieldy. Transfer of temperatures by means of

a disappearing-filament pyrometer, with a black-body source as the intermediary, is a possible solution.

4.6.2 Melting Points

The determination of a known melting point is the most common way to check a pyrometer. Calibration against known melting point has been discussed already on pp. 83–85 in conjunction with thermocouples, and the procedure is largely the same.

The melting points of a number of **metals** have already been given in Table 3.1, p. 63. Copper (1084.6 °C) is convenient for use in a graphite crucible. At higher temperatures, most of the metals listed are either very expensive or have inconveniently high melting points (Mo and W). An exception is Ni (1455 °C), as recommended by Kim, Gam and Kang (2001) and others. Nickel (and most other metals) may be melted in an alumina crucible. A lid with a suitable hole does not in this case give an adequate approximation to a black body, for two reasons: alumina is translucent and the molten metal is very glossy. Thus a sighting tube is required. A sighting tube with bottom will act as a 'black hole' in the metal, even when the tube itself is of translucent alumina. The sighting tube has to be weighted down, in order not to float out of the molten metal.

The melting points of non-metals, in particular **oxides**, are similarly used. Alumina may be melted in a molybdenum crucible (Gitlesen and Motzfeldt, 1965). A sighting tube is not required, but molten alumina is transparent, so it is recommended to introduce pieces of Mo foil or wire at the bottom of the crucible to counteract reflections. The above investigation was part of a joint effort to determine the melting point of Al_2O_3, resulting in the adopted result 2054 ± 6 °C (Schneider, 1970). More recent results, for example, Sakate, Sakuma and Ono (1995), are probably less accurate.

It may be noted that the above precautions to avoid reflections were *not* realized in the work of Gitlesen and Motzfeldt in 1965. Imperfect black-body conditions may be part of the reason why their result, 2041 °C, came out a bit low compared to the value adopted by the joint project.

In the joint project, tungsten was recommended as the container material, while several of the participants used molybdenum. It appears from

the results (Schneider, 1970) that the two materials are equally suitable for the purpose.

4.6.3 Metal-Carbon Systems

Carbon, in the form of graphite, is particularly suited for high temperature purposes, and metal-carbon systems may be used as fixed points in temperature measurements. Thus, Yamada *et al.* (2003) studied suitable furnaces for realizing metal-carbon eutectic points, with Re-C (2475 °C) as an example. A project named *High temperature, Metal-carbon Eutectic fixed points for Radiation Thermometry* (HIMERT) was established some years ago with participants from the standards laboratories in a number of countries (Machin *et al.*, 2003). Their preliminary conclusion may be summarized: '*Metal-carbon fixed points may well revolutionize the approach undertaken to realize and disseminate temperature scales.*' This and similar projects have resulted in the establishment of eutectic points for Ni-C (1329 °C) and Co-C (1324 °C) (Kim *et al.*, 2006) as well as for Pd-C (1492 °C), Pt-C (1739 °C) and Ru-C (1954 °C); see Anhalt *et al.* (2006); Lowe and Yamada (2006); Sasajima *et al.* (2006); Yamada, Wang and Sasajima (2006). The above temperatures are quoted here in degrees Celsius to the nearest °C; in the original papers the temperatures are given in Kelvin with two decimals, and with an agreement between different laboratories generally within 0.2 K. The agreement is impressive, and details of the various instruments are plentiful, while simple information about the preparation of charges is sometimes missing. Also, the last mentioned three metals, unfortunately, appear rather expensive for the practical user.

Alternatives to eutectics are peritectic points, as shown by Yamada, Wang and Sasajima (2006), with the systems WC-C (2749 °C), Cr_2C_3-C (1826 °C) and Mn_7C_3-C (1331 °C) as examples. In this context the system Al_4C_3-C may be suggested as a promising candidate. The phase diagram for the system Al-C given in Massalski (1990), however, is shockingly incorrect, with impossible curves and a suggested peritectic decomposition at about 2500 °C. In reality the decomposition takes place at 2150 °C as determined by Gjerstad in 1968, see Motzfeldt *et al.* (1989). More recent and accurate values are not known, and a redetermination would appear valuable. The vapour pressure of

aluminium at the peritectic temperature is about 0.1 bar, and this should not pose a problem when the heating takes place in 1 bar of argon.

Some further notes are in place with respect to Al_4C_3. First of all the compound is hygroscopic and should be kept in a desiccator. Any slight reaction does no harm, however; during heating the hydrous oxide will react with the graphite container and form carbide again.

The decomposition of Al_4C_3 takes place to pure carbon and a liquid containing about 19 atom% C. This liquid appears to exhibit perfect wetting to graphite and has a tendency to crawl out of the crucible. Thus prolonged overheating should be avoided. Apart from that, the peritectic decomposition is easily observed and reproduced.

4.7 PRACTICAL HINTS

4.7.1 The Object Inside a Furnace

A hot object inside a furnace emits radiation which eventually reaches the pyrometer. At the same time, radiation from the furnace walls is in part reflected from the object and also reaches the pyrometer. In principle the furnace wall must be hotter than the object being heated, thus it is impossible to tell whether the object (crucible, charge) is really hotter or colder than the temperature indicated by the pyrometer. Any attempt at estimating the emissivity is futile in this connection. The only solution to the problem is to read the pyrometer sighting into a black cavity.

It is known by anybody who has gazed into a potter's kiln that during heating, the objects appear dark against the bright internal walls of the hot kiln. During cooling the situation is reversed; the objects appear brighter on a dark background. But at a certain point during the cooling, the observer does not see any objects at all. At this point the kiln interior behaves like a black body.

As regards a laboratory furnace the ideal is that the whole working space of the furnace is at a uniform temperature. A 'state of invisibility' may be taken as an indication of this; if details like an orifice in the crucible lid do not show up at all, it means that the situation is close to that of a black body.

4.7.2 More about the Black Body

In precision pyrometry the best possible approximation to a black body is essential. A large number of publications deal with various possible configurations and mathematical treatments to attain emissivity $\varepsilon = 0.999+$. The book by Quinn (1990) offers 29 pages on the subject; the paper by Saunders and White (1995) may serve as another example.

A number of the papers discuss configurations in which black-body conditions may be achieved by means of highly reflecting surfaces, compare Usadi (2006). Various configurations may be of interest in low-temperature radiometry, while at high temperatures it should be kept simple. A rule-of-thumb is that a hole, or more strictly a cylindrical cavity, should have a depth 6 times its diameter to serve as an acceptable approximation to a black body. According to Prokhorov and Hanssen (2004) the bottom should be inclined; they did extensive theoretical studies of a cylindrical cavity with an inclined flat bottom by means of the Monte Carlo method. Alternatively the bottom may be cone-shaped, as it will be by the use of an ordinary twist drill.

When conceiving black-body conditions it is essential that the whole body is kept at a uniform temperature. For this reason it is an advantage that the body is not too large. The practitioner will assume that a graphite crucible some 20 to 30 mm inside diameter, and a matching lid with an orifice no more than one-fourth that of the inside diameter of the crucible, represents a good approximation to a black body. For metal crucibles, the bottom should be made non-reflecting by grooves if the contents are translucent or transparent.

4.7.3 Increasing the Apparent Emissivity of an Exposed Surface

So far, the discussion has centred around experiments where the object or the specimen is located inside a laboratory furnace. But sometimes the experimenter may be called upon to measure the temperature of a hot surface more or less exposed to the surroundings. As indicated above, the estimation of emissivities is always uncertain (cf., e.g. Michalski *et al.* 2001, pp. 469–470).

We will assume that the surface in question shows a visible structure, if not it may be provoked by a sharp object. Then a 'state of invisibility'

may be established by external illumination, increasing the intensity of the illumination until the details in the surface structure cannot be discerned. It may then be assumed that the reading of the pyrometer, as the result of internal and external radiation, shows the true temperature.

The method should preferably be used with a pyrometer that has effective wavelength within the visible range. It may be useful in the temperature range where the reflected radiation from the external lamps may equal or exceed the radiation from the hot surface itself; say, up to some 1200 °C. In this range it should represent a valuable adjunct to the mere estimation of emissivities.

REFERENCES

Anhalt, K., Hartmann, J., Lowe, D. *et al.* (2006) Thermodynamic temperature determination of Co-C, Pd-C, Pt-C and Ru-C eutectic fixed-point cells. *Metrologia*, **43**, S78–S83.

Bansal, N.P. and Doremus, R.H. (1986) *Handbook of Glass Properties*, Academic Press, Inc., New York, 680 pp.

Boltzmann, L. (1884) Ableitung des Stefan'schen Gesetzes, betreffend die Abhängigkeit der Wärmestrahlung von der Temperatur aus der electromagnetischen Lichttheorie. *Annal. Phys. Chem., Neue Folge (Wiedemanns Ann.)*, **22**, 291–294.

DeWitt, D.P. and Nutter, G.D. (eds) (1988) *Theory and Practice of Radiation Thermometry*, John Wiley & Sons, New York, 1138 pp.

Forsythe, W.E. (1941) *Optical Pyrometry, in "Temperature, Its Measurement and Control in Science and Industry" (TMCSI 1*), Reinhold Publ. Co., New York, pp. 1115–1131.

Forsythe, W.E. and Adams, E.Q. (1945) The disappearing-filament optical pyrometer calibration and use. *J. Sci. Lab. Denison U. Bull.*, **39**, 1–48.

Gitlesen, G. and Motzfeldt, K. (1965) The melting point of alumina and some related observations. *Acta Chemica Scandinavica*, **19**, 661–669.
The same paper is also published in French translation, together with a number of other papers on the melting point of Al_2O_3, see *Rev. Hautes Temp. Réfractaires*, **3** (1966) 301–361.

Ibach, H. and Lüth, H. (2003) *Solid-State Physics: An Introduction to Principles of Materials Science*, 3rd edn, Springer, New York, 501 pp.

Kim, Y.-G., Gam, K.S., and Kang, K.H. (2001) A nickel freezing point cell for thermocouple calibration. *Metrologia*, **38**, 319–323.

Kim, Y.-G., Yang, I., Kwon, S.Y., and Gam, K.S. (2006) Features of Co/C and Ni/C eutectic transitions for use in thermocouple thermometry. *Metrologia*, **43**, 67–70.

Kirchhoff, G. (1860) Ueber das Verhältniss zwischen dem Emissionsvermögen und dem Absorbtions-Vermögen der Körper für Wärme und Licht. *Ann. Phys.-Leipzig*, **109**, 275–301.

Lowe, D. and Yamada, Y. (2006) Reproducible metal-carbon eutectic fixed points. *Metrologia*, **43**, S135–S139.

Machin, G., Beynon, G., Edler, F. *et al.* (2003) HIMERT: A Pan-European project for the development of metal-carbon eutectics as temperature standards. *TMCSI*, **7**, 285–290.

Massalski, T.B. (ed.) (1990) *Binary Alloy Phase Diagrams*, Vol. I, ASM International, Materials Park, Ohio, pp. 130–131.

Matveyev, M.S., Pokhodun, A.I., and Sild, Yu.A. (2003) Should tungsten ribbon lamps be replaced or not? *TMCSI*, **7**, 675–680.

Michalski, L., Eckersdorf, K., Kucharski, J., and McGhee, J. (2001) *Temperature Measurement*, 2nd edn, John Wiley & Sons, Ltd., Chichester, 501 pp.

Motzfeldt, K., Kvande, H., Schei, A., and Grjotheim, K. (1989) *Carbothermal Production of Aluminium*, Aluminium-Verlag, Düsseldorf, 218 pp.

Nutter, G.D. (1972) A high precision automatic optical pyrometer. *TMCSI*, **4**, 519–530.

Nutter, G.D. (1988) Spectral-band radiation thermometers, in *Theory and Practice of Radiation Thermometry* (eds D.P. De Witt and G.D. Nutter), John Wiley & Sons, Chapter 5, pp. 341–458.

Planck, M. (1900) Entropie und Temperatur strahlender Wärme. *Ann. Phys. (Vierte Folge)*, **1**, 719–737.

Planck, M. (1913) "Vorlesungen über die Theorie der Wärmestrahlung", Zweite Auflage, J. A. Barth, Leipzig, 206 pp; translation by M. Masius, "Theory of Heat Radiation" (1914), Blakiston, Philadelphia; republ. Dover Publ., New York.

Prokhorov, A.V. and Hanssen, L.M. (2004) Effective emissivity of a cylindrical cavity with an inclined bottom: I. Isothermal cavity. *Metrologia*, **41**, 421–431.

Quinn, T.J. (1990) *Temperature*, 2nd edn, Academic Press Ltd., London, 495 pp.

Saunders, P. and White, D.R. (1995) A theory of reflections for traceable radiation thermometry. *Metrologia*, **32**, 1–10.

Sakate, H., Sakuma, F., and Ono, A. (1995) Observation of Al_2O_3 melting and freezing plateaus using a cavity-type tungsten crucible. *Metrologia*, **32**, 129–131.

Sasajima, N., Yoon, H.W., Gibson, C.E. *et al.* (2006) The NIST eutectic project: construction of Co-C, Pt-C and Re-C fixed-point cells and their comparison with the NMIJ. *Metrologia*, **43**, S109–S114.

Schneider, S.J. (1970) Cooperative determination of the melting point of Al_2O_3. *Pure Appl. Chem.*, **21**, 117–122.

Usadi, E. (2006) Reflecting cavity blackbodies for radiometry. *Metrologia*, **43**, S1–S5.

Wien, W. (1894) Temperatur und Entropie der Strahlung. *Annal. Phys. Chem., Neue Folge (Wiedemanns Ann.)*, **52**, 132–165; Ueber die Energievertheilung eines schwarzen Körpers. ibid. **58** (1896) 662–669.

Yamada, Y., Sasajima, N., Gomi, H., and Sugai, T. (2003) High-temperature furnace system for realizing metal-carbon eutectic fixed points. *TMCSI*, **7**, 985–990.

Yamada, Y., Khlevnoy, B., Wang, Y. *et al.* (2006) Application of metal (carbide) – carbon eutectic fixed points in radiometry. *Metrologia*, **43**, S140–S144.

Yamada, Y., Wang, Y., and Sasajima, N. (2006) Metal carbide-carbon peritectic systems as high temperature fixed points in thermometry. *Metrologia*, **43**, L23–L27.

5

Refractory Materials in the Laboratory

CONTENTS

High Temperature Experiments in Chemistry and Materials Science, First Edition.
Ketil Motzfeldt.

Preamble

The purpose of this chapter is to give a survey of the refractory materials most often encountered in the high temperature laboratory.

The word 'refractory', in a technical context, means '*Heat resistant; hard to melt or fuse*' (*The Concise Oxford Dictionary*, 10th Edn. 2001). The definition does not say anything about resistance to oxidation. Thus, while the largest class of refractories are oxides or oxidation resistant compounds, the discussion also includes carbon and graphite as well as a number of high-melting metals.

While the main intent has been a brief survey, a number of refractory materials also serve as objects of study within the area of 'High Temperature Experiments'. Thus, the discussion in some places reflects the interests of the author.

A thorough review of the whole area of ceramic materials is found in the encyclopaedia edited by Brook (1991); see also 'Modern Ceramic Engineering' by Richerson (2006). A useful handbook of properties has been compiled by Morrell (1989).

5.1 OXIDES

A major part of the refractory materials in common use consists of high-melting oxides. Industrial refractories are most often composite materials (chamotte, firebrick), while in the laboratory pure (or nearly pure) oxide materials are usually preferred. A survey of the commonly used oxides is given in Table 5.1. In the present context, special consideration is given to materials that are commercially available as tubes and crucibles for laboratory use. All of these oxides are available as dense-sintered, gas-tight materials (with the possible exception of magnesia). The same oxide materials are also available as porous tubes and other shapes.

The refractoriness of an oxide is associated with a large negative Gibbs energy of formation, as illustrated in Figure 5.1. It is noted that the lines for the various oxides run nearly parallell. The reason is that the various reactions of formation are written for the same amount of oxygen, each reaction consuming one mole of $O_2(g)$, and the entropy change of a reaction is primarily dependent upon the consumption or production of gas. For the change of Gibbs energy with temperature we have $\partial \Delta G^0 / \partial T = -\Delta S^0$, hence all the slopes are nearly identical.

The melting points for the reactant metals lie within the temperature range of Figure 5.1, but the entropies of melting cause only minor

Table 5.1 Properties of refractory oxide materials.

Material	Melting point °C	Density g/cm^3	Thermal expansion 10^{-6} K^{-1}	Max. temp. °C with	
				oxidizing atmosphere	carbon present
Pyrex glass	(~600)	2.4	3.2	—	—
SiO_2 glass	(~1600)	2.2	0.62	1400	1100
Mullite	~1820	2.6	~ 6	1600	1400
Al_2O_3	2054	3.9	7.7	1800	1500
MgO	2830	3.6	11.6	2000?	1500
BeO	2500	3.0	10	2300?	2000
ZrO_2	2680	5.6	11	2400?	2000
ThO_2	3390	9.9	10	2600?	>2000

Notes: The melting point of alumina is given with fair accuracy (2054 ± 6 °C), while the higher melting points are given with accuracy varying from ± 30 to ±100 °C.

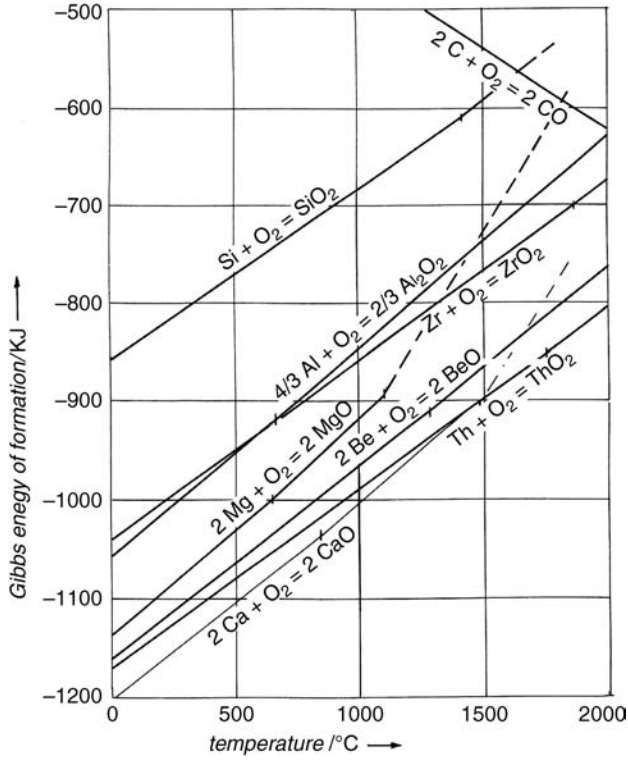

Figure 5.1 Gibbs energy of formation for refractory oxides, plotted as functions of the temperature in centigrade. (Data from NIST-JANAF Thermochemical Tables, 1998.)

changes of slope. Entropies of vaporization, on the other hand, cause large changes, as is seen in the lines for MgO where magnesium changes to Mg(gas) at 1100 °C, and correspondingly for CaO with the boiling point of Ca at 1485 °C.

Calcium oxide is included in Figure 5.1 because thermodynamically it appears to be the most stable of all oxides. Unfortunately it is so markedly hygroscopic that it is not much used as a refractory.

Included in the upper right-hand corner is also the line for the oxidation of carbon to carbon monoxide. It is seen from the reaction equation that in this case one extra mole of gas is *produced*, hence this line has nearly the same slope with opposite sign.

From the temperatures where the carbon line crosses the lines for SiO_2 and Al_2O_3, one might infer that these oxides react with carbon to form

metal and CO at about 1650 and 2000 °C, respectively. In reality the reaction temperatures are somewhat lower because of the formation of carbides.

5.1.1 Silica, SiO_2

In the laboratory, silica is used only in the form of silica glass, but we will take a brief look at other forms. Silica appears in a number of different crystal modifications. For a main classification we note that *quartz* appears as the stable modification to 870 °C, above this temperature *tridymite* may appear, and above 1470 °C *cristobalite* is the stable phase. These phase changes are termed *reconstructive* because they involve complete rearrangements of the structure, and they appear sluggish. Thus, a sample that has been transformed to cristobalite at high temperature may remain as cristobalite also at low temperatures. (To complicate matters, it has never been definitely settled whether tridymite is a phase in the pure SiO_2 system or depends upon the presence of foreign ions.)

In contrast, *displacive* transformations involve only minor changes of structure and hence take place almost without time lag. Quartz has a displacive transformation at 573 °C, while cristobalite has one at 270 °C. Both involve volume increase of 0.8 and 2.8%, respectively. In particular the latter may lead to cracking or disruption of the material unless accounted for. Addition of various foreign oxides may alter the course of events. In short, the production of silica-based refractories is an art in itself, and we will leave it at that.

The raw material for any kind of silica is the mineral quartz, hence the vitreous product is often termed quartz glass, while *silica glass* is a more proper name. One of the virtues of silica glass is the very low coefficient of thermal expansion; a tube of silica glass may be heated to 1000 °C and immersed in cold water without cracking. Pyrex, a brand of borosilicate glass, is included in Table 5.1 for comparison.

Glasses in general are thermodynamically unstable relative to the crystalline phases, but for most glasses the crystallization takes place only very slowly. Silica glass may show incipient crystallization at temperatures around 1100 °C or somewhat higher. It appears that the crystallization starts at the surface and may lead to flaking. It appears also that the crystallization is enhanced in reducing environments.

On the other hand, silica crucibles are used industrially for the melting and recrystallization of pure silicon with a melting point of 1410 °C. Thus the upper limit of use depends on the purpose and the expected lifetime. In the above process each crucible is used only once. The product is pure silicon for solar cells, or ultra-pure for the semiconductor industry. It appears that silica is the only crucible material employed for these purposes at present, but silicon nitride may be a contender in the future.

The usual silica glass is made by the melting of pure quartz at temperatures around 2000 °C, and the products are expensive. An alternative is the *Vycor* brand (Corning Glass Works, USA). This is made by a multistep process where the desired shape is first formed in a lower-melting glass which contains sodium and boron oxides in addition to silica. Next, the shape is heat-treated to achieve a phase separation, and then leached in hot acid to remove the sodium borate. The remaining, porous product is heat-treated to shrink into a clear glass with some 96% SiO_2. The advantage of the process is lower price, and for most purposes Vycor glass is equivalent to the more costly pure silica glass.

Another alternative is the translucent or 'milky' silica used for larger sizes of tubes, usually delivered with molten or glazed surfaces so that the product is gas tight. For use as furnace tubes it is as good as the transparent type, and much cheaper. However, for use as furnace tubes, silica in general has few advantages except for its resistance to thermal shock.

5.1.2 Mullite, $3Al_2O_3 \cdot 2SiO_2$

As the formula implies, mullite represents a compound in the system alumina-silica (in fact the only stable one). It has a fairly narrow range of homogeneity, and is assumed to melt incongruently at about 1830 °C. Its heat of formation from the component oxides is close to zero, and it appears that mullite is entropy-stabilized. However this may be, mullite appears as a stable compound and is the major phase in household porcelain and pottery.

Porcelain consists of a crystalline phase of mullite and a bonding phase of vitreous silica. By reducing the excess of silica compared to the composition of mullite, and at the same time securing a low content of alkali and alkaline earths, a product is obtained which can withstand higher temperatures than ordinary porcelain. It is marketed as 'Mullite'

or 'High-Alumina Porcelain' or under trade names such as 'Pythagoras'.[1]

The composition of mullite as given above corresponds to 71.8 weight% of Al_2O_3. Pythagoras is reported to contain 60 weight% Al_2O_3, thus it is still on the silica-rich side. Nevertheless, Pythagoras tubes may be used at temperatures to 1600 °C, and they have been found to be vacuum-tight up to the maximum temperature. Above 1500 °C some creep occurs. Thus, when used under vacuum for a period of hours, it finally caves in at temperatures of 1500 to 1550 °C.

In addition to the said quality, special qualities are available with alumina contents 65 and 78 weight%, reported to be useful to 1700 and 1800 °C respectively.

5.1.3 Alumina, Al_2O_3

Various modifications of aluminium oxide are known, but there is only one stable modification at all temperatures up to the melting point; the rhombohedral α-Al_2O_3. The usual, gas tight tubes, crucibles, and so on are reported to contain 99.6 to 99.7 weight% Al_2O_3, and the melting point should then be close to that of pure alumina: 2054 °C. The maximum useful temperature, however, is considerably lower. It appears that alumina exhibits some form of pre-melting; at temperatures around 1900 °C the material shows hardly any mechanical strength. The maximum useful temperature may be set at 1800 °C.

As evident from Figure 5.1 (p. 132), alumina – is thermodynamically markedly more stable than silica. It should be noted that the activity of silica in mullite is nearly the same as that of pure silica at the same temperature; for this reason, alumina should be preferred whenever the presence of silica is unwanted. This concerns (among other things) insulation and protection tubes for noble-metal thermocouples (cf. p. 75).

Apart from this, alumina offers no particular advantage compared to mullite-based materials for temperatures up to 1600 °C, while the cost of alumina is much higher. In fact, mullite-based materials may offer some advantages, in particular as regards thermal shock or steep thermal gradients, see Section 5.1.8.

[1] W. Haldenwanger Technische Keramik GmbH, Germany; a member of the Morgan Crucible Co., England.

5.1.4 Magnesia, MgO

Refractories based on magnesia are used on a large scale industrially, primarily in the iron and steel industry (see, e.g. Seltveit, 1992). In the laboratory, on the other hand, materials of essentially pure MgO are used only for special purposes. Tubes of dense-sintered magnesia would be expected to be prone to cracking because of the high coefficient of thermal expansion.

Magnesia crucibles are used where a 'basic' material is required. Fine powders of MgO may be pressed and sintered to reasonably dense products at temperatures around 1500 °C, but the shrinkage may cause problems. In contact with carbon or graphite, the materials react and disappear as $Mg(g) + CO(g)$ with $P_{tot} = 1$ bar around 1800 °C (cf. Figure 5.1).

Magnesium oxide powder absorbs moisture and is slowly converted to $Mg(OH)_2$, although it is not nearly as hygroscopic as calcium oxide. MgO is used for electrical insulation in MIMS thermocouples (cf. p. 77).

5.1.5 Beryllia, BeO

Dense-sintered beryllium oxide is noted for its high thermal conductivity. At the same time it shows good resistance against reaction with carbon. For these and other reasons it was formerly considered a promising ceramic material for various applications. Unfortunately, powdered BeO is very poisonous, particularly in the form of dust or vapours that may give severe lung disease (berylliosis). Water soluble beryllium compounds applied to the skin may give skin disease. Thus a number of ceramic manufacturers discontinued the production of beryllia ware, and it now finds only limited applications, primarily in the nuclear industry.

5.1.6 Zirconia, ZrO_2

This oxide appears in three different crystal forms:

$$ZrO_2(\text{monoclinic}) \underset{1000-1200\,^\circ C}{\rightarrow} ZrO_2(\text{tetragonal}) \underset{\sim 2300\,^\circ C}{\rightarrow} ZrO_2(\text{cubic}).$$

The transition from monoclinic to tetragonal is accompanied by a volume increase of about 7% with resultant cracking, so that pure ZrO_2

cannot be used as a ceramic material. It has been found, however, that a suitable addition of a lower-valent oxide stabilizes the cubic structure. About 10% of CaO is common, while Y_2O_3 may also be used. Such 'stabilized zirconia' is very refractory and resistant against thermal shock, thus it is used industrially in particularly exposed parts such as nozzles for liquid steel.

The addition of a lower-valent oxide also causes another effect. When a lower-valent cation replaces Zr^{+4} in the cation lattice, a corresponding vacancy is created in the anion lattice to preserve neutrality. Vacancies in the oxygen lattice give increased mobility for the oxygen ions, with the result that the material behaves like an oxygen ion conductor at temperatures of 500–600 °C and higher. This sort of oxide material has found various applications as 'solid electrolytes' in electrochemical cells. Stabilized zirconia may be used in cells for determination of the oxygen potential (or the oxygen partial pressure) in high temperature chemistry and metallurgy. The oxide is commonly used in the form of a gas-tight tube with closed bottom, with a known oxygen potential on the inside and the unknown on the outside of the tube. Another application is the use as solid electrolyte in fuel cells. Dahl *et al.* (2007) studied the densification of yttrium-stabilized zirconia by three different sintering methods, with the aim of obtaining improved electric conductivity at moderate cell temperatures.

Yet another aspect of stabilized zirconia is its resistance against reduction by carbon, related to the fact that zirconium does not form a suboxide.

5.1.7 Thoria, ThO_2

This oxide has an even higher melting point than zirconia, and also a greater thermodynamic stability. In contrast to zirconia it occurs only with a cubic structure, thus 'stabilization' is not necessary. As for zirconia, addition of a lower-valent oxide gives markedly increased electrical conductivity.

Thoria with CaO or Y_2O_3 in solid solution has found some application as a solid electrolyte, in particular for the measurement of very low oxygen potentials (P_{O2} in the range of 10^{-20} to 10^{-30} bar) where stabilized zirconia cannot be used. Note that thorium and its compounds are radioactive.

5.1.8 General Notes on Materials' Properties

The refractory oxides generally may be considered ionic compounds. They melt congruently, with a certain mobility of the ions also in the solid state at elevated temperature. As a consequence, when an article is shaped by compression of oxide powder and then fired at sufficient temperature, sintering will occur, with shrinking of the dimensions until eventually a body with near-theoretical density is obtained.

On the other hand, the nitrides and carbides discussed in the next sections are covalent structures. They melt incongruently or not at all; the mobility of each atom in the structure is very limited, and it is next to impossible to produce dense bodies of these materials by sintering at normal pressures.

Returning to oxide materials, we may ask about properties of particular interest for a specific application, for example, as a furnace tube in a wire-wound furnace. We assume that the furnace tube must be dense (gas tight); apart from that there are no special requirements as to mechanical strength and so on. It is a common experience, however, that furnace tubes of more than 5–6 cm diameter have a tendency to crack as a result of the steep thermal gradient from the hot furnace to the cold ends of the furnace tube. This leads us to consider the thermal shock resistance.

Various *thermal shock resistance parameters* have been proposed, but we will stick to the simplest expression:

$$R = \frac{\sigma(1-\nu)}{\alpha E} \tag{5.1}$$

σ = strength of the material. ν = Poisson's ratio ($\sim$0.2 for ceramic materials).
α = thermal expansion coefficient. E = elastic modulus.

The parameter R has the dimension of temperature (or rather a temperature difference) but we will consider it only as a qualitative expression. We may use it for a comparison between alumina and mullite.

For sintered alumina (Alsint), $\sigma = 300$ Mpa, $\alpha = 7.8 \times 10^{-6}\,\mathrm{K}^{-1}$, and $E = 370$ Gpa. For a mullite material (Pythagoras) the corresponding figures are 120 Mpa, $5.4 \times 10^{-6}\,\mathrm{K}^{-1}$, and 110 Gpa.[2] Inserted in Eq. (5.1),

[2] All data from Haldenwanger, loc. cit.

this gives R = 83 and 162 K for the two materials, respectively. Thus the numbers confirm experience from the laboratory, that sintered alumina is more prone to cracking than mullite materials under the same conditions of thermal gradients.

The same comparison may also be stated in simpler terms. It is seen from the data that alumina has a somewhat higher coefficient of thermal expansion but the big difference lies in the elastic modulus, 370 versus 110 Gpa. A certain stress, caused by a temperature gradient in the material, will be taken up by elastic strain in a 'soft' material, while a 'hard' material may crack. Thus, alumina may crack in spite of its higher strength.

An alternative thermal shock resistance parameter R' also includes the thermal conductivity λ of the material. The thermal conductivity of alumina is around ten times that of Pythagoras (26 and 2 $W\,m^{-1}\,K^{-1}$, respectively)[2] but experience indicates that this difference is of secondary importance as regards the tendency to cracking. Hence the simplest expression R is preferred.

In a different context the high thermal conductivity of alumina may be a disadvantage. For instance, the tube furnaces in Figures 2.5 and 2.6 (pp. 25–26) are shown with flanges and gaskets at both tube ends. Using alumina tubes it is likely that the rubber gaskets will be damaged by the hot tube ends, caused by the heat flux along the tube.

5.2 CARBIDES

The carbides belong to a larger group of ***non-oxide refractory materials***, comprising essentially carbides, nitrides and, to a more limited extent, borides. Various texts treat these materials as one group. Thus, Pierson (1996) has presented a handbook of refractory carbides and nitrides, while the compilation edited by Weimer (1997) considers carbide, nitride and boride materials, in particular their high temperature syntheses including furnace design. In the following we consider some of the more common carbides separately, and in the next section, the corresponding nitrides.

5.2.1 Silicon Carbide, SiC

The only solid compound in the system Si-C is the hard and brittle SiC. It is unique among the non-oxide ceramic materials in that it is produced

in large tonnages, and it is used industrially in a number of fields. Thus a general survey may be in place.

The production process will be briefly reviewed (Motzfeldt, 1993; Guichelaar, 1997). The starting materials, mainly silica sand and coke (and eventually some wood or sawdust) are lumped onto a large bed (some 3 or 4 m wide and 10 to 25 m long) with a graphite core placed along the centre of the charge, and graphite electrodes at both ends. The bed is resistance-heated by passing a high amperage current through the core (some 2 to 5 MW power). The overall chemical reaction may be written

$$SiO_2(s) + 3C(s) = SiC(s) + 2CO(g) \qquad (5.2)$$

where the equilibrium value $P_{CO} = 1$ bar at 1520 °C. Considerably higher temperatures are needed, however, to achieve the desired recrystallization to coarse SiC.

After one or two days the innermost part of the bed has reached some 2500 °C. The current is then discontinued, and after a few days of cooling, the bed is excavated. The innermost part then consists of pure graphite, then follows a layer of coarsely crystalline α-SiC which is the most valuable part of the product. Further out is found the less well crystallized material that may be used to produce silicon carbide bricks and as additions in the steel industry. The outermost zone contains material which is only partly reacted and is returned to the next batch. The process means rough work, but it is still the best method. The world production is estimated to be close to 1 million tons annually, of this an estimated 400 000 tons goes to abrasives and materials.

Properties. Pure SiC is golden yellow or greenish, but the industrial material may vary from dark green or blue to black, depending on the doping effects of aluminium or nitrogen. The crystalline product from the industrial process is always hexagonal α-SiC. When produced at lower temperatures, on the other hand, the cubic β-SiC is usually formed. From this one might conclude that the two are respectively low- and high temperature forms, but this may not be correct. Knippenberg (1963) concluded that the transformation $\beta \rightarrow \alpha$ is irreversible, and thus that α is the stable form at all temperatures.

Differences in the tabulated thermodynamic data for the two forms are too small to be significant.

Structure. In silicon carbide, each C-atom is surrounded by 4 Si-atoms and vice versa (as one would expect from the known tetrahedral configuration around both C and Si). Stacking of these CSi_4 (or SiC_4) tetrahedra with all of them pointing the same way results in the cubic β-SiC. Stacking with every second tetrahedron turned by 180° results in the hexagonal 2H α-SiC, where 2 stands for the number of layers before repetition and H stands for hexagonal. But numerous alternative stacking sequences are possible, resulting in a number of closely related structures that are all hexagonal or rhombohedral. These represent the many 'polytypes' of α-SiC. The distinction between different polytypes is of importance for semiconductor applications; for other uses it is of less importance.

Decomposition Temperature. Silicon carbide does not melt, but according to Scace and Slack (1959) it decomposes peritectically at $2830 \pm 40\,^{\circ}C$ to liquid Si with 19 atom% C, plus solid C.

Divergent data appear in the literature as regards both the peritectic temperature and the solubility of carbon in liquid silicon. The compilations of Moffat (1984), Massalski (1990) and Landolt-Börnstein (1992) all report the peritectic point at $2545 \pm 40\,^{\circ}C$ and 27 atom% C. This is taken from the review paper by Olesinski and Abbaschian (1984) who in turn took the data from a rather obscure paper by Dolloff (1960).

On the other hand, the review of Durand and Duby (1999) shows that the results of Oden and McCune (1987) and of Kleykamp and Schumacher (1993) are essentially in agreement with those of Scace and Slack, while the data of Dolloff are way off.

An explanation may be as follows: at the high temperatures in question, silicon has a significant vapour pressure. The silicon vaporization causes difficulties in optical pyrometry unless it is suppressed by an overpressure of inert gas. The experiments of Scace and Slack (1959) were done under 35 bar of argon, while the works of other authors were apparently done at 1 bar only. To quote from Dolloff (1960, p. 16): 'The (liquidus) line could not be determined above 2600 °C since the excessive vapour pressure of silicon at this temperature would result in prohibitive losses of material.'

Abrasives. Silicon carbide is among the hardest substances known, and it is extensively used as an abrasive. For this purpose the coarse α-SiC crystals are crushed, milled and classified to give high-quality abrasive powders, used in a number of industrial applications. The process of crushing, milling and screening to obtain micron-sized powders increases the value of the original silicon carbide by a factor of ten or more. One of the uses of this powder is in the slicing of ingots of ultra-pure silicon to produce silicon wafers for solar cells; a fast-growing market.

SiC Ceramics. As indicated above, it is typical for covalently bonded compounds that they do not melt congruently, and they do not sinter willingly. The coarser ceramic products, such as silicon carbide bricks for the lining of metallurgical furnaces, usually contain a binder phase of silica (or of silicon nitride, cf. below). The finer ceramic articles use fine powders to start, and various proprietary dopants to promote sintering. Still most of the commercial SiC articles have some 10% porosity (or more), but dense, pressureless sintered SiC articles are also on the market. Another approach is the silicon nitride bonded silicon carbide, usually produced by firing the silicon infiltrated material in a nitrogen atmosphere.

Both the carbide and the nitride may also be produced in the form of whiskers and fibres, to be used as reinforcement in composite materials (cf. Weimer 1997, pp. 409–453).

Typically, the silicon carbide based ceramic materials show high mechanical strength and good thermal shock resistance. In contrast to oxide ceramics they are practically free of creep or sagging under load at elevated temperatures.

Sidelining in Aluminium Cells. Traditionally the sidelining was made from carbon and chamotte, but improved cell design led to requests for better materials. After years of testing and industrial experience, the silicon nitride bonded silicon carbide qualities have turned out to be the preferred material for use in aluminium cell sidewalls (Sörlie and Öye, 2010, p. 253).

Oxidation in Oxygen. Silicon carbide is not thermodynamically stable in air or oxygen; it should react to carbon dioxide and silica. In practice it is quite stable due to a protective layer of silica. The temperature limit

for use of silicon carbide ceramics, including heating elements, is about 1600 °C, as determined by its resistance to oxidation.

A number of textbooks distinguish between 'active' and 'passive' oxidation. The active oxidation takes place at very low pressures of oxygen (1 millibar or less) where the oxidation goes to the volatile suboxide SiO(g) rather than the protective SiO_2. Under normal conditions (total pressure ~1 bar) the suboxide formation is negligible, and only the 'passive' oxidation is considered here.

For comparison, we consider first the oxidation of elemental silicon in oxygen. It is generally accepted that the process is diffusion controlled. With the silica film thickness s at the time t, we have the equation $s\ \mathrm{d}s/\mathrm{d}t = k$ where k is a rate constant. Assuming $s = 0$ for $t = 0$, we arrive at the familiar 'parabolic law' $s^2 = 2kt$ or $k = s^2/2t$.

Turning now to the oxidation of silicon carbide, we know that the protective layer is the same as for silicon. Assuming that the rate determining step in both cases is the diffusion of oxygen through the silica layer, one would expect that the rate constant k is the same in both processes (except for a factor of 2 to account for the oxidation of carbon):

$$\mathrm{SiC(s)} + 2\mathrm{O_2(g)} = \mathrm{SiO_2(s)} + \mathrm{CO_2(g)} \qquad (5.3)$$

Furthermore it might be expected that both processes may be correlated to data for the permeation of oxygen through silica glass. Based on the experimental data available at the time, Motzfeldt (1964) found that all three sets of data correlate surprisingly well over the whole temperature range from 850 to 1600 °C.

The experimental data for silicon carbide referred to by Motzfeldt were obtained for SiC grains, equivalent to polycrystalline materials. Single-crystal SiC, on the other hand, shows different rates of oxidation on the different crystal faces, and the rate-limiting steps may also be different, compare Song, Dhar and Feldman (2004).

The maximum temperature of use for SiC materials is set by the reaction

$$2\mathrm{SiO_2(s)} + \mathrm{SiC(s)} = 3\mathrm{SiO(g)} + \mathrm{CO(g)} \qquad (5.4)$$

The result of this reaction is evidenced as large gas bubbles in the silica skin if a silicon carbide heating element is overloaded. With a heating

element of molybdenum disilicide, on the other hand, this sort of reaction does not happen, hence the higher temperature limit of the latter (cf. Chapter 2, p. 27).

Oxidation in Water Vapour. It had already been observed 50 years ago that the oxidation of silicon carbide in a mixture of oxygen and water vapour proceeds more rapidly than in dry oxygen. Various volatile hydrous oxides were proposed at the time, but the exact mechanism remained in doubt.

To elucidate the matter, Cappelen, Johansen and Motzfeldt (1981) carried out oxidation experiments with a sample of 20 mesh SiC grains placed as a permeable plug in the central zone of an alumina tube. All runs were done with flowing gas at 1500 °C. Preliminary experiments with a Pt tube fitted as a condenser at the outlet revealed no weight gain, that is no condensate. Hence the most probable reaction with water vapour may be written

$$SiC(s) + 3H_2O = SiO_2(s) + CO(g) + 3H_2(g) \qquad (5.5)$$

To substantiate the mechanism, a gas train was fitted to the furnace (shown in Figure 2.8, p. 31), enabling the quantitative determination of CO(g), CO_2(g) and H_2(g). Oxidation was done alternately with $N_2 + O_2$, $N_2 + H_2O$, and $O_2 + H_2O$, each mixture with equal partial pressures of the two components. The results fitted the above reaction scheme perfectly.

The results may be summarized as follows: (i) Initial oxidation in $N_2 + O_2$ followed the usual parabolic law. (ii) In $N_2 + H_2O$ the oxidation proceeded roughly a factor of ten faster, and nearly linearly. (iii) Reverting to $N_2 + O_2$ the rate dropped almost to the previous level. (iv) Oxidation in $O_2 + H_2O$ showed a rate very similar to that of $N_2 + H_2O$.

Similar observations had already been made some 15 years earlier regarding the oxidation of *pure silicon* in oxygen and in water vapour, see Deal and Grove (1965). The explanation lies in the much larger solubility of water in vitreous silica. The dissolution may formally be written

$$H_2O + SiO_2 = SiO(OH)_2 \qquad (5.6)$$

where the OH^- groups are distributed at random in the lattice, disrupting the —O— bonds.

The effect of water vapour is of practical importance in all types of high temperature materials where silica serves as the protection against oxidation. Hence the subject has been extensively studied, see Opila (2003).

At elevated temperatures, water vapour may also lead to volatilization of oxidic materials, and eventually to the disruption of protective oxide layers. To take one example, the reaction

$$SiO_2(s) + 2H_2O(g) = Si(OH)_4(g) \qquad (5.7)$$

has been studied by mass spectrometry and by transpiration experiments. According to Opila *et al.* (2006), the equilibrium constant for reaction (5.7) is in the range 10^{-6} to 10^{-5} at the temperatures in question. Significant volatilization at these low partial pressures may occur in a rapidly flowing gas, as on the vanes of a gas turbine. Under ordinary conditions, however, the gaseous hydroxyl species are probably of little importance.

SiC as a Semiconductor. This topic is outside the scope of the present text, but merits a short mention. After a somewhat slow start, the interest in SiC for electronic purposes has increased steadily since about 1980, and has led to semi-annual conferences. The 13th international conference on silicon carbide and related materials was held in Nürnberg in 2009 (Bauer *et al.*, 2010). A readable account of the field has been given by Saddow and Agarwal (2004).

5.2.2 Aluminium Carbide, Al_4C_3

This compound is included in the presentation mainly to preserve the balance between carbides and nitrides. Al_4C_3 is of hardly any interest as a refractory material in the ordinary sense. Crucibles of aluminium carbide have been made and used for special purposes, but the material is very hygroscopic. When left in the open, aluminium carbide will react with the moisture in the air:

$$Al_4C_3(s) + 8H_2O(g) = 4AlO(OH)(s) + 3CH_4(g) \qquad (5.8)$$

Next morning, the material is transformed to a heap of hydrous alumina. The same is also seen with articles of graphite when partly reacted with alumina.

Aluminium carbide could be produced from alumina by carbothermal reduction at temperatures above 2000 °C, but the process has never been tried industrially. For experimental purposes the carbide may be produced by direct reaction between liquid aluminium and powdered graphite at about 1600 °C. The process is tedious, however, because the carbide first formed acts as a protective layer around each graphite grain, and repeated grinding and re-heating is necessary.

Aluminium carbide crystals are golden yellow and scratch glass. At high temperatures, Al_4C_3 decomposes to a metallic liquid plus solid carbon, with the peritectic point at 2150 °C and 19 atom% C (cf. Motzfeldt *et al.*, 1989).

Various properties of Al_4C_3 and the related oxycarbide Al_4O_4C were studied by Hanssen (1983). She found, among other things, that the carbide is a p-type semiconductor with relatively high conductivity, while the oxycarbide is a poorly conducting n-type semiconductor. To our knowledge, none of these compounds have found any practical application so far.

5.2.3 Boron Carbide, B_4C

This compound is noted primarily for its extreme hardness; next to diamond and cubic boron nitride it is the hardest substance known, and at the same time it shows good fracture toughness. Boron carbide has a peculiar structure; the structural units are linear chains of three carbon atoms and groups of twelve boron atoms arranged at the vertices of a regular icosahedron, producing a three-dimensional boron network.

The phase diagram B-C shows a wide homogeneity range in the solid state (~8 to 23 atom% C), but B_4C melts congruently at the stoichiometric composition, with a melting point of ~2450 °C (Massalski, 1990).

Boron carbide is produced from boron oxide and carbon at temperatures around 2500 °C. The coarsely crystalline product has to be intensively milled, yielding fine powders that are used in part as abrasives and in part for shaping and sintering articles that require extreme hardness, such as mortars for hard specimens. It is of limited use as a refractory.

5.3 NITRIDES

In analogy with the oxides, the nitrides are compounds of a (non-volatile) metal and a volatile gas. The oxides in general are so stable that the dissociation into metal + oxygen was not taken into consideration in the above discussion. As regards the nitrides, on the other hand, the thermal decomposition sets an upper limit of temperature for their use (dependent upon the total gas pressure and the partial pressure of nitrogen in the ambient atmosphere). Figure 5.2 shows the equilibrium nitrogen pressures as functions of temperature for three nitrides commonly used as refractory materials.

5.3.1 Silicon Nitride, Si_3N_4

This is a more recent material than the carbide, and it is produced in kilogrammes, rather than tons. Because of the prospects of obtaining

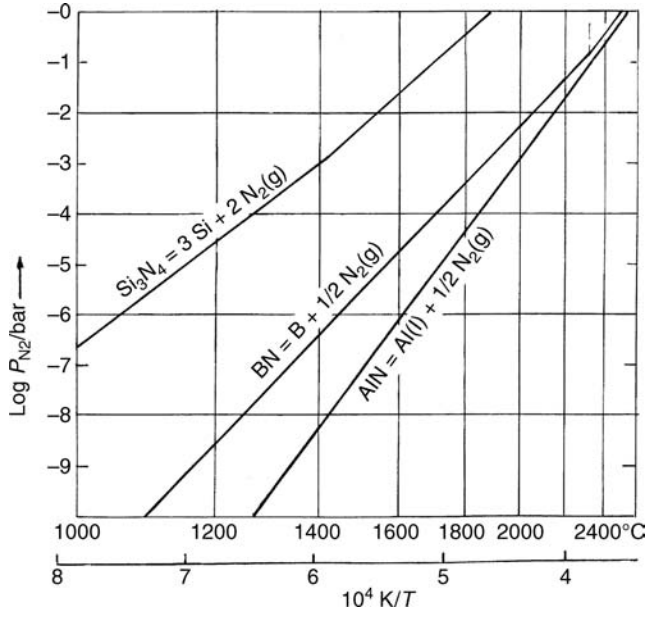

Figure 5.2 Equilibrium nitrogen pressures as functions of temperature for the thermal dissociation of some nitrides. (Data from NIST-JANAF Thermochemical Tables, 1998.)

strong, hard and heat-resistant materials of construction, silicon nitride and related materials have been the subjects of extensive research since about 1960; compare Jack (1976), Chen *et al.* (1993) and Hoffmann, Becher and Petzow (1994). This line of research is still continuing, see Belmonte, Miranzo and Osendi (2007).

Production. Silicon nitride may be produced directly from silica by reduction with carbon in a nitrogen atmosphere (endothermic), but more usually it is made by reaction between silicon powder and nitrogen (exothermic).

Silicon nitride occurs in two modifications, α- and β-Si_3N_4, both with fairly complicated crystal structures. When synthesized from silicon plus nitrogen at 1200–1400 °C, both modifications are formed simultaneously in varying proportions, presumably by two different reaction mechanisms. Most probably the α-Si_3N_4 is formed by a mechanism involving an Si-bearing vapour species, while β-Si_3N_4 is formed by reaction between N and condensed Si. It was formerly believed that the α-form is dependent upon a minor content of oxygen for stabilization, but Kari Blegen (1975, 1976) proved conclusively that both forms appear also in the absence of oxygen. On the other hand, in the presence of a suitable partial pressure of oxygen, the compound Si_2ON_2 is formed, with refractory properties comparable to those of the β-nitride, which is the stable form at all temperatures. The kinetics of nitridation of silicon powder were further studied by Myhre (1989), substantiating and completing the previous observations. Complete nitridation is difficult to achieve in a single step because of the formation of a protective layer of nitride around each grain.

It is difficult to grow Si_3N_4 single crystals, the products from synthesis appear as grey powders.

Properties and Uses. Silicon nitride does not melt, but it dissociates to liquid silicon and gaseous nitrogen, with $P_{N2} = 1$ bar at 1880 °C. The dissociation limits its use as a high temperature refractory, and the development work has mainly been focused on mechanical properties at more moderate temperatures.

It appears that the α form is preferred as starting material for ceramic work, since the transformation $\alpha \rightarrow \beta$ may aid in the sintering process. Sintering of covalent compounds, however, remains difficult, and various 'sintering aids' have to be used. Peng *et al.* (2006) used

additions of $MgSiN_2$ and found that a composite of α- and β-Si_3N_4 gave superior mechanical properties. More usually, oxides such as MgO, Al_2O_3 and Y_2O_3 have been added. As regards sintering techniques, it appears that spark plasma sintering (SPS) may open new possibilities for Si_3N_4 materials, compare Thompson (2002) and Shen *et al.* (2002).

It has been found that considerable fractions of Al^{3+} and O^{2-} ions can enter the lattice while still retaining the β-Si_3N_4 structure. This has led to a series of compositions known as *sialons* with interesting properties, see Section 5.3.3 below.

The oxidation resistance of silicon nitride materials in oxygen is similar to that of silicon carbide, as shown in the careful oxidation studies of Persson, Käll and Nygren (1993) and the review by Narushima *et al.* (1997). Their behaviour in water vapour is also similar to that of SiC, according to Opila (2003).

Silicon nitride may have a future in mechanical engineering, it has also been a successful bonding material in silicon carbide refractories, but it has not gained much acceptance as a refractory in its own right.

However, a new application for pure Si_3N_4 is just emerging. Until now, the crystallization of silicon for solar cells has universally been performed in crucibles of vitreous silica. Typical crucibles today may have square form, some 70×70 cm. These crucibles are costly, and they can be used only once. A recently formed Norwegian company[3] aims at producing silicon nitride crucibles that shall perform equally well or better, and may be re-used at least ten times. An interesting part of the process is that the crucibles are shaped from Si powder alone, and subsequently nitrided in nitrogen. The crucible walls remain porous, and the performance thus rests on the non-wetting of Si_3N_4 by molten Si. The development work is going on, and if successful it may mean important progress for the solar industry.

5.3.2 Aluminium Nitride, AlN

Fifty years ago, Long and Foster (1959) had already proposed aluminium nitride as a promising material for the containment of liquid

[3] CruSiN A/S, N-7491 Trondheim, Norway.

aluminium. It appears, however, that AlN was never established as a crucible material for industrial use. Major interest today centres around its properties as an electrically insulating material with a high thermal conductivity, for use in integrated circuits. We will start, however, with an older approach.

The Serpek Process. One obvious route is by carbothermal reduction:

$$Al_2O_3(s) + 3C(s) + N_2(g) = 2AlN(s) + 3CO(g) \qquad (5.9)$$

This, in essence, is the Serpek process for the manufacture of aluminium nitride, patented by Ottokar Serpek in 1905, see, for example, Richards (1913). The ultimate aim of the process was to make ammonia by subsequent hydrolysis of the nitride, or rather, ammonium sulphate by treatment of the nitride with sulphuric acid.

In this context a story may be retold, related to early electrochemical industry in Norway. It was at a time when the supplies of natural nitrogen fertilizers were dwindling, and the Birkeland–Eyde process, producing nitrogen oxides in an electric arc, was just in its infancy. The French company Pechiney had faith in the Serpek process and established the subsidiary Societé Générale des Nitrures. In order to utilize the hydroelectric power available in Norway, a joint French–Norwegian company was established in 1912 under the name 'Det Norske Nitridaktieselskap'. Work on the site in Eydehavn, some miles east of Arendal, began immediately. In the meantime, however, the French experiments with the Serpek process continued, and in 1913 it was concluded that the process would never be economical. Thus it was decided that the buildings already erected should be converted to aluminium electrolysis, and the production of aluminium started in May 1914. The name DNN, however, was retained, even though there was never any nitride produced on the premises (cf. Kollenborg, 1962).

It should be noted, finally, that the same route to ammonia has recently been proposed anew by Gálvez, Halman and Steinfeld (2007), using concentrated solar energy as the source of heat for the carbothermal reduction.

Production of AlN. Long and Foster (1959) produced their nitride by striking an electric arc between aluminium electrodes in a chamber filled

with nitrogen. This was a small-scale batch process only, not suited for industrial production.

The reaction $Al(l) + 1/2\,N_2(g) = AlN(s)$ is strongly exothermic and would appear straightforward as an industrial process, but apparently it is not that simple. For use as a starting material for ceramics, the nitride powder should have extremely small grain size, and at the same time it should contain no unreacted aluminium and no oxide. Starting with aluminium powder it will inevitably contain aluminium oxide, while the reaction with coarser pieces may leave cores of unreacted aluminium. Fu *et al.* (2005) have experimented with a self-propagating high temperature, high-pressure synthesis, starting with a mixture of Al and AlN powders ignited in nitrogen at 80 bar, with highly crystalline AlN powders as the combustion product.

The other main industrial method is the carbothermal reduction of alumina, essentially represented by Eq. (5.9). It is known from the carbothermal production of aluminium, however, that the oxycarbide Al_2OC, which is not a stable phase in the Al—O—C system, appears as a separate phase as soon as some nitrogen is present in the system. Conversely, it is to be expected that the oxycarbide also appears in the synthesis of the nitride, causing impurities. The atom pairs O—C and N—N are iso-electronic, and the two compounds AlN and 'Al_2OC' are isomorphic.

In addition to these two main methods for preparing AlN, a range of other methods have been suggested. A thorough review of synthesis methods for AlN has been given by Haussonne (1995), including methods for purifying the powders produced, and treatments for making the surface of each particle less sensitive to air or moisture. Because of the technological interest, a large number of the suggestions and methods have been patented.

Properties and Use. It was mentioned in the introduction that aluminium nitride is of special interest because of its high thermal conductivity. The thermal conductivity of AlN ceramics, however, depends on its purity. An impurity content of 1% of oxygen in the starting powder may lead to 30% lower thermal conductivity according to Haussonne (1995). Motzfeldt (1997) indicated that the oxide may be removed by heat treatment according to the net reaction

$$Al_2O_3 + 4\,AlN = 3\,Al_2O(g) + 2N_2(g) \qquad (5.10)$$

As it turns out, this reaction was suggested and experimentally verified already by Slack and McNelly (1976, 1977) when they developed methods to produce pure single crystal AlN from the vapour phase. The thermal conductivity of pure AlN between 0.4 and 1800 K was published by Slack *et al.* (1987). Their value at 300 K is 320 $W\,m^{-1}\,K^{-1}$. This is on the level of copper and pure aluminium, and is outstanding for a ceramic material.

At the same time AlN is a good electric insulator, and it has a coefficient of thermal expansion about $2.5 \times 10^{-6}\,K^{-1}$, that is, close to that of silicon ($2.6 \times 10^{-6}\,K^{-1}$ at 300 K). Hence it is a leading candidate for the insulation, or 'packaging' of integrated electronic components, where the evolved heat must be dissipated.

The sintering of pure AlN ceramics, however, gives problems. Some 'sintering aid' is usually added; CaO or Al_2O_3 plus Y_2O_3 are most common. The idea is to obtain a small amount of liquid phase at the firing temperature, thus attaining liquid-phase sintering. A balance has to be struck between the gain in density and the loss in thermal conductivity by the various additions and sintering methods. Values of the thermal conductivity for commercial AlN-ceramics are in the range 100 to 200 $W\,m^{-1}\,K^{-1}$, but this is still high. (The corresponding value for alumina is 25 to 30 $W\,m^{-1}\,K^{-1}$.)

The crystal structure of AlN is isomorphic with that of 2H-SiC, and the two form homogeneous solid solutions above 2000 °C (Tian and Virkar, 1996). In contrast to silicon carbide, pure AlN normally occurs only with the 2H structure (cf. SiC, p. 141). However, with small additions of alumina and heating above 1900 °C, a number of polytypes appear. The materials thus obtained may be considered composites of different AlN polytypes, with potentially interesting mechanical properties (Tangen, 2005).

It was mentioned above that Long and Foster (1959) primarily considered AlN as an interesting material for metallurgical purposes. It appears, however, that it has never been used on a larger scale; this may be due to the lack of a low-cost production method. On the other hand, the interest within the semiconductor industry is increasing, in particular as regards the production of high-purity or single-crystal AlN, compare Slack *et al.* (2004) and Bondokov *et al.* (2006).

5.3.3 Sialons

The name is shorthand for the quaternary system Si—Al—O—N. Restricting the consideration to the normal valences, with equivalent amounts in each corner, we have the square

$$Si_3N_4 \text{ —} Al_4N_4 \text{ —} Al_4O_6 \text{ —} Si_3O_6.$$

This is an interesting system, but one that is well outside the frame of the present communication. Thus, it is only briefly summarized here.

The studies, originally a British initiative, started around 1960 with the intention of finding non-metal materials of construction that could be used at higher temperatures than the metal alloys. The objective is clear: raising the maximum temperature inside a combustion engine means raising its efficiency, according to the Second Law of Thermodynamics. Furthermore, ceramic components will be lighter than the corresponding metal parts, giving another gain in efficiency.

The starting point was silicon nitride, which was found to give light and strong materials, and yet, according to one of the pioneers in the field, K. H. Jack (1976, 1988); ' . . . *it is only the first of a wide field of nitrogen ceramics, other members of which offer better prospects for technological exploitation*.'

The square phase diagram is shown to contain a large number of phases with different properties. Enlarging the field by adding MgO, Y_2O_3 and other 'sintering aids' gives a wealth of new materials. They may be sufficiently hard and tough to replace hard metals as cutting tools, or they may be strong enough to replace steel in moving machinery, where low weight of the component is an advantage. Thus, β-Si_3N_4 and its derivatives have been considered 'the materials of the future' for advanced structural application.

5.3.4 Boron Nitride, BN

This nitride may be synthesized in the same way as AlN, by heating of the oxide plus carbon in a nitrogen atmosphere. More commonly it is produced by reaction between molten boric oxide and ammonia, or the oxide plus urea or some other organic nitrogen compound, in a nitrogen

atmosphere. The milled product is a light-grey powder that may be shaped by ceramic techniques. Thin films of boron nitride may be obtained by chemical vacuum deposition from boron trichloride and some nitrogen precursor.

Boron nitride has a hexagonal structure similar to that of graphite with sheets of hexagonal rings, except that in boron nitride the B and N atoms alternate in the ring. A further structural difference is that the sheets are in register, that is each B—N ring is directly on top of the one underneath.

The material is soft, has a low friction against steel, and resembles graphite in many respects. However, the polar B—N bonds do not give delocalized electrons, and as a consequence boron nitride is colourless (white) and electrically insulating. In analogy with AlN it has a high thermal conductivity.

In compact form the light-grey, hexagonal boron nitride is of considerable interest as a refractory material in the laboratory. It is easily machined, hence it finds applications for parts that should be electrically insulating, thermally conducting and not easily wet by molten metals. From Figure 5.2 (p. 148) it is seen that it may be used in a high vacuum to 1200–1300 °C, or in an inert atmosphere to about 2000 °C.

Boron nitride powder, on the other hand, is used as a 'solid lubricant', which may also be used for moving parts in a high vacuum.

Boron nitride also occurs with a cubic structure analogous to that of diamond. In analogy with diamond, the conversion hexagonal–cubic takes place only at high temperatures and very high pressures. The high temperature is necessary for kinetic reasons, that is, to make the substance reactive. But then we have the Clapeyron equation for phase changes:

$$\frac{dP}{dT} = \frac{\Delta S_{trans}}{\Delta V_{trans}} \tag{5.11}$$

Here, ΔV_{trans} is certainly negative for a transition that is caused by high pressure. Most often ΔS_{trans} is also negative for such a transition. But from Eq. (5.11) it is then seen that dP/dT is positive. This means that a higher temperature necessitates a higher pressure to bring about the transition. Thus, for both diamond and cubic boron nitride, pressures of 50 to 100 kilobar are necessary, in combination with temperatures of 2000 to 2500 °C.

5.4 CARBON AND GRAPHITE

5.4.1 Carbon: The Element

It is just element No. 6 in the periodic table, but it is the basic element for all life as we know it today. But it is also the general name for a more varied family of materials than any other single element. As a consequence of its versatility and its importance, the literature on *carbon* is very extensive and expanding every year (not counting carbon chemistry). A comprehensive survey of carbon materials is given by Pierson (1993), while Urry (1989) has given an entertaining account of its elementary equilibrium chemistry. The terminology of carbon as a solid has been compiled by Fitzer *et al.* (1995).

The thermodynamically stable form of carbon is ***graphite***. The structure of graphite may be described as planar sheets of fused hexagonal rings of carbon with sp^2 bonds, with weaker π bonds between each layer. In hexagonal graphite each layer is displaced from the one above or below, so that one carbon atom falls in the centre of the carbon ring immediately below (ABABA - - stacking). (In contrast, the layers in hexagonal boron nitride are stacked directly on top, AAA - - stacking, cf. p. 154.) Because of the layered structure, a graphite crystal is markedly anisotropic, with higher thermal and electrical conductivity along the sheets than in the c-direction. (The anisotropy, however, does not markedly influence the properties of the polycrystalline materials, cf. below.)

The ideal density of graphite is 2.25 g/cm^3, while real graphite materials hardly ever attain this value.

Graphite also occurs with every *third* layer superimposed (ABCABC -), this gives a rhomboedral structure. Rhomboedral graphite is never found in pure form but always in combination with hexagonal graphite. It is thermodynamically unstable, and usually reverts to the hexagonal form during heat treatment above 1300 °C.

Carbon/graphite does not melt at normal pressures, but sublimes with 1 bar total pressure at about 3700 °C. This vaporization without melting may be observed quite simply in an electric arc between graphite electrodes, while accurate determination of the temperature is more difficult. The dominant vapour species is C_3, with lower partial pressures of C_1 and C_2, as determined by mass spectrometry. A melting point has been estimated at 120 bar and 3850 °C (cf. NIST-JANAF, 1998).

Diamond is another allotrope of carbon, with sp^3 bonds giving the tetrahedral coordination, and a density of $3.50\,g/cm^3$. Ordinary diamond is cubic, and is considered the hardest substance known. Upon heating it converts to graphite and thus is of no value as a refractory.

A third form of carbon has been found more recently and has been a subject of research since its discovery in 1985. It may be found in various forms of soot and forms a class of ball- or dome-like carbon structures. It has been named fullerenes after the distinguished architect Buckminster Fuller, who designed the first dome built upon the same principle of pentagons and hexagons as found in the carbon molecules. The most prominent member of the class is the molecule C_{60}, with 12 pentagons and 20 hexagons (the numbers may be checked by observation on a modern football). Other shapes may be cylinders or tubes with domes at the ends; generally known as nanotubes because of their molecular dimensions (the distance across a graphite hexagon is 0.246 nanometres).

5.4.2 Occurrence of Carbonaceous Materials

Natural graphite is a soft and flaky mineral found in many parts of the world. It is mined and used for special applications. The majority of commercial graphite products, however, are made by heat treatment of carbon materials from various sources (see next section).

Diamonds are found as a mineral in various places, in particular in South Africa. Larger specimens are used as valuable gems, while the smaller may be used for abrasives. Nowadays, diamonds for industrial use are synthesized from carbon at high temperatures and pressures with the aid of a solid catalyst.

The overwhelming majority of carbonaceous material is found as coal beds in various places all over the world. Its prime use is as fuel to satisfy the ever growing global demand for energy, while a smaller part is refined to carbon materials. In this sense it is comparable to crude oil; most of it is consumed as fuel, while the less volatile components end up as tar, pitch, or petrol coke which in turn is used to produce graphitic materials.

The story of coal and oil, from its first formation until its excavation and consumption, is a fascinating one; it also touches on the hottest topics of our world today. It is believed that, some three billion (3×10^9) years ago, the atmosphere on the Earth consisted

predominantly of carbon dioxide. But at that time, some form of *life* occurred. The process of photosynthesis began and proved successful, with the conversion of carbon dioxide to organic matter and the simultaneous production of free oxygen. In the course of a billion years, the proportion of oxygen in the atmosphere increased from nothing to the present 20% while the contents of carbon dioxide dwindled to about 0.03%.

The carbon cycle as we know it consists of carbon dioxide assimilation and production of oxygen, but when living tissue dies and rots, the process is reversed and carbon dioxide is restored. And yet there is so little of it in the atmosphere today. This raises a question: where did the rest of the carbon dioxide go?

One type of capture took place in the oceans through reaction between the dissolved carbon dioxide and the dissolved calcium ions, forming solid carbonates. It has taken place directly, and also indirectly by the interaction with living organisms, forming calcium carbonate shells that remain when the organisms die. The precipitated carbonate silt has in time been converted to rocks of limestone. The mineral dolomite was probably formed at a later stage by exchange between $CaCO_3(s)$ and Mg^{2+} in the seawater, see Krauskopf and Bird (1995) p. 79 and 574.

Another mechanism had its origin in warmer periods with abundant plant life on Earth. Withering vegetation was only partly decomposed, and the carbon-rich remains accumulated. By the action of heat and compression they ended up as coal beds of varying quality, from brownish lignite to hard and black anthracite. Similar processes also took place with animal tissue, converting it to oil deposits.

Thus the formation of coal and petroleum must be considered lucky incidents that decreased the carbon dioxide content, making our present world habitable to beast and man. But this development, taking millions if not billions of years, is now being reversed by the excavating and burning of the same coal and oil in the course of just a few hundred years. It appears to be a problem with no immediate solution.

5.4.3 Carbon and Graphite

The first step in converting coal to carbon materials is a heat treatment, up to 1200 °C, to drive off volatiles. The product, coke, still contains most of the inorganic impurities present in the original coal. For this

reason, coke derived from anthracene may be adequate for coarser products only, while coke derived from the residue in petroleum refining, petrol coke, is preferred for production of graphitic materials.

Carbon Materials. For further processing to produce carbon materials, the coke is ground or milled and mixed with some 15% binder, usually coal-tar pitch. It is then moulded into the desired shape and baked at some 1200 °C.

The largest consumption of this type of carbon material takes place within the primary aluminium industry. In the aluminium electrolysis, the carbon anode serves as an electrode and at the same time is consumed as reducing agent. The annual world production of primary aluminium is about 30 million tons (2006), corresponding to a consumption of 12–13 million tons of anode carbon. Formerly, self-baking anodes of the Söderberg type were used, while modern cells use prebaked anodes.

The cathode in the aluminium electrolysis cell is also made of carbon, but the cathode should last unimpaired for a number of years. For this reason the requirements for the two types of carbon are different; the anode carbon is consumed and hence must be reasonably priced, while an extended lifetime for the cathode warrants a more expensive material, turning towards graphite. The sheer size of this industry has warranted extensive research and development to find the best carbon material for each purpose, compare Foosnæs and Naterstad (1993), Tkac (2007) and Sörlie and Öye (2010).

Graphitization. A number of processes take place within the material in the coking, including partial graphitization. For further processes the coke is ground, milled and mixed with a binder as above. The mixture is then moulded by extrusion or pressing, and baked at slowly increasing temperature up to 2500 °C or even higher. This graphitization process takes place in furnaces of the original Acheson type (similar to those described for the production of silicon carbide, p. 140) or nowadays also in medium-frequency induction furnaces.

Graphite Materials. All the steps, from selection of raw materials through crushing, milling and so on to the final baking, influence the properties of the product. 'Graphite' is thus a common designation for a whole range of materials, and the specific producer should be consulted with respect to the properties of a given product.

From the short description above it appears that moulded graphite is produced from carbon grains plus a binder, quite analogous to conventional ceramics. In analogy with ceramics it is found that the particle size of the grains has a marked influence on the properties of the product. For example, a specific grade of graphite with an average grain size of 75 μm had a density of 1.72 g/cm^3 and flexural strength of 28 Mpa, while a similar grade with grain size 10 μm had a density of 1.90 g/cm^3 and flexural strength of 77 Mpa (Pierson, 1993, p. 99). Thus, the reduced grain size resulted in a substantial increase in both apparent density and mechanical strength. It also led to a marked increase in the coefficient of thermal expansion, but this may be of less significance.

Generally speaking, coarse components like the electrodes in an arc furnace may be made from coarser (and less expensive) material, while a dense and fine-grained graphite should be selected for details machined to close tolerances. 'Dense' in this connection should not be mistaken for 'gas tight'; all conventional graphite products are porous and permeable. Gas tight graphite exists, but then as a special quality; see also vitreous carbon below.

Concerning the mechanical properties of graphite, it is noted that the bending strength *increases* with increasing temperature, up to about 2500 °C. This is in contrast to any metal and seems almost unnatural. The explanation is found in its similarity to ceramics. The bonding phase in graphitic materials is generally hard and stiff at room temperature, so that the material is subject to brittle fracture. With increasing temperature, the bonding phase becomes more flexible, so that fracture is avoided. From an elementary practical viewpoint, it is good to know that any design of graphite which is able to support itself at room temperature will not sag at any temperature within our range of interest.

This section concludes with a repetition: technically 'graphite' is a whole family of materials. Different companies use different designations for their qualities, and the producer's catalogues should be consulted for information on the properties of any specific grade.

5.4.4 Vitreous Carbon

Three-dimensionally cross-linked synthetic resins, such as phenolic or furan resins, do not easily graphitize. Heat treatment leads instead to a glassy form of carbon. The precursor polymer may be shaped by

standard plastic processing, taking account of the large shrinkage that will occur. Carbonization takes place in an inert atmosphere with very slow heating up to about 1000 °C, and further heating to some 1800–2000 °C.

The product is essentially vitreous, that is, hard and brittle like a glass, not to be shaped by ordinary machine tools. It has a low density (about 2/3 that of the ideal graphite crystal) and yet it is essentially impermeable to gases. The surface is non-porous and free of surface defects, and it possesses greater resistance to corrosion and oxidation than does normal electrographite (see Pierson, 1993, p. 134). It is used as vessels for chemical processing and crucibles for melting the more noble metals. The excellent thermal shock resistance permits high rates of heating and cooling.

5.4.5 Carbon Fibres and Graphite Felt

It was said in the introduction that carbon forms a large family of different materials, and this includes a variety of carbon fibres for various purposes. The fibres are generally produced by heat treatment and carbonization of synthetic thread or textiles. It is general knowledge that reinforcement of carbon fibres gives strength and stiffness to such items as golf clubs and ski poles as well as more advanced products. For the present purpose, however, we are particularly interest in graphite felt, used for thermal insulation in furnaces with graphite heating elements.

A retrospective may be in order at this point. It is now more than 50 years since my first graphite-tube furnace was put into operation. The thermal insulation at that time consisted of three thin-walled, concentric cylinders as radiation shields around the heating element (50 mm OD). The low-voltage transformer had a nominal capacity of 25 kW, but it got uncomfortably hot when the furnace should attain 2200 °C. Then, one or two years later, a salesman came around with the first samples of graphite felt. Once ordered and put to use (some 6 or 12 mm thickness) the power consumption fell to about 15 kW for the same temperature. Thus the introduction of graphite felt really meant a change in our work at that time.

Manufacturers usually distinguish between carbon and graphite in this context; the two types of felt having largely the same thermal

characteristics. One notable difference, however, is the contents of volatiles. The use of carbon felt in a high-vacuum furnace leads to a prolonged period of degassing and poor vacuum, hence graphite felt should be preferred (even when a high vacuum is not strictly required).

The thermal conductivity of graphite is generally low, but increases markedly with increasing temperature. The scanty information retrieved indicates that the thermal conductivity of graphite felt is in the same range as that of the fibrous Kaowool, see Figure 2.14 curves (3) and (4) on p. 39.

More exact data are not necessarily valuable to the designer. For one thing, the total power loss of a furnace depends markedly on the design. Also, the thermal loss observed for a furnace in argon will be considerably larger than in a vacuum at the same temperature. With helium it is still larger. Generally it is sensible for the user to provide a power source with ample capacity for the task in question.

5.5 REFRACTORY METALS

5.5.1 Base Metals and Alloys

Most commonly used high temperature metals are alloys containing nickel, chromium and iron, including the Kanthal alloys described on p. 14. Their main uses in our context are as wire or ribbon for electric heating elements, see Table 2.1, p. 14. Pure nickel is commonly used for crucibles, while heat resistant steels are available in sheet, rods, tubes, and so on. Another important use for our purposes is in thermocouples, see pp. 69–74.

5.5.2 Noble Metals

Above some 1200 °C in oxidizing atmospheres, one has to resort to noble metals. We recall the whole platinum group, including their melting points:

Ru	(2250 °C);	Rh	(1963 °C);	Pd	(1555 °C)
Os	(3000 °C);	Ir	(2446 °C);	Pt	(1768 °C)

It is seen that the melting points, and hence the hardness, increase from right to left and from the upper to the lower row. Hence the

metal to the lower left, osmium, is described as extremely hard and brittle; it finds applications only as a minor component in alloys to make them hard. The same is true for the metal right above, ruthenium. To the lower right is platinum, with a suitable combination of ductility and high melting point. Rhodium is harder, and not much used in pure form, but widely applied in alloys with platinum. The phase diagram Pt-Rh was shown previously, Figure 3.5 p. 73. It is seen that already a small addition of Rh causes a steep increase in the melting temperature of the Pt-alloy. Equally important, a modest addition of rhodium greatly improves the tensile strength and hardness.

The phase diagrams of Ir-Rh, Ir-Pt and Pd-Rh are similar to that of Pt-Rh in that they show complete miscibility in both solid and liquid states. Alloying with iridium gives hardness and corrosion resistance. An alloy of 10 Ir 90 Pt is considered the most corrosion resistant alloy known. It was used for the standard metre in Paris; similar alloys are also used for crucibles.

To the upper right in the row is palladium, the softest metal in the group. It finds uses in alloys with rhodium. A property of Pd (and to some extent Pt) is that the metal shows high solubility and diffusivity for hydrogen.

It should be noted that although platinum and its neighbours are called 'noble metals', they are not strictly inert. Under neutral or reducing conditions platinum dissolves or forms compounds with almost any other element (with carbon as a noteworthy exception). Some examples are given in the discussion of noble-metal thermocouples, Chapter 3 pp. 72–74; see also Brewer (1967).

5.5.3 Molybdenum and Tungsten

Both metals are high-melting, but with notably different melting points, 2622 and 3414 °C, respectively. In line with this difference, tungsten is stiffer and more difficult to shape. Apart from that, they exhibit a number of similarities. At elevated temperatures they are easily oxidized and form volatile oxides; MoO_3 has boiling point about 1100 °C, WO_3 about 1800 °C. Furthermore both metals react with carbon; the most stable carbides are Mo_2C, respectively WC. Hence their uses are preferably confined to neutral atmospheres or vacuum.

Both metals are commercially available as wire, sheet and other shapes, thus the choice depends primarily on the ease of handling and the required temperature.

Molybdenum in pure form has a tendency to grain growth at elevated temperatures. Hence the commonly used quality contains minor amounts of alloying elements to improve the high temperature stability.[4] From the user's point of view, however, the alloy denoted TZM may be considered equivalent to pure molybdenum with improved properties.

Molybdenum wire is used as heating element in high temperature furnaces (cf. Figure 2.8, p. 31), and thin sheet may be shaped to serve as container materials. Mo wire or sheet is readily bent or shaped at room temperature, with the restriction that the bending radius should not be less than 1.5 times the sheet thickness.

Tungsten appears considerably stiffer. Attempts to bend a tungsten wire at room temperature results in fracture, usually revealing a stringy structure that is caused by the rolling or drawing of this high-melting metal. Bending or shaping of tungsten has to be done at elevated temperatures.

In this context, the brittle-ductile transition temperatures of molybdenum and tungsten are shown in Figure 5.3 as functions of the sheet thickness. From the diagram it appears that a molybdenum sheet of up to 1 mm thickness may be bent with success at room temperature, while a similar bending of even the thinnest sheet of tungsten will result in failure (in agreement with a practitioner's experience). Bending of tungsten may be done, for example, with a gas torch. When done in open air, it has to be done quickly because of the rapid oxidation. From Figure 5.3, however, it appears that bending of tungsten sheet or wire may also be done at fairly moderate temperatures where the oxidation rate is not yet very high.

The oxidation of these metals in air may be used to advantage in identifying an unknown piece of wire. Heating the piece in a gas torch without visible reaction, it is probably Kanthal or some similar alloy (or possibly platinum). If it gives off white smoke, it is either molybdenum or tungsten, with the more intense smoke from molybdenum.

[4] Molybdenum, tungsten and other high-melting alloys are manufactured by Metallwerk Plansee AG, Reutte, Austria. Their most commonly used Mo alloy is designated TZM and contains about 0.5% Ti, 0.07% Zr and 0.05% C. Their common tungsten alloy is likewise 'doped' and heat treated to obtain high temperature stability.

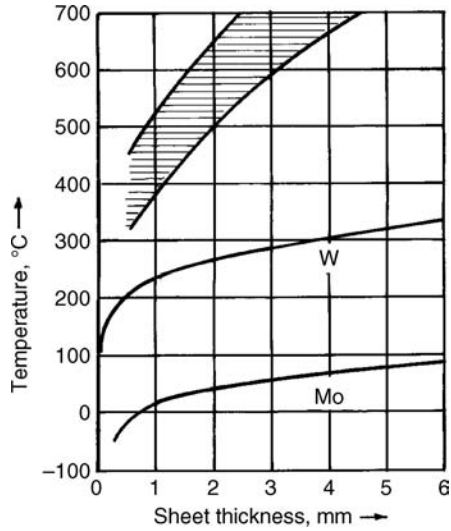

Figure 5.3 Brittle-ductile transition temperatures for molybdenum and tungsten sheet as functions of sheet thickness. It should be noted that the transition temperatures are in reality not sharply defined; the curves should be considered more as guidelines. The hatched area indicates *recommended* temperatures for shaping of molybdenum. The recommended area for tungsten is similar, not shown here. (Adapted from graphs given in catalogues from Metallwerk Plansee.)

In addition to heating elements and furnace furniture, molybdenum and tungsten are useful as crucibles for the melting of various materials. For example, determination of the melting point of alumina (p. 123) was made by aid of a molybdenum crucible (machined from solid stock). The industrial melting of silica glass takes place in large tungsten crucibles with induction heating.

5.5.4 Tantalum

Tantalum has a melting point of 3000 °C, considerably higher than molybdenum. At the same time it is very ductile, and hence would seem the ideal material for high temperature furnaces. Unfortunately, tantalum readily absorbs gases like oxygen, hydrogen and nitrogen. Tantalum with dissolved oxygen may be outgassed at high temperatures in a high vacuum (resulting in a loss of material and condensation

of oxide in the cooler parts of the apparatus). Outgassing of nitrogen also requires high temperatures, and outgassing in general is a tedious process.

Unexpected reactions may also occur between refractory oxides and tantalum at elevated temperatures. Even very stable oxides like alumina or magnesia are partially reduced. Altogether, the use of tantalum for heating elements and radiation shields is confined to furnaces that will be used with a high vacuum under clean conditions only. This makes it less suitable for high temperature experiments in general.

At moderate temperatures (below 150 °C) tantalum shows excellent corrosion resistance and is widely used as a construction material in chemical engineering, but that is another story.

Tantalum and carbon combine to give the very stable carbide TaC, which according to the C-Ta phase diagram melts congruently at 4000 ± 200 °C. It is the least volatile of all known substances.

5.5.5 Rhenium

Rhenium is unique among the refractory metals in that it does not form a carbide. The solubility of carbon in solid Re is also negligible. The melting point is 3180 °C, the metal is ductile, the tensile strength at elevated temperatures is higher than that of tungsten (Metals Handbook, 1990, p. 557) and rhenium would seem the ideal material for high temperatures in non-oxidizing atmospheres.

Unfortunately, the cost prevents more widespread use. But a thin disc or foil of rhenium may be worth its price, for example, as a barrier between graphite and oxide components in a high temperature furnace.

5.6 NOTES ON CRUCIBLE MATERIALS AND COMPATIBILITY

In the preceding text, reference has repeatedly been made to compatibility of materials. In general, this concept opens a field which is much too wide for any attempt at an overview. Thus only a few examples will be given, mainly limited to the problem of finding a suitable crucible material for a given charge.

5.6.1 A Line of Thought

When considering two (or more) materials in contact, the thinking should follow several steps: (i) What reactions are conceivable between the materials? (ii) Are these reactions thermodynamically feasible at the temperatures in question? Equilibrium calculations (however rough) may give the answers. (iii) If a reaction is thermodynamically feasible, will it take place, or is it kinetically hindered?

The fourth question concerns mutual solubility, which may be harder to predict. In the following, some combinations of materials will be considered.

5.6.2 Graphite plus Metals

Graphite is a first choice in many cases because of its refractoriness, low vapour pressure and ease of machining. To take a simple example: may a graphite crucible be used to melt aluminium (m.p. 660 °C)? The likely reaction is a formation of the stoichiometric compound Al_4C_3, and thermodynamic data tells that this should happen at all temperatures. But in practice it does not; aluminium may be molten and heated several hundred degrees above the melting point with nothing happening. The latter statement, of course, is not quite true; a thin layer of the carbide is formed on the crucible wall, protecting it from further reaction. This kinetic hindrance in general is hard to predict; in the case of graphite the maximum allowable temperature for molten metals is very much dependent on the graphite quality. In the case of molten silicon (m.p. 1410 °C) only very special qualities will survive, otherwise reaction to SiC will occur.

A further question is the solubility of carbon (or really, solubility of the carbide) in the metal. The answer is that for the metals mentioned above, the solubility is negligible several hundred degrees above the melting point. Similarly, the solubility of the metals in carbon/graphite is essentially nil.

In general, the various compilations of binary alloy phase diagrams give useful information about the formation of compounds as well as their solubilities in both solid and liquid states. To take one more example: copper forms no compound with carbon, and the solubility of carbon in liquid copper is negligible. Hence graphite is the ideal material for

crucibles to calibrate thermocouples by means of the melting point of copper (pp. 83–84).

5.6.3 Ceramics plus Metal

When the metal dissolves or reacts with carbon, some ceramic material is usually the next choice. To take an example: is alumina suitable for the melting of silicon? Disregarding the possible reaction between the oxides to form mullite, a possible reaction may be written:

$$2\,Al_2O_3(s) + 3\,Si(l) = 4\,Al(\text{in Si})(l) + 3\,SiO_2(s)$$

A quick calculation indicates that the liquid Si at equilibrium will contain about 1% Al. This is way too much if pure Si is required. In fact, the suitable container material for melting of a pure, reactive metal is often a compound of that metal plus a non-metal. For example, for the melting of solar grade silicon, SiO_2 and Si_3N_4 are the only materials in question.

5.6.4 Molten Salts and Slags

To start with the simplest: binary salts like NaCl and their mixtures may be melted in graphite crucibles, which are cheap and convenient. For oxy-salts like Na_2SO_4, Na_2CO_3 and so on, platinum (or a Pt alloy) is generally used in the laboratory. Platinum also works well for oxide mixtures provided that none of the cationic metals are easily reduced. In, for example, mixtures involving Fe^{3+} and Fe^{2+}, a Pt crucible will be contaminated with iron, this may influence the experiment, and eventually the crucible will be ruined.

In the classical experiments of Muan (1966) the problem was overcome by using alloys of silver and palladium. Silver has a very low solubility for iron, and by alloying with palladium the metal melting point (961.8 °C for pure Ag) was markedly increased without significant increase in the iron content of the alloy. The maximum allowable Pd content is dependent on the oxygen potential of the slag system, see Muan. This solution, however, is limited to fairly moderate temperatures, and for many slags of commercial interest, no usable crucible material has been found.

In larger, industrial electric arc furnaces, this problem is generally solved by a water-cooled shell, giving a solidified layer inside the shell that actually works as a container for the melt. On a laboratory scale this is not equally simple to realize. However, a recent development, the 'cold crucible' induction furnace, in essence has solved the problem. The water cooled copper container is split in narrow vertical sections so that it does not form a complete loop for the induction current. The susceptor is effectively formed by the frozen layer next to the cold copper, and the melt next to the frozen layer (cf. Chapter 2, p. 32). A recent example of the use of this type of furnace is given by Elstad *et al.* (2007) and Eriksen, Robles and Rosenqvist (2007) in the study of a Ti—Fe—O slag.

5.6.5 Chemical Transport Reactions

The concept was initially introduced in the classical book by Schäfer (1964). In the present context we consider gaseous transport in particular. An example of current interest is the production of aluminium nitride single crystals. In the thorough work of Slack and McNelly (1976) they investigated various processes for the production of pure AlN, with sublimation-condensation as the final step to obtain single crystals. Tungsten was used as the container material. More recently, Slack *et al.* (2004) presented a discussion of various container materials for the purpose, such as pyrolytic graphite, BN, W and TaC. The discussion is interesting, although they left the final choice for future development of single crystal AlN.

5.6.6 Special Materials

As indicated in the introduction, the number of possible combinations of materials is almost infinite, and any attempt at a survey will be futile. However, special problems require special solutions.

Only one example will be cited. During the Second World War, scientists in the USA had a problem with the melting and casting of uranium metal. Somebody came up with the idea of cerium sulphide as a suitable ceramic material. Now, cerium sulphide is not (or was not) commercially available in the form of ceramic crucibles, so the working group

had to make their own. Figure 5.4 is a drawing of the pressing tools they used, adapted from Eastman *et al.* (1951).

The dimensions of Figure 5.4 are reduced by a factor of about 0.62 compared to the original, to make the tool suitable for small-scale work. (The uneven scale factor stems from the simultaneous change from inches to the metric system.)

The idea behind reproducing the drawing is that experimentalists even today may encounter situations where crucibles of some unusual ceramic material are desired. A special feature of the die is the slight taper in the lower part. The purpose is to allow uniform expansion of the compact as it is ejected from the die. Experience shows that the ejection of a perfectly cylindrical compact often causes fractures at the edge of the block.

It should be noted that the die is a precision tool. Before use, each moving part is lubricated with a fatty acid such as stearic or caprylic,

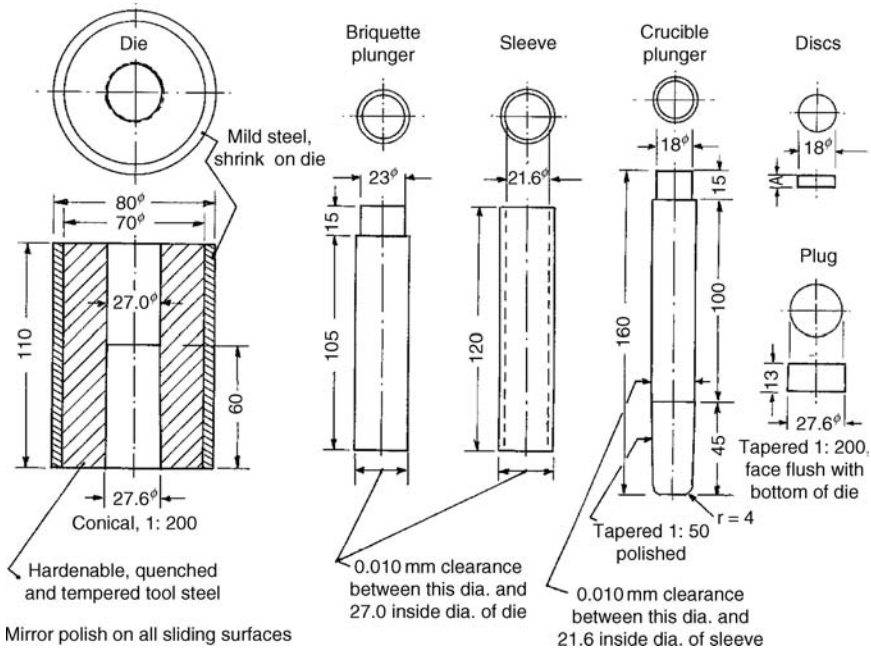

Figure 5.4 Details of equipment used for uniaxial pressing to make ceramic crucibles, adapted from Eastman *et al.* (1951) with about 40% reduction of dimensions compared to the original.

dissolved in ether. The ether should be carefully evaporated before the parts are assembled. The ceramic powder, with a suitable temporary binder, is preferably loaded into the die in an inverted position. Next it is put upright and placed in a hydraulic press. The purpose of the discs on top of the plunger is to allow the alternate application of pressure to the sleeve and the plunger, see Figure 5.5. According to Eastman *et al.* (1951) suitable pressures range from 3.5 to 7 ton/cm^2. The cross-section of the plunger in Figure 5.4 is about 2 cm^2, which corresponds to a maximum of 15 ton total. It appears advisable to consult an experienced press operator before applying these pressures.

After pressing, the compact *and the plunger* are ejected *in the direction of the pressing* (that is, downwards). Any attempt at moving the plunger in the reverse direction may cause it to get stuck because of the taper in combination with traces of ceramic particles. Eventually it gets stuck forever.

Details of the preparation of powders and the further pressing process are given in the paper by Eastman *et al.* (1951), which should be consulted. Uniaxial pressing is also discussed, for example by Richerson (2006) pp. 403–417.

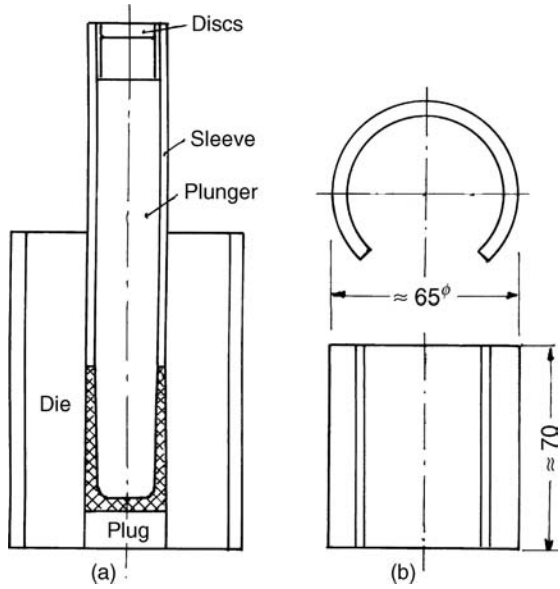

Figure 5.5 (a) Assembly drawing showing crucible compact during pressing. (b) An auxiliary tool to aid in the ejection of the compact after finished pressing (not included in the original drawing).

Another possibility, in combination with, or as an alternative to, uniaxial pressing, is isostatic pressing, see Richerson pp. 417–420.

5.6.7 A Note on Safety

The preparation of ceramic materials often involves the handling of powders or dust that presents a potential health hazard. Fibrous materials are even worse in this respect. Thus a dust mask should be worn whenever dry powder or fibrous materials are handled.

REFERENCES

Bauer, A.J., Friedrichs, P., Krieger, M., Pensl, G., Rupp, R., and Seyller, T. (2010) Silicon Carbide and Related Materials 2009. (The 13th International Conference), Trans Tech Publications, Stafa-Zurich (2 vols.), 1260 pp.

Belmonte, M., Miranzo, P., and Osendi, M.I. (2007) Mechanical properties and contact damage behavior in aligned silicon nitride materials. *J. Am. Ceram. Soc.*, **90**, 1157–1163.

Blegen, K. (1975) Equilibria and kinetics in the system Si-N and Si-N-O, in *Special Ceramics*, (ed. P. Popper), vol. **6** Brit. Ceram. Soc., Manchester, pp. 223–244.

Blegen, K. (1976) *Equilibria and Kinetics in the Systems Si-N, Si-O-N, and Si-C-O-N*, Dr. Ing. Thesis, N.T.H. (now The Norwegian University of Science and Tehnology), Trondheim 259 pp.

Bondokov, R.T., Morgan, K.E., Shetty, R.L.W., *et al.* (2006) Defect content evaluation in single crystal AlN wafers. *Materials Research Society Symposium Proceedings*, **892** (2006) (GaN, AlN, InN and Related Materials), 736–738.

Brewer, L. (1967) A most striking confirmation of the Engel metallic correlation. *Acta Met.*, **15**, 553–556.

Brook, R.J. (ed.) (1991) *Concise Enclyclopedia of Advanced Ceramic Materials*, Pergamon Press, Oxford, 588 pp.

Cappelen, H., Johansen, K.H., and Motzfeldt, K. (1981) Oxidation of silicon carbide in oxygen and in water vapour at 1500 °C. *Acta Chem. Scand.*, **A35**, 247–254.

Chen, I-.W., Becher, P.F., Mitomo, M., *et al.* (eds.) (1993) Materials research society symposium proceedings, in *Silicon Nitride Ceramics*, vol. **287**, MRS, Pittsburgh, Penn, 550 pp.

Dahl, P., Kaus, I., Zhao, Z., *et al.* (2007) Densification and properties of zirconia prepared by three different sintering techniques. *Ceram. Int.*, **33**, 1603–1610.

Deal, B.F. and Grove, A.S. (1965) General relationship for the thermal oxidation of silicon. *J. Appl. Phys.*, **36**, 3770–3778.

Dolloff, R.T. (1960) WADD Technical Report 60–143: 'Research Study to Determine the Phase Equilibrium Relations of Selected Metal Carbides at High Temperatures', Wright-Patterson Air Force Base, Ohio, 22 pp.

Durand, F. and Duby, J.C. (1999) Carbon solubility in solid and liquid Si – A review. *J. Phase Equilibr.*, **20**, 61–63.

Eastman, E.D., Brewer, L., Bromley, L.-R.A., *et al.* (1951) Preparation and tests of refractory sulfide crucibles. *J. Am. Ceram. Soc.*, **34**, 128–134.

Elstad, H., Eriksen, J.M., Hildal, A., *et al.* (2007) Equilibrium between titania slags and metallic iron. *Proceedings of The 6th International Heavy Minerals Conference 'Back to Basics'*, The South African Institute of Mining and Metallurgy, Johannesburg, pp. 35–42.

Eriksen, J.M., Robles, E.C., and Rosenqvist, T. (2007) Equilibrium between liquid Fe-Ti-O slags and metallic iron. *Steel Res. Int.*, **78**, 671–675.

Fitzer, E., Kochling, K-.H., Boehm, H.P. and Marsh, H. (eds.) (1995) Recommended terminology for the description of carbon as a solid. *Pure Appl. Chem.*, **67**, 473–506.

Foosnæs, T. and Naterstad, T. (1993) Carbon, Basic and Principles, Chap. 4 in *'Introduction to Aluminium Electrolysis'*, (eds K. Grjotheim and H. Kvande), Aluminium-Verlag, Düsseldorf, pp. 87–138.

Fu, R., Chen, K., Xu, X., and Ferreira, J.M.F. (2005) Highly crystalline AlN particles synthesised by SHS method. *Mater. Lett*, **59**, 2605–2609.

Gálvez, M.E., Halman, M., and Steinfeld, A. (2007) Ammonia Production via a Two-Step Al_2O_3/AlN Thermochemical Cycle. **1**. Thermodynamic, Environmental and Economic Analyses. *Ibid.* (with A. Frey) pp. 2047–253: '**2**. Kinetic Analysis'. *Ind. Eng. Chem. Res.*, **46**, 2042–2046.

Guichelaar, P.J. (1997) Chap. 4 in Weimer (1997), 'Acheson Process', pp. 115–129.

Hanssen, K.O. (1983) Fremstilling og egenskaper for materialer av aluminium-oksynitrid og aluminiumnitrid, Dr. Ing. Thesis, Inst. uorganisk kjemi, NTH (now NTNU), Trondheim, 123 pp.

Haussonne, F.J.-M. (1995) Review of the synthesis methods for AlN. *Mater. Manuf. Process.*, **10**, 717–755.

Hoffmann, M.J., Becher, P.F. and Petzow, G. (eds) (1994) *Proceedings of the International Conference 'Silicon Nitride 93'* (held in Stuttgart Oct. 4–6, 1993) Trans Tech Publications, Stuttgart, 1–782.

Jack, K.H. (1976) Review: Sialons and related nitrogen ceramics. *J. Materials Sci.*, **11**, 1135–1158.

Jack, K.H. (1988) Sialons and Related Ceramic Alloys, pp. 447–488 in *Alloying* (eds. J. L. Walter, M. R. Jackson and C. T. Sims), ASM International, Metals Park, Ohio.

Kleykamp, H. and Schumacher, G. (1993) The constitution of the silicon – carbon system. *Ber. Bunsenges. Phys. Chem.*, **97**, 799–805.

Knippenberg, W.F. (1963) Growth phenomena in silicon carbide. *Philips Res. Rep.*, **18**, 161–274.

Kollenborg, E. (1962) *Det Norske Nitrideaktieselskap 1912–1962*, Rambaeks Trykkeri, Oslo, 142 pp.

Krauskopf, K.B. and Bird, D.K. (1995) *Introduction to Geochemistry*, 3rd edn, McGraw-Hill Book Co., Singapore, 645 pp.

Madelung, O. (ed.) (1992) *Landolt-Börnstein*, New Series, vol. **5**, subvol. b, Springer-Verlag, Berlin, 309 pp.

Long, G. and Foster, L.M. (1959) Aluminum Nitride, a Refractory for Aluminum to 2000 °C. *J. Am. Ceram. Soc.*, **42**, 53–59.

Massalski, T.B. (ed.) (1990) *Binary Alloy Phase Diagrams*, 2nd edn, ASM International, Ohio, pp. 882–883.

Metals Handbook (1990) *Metals Handbook*, 10th edn, vol. **2**, ASM International Handbook Committee, 1328 pp. ('Refractory Metals and Alloys' pp. 557–585).

Moffat, W.G. (ed.) (1984) *The Handbook of Binary Phase Diagrams*, Genius Publ. Corp., Schenectady, NY, (loose-leaf binder, 5 vol.s).

Morrell, R. (1989) *Handbook of Properties of Technical & Engineering Ceramics, Part 1*, Revised edn, National Physical Laboratory/Her Majesty's Stationery Office, London, 348 pp.

Motzfeldt, K. (1964) On the rates of oxidation of silicon and of silicon carbide in oxygen, and correlation with permeability of silica glass. *Acta Chem. Scand.*, **18**, 1596–1606.

Motzfeldt, K. (1993) *Engineering Ceramics '92* (ed. M. Haviar), Slovac Academy of Science, Bratislava, pp. 1–36: 'Silicon Carbide: Synthesis, Structure and Sintering'.

Motzfeldt, K. (1997) Chemical thermodynamics in ceramics, in *Engineering Ceramics '96: Higher Reliability through Processing* (eds G.C. Babini, M. Haviar, and P. Sajgalík), Kluver Academic Publishers, The Netherlands, pp. 189–196.

Motzfeldt, K., Kvande, H., Schei, A., and Grjotheim, K. (1989) *Carbothermal Production of Aluminium*, Aluminium-Verlag, Düsseldorf, 218 pp.

Muan, A. (1966) Equilibrium measurements involving oxide and alloy phases at high-temperatures, in *Selected Topics in High-Temperature Chemistry* (eds T. Förland, K. Grjotheim, K. Motzfeldt, and S. Urnes), Universitetsforlaget, Oslo, pp. 125–139.

Myhre, B. (1989) Kinetics of the Nitridation of Silicon, Dr. Ing. Thesis, Inst. Inorganic Chem., NTH (now NTNU), Trondheim 208 pp.

Narushima, T., Goto, T., Hirai, T., and Iguchi, Y. (1997) High-temperature oxidation of silicon carbide and silicon nitride. *Materials Trans., JIM*, **38**, 821–835.

NIST-JANAF (1998) *Thermochemical Tables*, 4th edn (ed. M.W. Chase, Jr.), Part I+II, Am. Chem. Soc./Am. Inst. Physics, New York, 1950 pp.

Oden, L.L. and McCune, R.A. (1987) Phase equilibria in the Al-Si-C system. *Metall. Trans.*, **A18**, 2005–2014.

Olesinski, R.W. and Abbaschian, G.J. (1984) The C-Si system. *Bull. Alloy Phase Diagrams*, **5**, 486–489.

Opila, E.J. (2003) Water vapor effects on high-temperature oxidation and volatilization of ceramics. *J. Am. Ceram. Soc.*, **86**, 1237: (introduction to Special Issue, pp. 1237–1306). *Ibid*. pp. 1238–1248: 'Oxidation and Volatilization of Silica Formers in Water Vapor'.

Opila, E.J., Jacobson, N.S., Myers, D.L., and Copland, E.H. (2006) Predicting oxide stability in high-temperature water vapors. *JOM*, **58**, 22–28.

Peng, G., Jiang, G., Li, W., Zhang, B., and Chen, L. (2006) Fabrication of hard and strong α/β-Si_3N_4 composites with $MgSiN_2$ as additives. *J. Am. Ceram. Soc.*, **89**, 3824–3826.

Persson, J., Käll, P.-O., and Nygren, M. (1993) Parabolic – non-parabolic oxidation kinetics of Si_3N_4. *J. European Ceram. Soc.*, **12**, 177–184.

Pierson, H.O. (1993) *Handbook of Carbon, Graphite, Diamond and Fullerenes*, Noyes Publications, Park Ridge, NJ, 399 pp.

Pierson, H.O. (1996) *Handbook of Refractory Carbides and Nitrides*, Noyes Publications, London, 340 pp.

Richards, J.W. (1913) The Serpek process for the manufacture of aluminium nitride. *J. Ind. Eng. Chem.*, **5**, 335.

Richerson, D.W. (2006) *Modern Ceramic Engineering*, 3rd edn, Taylor & Francis Group, Boca Raton, Florida, 707 pp.

Saddow, S.E. and Agarwal, A. (eds.) (2004) *Advances in Silicon Carbide*, Artec House, Inc., Boston and London, 212 pp.

Scace, R.I. and Slack, G.A. (1959) Solubility of carbon in silicon and germanium. *J. Chem. Phys.*, **30**, 1551–1555.

Schäfer, H. (1964) *Chemical Transport Reactions*, Academic Press, New York, 142 pp.

Seltveit, A. (1992) *Ildfaste materialer*, Tapir Forlag, Trondheim, 496 pp.

Shen, Z., Johnsson, M., Zhao, Z., and Nygren, M. (2002) Spark plasma sintering of alumina. *J. Am. Ceram. Soc.*, **85**, 1921–1927.

Shen, Z., Zhao, Z., Peng, H., and Nygren, M. (2002) Formation of tough interlocking microstructures in silicon nitride ceramics by dynamic ripening. *Nature*, **417**, 266–269.

Slack, G.A. and McNelly, T.F. (1976) Growth of high purity AlN crystals. *J. Cryst. Growth*, **34**, 263–279. *Ibid.* **42** (1977) 560–563: 'AlN Single Crystals'.

Slack, G.A., Tanzilli, R.A., Pohl, R.O., and Vandersande, J.W. (1987) The intrinsic thermal conductivity of AlN. *J. Phys. Chem. Solids*, **48**, 641–647.

Slack, G.A., Whitlock, J., Morgan, K., and Schowalter, L.J. (2004) Properties of crucible materials for bulk growth of AlN. *Mater. Res. Soc. Proc.*, **798**, 293–296: (GaN and Related Alloys).

Song, Y., Dhar, S., and Feldman, L.C. (2004) Modified Deal Grove model for the thermal oxidation of silicon carbide. *J. Appl. Phys.*, **95**, 4953–4957.

Sörlie, M. and Öye, H.A. (2010) *Cathodes in Aluminium Electrolysis*, 3rd edn, Aluminium-Verlag, Düsseldorf, 662 pp.

Tangen, I.-L. (2005) Preparation and characterisation of silica-doped aluminiumnitride - aluminiumnitride Poly- typoid composites. *Ceram. Int.*, **31**, 591–598.

Thompson, D.P. (2002) Cooking up tougher ceramics. *Nature*, **417**, 237.

Tian, Q. and Virkar, A. (1996) Interdiffusion in SiC-AlN and AlN-Al_2OC systems. *J. Am. Ceram. Soc.*, **79**, 2168–2174.

Tkac, M. (2007) Porosity Development in Composite Carbon Materials During Heat Treatment, Ph.D. Thesis, Dept. of Materials Tech., NTNU, Trondheim 173 pp.

Urry, G. (1989) *Elementary Equilibrium Chemistry of Carbon*, John Wiley & Sons, New York, 223 pp.

Weimer, A.W. (1997) *Carbide, Nitride and Boride Materials Synthesis and Processing*, Chapman and Hall, London, 671 pp.

6

Vacuum in Theory and Practice

CONTENTS

High Temperature Experiments in Chemistry and Materials Science, First Edition.
Ketil Motzfeldt.

Preamble

The purpose of evacuation and degassing of high temperature systems is essentially the same as that of thorough cleaning of the glassware in aqueous chemistry. The methods, however, are a bit more demanding. Furthermore, in experiments involving gases the careful control of gas pressures is essential.

6.1 BASIC CONCEPTS

6.1.1 Why Vacuum?

The word 'vacuum' stands for empty space, or a space in which all or nearly all of the gases normally present have been removed. There may be several reasons for this removal:

- A number of modern instruments, such as electron microscopes and mass spectrographs, are entirely dependent on a high vacuum in parts of the system because electrons or ions shall be accelerated through the system without colliding with other ions or molecules.
- More specifically, studies in high temperature chemistry often involve substances that may react with oxygen or other gases initially present in the system. A common procedure in such cases is to flush the system with an inert gas (e.g. argon). Thorough evacuation, however, followed by admission of inert gas, is a much more efficient procedure. We will have occasion to return to this topic, with 'degassing' as a key word.

A number of objects in everyday life have been evacuated, degassed, and then permanently sealed. In such cases we talk about a *static* vacuum. In other cases, like the electron microscope or the mass spectrometer, a vacuum is maintained through constant pumping. We then have a *dynamic* vacuum. For our purposes we will only consider dynamic vacua.

6.1.2 Units of Gas Pressure

Pressure is defined as *force per unit area*. In the Systéme International (SI), the unit of force is *newton*, and that of area is *square metre*. Hence the unit of pressure, which is given the name *pascal*:

$$1\ \mathrm{N/m^2} = 1\ \mathrm{Pa\ (def)} \tag{6.1}$$

In chemistry we are generally more interested in concentration, or *contents per unit volume*. But the concentration of a gas is related to its pressure. With n mol of gas in a confined volume V at the absolute temperature T, introducing also the universal gas constant $R = 8.314\ \mathrm{N\,m\ K^{-1}\,mol^{-1}}$, the gas concentration is

$$\frac{n}{V} = \frac{P}{RT} \tag{6.2}$$

Thus the pressure is a convenient equivalent of the gas concentration. Strictly speaking, Eq. (6.2) is valid only for an ideal gas, but the behaviour of a real gas approaches that of the ideal one as the gas is rarefied (or the temperature increased).

In the SI system it is agreed that every third power of the basic unit shall have its own designation, thus $1\ \mathrm{kPa} = 10^3\ \mathrm{Pa}$, $1\ \mathrm{MPa} = 10^6\ \mathrm{Pa}$. But it so happens that the normal atmospheric pressure is close to 10^5 Pa. For practical reasons, then, a separate unit has been introduced:

$$1\ \mathrm{bar} = 10^5\ \mathrm{Pa\ (def)} \tag{6.3}$$

In chemical thermodynamics the pressure 1 atm was formerly established as the pressure of the standard state. By decision of the International Union of Pure and Applied Chemistry (IUPAC) in 1982, the standard pressure is now 1 bar. The conversion factor is

$$1\ \mathrm{atm} = 1.0132\ \mathrm{bar} \tag{6.4}$$

In retrospect, it may be of interest to see the origin of the conversion factor. The pressure 1 atm was defined as the pressure exerted by a 760 mm high column of mercury at 0 °C. The density of mercury at this temperature is $13\,595\ \mathrm{kg\,m^{-3}}$, and the gravity at 45° latitude is $9.8062\ \mathrm{m\,s^{-2}}$. Thus

$$0.760\ \mathrm{m} \times 13595\ \mathrm{kg\,m^{-3}} \times 9.8062\ \mathrm{m\,s^{-2}} = 1.0132 \times 10^5\ \mathrm{Pa}.$$

The change in standard pressure did not result in any notable changes in the thermodynamic data for solids and liquids, and only very small changes in the standard entropy for gases, see IUPAC (1982); Freeman (1983).

Another unit which was commonly used in vacuum technique, is 'millimetres of mercury' which was given the name *torr* (in honour of E. Torricelli, 1608–1647). When the unit torr was abandoned, it was convenient to have another unit of approximately the same magnitude. It is seen that 1 torr = 1/760 atm ≅ 1/1000 atm. Correspondingly, 1/1000 bar = 1 millibar.

Commercial instruments for the measurement of pressure in the vacuum region are usually graduated in mbar. Sometimes, *hectopascal* is used. But 1 hPa = 100 Pa = 1 mbar, so this is really two names for the same unit.

In addition to torr or mm Hg, 1/1000 torr was also used as a unit in the vacuum region. It is seen that 1/1000 torr = 10^{-3} mm Hg = 10^{-6} m Hg = 1 μm (Hg), abbreviated to 1 micron (μ). A corresponding unit in modern terms is 1/1000 mbar = 1 μbar.

6.1.3 Elements of a Vacuum System

Before entering into the necessary details, it may be helpful for the reader to have an overall idea of what a vacuum system may look like. Of course it may take on a variety of forms, the semi-schematic diagram in Figure 6.1 is given only to show a number of parts that are usually present.

Starting from the high-pressure end (atmospheric pressure) a mechanical, rotary pump **RP** is shown. A two-stage rotary pump may bring the pressure in the system down to about 10^{-2} mbar or slightly lower. For clean work, however, a lower pressure (or a 'better vacuum') is required, as related below. Hence a high-vacuum pump, usually an oil diffusion pump **DP**, is added. This type of pump does not function until the pressure on the forevacuum side is down to a few tenths of a millibar, but then it may bring the pressure further down to about 10^{-5} or 10^{-6} mbar.

Next is shown a high-vacuum valve **V**, which may be an angle valve as shown, or the straight-through type. Its purpose is to shut the connection between the pumps and the vacuum chamber **C**, so that the chamber may eventually be filled with gas (or opened to the atmosphere) while the diffusion pump remains under vacuum.

The 'bypass' line **B** serves to re-evacuate the chamber once it has been opened, without admitting air into the diffusion pump. Included in the forevacuum/bypass line are two valves (indicated by crosses) to allow

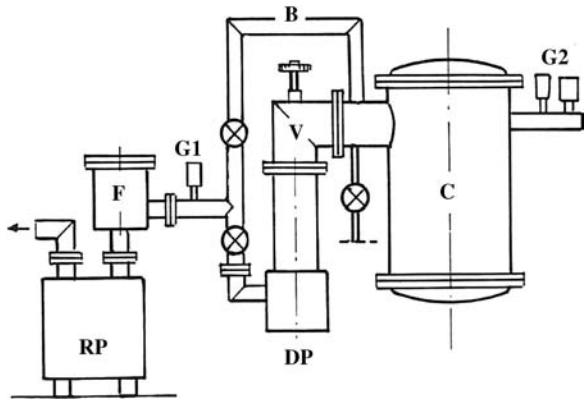

Figure 6.1 The various components of a typical vacuum system. **RP**: Rotary pump. **F**: Dust filter. **G1, G2**: Vacuum gauges. **DP**: Diffusion pump. **V**: High-vacuum valve. **B**: Bypass line. **C**: Chamber (working space).

the alternate evacuation through the bypass or the diffusion pump. A third, separate valve is added without further specification, to indicate the need for gas inlet and air admittance.

As drawn in Figure 6.1, the connection between the diffusion pump and the chamber is short and wide, as it should be to ensure a high rate of evacuation (or a high 'pumping speed') at low pressures.

Attached to the system are a number of pressure and vacuum gauges, one at **G1** to check the forevacuum pressure, and at least one more at **G2** to gauge the system pressure in the various ranges from 1000 to 10^{-6} mbar. Only the gauge heads are shown; the electronic circuits and display are supposedly located with other control elements on an instrument panel, not included in Figure 6.1.

Finally, **F** indicates a dust filter, fitted to the inlet of the mechanical pump; a detail quite often ignored. Its purpose is to prevent the entrance of abrasive dust into the mechanical pump, it may otherwise be ruined in a short time.

Alternatively, a turbo pump could be fitted in place of the oil diffusion pump. The turbo pump produces a better end vacuum, but it is a rather delicate piece of equipment which operates at some 50 to 100 000 rpm, and is very sensitive to contamination by solid particles. In contrast, the oil diffusion pump contains no moving parts, is very durable, and its end vacuum is satisfactory for almost any purpose in chemistry and metallurgy. Hence the oil diffusion pump is preferred in the present discussion.

This was a quick preliminary tour through some of the relevant components of a vacuum system, before returning to the basic principles.

6.2 EXPRESSIONS FROM THE KINETIC THEORY OF GASES

The foundation of the kinetic theory of gases is given by Maxwell's and Boltzmann's equations for the distribution of velocities of molecules in an ideal gas. This is treated in standard texts in physical chemistry. We will not here give any summary of the theory, but only reproduce some of the results that are useful for our purposes.

6.2.1 The Mean Free Path

It is defined as the distance a molecule in the gas on an average travels between two collisions. For a gas of molecules with collision diameter δ at the temperature T and pressure P, the mean free path is

$$\lambda = \frac{kT}{\sqrt{2}\pi P \delta^2} \tag{6.5}$$

where k is Boltzmann's constant. As an example of the use of SI units, we may assume $\delta = 3.8 \times 10^{-10}$ m (which is a suitable value for N_2), and temperature 20 °C = 293 K. This gives

$$\lambda = \frac{1.381 \times 10^{-23} \times 293}{\sqrt{2}\pi P (3.8)^2 \times 10^{-20}} = \frac{6.3 \times 10^{-3}\ \text{m}}{(P/\text{Pa})}. \tag{6.6}$$

The expression P/Pa in the denominator indicates that the pressure P divided by the unit 1 Pa is a dimensionless number.

For our purposes we are mainly interested in the *order of magnitude* of the mean free path. Hence we will express the result of Eq. (6.6) in round figures, and at the same time we give the length in mm and the pressure in mbar. This gives

$$\lambda \cong \frac{0.1\ \text{mm}}{P/\text{mbar}} \tag{6.7}$$

From this expression we may display the connection between gas pressure and mean free path (with figures that are close to correct for nitrogen at a temperature of $293 \times 10/6.3 = 465\,\mathrm{K} \cong 200\,^{\circ}\mathrm{C}$):

P/mbar	1000	100	10	1	0.1	10^{-2}	10^{-3}	10^{-4}	10^{-5}	10^{-6}
λ/mm	10^{-4}	10^{-3}	10^{-2}	10^{-1}	1	10	100	1 m	10 m	100 m
		Rough vacuum				Fine vacuum			High vacuum	

Below the numbers are given the usual designations for the different pressure ranges, although the limits are not sharp. At pressures of 10^{-7} mbar and lower we have 'ultra-high vacuum', but vacua in this range are usually not needed in high temperature chemistry.

The mean free path has a direct bearing on the transport process for a gas, for example, through a tube connecting the system with the vacuum pump. The transport occurs as *viscous flow* if the mean free path in the gas is much smaller than the tube diameter (disregarding turbulent flow). On the other hand, at very low pressures where the mean free path is much larger than the tube diameter, the transport occurs as *molecular flow*. Between these two extremes there is a transition region. We will return to this in Section 6.4.

6.2.2 Collision Frequency on a Plane Surface

Collisions between molecules in the gas gave rise to the concept of mean free path. We are also interested in collisions between the gas molecules and a plane wall in the system. In kinetic theory, the gas concentration is usually given as the number N of molecules per unit volume. With molecular mass m, an expression is derived for the number Z of collisions per unit area in unit time:

$$Z = N\sqrt{\frac{kT}{2\pi m}} \tag{6.8}$$

With the mass M of one mole[1] and Avogadro's number N_A we have the molecular mass $m = M/N_A$. Furthermore, $k = R/N_A$. Rather than the

[1] Remember that for a consistent numerical calculation in the SI system, M should be expressed in kilogrammes.

collision number Z, we want the number of moles of gas which hit a plane with area A in unit time. With n for the number of moles we have the time derivative $n^{\bullet}$, and $Z = N_A \times n^{\bullet}/A$. Furthermore we introduce the ideal gas law $n/V = P/RT$. Expression (6.8) may then be transformed to

$$\frac{n^{\bullet}}{A} = P\sqrt{\frac{1}{2\pi RTM}} \tag{6.9}$$

Assuming a plane with area A placed in a gas with molar mass M and gas pressure P, Eq. (6.9) gives an expression for the number of moles of gas which hit this area in unit time. On the other hand, if A represents the area of a *hole* in this plane, Eq. (6.9) expresses the rate of gas transport through the hole, in this case limited to low pressures where the mean free path is larger than the cross-section of the hole. This will be further discussed in Section 6.4: Pumping speed.

6.3 VARIOUS APPLICATIONS

6.3.1 Rate of Oxidation

We will consider a high temperature vacuum furnace where the heating element may react with oxygen to form volatile oxides. We ask the question: How 'good' a vacuum is necessary in order that no harmful reaction occurs? In other terms, what is an acceptable upper limit for the oxygen pressure in the system?

In order to use Eq. (6.9) we have to decide on a temperature, say, 2000 K. We assume that the gas and the heating element are at the same temperature. For oxygen, $M = 0.032$ kg, and we have

$$\frac{n^{\bullet}}{A} = P(2\pi \times 8.314 \times 2000 \times 0.032)^{-1/2} = 0.0173\frac{P}{\text{Pa}}\,\text{mol}\,\text{s}^{-1}\,\text{m}^{-2}$$

Conversion to pressure in mbar, time in minutes and area in cm^2 gives

$$\frac{n^{\bullet}}{A} = 1.73 \times 10^{-4}\left(\frac{P}{\text{mbar}}\right) \times 60 = 1.0 \times 10^{-2}\left(\frac{P}{\text{mbar}}\right)\text{mol}\,\text{min}^{-1}\,\text{cm}^{-2} \tag{6.10}$$

Assuming that all collisions with oxygen molecules result in reaction, the rate of deterioration of the material may be calculated from Eq. (6.10). We may use graphite as an example. Assuming an apparent density of $1.7\,\mathrm{g/cm^2}$ (for an ordinary, porous quality of graphite) gives an apparent molar volume of $7.0\,\mathrm{cm^3}$. Assuming reaction according to the equation $2\ \mathrm{C} + \mathrm{O_2(g)} = 2\mathrm{CO(g)}$, one molecule of oxygen removes two atoms of carbon. The linear rate of reduction of the graphite material is then

$$2 \times 7.0 \frac{\mathrm{cm^3}}{\mathrm{mol}} \times 0.010 \left(\frac{P}{\mathrm{mbar}}\right) \frac{\mathrm{mol}}{\mathrm{min\,cm^2}} = 1.4 \left(\frac{P}{\mathrm{mbar}}\right) \frac{\mathrm{mm}}{\mathrm{min}} \qquad (6.11)$$

Note first that with an oxygen pressure of 1/1000 bar (which is already a fairly good vacuum), the graphite material will be consumed at a rate of 1.4 mm/min, or destroyed in a few minutes according to Eq. (6.11).

An ordinary two-stage rotary vacuum pump in practice gives an end vacuum of about 10^{-2} mbar. Assuming that 1/5 of this gas is oxygen, insertion in Eq. (6.11) indicates a reduction in thickness of the material of roughly 0.2 mm/hour, or that the heating element would be destroyed in a few hours.

Admittedly this is a rough illustration, since the oxygen initially in the system will be consumed by reaction with the graphite and the reaction will stop (unless air is continuously admitted through leaks in the system). Nevertheless the example serves to demonstrate that a pressure of 10^{-2} or 10^{-3} mbar (one-millionth of an atmosphere) is *not* sufficiently low to ensure the absence of reactions with the gas in an evacuated system.

In conclusion: when designing (or purchasing) a vacuum furnace for scientific work, one may as well do a proper job from the beginning, and aim at an end vacuum of 10^{-5} mbar or better. How this is done is the main topic of this chapter.

6.3.2 Evaporation Processes

For the sake of argument we consider an evacuated and closed container made of a non-volatile material, containing a sample with a measurable vapour pressure. The container with the sample is heated to the

temperature T, part of the sample will evaporate, and an equilibrium will be established between the sample and its vapour with the vapour pressure P. In this situation, molecules of the vapour will hit the surfaces of the sample at a rate which is given by Eq. (6.9). We may assume that all molecules which hit the surfaces of the sample will also condense. But in order to maintain equilibrium, an equal number must then at the same time evaporate. This reasoning brings us to the conclusion that Eq. (6.9) also gives an expression for the *rate of evaporation* for a substance with the vapour pressure P.

The assumption that all molecules which hit the surface of the sample will condense is not necessarily true. If only a fraction condenses, then the rate of evaporation must be reduced by the same fraction. Thus we conclude that Eq. (6.9) represents the *maximum possible* rate of evaporation for a given equilibrium vapour pressure. The fraction of all incoming molecules which condense, may be called the condensation coefficient α. It appears from the above argument that it may then also be regarded as an evaporation coefficient. For $\alpha = 1$, the rate of evaporation is given by Eq. (6.9). For a majority of 'simple' evaporation processes, as for example the vaporization of a metal to a monatomic vapour, α has been experimentally found to be close to 1.

Kinetic hindrance has been found in particular in the cases where the molecules in the equilibrium vapour have a structure which is not immediately present in the condensed phase. An extreme example is arsenic, where the equilibrium vapour consists of tetrahedral As_4 molecules which are not present in the structure of crystalline arsenic. In this case, α is in the order of 10^{-6} (cf. Brewer and Kane, 1955).

The equilibrium situation inside our conceptual crucible above is analogous to the concept of the black body, illustrated in Figure 4.3a on p. 98. If we now make a small hole in the crucible, some of the vapour will escape, but if the hole is small, the equilibrium will essentially be maintained *even if the vaporization coefficient* $\alpha < 1$. This is quite analogous to the radiation example in Figure 4.3b, where equilibrium radiation is emitted from a hole in the cavity. In the case of vaporization, a container with a small hole forms the basis for measuring equilibrium vapour pressures by the Knudsen effusion method, to be discussed in Chapter 8.

After this discussion of principles we return to a real material, once again choosing graphite as an example. The vapour pressure of graphite is low, but has to be taken into account at temperatures above 2000 °C.

Graphite/carbon vaporizes as both monomer and dimer, but the dominating vapour species at elevated temperature is the trimer C_3. At, for example, 2200 °C, the equilibrium pressure of the trimer is 3.4×10^{-4} mbar (interpolated from NIST-JANAF, 1998). From Eq. (6.9) this gives a maximum rate of evaporation of 3.0×10^{-6} mol min^{-1} cm^{-2}. This is calculated for C_3, considered as graphite atoms the rate is three times higher. Assuming an apparent molar volume of 7 cm^3 as before, we find that a graphite heating element at 2200 °C will have its thickness reduced at a rate of about 6×10^{-4} mm/min because of evaporation, or about 0.1 mm in 6 hours. Assuming a relatively thin-walled element, this rate can hardly be tolerated.

In practice the rate of vaporization may be slower than that calculated above, since we would expect the evaporation coefficient for carbon in the form of C_3 to be less than unity. Nevertheless, 2200 °C may be considered an upper limit for the use of graphite as a material of construction in a vacuum. Similar estimates of maximum permissible temperature may be made for other materials once the vapour pressure is known.

6.3.3 Processes in the Presence of an Inert Gas

Thus far we have discussed processes taking place in a vacuum. The presence of an inert gas markedly changes the situation. At 1 bar pressure the inert-gas molecules have a mean free path of the order of 10^{-4} mm, and their presence greatly impedes any transport processes.

Consider first an evaporation process, assuming a hot surface of a material with a vapour pressure P, located in an inert gas. The space next to the surface of the evaporating material will soon be saturated with the vapour. Further transport must occur by diffusion of the vapour molecules through the inert gas. This diffusion, and hence the vaporization, takes place much more slowly than free evaporation.

A quantitative estimate of the effective rate is difficult. The relevant diffusion coefficients may be known, but transport by convection may be equally important. Generally one may assume that the rate of evaporation in 1 bar of inert gas will be about two powers of ten lower than in a vacuum at the same temperature, and that the maximum permissible temperature may be raised accordingly. For example, for graphite in 1 bar inert gas, the maximum permissible

temperature may be increased to about 2400 °C (dependent on the expected lifetime).

Processes in an inert gas do not necessarily take place at 1 bar total pressure. It is important, then, to note that *the coefficient of diffusion in a gas is inversely proportional to the total pressure*. Thus it is expected, for example, that the rate of evaporation of a given material in an inert gas pressure of 0.5 bar would be roughly twice that in 1 bar, or ten times at 0.1 bar.

A protective gas is used to avoid undue vaporization *and* undesired reactions between the charge and the environment. For this latter purpose, the required purity of the gas and its environment depends on the requirements of the process.

6.3.4 Outgassing

All solid objects left in the surrounding atmosphere will have gas molecules adsorbed to the surfaces. For example, oxygen is rather tightly bound to most metal surfaces, while water vapour is bound to oxides (forming hydroxyl groups). When a system is evacuated, the adsorbed gas will gradually be released from the surfaces, but it takes time. (Certain materials also *dissolve* gases; in these cases the outgassing also involves solid-state diffusion.)

As an example we may assume that in a system there remains adsorbed water vapour in an amount of 0.01 mol (0.18 g). We may further assume that this remnant water is adsorbed to the surfaces (including the internal surfaces of porous materials) in such a way that the apparent vapour pressure is 10^{-5} mbar.

At room temperature and 1 bar pressure, an amount of 10^{-2} mol gas has a volume of about 0.25 litre. At a pressure of 10^{-5} mbar = 10^{-8} bar, the volume amounts to 2.5×10^7 litre. With a pumping speed of 250 l/sec (as for a 10 cm dia. oil diffusion pump), the required time will be

$$2.5 \times 10^7 \text{ litre}/250 \text{ litre s}^{-1} = 10^5 \text{ s} \cong 28 \text{ hours!} \qquad (6.12)$$

The example serves only as an illustration and should not be taken quantitatively. It does, however, show why we normally do not obtain

vacua much below 10^{-5} mbar: at these low pressures the volume of remaining gas gets very large, and the required pumping time correspondingly long.

Now, it is a common experience that, as soon as you start heating a vacuum furnace, the pressure increases by one or two powers of ten as seen on the vacuum gauges. A burst of adsorbed gases is given off. This means that it is a waste of time to outgas the system at room temperature.

For example, the equilibrium vapour pressure of water at 20 °C is 23 mbar. Already at 32 °C the vapour pressure is doubled (46 mbar), and at 65 °C it is larger by a power of ten (250 mbar). It may be assumed that the apparent 'vapour pressure' of adsorbed water vapour shows a corresponding increase with increased temperature. From this it follows that already a relatively moderate heating of the system may drastically reduce the time required for outgassing. We may take advantage of this, for example, by arranging an inlet for hot water to the cooling-water system of the furnace enclosure.

Concerning the furnace proper, outgassing may be effected at a higher temperature, provided the temperature is kept well below that required for any chemical reaction to occur in the studied system. A time-saving habit is to have the sample and the furnace ready in the afternoon. Evacuate the system, increase the temperature to the desired level for outgassing, and leave it overnight with pumps running. Next morning, read the gauges and start the run. This should ensure clean work.

6.4 THROUGHPUT, CONDUCTANCE AND PUMPING SPEED

The quantity of gas which passes through a given conduit or vacuum component in unit time is called the *throughput,* Q. It is a measure of the amount of gas (volume · pressure, or number of moles) that passes in unit time. The throughput is dependent upon the pressure drop through the component. Hence for a given component we define its intrinsic *conductivity*, $C = Q/(P_1 - P_2)$.

A closely related quantity is the *pumping speed*, $S = Q/P$. Texts on vacuum technology distinguish between the two concepts; C refers to the pressure difference $(P_1 - P_2)$ while S refers to the pressure P across a plane in the system (cf. O'Hanlon (2003) p. 27 and 123).

For the present purposes, however, the distinction appears superfluous. We will use the concept *pumping speed S* only for both pumps and other components.

The pumping speed of a given tube depends on the pressure range. On p. 182 a survey of mean free path in dependence of pressure was given. Two types of gas transport were mentioned: viscous flow at high pressures (small mean free path), and molecular flow at low pressures (large mean free path).

Which of the two types of flow is dominating in a specific case is determined by the relation between the mean free path and the diameter d of the tube, often termed the 'Knudsen number'

$$\mathrm{Kn} = \lambda/d \,(\mathrm{def}) \tag{6.13}$$

For $\mathrm{Kn} < 0.01$ we assume viscous flow, for $\mathrm{Kn} > 1$ we have essentially molecular flow. The range $0.01 < \mathrm{Kn} < 1$ represents a transition region.

6.4.1 Viscous Flow

At the start of a pumping sequence, the flow in the forevacuum line may be turbulent, but as the gas density is reduced it will revert to laminar, or *viscous* flow. The volume rate of flow for a gas with viscosity η through a tube with diameter d and length $L \gg \mathrm{d}$ is given by Poiseuille's equation:

$$S_{visc} = \frac{\pi r^4}{8\eta L} P = \frac{\pi d^4}{128\eta L} P \tag{6.14}$$

The viscosity of a gas is essentially independent of its pressure, while it increases with temperature. The viscosity of air at 20 °C is about $1.85 \times 10^{-5}\,\mathrm{Ns/m^2}$. With consistent use of SI units, Eq. (6.14) gives $S_{visc} = 1330\, d^4/L \cdot P\ (\mathrm{m^3/s})$, where P is the pressure drop in pascal.

Here we meet (again) the practical problem of 'suitable' dimensions. In the above examples (pp. 183–184) area was repeatedly expressed in $\mathrm{cm^2}$, for the simple reason that $1\,\mathrm{m^2}$ is too big to be conceived on a laboratory desk, and $1\,\mathrm{mm^2}$ is too small. Hence we diverge from the standard engineering practice with powers of 10^3, and express dimensions in

centimetres. Converting to d and L in cm, Eq. (6.14) yields $S_{visc} = 1330\ d^4/L \cdot P\ (\mathrm{cm}^3/\mathrm{s}) = 1.33\ d^4/L \cdot P$ (litre/s). Converting also to P in millibar, we have

$$S_{visc} = 133 \frac{d^4}{L} P\ (\mathrm{litre/s}) \tag{6.15}$$

Equation (6.15) is valid for tubes with $L \gg d$, as is the usual case with a forevacuum line. Expressions for short tubes in the viscous region are of little importance for our purposes.

6.4.2 Molecular Flow

As stated above, molecular flow is dominant for $\lambda > d$, where d is an inside diameter. It is worth noting that this expression is valid down to microscopic dimensions; hence it follows from the table on p. 182 that gas flow in pores of cross-section 1 μm or less is essentially molecular even at 1 bar pressure. For the present, however, we consider tubes and openings of macroscopic dimensions.

In the region of molecular flow, the concept of viscosity loses its meaning, and the pumping speed is given by the expression:

$$S_{mol} = \frac{1}{3} \sqrt{\frac{\pi RT}{2M}} \frac{d^3}{L} (\mathrm{m}^3/\mathrm{s}) \tag{6.16}$$

For air ($M = 0.029$) at 20 °C, with d and L in cm and S in litre/s:

$$S_{mol} = 12.1 \frac{d^3}{L}\ (\mathrm{l/s}) \tag{6.17}$$

Note that the pumping speed in the range of molecular flow is independent of the pressure. In other words, the transport process is not the result of pressure differences as such, but rather the net result of random movements of molecules within a space with gradients in concentration. In this sense it is analogous to diffusion, whence the name *diffusion pump* for pumps used in this range.

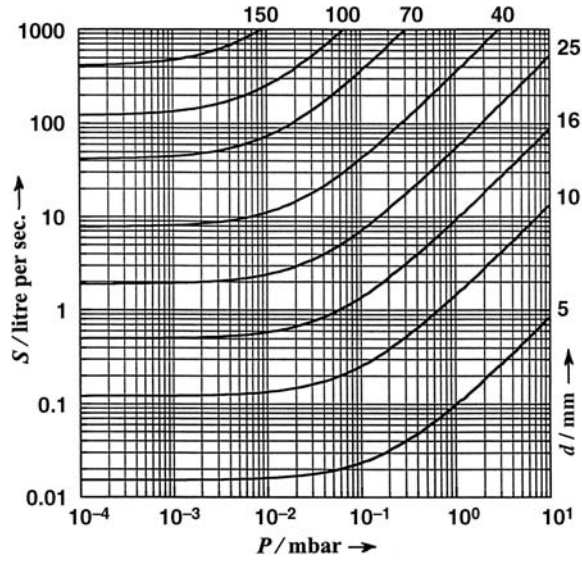

Figure 6.2 The pumping speed S of round tubes in dependence of gas pressure P, calculated from Eq. (6.18) for tube length $L = 1$ metre and various diameters d.

6.4.3 The Transition Region

The pumping speed in the pressure range between roughly 1 mbar and 10^{-3} mbar is most simply treated as the sum of the two independent contributions from viscous and molecular flow, that is

$$S = 133\frac{d^4}{L}P + 12.1\frac{d^3}{L}(\text{l/s}) \qquad (6.18)$$

The results of Eq. (6.18) are shown graphically as a function of pressure for a number of tube diameters in Figure 6.2. It should be noted in particular that as the tube diameter is increased, the transition from viscous to molecular flow stretches to lower pressures.

6.4.4 Molecular Flow, Short Tubes

The rate of transport, or pumping speed, for molecular flow through a short tube is usually given as the transport rate for an opening in a thin

wall ($L = 0$), multiplied by a factor which is a function of the ratio between length and diameter.

Thin Wall (L = 0). The collision frequency $n^\bullet$ (mol/s) on the area A was given in Eq. (6.9) (p. 183) as a function of the gas pressure P. Converting to pumping speed $S = V^\bullet = n^\bullet RT/P$, this gives the pumping speed for zero length:

$$S_0 = A\sqrt{\frac{RT}{2\pi M}} \tag{6.19}$$

By use of SI units, Eq. (6.19) gives the pumping speed in m^3/s. Changing to lengths in cm and volume in litre, with the molar mass for air (0.029 kg/mol) and 20 °C = 293 K:

$$S_0 = 11.6\ (A/\mathrm{cm}^2) = 9.1\ (d^2/\mathrm{cm}^2)\ (\mathrm{l/s}) \tag{6.20}$$

As a memory aid it may be noted that the pumping speed of an opening is about 10 l/s per cm^2 area of the aperture.

Short Tube (0 < L/d < 50). The pumping speed for a short tube is usually expressed in terms of the speed S_0 for the cross-section, times a factor W which is less than unity:

$$S_l = S_0 W \tag{6.21}$$

The factor W expresses the probability that a molecule which enters into one end of the opening will eventually exit through the other end; planes A-A and B-B in Figure 6.3a. The letter W stems from the German *Wahrscheinlichkeit* = probability. It is also called the 'Clausing factor', named after P. Clausing who made the first calculations in 1932.

It is of some interest to take a look at the physical basis for the calculation of W. The basic assumption is that a molecule which hits the wall of the tube, leaves again in a direction which is independent of the angle of incidence. The reason is that the molecule remains adsorbed to the inside wall for some time, however short. When the molecule re-evaporates, its exit direction is statistically distributed according to the 'cosine law' $I = I_o \cos \varphi$, where I_o is the maximum probability at right

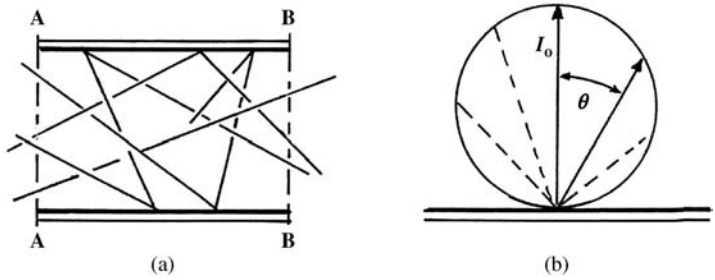

Figure 6.3 (**a**): The path of molecules through a short tube at conditions of molecular flow (schematic). (**b**): The probability distribution of exit direction θ for a molecule desorbed from a solid wall.

angle to the wall, compare Figure 6.3b (compare also the optical equivalent on p. 96, Figure 4.1a).

The calculations of net transport rates are quite complicated, and the results are usually given in tabular form. Table 6.1 gives only abbreviated results for circular tubes; more complete tables are given by, for example, O'Hanlon (2003).

Accurate calculations of the transition probability W for short circular channels are of considerable interest in connection with vapour pressure determinations by the Knudsen effusion method, to be discussed in

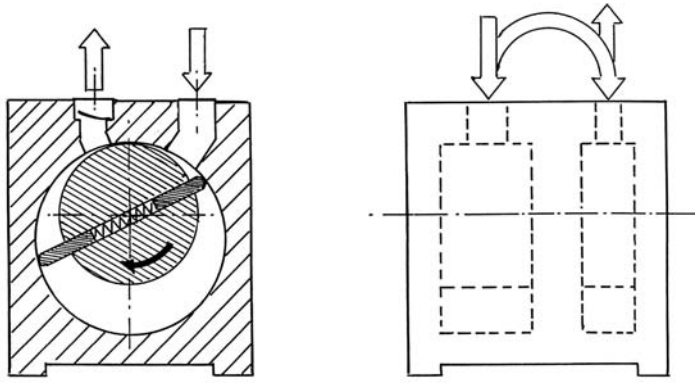

Figure 6.4 (**a**): Principle of an oil-sealed rotary vane pump. The two vanes are spring-loaded and slide in slits within the rotating body. (**b**): Simplified side view of a two-stage pump, showing the path of the gas from the first stage to the second and out.

Table 6.1 Transmission probability W for round tubes in dependence of the ratio between length and diameter, L/d.

L/d	W	L/d	W	L/d	W
0	1.000	0.4	0.718	3.0	0.275
0.05	0.952	0.5	0.672	4.0	0.225
0.10	0.909	0.7	0.597	5.0	0.191
0.15	0.870	1.0	0.514	10	0.109
0.20	0.834	1.5	0.420	20	0.059
0.30	0.771	2.0	0.357	50	0.025

Chapter 8. In a brief discussion of vacuum technique, on the other hand, it is probably sufficient to state that channels in the range of molecular flow should be made as short and wide as possible, compatible with the rest of the apparatus. As a rule of thumb it may be noted that for a tube with length equal to the diameter, $W \approx 0.5$.

6.5 FOREVACUUM PUMPS

As indicated on Figure 6.1 (p. 180) it is standard practice that a high-vacuum system includes a forevacuum pump in series with a high-vacuum pump.

6.5.1 The Oil Sealed Rotary Vane Pump

This is the most commonly used forevacuum pump in the laboratory. A detailed knowledge of the mechanism or working of a rotary pump is not essential to the user, hence only the principle of the pump is shown in Figure 6.4. The gas (air) is sucked into one side where the volume expands due to the rotation, and it is compressed and ejected at the other side where the volume is decreasing. A number of necessary details, such as the condenser that prevents loss of oil, are omitted on the drawing.

In order to achieve a better and more reliable vacuum, two-stage pumps are usually preferred. The two stages are arranged side by side on the same shaft, with the exit from the first stage leading directly to the inlet stage of the second.

The pump is powered by an electric motor that does not require further comment here. Formerly, the speed of the pump (rpm) was generally lower than the speed of the motor, so that a belt drive was required. With improved technology, pumps were made with higher speed of rotation (and thus smaller size for the same pumping capacity), and direct drive between pump and motor is now the standard.

It is important to note that a rotary vacuum pump is a precision device. The vanes shall provide vacuum tight sealing against the cylindrical housing as well as the flat end walls. For one thing, it is very important that no abrasive particles are admitted into the pump.

A dust filter in the pump entrance is highly recommended, not least in conjunction with vacuum furnaces. Various high temperature vapours, such as SiO or Al_2O, may give rise to fine dust that passes though the system and ends up as finely divided abrasives in the pump oil, eventually ruining the pump. A suitable design of a dust filter is indicated in Figure 6.5, intended for direct fitting to the top of the forevacuum pump.

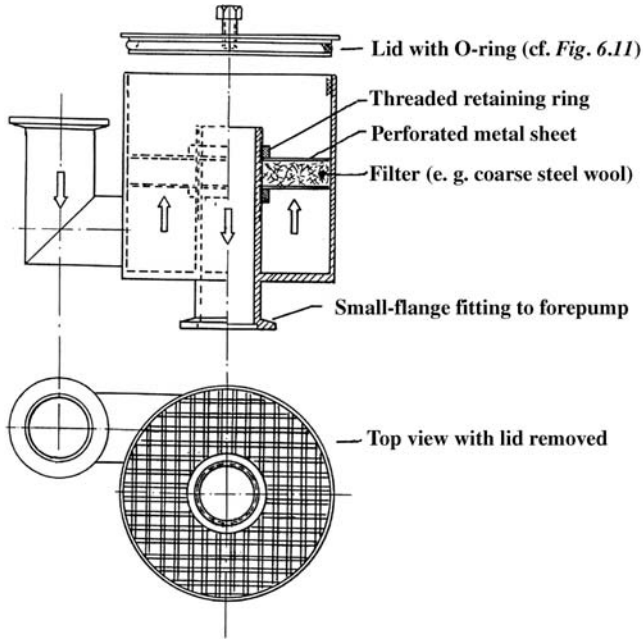

Figure 6.5 A dust filter fitted directly on top of the inlet flange of a forevacuum pump.

The filter medium deserves special attention. In Figure 6.5, coarse steel wool is suggested; a mass of copper wire has also been used. The filter is drenched in pump oil before use. During the passage of the gas through the tortuous path in the filter, the dust particles will adhere to the oil film. After prolonged use the filter may be removed, cleaned in kerosene and re-installed.

A number of different forevacuum filters are commercially available. Some of them utilize 'cardboard' filter materials of the kind used in air filters for car engines. In this context it should be noted that the filter may become wet with oil, whether intended or not, because of back-diffusion of oil from the pump. The pumping capacity of a finely porous material wet with oil may be in doubt, hence a coarser material is suggested above.

A filter will necessarily decrease the pumping capacity of the fore-pump. No definite figures will be given, but it seems that a loss of some 30% of the full capacity is a reasonable fee to pay in order to prevent the pump from being ruined.

The pump oil should have good lubricating properties. At the same time it should have a low vapour pressure, but the lubricating properties have priority. Note that a rotary pump while running causes mechanical work which is converted to heat. The temperature of the oil in a normally running pump may well be around 80 °C, and the vapour pressure of the oil in the pump is correspondingly high. Used alone and directly connected to a chamber at room temperature, pump oil will slowly distil from the pump into the chamber (as also indicated above).

The end vacuum of a commercial two-stage rotary pump may be given by the manufacturer as 10^{-4} or even 10^{-5} millibar, but these numbers indicate the end pressure of permanent gases under ideal conditions. The total pressure seldom goes much below 10^{-2} millibar due to the vapour pressure of the oil. But this is amply sufficient since the required forevacuum for an oil diffusion pump is at least an order of magnitude larger.

The manufacturer's recommendations should be followed regarding the proper oil for a given pump, and the periods for oil change. (The recommended oil may usually be obtained directly from one or another of the oil companies.)

The gas ballast valve, fitted to most two-stage pumps, deserves some explanation. With the valve open, some air is automatically admitted to the entrance of the second stage during each revolution. This acts as a

'carrier gas' so that condensable gases (such as water vapour) may be exhausted rather than dispersed in the oil. With the gas ballast valve open, the end vacuum is not quite as low, but generally it is still ample for satisfying the required forevacuum.

6.5.2 The Rotary Piston Pump

This is considered somewhat more robust than the vane pump, and for this reason it is preferred for larger, industrial vacuum systems. Otherwise the ranges of service are the same for the two types, as are also the precautions mentioned above.

6.5.3 Other Forevacuum and Medium-Pressure Pumps

Some applications require oil-free or 'dry' pumping. The **diaphragm pump** serves the purpose, but does not attain end vacuum better than some 2 mbar. The **Roots pump** or **lobe blower** is another type of dry pump. It contains two rotors on parallell shafts, which rotate in opposite directions. Each rotor has two lobes, like a figure 6.8 (or even three lobes), designed to fit into each other during the rotation. The clearances between the two rotors and between the rotors and the elongated housing may be some 0.2 mm. It runs oil-free at speeds of some 2000–3000 rpm and provides large pumping capacity at medium pressures, with end pressures of a few millibar. The **scroll pump** is a further development along the same lines, designed to run without any lubricant and hermetically sealed, with end vacua below 0.1 mbar. Such pumps, however, are of only marginal interest for the present purposes.

6.6 HIGH-VACUUM PUMPS

6.6.1 The Oil Diffusion Pump

A typical oil diffusion pump is seen in longitudinal section in Figure 6.6. Note that this sort of pump contains no moving parts, and for this reason it is rugged and durable. But it does not act as a pump unless the

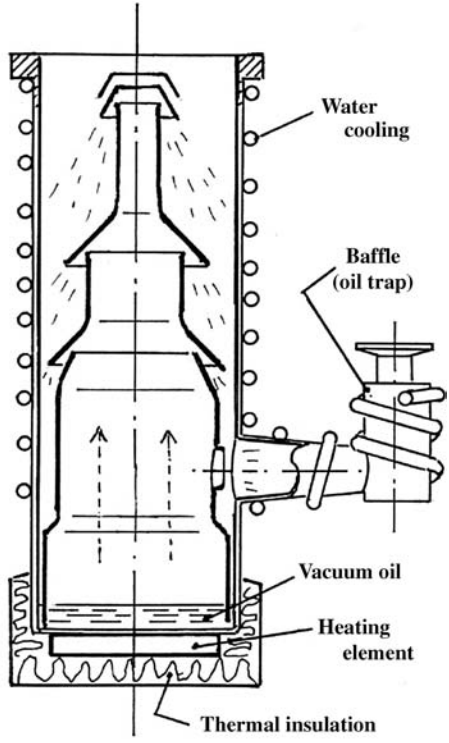

Figure 6.6 Section through an oil diffusion pump. The pump body is usually made of stainless steel with outside water cooling, while the internal parts may be made of aluminium.

forevacuum pressure is below a certain critical limit, which for different designs may lie between 0.3 and 1.0 mbar.

To explain the working principle, we note first the heating element beneath the bottom of the pump. On the bottom floats a layer of high-vacuum oil, usually to no more than some 10–15 mm depth. When heated, this oil is brought to boiling under the reduced pressure created by the forepump. The vapour streams upwards through the tubular inner body, is directed downwards by the conical hoods, and is forced out through the narrow passages forming circular, downwards-directed jets. Any gas molecule that happens to drift into the uppermost vapour jet is likely to be knocked downwards by the vapour molecules, and eventually forced out through the forevacuum outlet. The oil vapour is condensed when hitting the water-cooled walls, and it runs down the

walls and back to the oil pool. A water-cooled baffle is often fitted to the top of the pump to avoid back-streaming of oil vapour.

The interior parts are usually made of aluminium, which has negligible vapour pressure at the temperatures in question and excellent thermal conductivity. The outer casing is made from stainless steel which is a poor conductor of heat, hence the short distance between cooling turns as seen in Figure 6.6.

The illustrated, cylindrical pump has three stages, plus a fourth compression stage directed into the forevacuum line. The outer shape as well as details may vary for different makes, sizes and purposes. For 'scientific' pumps, the body may be pear-shaped to give more room for the top stage.

In earlier models the tubular section of the top stage in Figure 6.6 (or both the first and second) extended all the way downwards into the oil pool. The idea was that the fraction of the oil with the highest boiling point would evaporate from the central bottom area and hence reach the top stage of the vapour ejectors. This fractionation is probably of less importance today with pump fluids of homogeneous composition.

Diffusion pump fluids have undergone considerable development, from the early hydrocarbon oils to the present silicone fluids. An early cause of failure was carbonization of the pump oil due to overheating, caused by accidental air inlet or by failure of the forevacuum. The subsequent removal of the carbon residue was a tedious job. The present silicone fluids (and some polyphenyl ethers), have much better stability at high temperatures and against oxidizing gases such as air. Still it is recommended to keep the pump under vacuum until the fluid is cold. In fact it may to advantage be kept under vacuum at all times, using the bypass line of Figure 6.1 (p. 180).

The end vacuum obtainable with a diffusion pump depends on the pump fluid. Fluids with the lowest vapour pressures also have the lowest attainable end pressures, of the order of 10^{-9} mbar. However, for a number of reasons these very low pressures may not be attained in practice, and they are usually not even needed. A pump fluid with somewhat higher vapour pressure will tolerate a higher forevacuum, and it may give as good or better pumping performance in the range from 10^{-1} to 10^{-5} mbar. Better end-vacua than this are seldom needed in high temperature chemistry.

The first diffusion pumps, about a hundred years ago, used mercury as the pump fluid, with the pump body made of glass. Mercury has a

vapour pressure of about 10^{-3} mbar at room temperature, and hence a cold trap was definitely needed, often with solid carbon dioxide as the cooling medium.

As is well known, mercury vapour is toxic, and mercury diffusion pumps are now mainly of historic interest. The only application where they offer special advantages is in mass spectrometry, because the mercury atom does not decompose and its mass is easily identified. But even in this area they are being displaced by more modern high-vacuum pumping systems.

6.6.2 Vapour Booster Pumps

These are similar to diffusion pumps, but specifically designed to give large throughput in the medium–high vacuum region. To this end the pump body is cone-shaped, widening upwards. The end vacuum is generally higher than 10^{-5} millibar, while the critical forevacuum may be several millibars. Vapour boosters are primarily made for industrial use. They are mentioned in the present context, however, because they seem well suited to metallurgical reduction and refining processes at reduced pressures.

6.6.3 Turbomolecular Pumps

These are designed to give pressures lower than attainable with the best oil diffusion pumps, while the throughput is of secondary importance. A turbo pump is akin to a gas turbine but with the opposite purpose: in the turbo pump energy is consumed to move the gas molecules. The speed of rotation of a turbomolecular pump may be some 30 000 rpm or even higher. At these high speeds, any gas molecule hitting a vane in the pump is not adsorbed like discussed on p. 193, but rather knocked off in a direction similar to specular reflection. By a large stack of interspaced vanes, the molecules are forced through the pump and out through the forevacuum line.

The high speed of rotation demands a separate electronic control unit which adds to the cost. The pump itself is prone to failure if foreign particles hit the rotor during use. Generally speaking, the turbomolecular pump is a costly and fragile piece of equipment. It is preferred where ultra-low pressures and clean conditions are required, like in mass spectrometers and electron microscopes, and for the study of surfaces.

6.6.4 The Ion Pump

The ion pump (or ion sputter pump) is used to attain ultra-high vacua. It employs a strong electrical potential in combination with a strong magnetic field. Incoming atoms or molecules are ionized, accellerated and finally trapped in the solid cathode, which is usually of titanium. The ion pump has no pump outlet, hence it is suitable only for systems with a very modest release of gases.

6.7 EVACUATION TIME AND CHAMBER MATERIALS

6.7.1 Evacuation Time

We assume a pump with pumping speed S, working in a vacuum chamber with the gas pressure P. During the short time interval $\mathrm{d}t$, the amount of gas transported is $PS\mathrm{d}t$. With the chamber volume V, the amount of gas removed from the chamber during the same time is $V\mathrm{d}P$. Thus we have the equation

$$V\mathrm{d}P = PS\mathrm{d}T$$

By integration:

$$t = 2.30\frac{V}{S}\log\frac{P_0}{P_t} \tag{6.22}$$

Assume as an example a chamber volume $V = 50$ l, a starting pressure $P_0 = 1000$ mbar and an end pressure $P_t = 0.1$ mbar (four powers of ten). A forevacuum pump with a pumping speed $S = 1.5$ l/s does the job in $307\,\mathrm{s} \approx 5$ min, according to Eq. (6.22). From this point of view the said forevacuum pump capacity is ample.

6.7.2 The Suitable Pump Combination

As an example, we choose an oil diffusion pump with an internal diameter of 10 cm. According to Eq. (6.20) this has a theoretical pumping speed of 910 l/s at the plane of the pump entrance. However, the pump

may be likened to a short tube with a length twice the diameter; $L \approx 2d$. This gives the Causing factor $W = 0.35$, and hence a pumping speed $S \approx 300$ l/s. This is roughly the pumping speed quoted by the manufacturers for a 10 cm diameter pump.

Now suppose that this speed shall be maintained at a high-vacuum pressure of 10^{-3} mbar and a forevacuum pressure of 0.2 mbar. The required capacity of the forevacuum pump is then $(10^{-3}/0.2)$ $300 = 1.5$ l/s or about 5 m^3/h. This is just about the backing pump capacity recommended by the manufacturers for the said size diffusion pump.

The assumed pressure of 10^{-3} mbar may seem high, and just on the verge with respect to maintaining the pumping speed of a diffusion pump. After sufficient pumping time, the pressure may be two orders of ten lower. The example, however, is chosen to illustrate the situation during initial start-up and outgassing.

Practical Considerations. From the construction of an oil diffusion pump (Figure 6.6) it is clear that it takes some time from the point that the heater is turned on until the oil starts boiling; usually some 15–20 min. With an ample forevacuum capacity as indicated above, it is convenient to turn on the forevacuum pump and the diffusion pump at the same time, resting assured that the required forevacuum will be attained before the diffusion pump starts working.

Once the diffusion pump starts working, the next drop in the powers of ten should be reached in a very short time due to the large pumping speed of the diffusion pump, compare Eq. (6.22). Right enough, the first sharp drop in pressure occurs almost at once, as observed on a vacuum gauge. But then the outgassing takes over, as discussed already on pp. 187, 188, and the further drop to 10^{-4} and 10^{-5} mbar may take hours, depending on the materials in the chamber.

6.7.3 Materials and Outgassing

The materials of the chamber wall should be gas tight, non-volatile and preferably with smooth surfaces.

Glass. This was the classical material for vacuum lines in the old days. An experienced glass blower could make almost anything out of glass, including mercury diffusion pumps and cold traps. For a chemist, and particularly in synthetic organic chemistry, glass vacuum lines are essential, see Plesch (1989). In this context, the operator must be familiar with at least the elements of glass blowing and the use of a hand torch (Plesch, p. 18).

Larger flanged tubes of borosilicate glass with rubber gaskets are used both in chemical industry and in the laboratory. The first high vacuum system I ever encountered (in California half a century ago) was built in this way, with 4 in. Pyrex tubing. Through a ground glass joint it was connected to a vertical, round-bottom silica glass tube with the sample inside and the high-frequency induction coil on the outside. Glass is still a favourite container material for induction heating in the laboratory, compare Figure 2.11 p. 35.

A point against the use of large glass chambers is the risk of implosion. A glass chamber that breaks while under vacuum will implode with a violence much like that of an explosion. For safety, a glass 'bell jar' for vacuum use should be covered by an outside metal screen before evacuation.

Metals. The commonly used metals of construction, like steel (including stainless), copper and aluminium, have negligible vapour pressures and are generally suited for vacuum constructions. An exception is brass, an alloy of Cu with 30 to 40 wt% Zn. Metallic zink has a vapour pressure of 10^{-3} mbar already at 300 °C, and this is reflected also in its alloys with copper. Water-cooled chambers may be made of brass, while inside brass screws or other items that get hot must be avoided. More on this topic in Chapter 7.

Thermal Insulation. This topic was already discussed on pp. 38–40. When used in a vacuum furnace, the large surface area and the tendency to gas adsorbtion is a problem with fibrous materials. Porous materials with partly closed pores may be even worse.

A partial solution is to always keep the furnace in the chamber under vacuum when not in use. It should be exposed to the atmosphere only for the short periods needed for exchanging samples or other alterations. Absorbtion and desorbtion of gases take time, and keeping the system under vacuum aids in shortening the time necessary for outgassing. This

statement is not a result of theoretical considerations; it is a matter of practical experience.

6.8 FLANGE FITTINGS

6.8.1 The Flange and the O-Ring

Once upon a time, when lecturing on the basic facts of vacuum systems, one of the students asked me: *What is a 'flange?'* So, here is the answer according to *The Concise Oxford Dictionary*: *A protruding rim*. In connection with plumbing or vacuum systems, it is the rim of a tube, made to be fastened to a similar rim on the next piece of tubing.

A simple sort of flange joint is shown in Figure 6.7. As drawn, it is fastened by hexagonal bolts and nuts through holes around the flanges. In the 'old days' (before ~1950), such flange joints were usually made tight by means of a flat gasket between plane flange surfaces. It is clear, however, that a flat gasket gives little play for uneven surfaces; a misfit of a few tenths of a mm might be enough to cause a leak. It was a

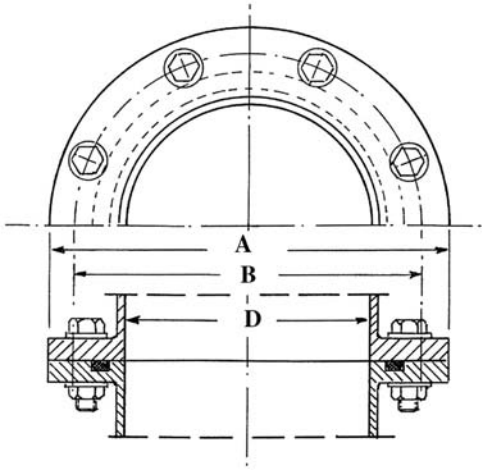

	A	B	D	Holes: Dia.	Holes: No.
ISO63	130	110	70	9	4
ISO80	145	125	83	9	8
ISO100	165	145	102	9	8
ISO160	225	200	153	11	8
ISO200	285	260	213	11	12
ISO250	335	310	261	11	12
ISO320	425	395	318	14	12
ISO400	510	480	400	14	16
ISO500	610	680	501	14	16
ISO630	750	720	630	14	20

Figure 6.7 A flange joint with O-ring groove on the lower flange. Standard dimensions according to ISO (the International Standards Organization) are given in mm for the outside flange diameter, hole circle and internal diameter, for sizes from ISO63 to ISO630.

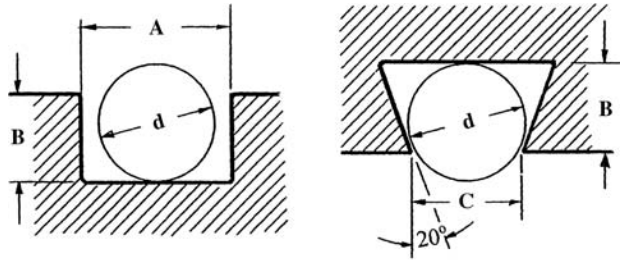

Figure 6.8 Suitable dimensions of O-ring grooves in dependence of the O-ring thickness *d*. Tolerances are given so that the real dimensions may be adjusted to the nearest tenth of a millimetre for a given O-ring. (**a**): Rectangular (open) groove. (**b**): Dovetail (retaining) groove.

great leap forwards in vacuum technology when the *O-ring* was introduced.[2] The circular cross-section of the O-ring requires less force to obtain a given reduction in height, and hence has a better ability to provide vacuum tight joints.

It should be noted that elastomers or rubber-like materials from which O-rings are made, may deform under load, but like other materials they are essentially incompressible. For illustration, compare with water: it may change its form, but under normal pressures it does not markedly alter its volume. This is of importance for the dimensioning of an O-ring groove. In order to avoid damaging the O-ring, the cross-section area of the groove (height times width) should be some 20 to 25% larger than the cross-section area of the O-ring ($\pi d^2/4$). Suitable dimensions for O-ring grooves are shown in Figure 6.8.

Horizontal flange joints that are often opened (like the flanges of a furnace chamber) should have the O-ring groove retained on the upper flange when in open position, to reduce the risk of dirt dropping onto the exposed O-ring. With this in mind, suitable dimensions for a dovetail groove are shown to the right in Figure 6.8.[3]

[2] The O-ring was patented in the USA in 1938, and is now used throughout all kinds of industry.

[3] Manufacturers of vacuum equipment have not always been aware of this requirement of sufficient volume. Thus, commercial vacuum equipment disassembled after some years' use has shown O-rings that are cracked due to excessive compression. On the other hand, experience shows that O-rings mounted with adequate space may be in good shape after 20–30 years of service.A dovetail groove may mean an important convenience to the user, but it is rarely seen on commercial equipment.

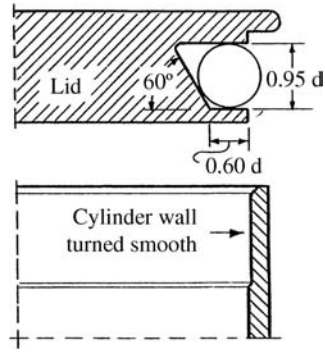

Figure 6.9 Space- and material-saving design for a lid at one end of a tube.

In cases where a tube should terminate with a lid only, regular flanges are not strictly necessary. Figure 6.9 gives the suitable shape and dimensions for an O-ring groove in a lid to be pressed onto the matching cylinder.

A final note: the cross-section diameter d of the O-ring is a critical value (to the nearest tenth of a mm), while the larger diameter D of the ring is less critical.

6.8.2 Small Flange Fittings

With the development of vacuum technology during the last half century, the International Standards Organization (ISO) established a set of standard shapes and sizes for essentially three different types of flanges.

For the smallest flanges, up to 50 mm inside diameter, the joining with bolts and nuts seemed unwieldy. A simpler system was designed, as illustrated in Figure 6.10. The two opposing flanges are identical, with an O-ring inbetween, held in place by a centring ring. The outside face of each flange is slightly conical (15°), and the assembled flanges are secured by a clamping ring with insides shaped to fit the conical faces.

These flanges were originally developed in Germany, and they have variedly been designed ISO-KF (for *Kleinflansch* = small flange) or NW (*Nennweite* = nominal width). All kinds of small-flange fittings are

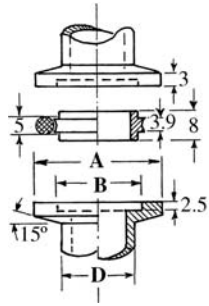

	A	B	D
NW10	30	12.2	14
NW16	30	17.2	20
NW20	40	22.2	25
NW25	40	26.2	28
NW32	55	34.2	38
NW40	55	41.2	44.5
NW50	75	52.2	57

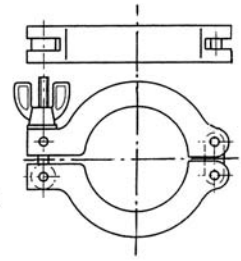

Figure 6.10 Left: Two identical, opposed small flanges with O-ring and centring ring in-between. Right: Clamping ring, to fit the outer diameter as given in column A of the table (four different sizes). The table plus the drawing gives the relevant dimensions for the seven sizes of small flanges.

available commercially, such as elbows, tees, crosses, and so on, made from aluminium (alloy) or from stainless steel. In Figure 6.10 the relevant dimensions in mm are tabulated, in case a flange or two should be made in a lathe at short notice.

Historically the small-flange series included NW10, 20, 32 and 50. At a later date it was found that most of these standard flanges were rather roomy, thus NW10 was supplemented with NW16 with the same outer diameter; NW25 came in addition to NW20, and NW40 in addition to NW32. Only NW50 remained unchanged. Thus it is seen from the table in Figure 6.10 that there are seven different varieties of small flanges, but (fortunately) only four different sizes of clamping rings.

The larger-size internal diameter never does any harm, thus the sizes 10, 20 and 32 could be omitted. However, with a lot of equipment already in use, all sizes are still available, including adapters for combinations 10/16, 20/25, and so on.

6.8.3 Rotatable, Collar, and Clamping Flanges

From an internal diameter of 63 mm upwards, the more usual design of flanges with bolts and nuts was retained, compare the table of dimensions in Figure 6.7. However, the O-ring groove was omitted, and a set of centring and retaining rings were designed to keep the O-ring in place,

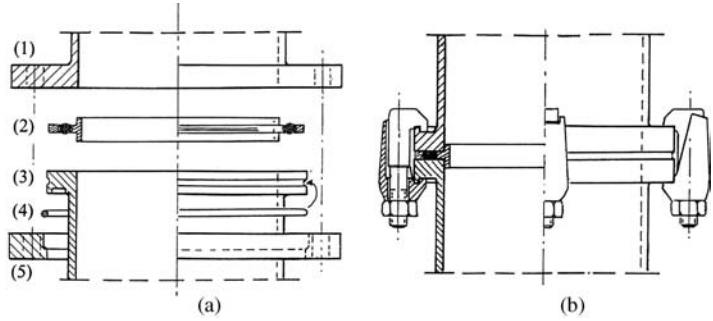

Figure 6.11 (**a**): Assembly drawing of a fixed and a rotatable flange. (1): Fixed flange. (2): O-ring with centring and retaining rings. (3): Collar flange. (4): Split steel ring. (5): Outer flange with bolt holes (as on Figure 6.7). (**b**): Two opposing collar flanges, secured by claw clamps.

compare Figure 6.11a. An obvious advantage is that all flanges of the same nominal size are flat and may be interchanged.

Another change is the introduction of the rotatable flange, making it possible to fasten a component at any angle regardless of the position of the bolt holes. As seen on Figure 6.11a it consists of an inner collar flange (3) and an outer rotatable flange (5), secured by a steel ring (4) clipped onto the collar.

A further alternative is that the outer flanges and bolts are omitted altogether, while the two opposing collar flanges are secured by claw clamps as illustrated in Figure 6.11b. Four, six or eight clamps are used according to the size of flanges.

Commercially, all kinds of combinations between claw flanges and fixed flanges are available. For workshop production, on the other hand, the old-fashioned fixed flange with groove (Figure 6.7) may still be the simplest.

6.8.4 ConFlat (CF) Flanges

This is a series of flanges designed for ultra-high vacuum where elastomer gaskets (O-rings) are not adequate. A CF flange is made of steel with a sharp, circular edge where it faces the flat metal gasket. Copper is the usual gasket material. Two identical, opposed flanges are tightened by bolts and nuts so that the steel edges cut partly into the soft

copper. Compared to a normal vacuum flange, about the double number of bolts are used to provide an adequate compression. The result is a very reliable seal, as further discussed by, for example, O'Hanlon (2003) p. 316. However, for the present purposes, ultra-high vacua are generally not required.

6.9 VALVES

6.9.1 High-Vacuum Valves

The connection between diffusion pump and working space must permit closing and opening. A further consideration shows that the diffusion pump should not be attached directly below the bottom of the work space, because of the chances for foreign material to drop into the pump. In conclusion, an angle valve is preferred, as already indicated on Figure 6.1.

A classical design of a high-vacuum valve is shown in Figure 6.12a. The original design is more than 50 years old, initially made from brass with silver solder. An improved design, permitting a higher pumping speed for the same size flanges, is shown in Figure 6.12b. Modern,

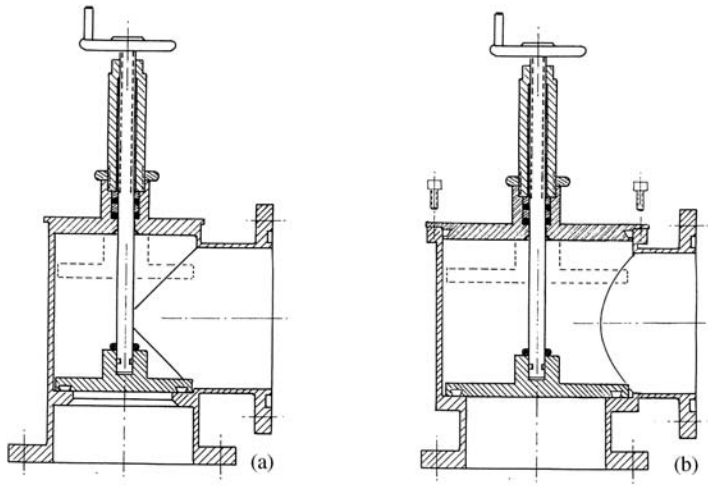

Figure 6.12 (**a**) A classical design of an angle valve. (**b**): An improved version, giving larger pumping speed on the same size flanges.

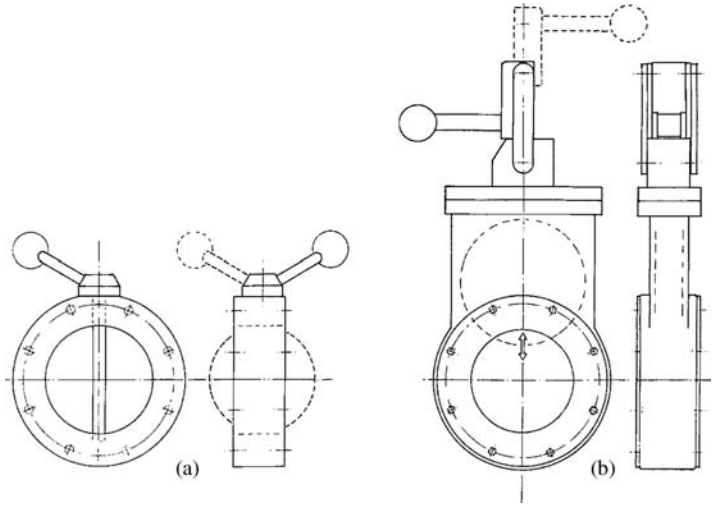

Figure 6.13 Two types of straight-through, space-saving high-vacuum valves. (**a**): Butterfly valve, with O-ring around the rim of the plate. (**b**): Gate valve, with O-ring groove in the plane. Both types require some design considerations in order to close the vacuum tight.

commercial angle valves are usually built on a cast-alloy body, eventually with some quick-release mechanism to open or close, but the principles are the same.

The valves in Figure 6.12 are shown with the stem tightened by means of packing glands with O-rings (cf. next section). An alternative way is to transfer the sliding motion by means of flexible bellows to avoid possible leaks. These are more expensive, less durable, and generally not needed for the present purposes.

A variety of high-vacuum valves are available commercially, including space saving models. Two of them are shown in outline in Figure 6.13. Both require more sophisticated engineering than the simple angle valve, which remains the preferred one for our purposes.

6.9.2 Forevacuum and Gas Admittance Valves

As regards the smaller valves needed in the forevacuum line, it makes no difference whether angle or straight-through models are used. It is

important, however, to provide adequate pumping speed, most simply by using valves and fittings of at least the same size as that represented by the flange on the forepump.

As regards air and gas admittance valves, smaller sizes may be used, down to 6 mm or 1/4″. Such small valves may as well be purchased from companies specializing in pipe fittings (Hooke, Swagelock, etc.). Valves down to 6 mm are available with O-ring fittings that make them entirely adequate for vacuum use. The glass tubes and stopcocks of old days are conveniently replaced by copper tubing and brass fittings. Tubes and fittings of stainless steel are more expensive, less easily handled, and unnecessary for general use.

6.10 FEEDTHROUGHS

6.10.1 Packing Glands

A very simple way of introducing a stationary rod or tube is shown in Figure 6.14a. The more professional solution, suitable also for moving

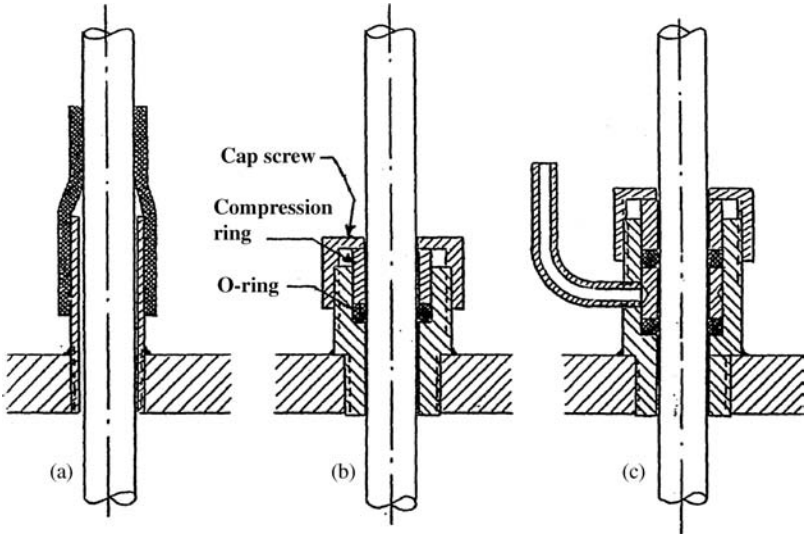

Figure 6.14 (**a**): A short, thin-walled pipe with a piece of rubber hose. (**b**): Packing gland with one O-ring. (**c**): Packing gland with two O-rings and compression rings, and (optional) side stud for extra lubrication.

shafts, is a packing gland with O-rings. In principle, one O-ring and one compression ring should suffice, as shown in Figure 6.14b. For added reliability, two each may be used. A side tube between the two O-rings may be provided as shown in Figure 6.14c, with a small quantity of silicone oil in the tube. Alternatively the side tube is omitted, while a small amount of silicone grease provides sufficient lubrication.

The space between the shaft and the gland should be just slightly smaller (some 0.1 mm less) than the smaller diameter d of the O-ring, and the collar nut should be tightened by hand only. If (by mistake) the gland appears too roomy, it may be noted that O-ring producers now offer a selection of O-rings with different thicknesses d for the same outward diameter D.

6.10.2 Electric Leads

The very simplest solution is the drilling of holes in a rubber stopper and forcing the leads through (with some silicone grease for lubrication). A more permanent solution is provided by using short pieces of ceramic tubing in holes in the metal flange, and copper leads inside the ceramics, as shown in Figure 6.15. Epoxy resin (e.g., Araldite) is used to seal the copper, ceramics and flange metal. The use of epoxy resin in vacuum technology is discussed by Roth (1994) pp. 248–258. The specific design will depend upon the requirements of high current or high voltage.

Reliable, vacuum-tight multipin leadthroughs with corresponding connectors are commercially available, and convenient in connection

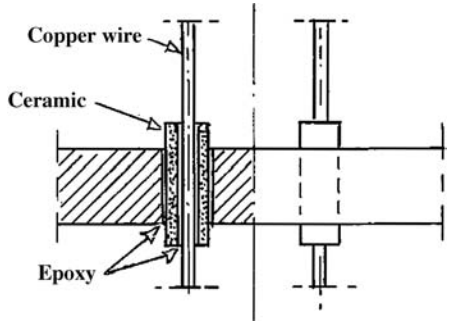

Figure 6.15 Electric leads through a metal flange.

with, for example, electronic thermobalances. In the end it is a question of needs, prices and availability.

Arrangements for high currents (several thosand ampéres) will be described in the next chapter.

6.10.3 Windows

In a metal system, windows are most simply made with the aid of an O-ring as illustrated in Figure 6.16, with groove dimensions as in Figure 6.8. Because of the smooth and glossy surface of the glass, hardly any compression is needed to provide tightness. A 40 mm dia. glass on a 25 mm dia. opening has been found suitable for general use. The nuts should be tightened by hand only; using a wrench is likely to result in cracked glass.

Windows in a vacuum furnace are likely to get coated by evaporating matter from the hot interior. This may cause difficulties in temperature measurement by optical means, see also Chapter 4, pp. 116–121. One solution that has been used is to provide a light flap of sheet iron hinged underneath the window, and a horseshoe magnet on the outside. Thus the window is subjected to the direct molecular beam only during the shorter intervals of temperature measurement.

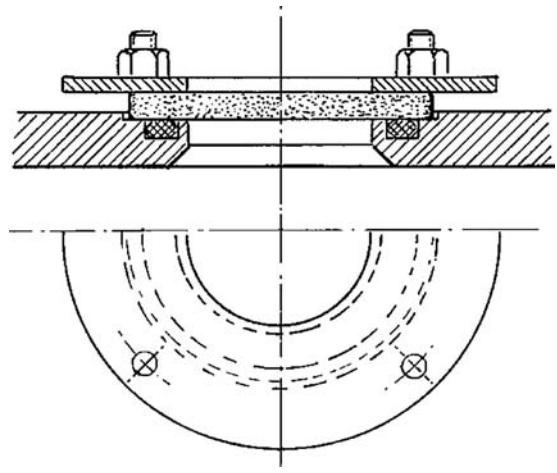

Figure 6.16 A glass window with retaining ring.

A better solution is to provide a 'carousel' with several windows, only one of which is exposed at a time. The design is shown in Chapter 7, pp. 256–259. But whatever solution is used, it is advisable to remove and clean the windows between each run.

6.11 PRESSURE AND VACUUM GAUGES

It appears customary to use the term manometer or pressure gauge for the range down to some 0.1 mbar, and vacuum gauge for the lower range, but the distinction is not important.

The most commonly used types of pressure and vacuum gauges are listed in Table 6.2. The first two are based on mercury as the manometric liquid and are now absent in most laboratories, but they are included for the sake of completeness. The next three in combination are (or should be) standard equipment in any high temperature chemistry laboratory. Each type is discussed separately in the next sections.

6.11.1 The Mercury Manometer

This is the classical pressure gauge, shown in Figure 6.17a. Considering the difficulty in transportation, it is likely to be 'homemade'. It is made from borosilicate glass tubing, with a 8 to 10 mm inside diameter to avoid excessive effect of the capillary depression. The shaping of the glass into a manometer requires some skill in glass blowing (or a professional glass blower).

An empty manometer, finished from the glass blower's hand, is shown in Figure 6.17b. A narrow section in or near the bend is recommended to

Table 6.2 Some pressure gauges, with their approximate pressure ranges.

Type	Range, *P*/millibars
Mercury manometer	10^{3}–1
McLeod gauge (mercury)	1–10^{-4}
Diaphragm	10^{3}–10^{-1}
Pirani/Thermoelectric	10^{-1}–10^{-3}
Penning (cold cathode)	10^{-1}–10^{-5}
Ionization (hot cathode)	10^{-2}–10^{-10}(?)

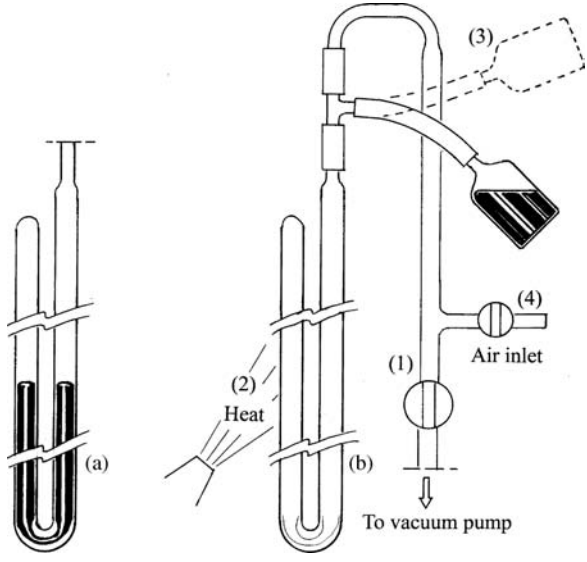

Figure 6.17 (**a**): A mercury manometer, shown with the vacuum system in evacuated position. (**b**): The same type manometer in an empty state. (1) Evacuation by rotary pump. (2) Heat to outgas the glass. (3) After cooling, fill in the required amount of mercury. (4) Close the valve to the vacuum pump, and slowly open the air valve. The design as shown permits mutual support of the two legs over the full height.

avoid too fast movement of the mercury in the event of sudden pressure changes.

The manometer is connected to a two-stage forevacuum pump and evacuated. Subsequently it is gently heated by a torch under continuous pumping to outgas the glass walls. After cooling, it is filled with mercury while still under vacuum. Finally, air is admitted, but carefully. The steps of the procedure are indicated in Figure 6.17b. The two legs of the manometer should be secured without strain, and the manometer sturdily mounted to avoid mishap.

Mercury is poisonous, as repeatedly pointed out, and many laboratories want to avoid it. The mercury manometer, however, is an 'absolute' gauge requiring no calibration. For this reason it still has its place when accurate gas pressure measurements in the 10 to 1000 mbar range are required.

6.11.2 The McLeod Manometer (H. G. McLeod, 1874)

This is a vacuum gauge based on mercury, as shown in Figure 6.18. This device enables measurement of the pressure of permanent gases down to

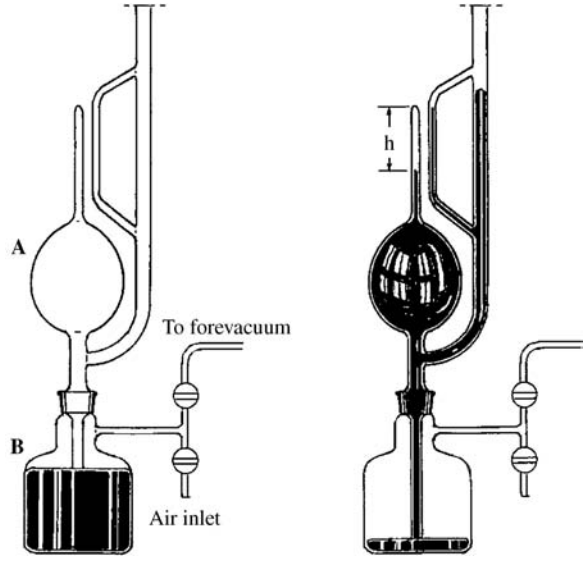

Figure 6.18 A McLeod manometer. Left: The gauge at rest. Right: Air admitted to bulb **B** until the mercury in the side capillary is level with the top of the capillary on **A**.

some 10^{-4} or 10^{-5} millibar. A McLeod manometer, however, might contain 10 kg or more of mercury, and due to the fragility of the glass bulb and the poisonous nature of mercury it is not much used any more. Still it deserves a short description.

The bulb **A** is the 'active volume' while the bulb **B** acts as a mercury reservoir. When both are evacuated, the mercury level is at a position where bulb **A** is open to the vacuum system. When a reading is to be taken, air is admitted to bulb **B**, causing the mercury level to rise so that the connection between the bulb **A** and the rest of the vacuum system is cut off. Further rise of the mercury level forces the gas trapped in volume **A** to be compressed into a steadily diminishing volume, and finally into the capillary on top of **A**. When the mercury in the capillary side-arm is level with the top of the capillary on **A**, the mercury level in **A** will remain somewhat lower because of the gas compressed into this capillary. The height h is a measure of the pressure initially in the vacuum system.

The capillary side-arm is a necessity to compensate for the capillary depression (the mercury level in the main vacuum connection rises higher). It is also noted that the time of the reading is the moment when

the mercury cuts off the main connection at the lower end of **A**. The resulting time lag, however, should make no difference if the bulb **A** is free of leaks.

In the 'old days', the reservoir **B** was connected to **A** by means of a rubber hose, and the mercury level was adjusted by moving **B** up or down. The use of partial vacuum in **B** to adjust the mercury level represents a modernized version. See also Roth (1982) pp. 289–297.

With a known volume of the bulb **A** and known internal diameter of the capillary, the relation between the measured height h and the pressure in the system may be calculated. The McLeod is thus an absolute gauge. It is noted, however, that it shows the pressure of permanent gases only.

6.11.3 Diaphragm Manometers

A diaphragm manometer has a thin membrane (a diaphragm) sealed between a good vacuum (or a reference pressure) and the pressure to be measured. Formerly, the movement of the diaphragm in response to changes in pressure was recorded by mechanical means. Nowadays, it is done by one or another form of digital electronics. It may be observed by changes in capacitance caused by movement of the diaphragm, or it may be done by means of a strain gauge. One type uses a thin disc of silicon, which thus acts as a combination of membrane and strain gauge.

The exact mode of operation is of minor interest to the user as long as the gauge works properly. For general use, a gauge with the range from 0.1 to 1000 mbar is recommended. The last digit may seem superfluous, and the zero point may vary between, for example, $+0.4$ and -0.4 (depending on room temperature, etc.). The last digit, however, is valuable in connection with leak detection, compare below. For this purpose, a scale in whole mbar is considered too coarse.

6.11.4 The Pirani and the Thermoelectric Gauge (M. Pirani, 1880–1968)

These are two variants of gauges based on the thermal conductivity of the gas. The sensing element is generally a thin metal wire heated

by a constant, low current. The temperature acquired by the wire will depend on the cooling effected by the surrounding gas, and this again depends on the pressure of the gas. The two types of instrument differ in the way of observing the temperature of the wire. In the Pirani instrument, the change in resistance of the wire is observed by making it one leg of a Wheatstone bridge (equivalent to a potentiometer, cf. p. 87). In the thermoelectric gauge, the temperature on the wire is observed by means of a fine thermocouple. Which of the two types is used is of less importance to the user since both are based on the same fundamental principle.

It is important, however, to note that the thermal conductivity of a gas varies markedly with its pressure only within a certain range. The thermal conductivity of a gas at 1 mbar is almost the same as at 1 bar, while at 10^{-3} mbar and below it is essentially zero. Thus these gauges are primarily used within the 1 to 10^{-3} mbar range, which coincides with the range of most forevacuum pumps.

At 1 mbar and above, the cooling of the wire is effected mainly by convection. By special design, this convection may be utilized to extend the measuring range to 10, 100 or 1000 mbar in commercial instruments. On a digital display it may look convincing, but the user is wise to regard the numbers with misgiving.

6.11.5 Hot-Cathode Ionization Gauge

In relation to Table 6.2 (p. 214), the hot cathode gauge is presented out of order for simplicity. In principle the hot cathode ionization gauge is similar to an old-fashioned vacuum tube, a triode, see Figure 6.19. It contains a heated filament serving as the cathode, a 'plate' or target serving as the anode, and between these a 'grid'. When used as a radio tube, the cathode was kept at a moderate glow, and the current between cathode and anode was varied or modulated by varying the voltage on the grid.

When in use as an instrument to measure low gas pressures, the tungsten filament cathode is kept white hot, and the grid is used as the positive electrode (the anode). The stream of electrons emitted from the cathode is accelerated towards the grid by a potential difference of, for example, 200 volt. A molecule in the gas phase that is hit by one of these electrons is likely to be ionized; that is, a valence

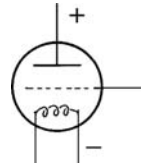

Figure 6.19 The principle of a vacuum tube, a triode.

electron is knocked off and the rest of the molecule is left as a positive ion. With the plate at a negative potential, the positive ions will be collected at the plate. With the proper design there is a linear relationship between the plate current and the gas pressure in the tube.[4]

This is still the basic principle of the hot-cathode ionization gauge, although the design may vary in order to achieve the highest possible sensitivity at very low pressures. It suffers from the weakness that, if exposed to pressures of air higher than some 10^{-3} mbar for only a few seconds, the tungsten filament burns off and has to be replaced. Thus, when very low pressures are not required, an instrument without a glowing filament is preferred.

6.11.6 Penning, or Cold-Cathode Ionisation Gauge (F. M. Penning, 1894–1953)

The principle is the same as the preceding one, with some differences. The cathode is kept cold, but with a larger surface area. The potential difference between cathode and anode is increased to a few thousand volts. And a magnetic field, in the form of a powerful permanent magnet, is positioned between the electrodes. The design is such that the (relatively few) electrons emitted from the cold cathode are accelerated in a spiral, covering a considerable distance before arriving at the anode. In this way, the limited number of electrons have an improved chance of hitting and ionizing gas molecules. The

[4] The grid is made of fine wire, and most of the electrons will miss the grid wires in the first pass. The electrons will oscillate radially before finally arriving at a grid wire, thus increasing the chances of hitting a molecule, cf. Roth (1982) p. 310.

ions are then attracted towards the negatively charged collector as above.

The Penning gauge originally covered the range down to about 10^{-5} mbar, but through improved design in the later years it now goes to some 10^{-6} or 10^{-7}, very ample in conjuction with the subject matter of the present text. It goes upwards to some 10^{-2}, but it is not ruined even by admitting 1 bar of air. It is to be noted, however, that any amount of magnetic dust or particles will accumulate inside the instrument; for this reason it may as well be kept under vacuum when not in use.

It should be noted finally that the various vacuum gauges show somewhat different responses for different gases at the same pressures. But, apart from the possible use in leak detection, these variations are of little concern for our purposes. Most of these vacuum gauges are fairly inaccurate anyway (unless carefully calibrated), and we are at best interested in the correct value within a factor of 2.

6.12 LEAK DETECTION AND MENDING

6.12.1 Preliminary Testing of Components

Commercially acquired parts are usually considered gas tight and thus should not need testing. Components made in the workshop, on the other hand, should be tested before assembly. In lieu of a helium leak detector (cf. below), a handy method is to test each part under water. The outlets are blanked with spare flanges, with a hose socket provided to pressurize the part to about 1 bar overpressure of air or nitrogen. If no tiny stream of bubbles appears when under water, the part may be considered tight.[5]

Testing by overpressure, with one or another test gas, has been applied also to complete systems, using a 'sniffer' to detect any test gas

[5] Because of the surface tension, the very smallest leaks may not show up, but experience shows that testing under water is adequate for ordinary high-vacuum use, though possibly not for ultra-high vacuum.

on the outside. For vacuum systems, however, this method is definitely not recommended.

6.12.2 A Note on Cleanliness

The best remedy against leaks is to avoid them. Clean the room before you start the installation, clean your hands, and carefully clean the mating parts and O-rings before assembly. This may save hours and days of subsequent leak hunting.

6.12.3 Leak Testing, First Step

A newly installed system, or one that has been standing idle for some time, may seem sluggish when first evacuated. Outgassing takes time (cf. pp. 187, 188). The fact that the system does not attain the desired low level within the allotted time does not necessarily mean that it is leaky. After prolonged pump-down, the recommended procedure is to close the main valve, note the pressure and go home.

The next morning, note the pressure and observe it once again after a few hours. If the rate declines, it may indicate outgassing, compare Figure 6.20. If the pressure shows a linear increase with time, there is a leak.

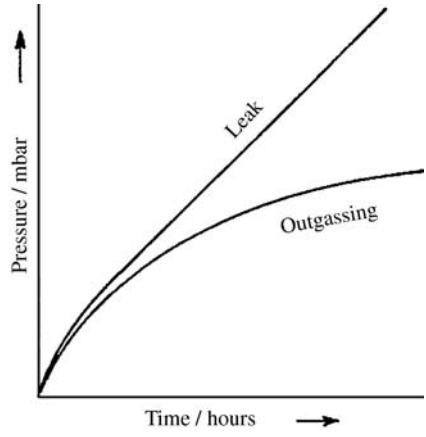

Figure 6.20 A quick graph of pressure against time allows the decision of whether the pressure rise is caused by outgassing or leaks.

6.12.4 Leak Rates

No vacuum system is absolutely tight. This may not be the ultimate truth, but for our practical purposes it is true. All systems have a leak rate.

To start, how do we measure a leak rate? Most simply by closing the system and noting the pressure rise as above. In order to arrive at a value for the leak rate, the volume of the system must be known or estimated. In connection with leak rates we choose to give the pressure in μbar, denoted μ for short (see p. 179). With volume in litres, and time in minutes, we have the leak rate

$$L = \textit{pressure increase}(\mu) \cdot \textit{volume}(\text{litre})/\textit{time}(\text{minutes})$$

Secondly, what is a tolerable leak rate? The answer depends on the purpose. But we may aim at a rate low enough that air leaks will not in any way interfere with our experiments. The example on pp. 183–184 indicated that in a vacuum, the pressure should be down to the order of 10^{-5} mbar. For example, we may assume that the high-vacuum pump has an effective pumping speed of 150 l/s while maintaining a pressure of 10^{-5} mbar. The figures correspond to a throughput of 1.5×10^{-6} bar·litre/sec, or roughly 100 μbar·litre/min.

Considered as a leak rate, however, this may be taken as an upper limit; the capacity of the diffusion pump is fully engaged to fight the leak. In practice we want lower leak rates. Thus we have a simple rule:

$$1\ \mu \cdot \text{litre/min} = \text{very good.}\ 10\ \mu \cdot \text{l/min} = \text{acceptable.}\ 100\ \mu \cdot \text{l/min} = \text{too much.}$$

Experience throughout the years indicates that this rule makes sense. In addition, it is easy to remember.

6.12.5 Leak Hunting

As stressed above, there is little point in searching for leaks until it is proven beyond doubt that the system *does* leak. Once this is established, the next question is: where?

In the case that the system consists of several parts separated by valves, all valves should be closed after evacuation. After some time, systematic opening of one valve at a time (and watching the gauges) may reveal which part is leaking.

More generally, a systematic search from one end to the other may be necessary, and some leak detection device is required. To this end, a helium leak detector without question is superior. But it is a costly instrument and not always available, hence some other possibilities are mentioned first.

Tesla Coil, Spark Tester (N. Tesla, 1856–1943). This is probably the oldest of the leak-detection devices. However, it can only be used on non-conducting materials, primarily on glass.

It consists in principle of a primary coil with a few turns and a secondary with many turns, tuned to resonance so that it acts as a high frequency, high voltage transformer. The spark tester has one visible electrode only (the other represents the more diffuse 'ground'). When held near solid object it may draw sparks of several centimetres' length.

Used on a glass system under vacuum, the sparks will wander at random on the glass surface. But if there is a leak, however small, the spark will stick to that spot with a luminous glow, pinpointing the leak. (In a certain pressure interval, between some 10 and 10^{-3} mbar, and independent of leaks, it also gives a bluish luminescence throughout the glass tubing.)

The spark tester may also be used on ceramic tubes. An alumina tube (the inner tube in the furnace Figure 2.8, p. 31) was originally found to be vacuum tight. After prolonged exposure at high temperature (1500 °C) under reducing atmosphere (H_2), the spark tester revealed a large number of tiny leaks.

Glass vacuum systems are not much used any more, and so the Tesla coil has mostly gone out of use. It is, however, a low-cost instrument, it still has its uses in leak testing, and it is fun for demonstrations.

Pirani, Thermo Gauges. As mentioned above, gauges based on the thermal conductivity of gases show increased response in the presence of hydrogen. This may be used to locate leaks. However, the response

is essentially zero for these gauges at pressures below 10^{-3} mbar, thus the leak testing should be done with the forepump only running, or with the high-vacuum valve partly shut so that the gauge shows a response before the testing starts.

Hydrogen should be admitted through a narrow nozzle only (remembering the fire hazard), and the search starts from the uppermost parts since hydrogen rises in the air. The observed increase in response is not expected to be large anyway, but a repeated small increase may reveal a leak.

Penning, Ion Gauges. These may be used much the same way as those above, except that the test gas may be a volatile organic liquid like acetone or ethanol. The sensitivity is expected to be higher since the test may be carried out at lower pressures. However, none of these methods based on the gauges of the system are very efficient, and hunting for moderate leaks in this way may be a waste of time.

Halogen Leak Detector. This instrument is based on the fact that the ion emission of glowing platinum is greatly enhanced in the presence of halogen-containing molecules. In practice, the gauge head contains a small heating element of platinum coiled on a ceramic support, surrounded by a platinum cylinder which acts as the negative electrode. This gauge head is mounted on a vacant flange on the set-up, with leads to the external electronics and display (like any vacuum gauge). The test gas was previously usually freon, one of a class of fluorochloromethanes, applied through a nozzle as for the other test methods.

The halogen leak detector has proved sufficiently sensitive to detect most leaks within our range of interest, and thus represents a useful alternative at a reasonable cost. Unfortunately, the compounds formerly used as test gases are now abandoned because of their harmful influence on the ozone layer. Other test gases might be used, but the future of the halogen leak detector is uncertain.

The Helium Mass Spectrograph. Mass spectrography in general is unrivalled for detection and identification of compounds at low concentrations. In vacuum technology it has been used to determine the partial pressures of residual gases. For our purposes, however, we will consider it for leak detection only.

For this purpose, the spectrograph is focused on a single mass, that of helium (4.00). The contents of helium in the Earth's atmosphere are extremely low; this makes it an ideal test gas for leak detection. (Although virtually absent in the atmosphere, helium is present in natural gases in some locations in USA, in amounts that makes it commercially available at reasonable cost.)

The helium leak detector is usually built as a self-contained unit with its own forepump and high-vacuum pump. Thus the vacuum system to be tested may be connected directly to the outlet of the leak detector, or (more usually) the system uses its own vacuum pumps for evacuation, and a small part of the residual gas is then diverted into the leak detector. The sensitivity of the helium leak detector is such that it exceeds the needs of ordinary high-vacuum users by several powers of ten. This also means that small leaks that may take at lot of time to discover by other means, may be located in minutes with a helium leak detector.

From what has been said it is understood that a research institution of any size, using vacuum equipment, should have a helium leak detector available. It is important, however, that there is a knowledgeable person in charge of the instrument, and also a concise set of instructions for use. In the author's experience, the latter requirements are not always fulfilled.

6.12.6 Mending

Once a leak is detected and located, it has to be tightened. A leak in a flange joint means that the parts have to be taken apart, inspected and cleaned. A human hair across an O-ring is enough to cause what seems like a big leak. A scar on the surface of a mating flange may be remedied with epoxy resin, finished with fine emery cloth after the resin has hardened.

Leaks in permanently joined parts (soldered, brazed, welded) may often be fixed by clear varnish. Remember that it is a matter of very tiny 'holes'. The paint or varnish should have low viscosity and good wetting properties so that it may eventually penetrate the hole; the chances that it goes right through before drying are minimal. A spray-can with clear varnish may work wonders, it also reaches otherwise inaccessible areas. Larger, visible fissures or cracks may be mended with epoxy resin

(preferably the slow-setting type); in spite of its higher viscosity it has good fluidity and good wetting properties.

And a final note: prevention is better than a cure. Clean and careful work may be the quickest way to the end result.

REFERENCES

Brewer, L. and Kane, J. (1955) The importance of complex gaseous molecules in high-temperature systems. *J. Phys. Chem.*, **59**, 105–109.

Freeman, R.D. (1983) Conversion of standard (1 atm) thermodynamic data to the new standard-state pressure, 1 bar (10^5 Pa). *High Temp. Sci.*, **16**, 279–295.

IUPAC (1982) A report of IUPAC commission 1.2 on thermodynamics. Notation for states and processes, significance of the word 'standard' in chemical thermodynamics, and remarks on commonly tabulated forms of thermodynamic functions. *J. Chem. Thermodyn.*, **14**, 805–815.

NIST-JANAF (1998) *Thermochemical Tables*, 4th edn, American Chemical Society/ American Institute of Physics, New York, Part I + II, 1950 pp.

O'Hanlon, J.F. (2003) *A User's Guide to Vacuum Technology*, 3rd edn, Wiley-Interscience, New Jersey, 516 pp.

Plesch, P.H. (1989) *High Vacuum Technique for Chemical Syntheses and Measurements*, Cambridge Univ. Press, Cambridge, 167 pp.

Roth, A. (1982) *Vacuum Technology*, North Holland/Elsevier, Amsterdam, 531 pp.

Roth, A. (1994) *Vacuum Sealing Techniques*, American Institute of Physics, New York, 845 pp.

7

High Temperature Furnaces and Thermobalances

CONTENTS

High Temperature Experiments in Chemistry and Materials Science, First Edition.
Ketil Motzfeldt.

Preamble

The preceding chapters discussed the necessary foundations for experiments at high temperatures, including the attainment, control and measurement of temperature, the control of furnace atmosphere, and a discussion of relevant materials. The present chapter goes a step further, showing the specific design of various high temperature furnaces and their combination with balances.

It is noted, however, that the original design of a piece of equipment may involve 10 or 20 drawings in various sizes up to A0 (840 × 1180 mm). A printed text, on the other hand, should have only a limited number of drawings and strict limits regarding size (less than A4). The present text is an attempt at a happy medium.

7.1 AIM AND SCOPE

7.1.1 High Temperature Furnaces

In the context of the present chapter, 'high temperatures' indicate that temperatures of 1800 °C and above may be attained. At these temperatures, graphite is one of the few resistor materials that does not melt and has low vapour pressures, and it is just about the only one that does not sag at high temperatures. In addition it lends itself easily to cutting and shaping. Thus, the designs described in the present chapter are all based on graphite as the resistor material. Alternatives would be molybdenum or tungsten. (In some cases the graphite was replaced by a heater of molybdenum foil, see p. 264.)

The mentioned materials are easily oxidized, thus they may be used only in a neutral or reducing atmosphere. The problems of experimenting

in an oxidizing environment above some 1600 °C were briefly mentioned in Chapter 2 (pp. 27–29) and will not be further discussed here.

7.1.2 Thermobalances

Temperature and pressure are the two most important variables in experimental thermodynamics, if not in experimental science at large. A third important variable, however, is the *mass*. Continuous observation of mass changes greatly adds to the scope of high temperature experiments. Thus most of the furnaces described below were designed to admit the addition of a balance, the completed apparatus thus constituting a thermobalance.

Thermobalances for use at more moderate temperatures are commercially available. Outfits for use above 1600 °C, on the other hand, are rare and merit some consideration.

7.2 GENERAL DESIGN PRINCIPLES

7.2.1 Graphite Heating Elements

As mentioned above, graphite is a preferred material for use at high temperatures. The heating elements, however, may take on various forms. A straight-through tube or rod of graphite will have a low electrical resistance, and hence demands a high current in order to attain a high temperature. Larger furnaces may use compound heaters, where each part has a zig-zag shape to increase the resistance. For smaller furnaces, a spiral, or a double spiral, may be suitable shapes. A split-tube heater with both terminals at one end has also been employed, as in the classical Tamman-furnace.

On the other hand, a straight-through tube is simple to make and rugged in use. An additional point of interest arises if the furnace is designed for use with a thermobalance. Used with a gas atmosphere, a compound or spiral-shaped element will necessarily admit a draught through the interspaces, which in turn will affect the apparent weight of the sample. In contrast, a straight-through tube with closed bottom provides a stagnant atmosphere, allowing accurate weighing. Thus, the straight-through graphite tube is the preferred type in the furnaces described below.

7.2.2 Current, Voltage and Terminals

As an example, we assume a straight graphite tube with an inside diameter of 50 mm, an average wall thickness of 3 mm and a length of 300 mm. With an assumed resistivity of 1.0×10^{-3} ohm cm (cf. Figure 2.1 p. 16) it will have a resistance of roughly 0.0060 ohms. This corresponds to, for example, 12 V and 2000 A (24 kV, not unreasonable for a furnace to reach 2400 °C). The rather large current, however, indicates that the terminal connections deserve some consideration.

Direct connection between the heating element and water-cooled copper terminals would mean excessive heat losses and should be avoided. The current should go from the heating element to some sort of graphite slab, and from these on to water-cooled copper terminals. An example is shown in Figure 7.1, where the heavy current is supplied through double-walled copper tubing.

The connection between smooth copper and smooth graphite does not give any trouble when adequate water cooling, sufficient contact area and secure clamping are provided. The bolts used for the clamping, however, require some consideration, see Figure 7.2. With the bolt heads and steel washers in direct contact with the graphite, a significant part of the current may go through the bolts, as indicated in Figure 7.2a. This current will heat the bolts, and all of a sudden a bolt may turn red hot and lose its strength. This happened to us repeatedly until we learned to place a mica washer underneath each steel washer on the bolt head, as seen in Figure 7.2b.

Experience has shown that a threaded joint between the graphite slab and the mating end of the heater tube does the job without trouble. Subsequently it was found that a smooth, tight fit works equally well. Thus the recommended arrangement now is to have one end threaded to keep the heating element in place, and the other end smooth to allow for thermal expansion during heating.

7.2.3 Obtaining a Zone of Uniform Temperature

This problem was discussed already in Chapter 2, pp. 17–20. For wire-wound furnaces the problem was solved by an uneven distance between the wire turns, compare Figure 2.2. The corresponding effect is obtained in a graphite tube heater by variable wall thickness along the length

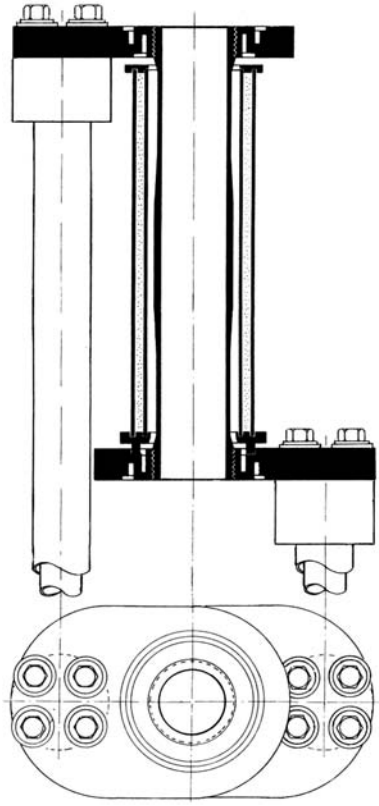

Figure 7.1 A tubular graphite heating element, screwed into mating graphite slabs which in turn are fastened to copper terminals by means of steel bolts.

of the tube, as shown already in Figure 7.1. (It may be noted that, in Figure 7.1, the graphite slabs have grooves in the area next to the ends of the heating element. This reduces the heat loss towards the heating element, but it increases the power lost to the graphite slabs.)

Referring to Figure 7.3, a short length at each end of the heating element has its full wall thickness to allow for the terminal connections. Next follows a length with smaller wall thickness to give increased power input towards both ends. For instance, half the wall thickness means twice the resistance and hence twice the power per unit length. Towards the mid-point the thickness is gradually increased to give full thickness and hence less power along the central part. In Figure 7.3 the relevant dimensions and the observed temperature profile are also given.

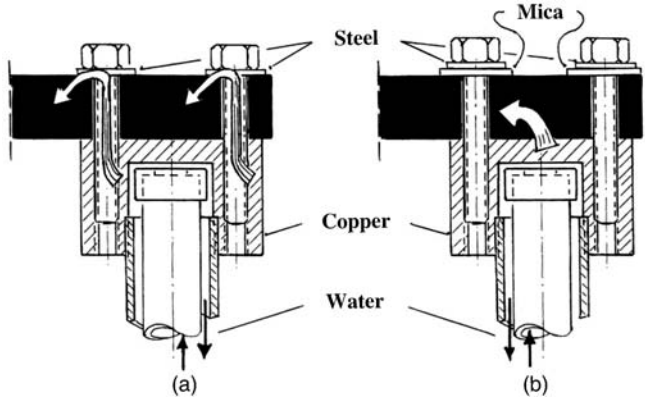

Figure 7.2 (**a**) Bolts with steel washers directly onto the graphite slab. The current may find its way through the bolts, as schematically indicated. (**b**) Mica washers beneath the steel washers prevent current through the bolts, and it flows through the interface between the copper terminal and the graphite slab.

Usually the element is made symmetrical with respect to the centre plane, as shown in the drawings.

It appears difficult to predict a temperature distribution by advance calculation, and the desired distribution is found by trial and measurement. The temperature may be scanned along the centre line by means of a thermocouple or, at the more elevated temperatures, by means of a small 'black body'. The probe is mounted on a sliding supporter, extending through the bottom flange by means of a packing gland such as shown in Chapter 6 (p. 211). In order to avoid the influence of heat conduction along the probe, arrangements such as those depicted in Figure 7.4 have been used. The scanning is most simply done in a vacuum with the horizontal radiation shields removed.

The temperature distribution within a given element depends upon the thickness of thermal insulation. Thus, observations of temperature distribution should be given with detailed reference to the conditions of the experiment.

The heating element shown in Figure 7.3 has a wall thickness of 2.0 mm in the narrow parts. Smaller wall thicknesses should be avoided because of the fragility. Note also that the manufacture of such an element requires accurate machining; a deviation of 0.1 mm in a 2.0 mm wall will give 5% difference in the power per unit length. This sort of

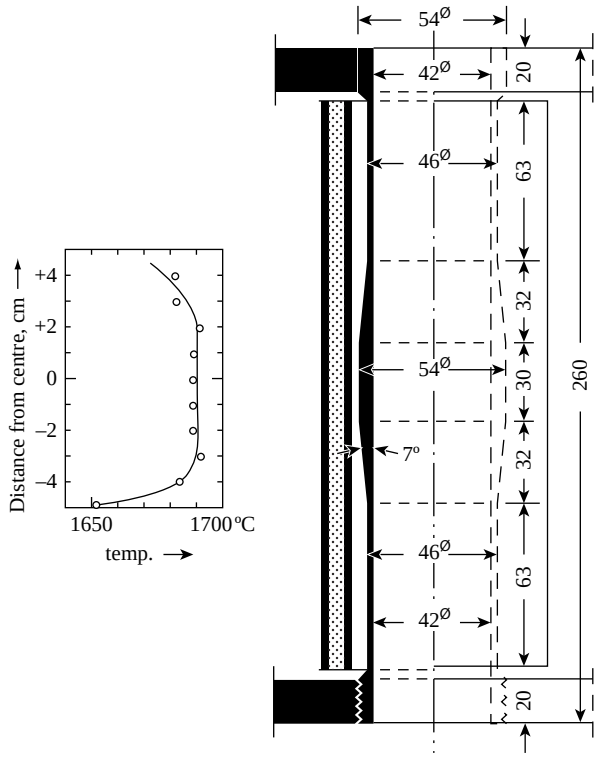

Figure 7.3 A graphite heating element, shaped to give a zone of uniform temperature in the working space. The graph shows experimental results for the temperature along the centre line of the element, obtained by means of an optical pyrometer and a small 'black body' on a movable stand (cf. Figure 7.4). The measurements were done with the furnace evacuated, and thermal insulation consisting of one layer (6 mm) of graphite felt between thin graphite cylinders. (From Sandberg, 1981.)

deviation in a part of the element may result in a rather lopsided temperature distribution.

7.2.4 Materials and Water Cooling

This topic was discussed at length in Chapter 2, pp. 36–42. Adequate water cooling of the furnace chamber is even more important as power input and furnace temperature increase for the same size receptacle.

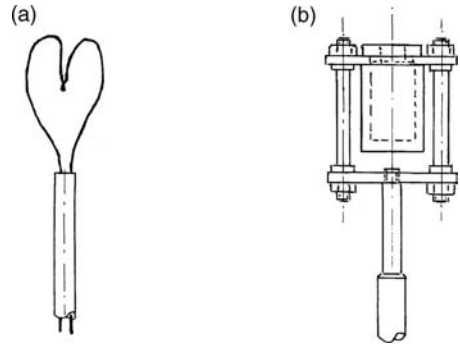

Figure 7.4 Configuration of thermal probes to avoid error due to thermal conduction through the support. (**a**) Thermocouple, naked wires in upper part. (**b**) A tiny graphite crucible with a sighting hole in the lid, serving as a small 'black body'. All parts of graphite, including threaded graphite rods and nuts.

In Chapter 2 (p. 44) it was pointed out that the heat transport from a heated object to the cooling water takes place through a surface film that represents a resistance to the heat transport, and also that this resistance is decreased by increasing the linear flow velocity of the water. Effective cooling in critical areas is thus effected by making narrow passages. This may be realized as indicated in Figure 7.2, where a brass cap is fitted over the end of the inner copper tubing.

It was also pointed out that stainless steel may create difficulties because of its very low thermal conductivity (Table 2.2, p. 41), and that copper and brass still appear to be the best choices for water-cooled furnace chambers. It was pointed out also that aluminium (suitably alloyed) would be the ideal material for the purpose if the problem of water cooling could be solved. A couple of smaller 'test furnaces' with water-cooled vacuum chambers of aluminium have worked satisfactorily, while the furnace chambers described in the next sections are all made from brass and copper.

7.2.5 Positions of Furnace and Balance

Some commercial thermobalances have the balance or weighing cell positioned underneath the furnace. A refractory rod is used to support the sample, protruding into the furnace from below. The apparent idea is to avoid the hot upwards draught of the furnace from interfering with the balance.

For the present purposes it appeared more expedient to place the balance on top, with the sample suspended into the furnace below. This requires some sort of heat shield between furnace and balance, but otherwise causes no problem.

The design of the furnace should permit ready access for introduction and removal of samples. This detail, however, depends on whether the sample rests on a stand (no balance) or is suspended from above (thermobalance). The successful design should take account of both possibilities. Various options exist, as indicated in Figure 7.5 a–d. Each of the four designs has been tried and will be discussed separately.

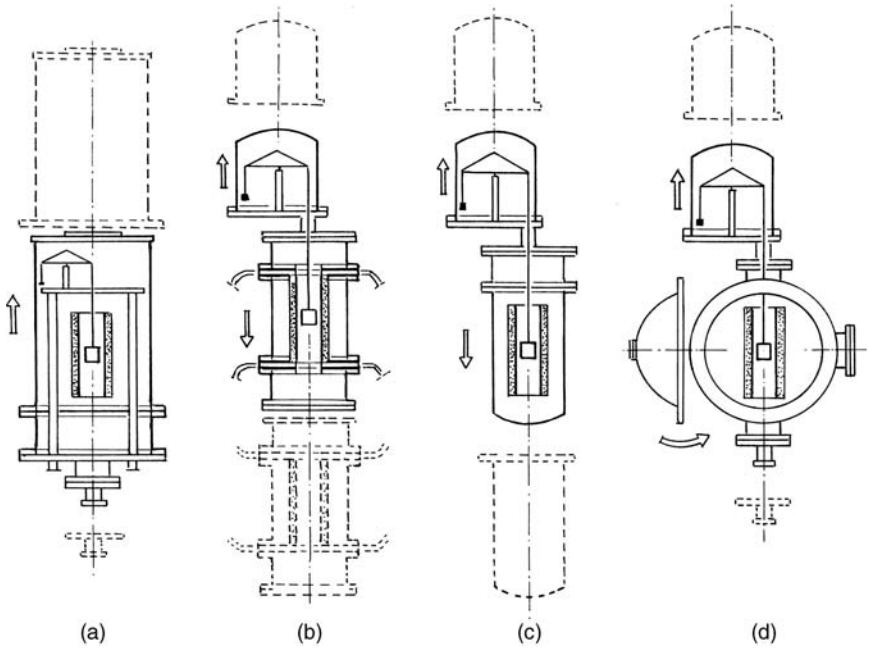

Figure 7.5 Four different thermobalance arrangements. All of the designs are intended for vacuum use, although the necessary valves, pumps, and so on are omitted in the simplified drawings. (**a**) Furnace and balance under one hat (a sort of bell jar). Insulated current terminals (not shown) fastened to the base plate. (**b**) Furnace sliding down; current supply by eight flexible cables. (**c**) Bell jar upside down, furnace stationary. (**d**) Furnace chamber with hinged front door. In all cases the *balance* is stationary, while in (b), (c) and (d) the accompanying bell jar may slide upwards. **Note:** In (**b**), (**c**) and (**d**), a separate tubular connection (not shown in the drawing) is necessary between the furnace and balance compartments to equalize pressure differences.

Certain features are common to all of the designs, in particular as regards the pyrometry. It is evident that the sighting path for optical pyrometry must be off-axis when the sample is suspended along the axis; furthermore some means should be provided to keep a clean window for the pyrometry. These matters will be dealt with after each of the four designs has been presented (cf. pp. 255–259).

7.3 SPECIFIC FURNACE/THERMOBALANCE DESIGNS

7.3.1 The Bell Jar Type: *Beljara*

This design was my first high-vacuum installation: furnace and balance are stationary, enclosed in a bell jar that could slide upwards, as indicated in Figure 7.5a. The real appearance is shown in Figure 7.6.

Some commercial vacuum furnaces have the diffusion pump attached directly beneath the base plate. This should be avoided, however, since it invites the dropping of foreign matter into the pump, with troublesome dismantling as a consequence. The pump opening should be off to one side (cf. Figure 6.1, p. 180). In the case of Beljara it was done through the lower, stationary part of the furnace chamber, with a wide, flattened opening for adequate pumping speed, see Figure 7.6.

The forevacuum tank (**E**) is a further peculiar feature, formerly common to many vacuum systems. The general idea of a forevacuum tank was to save the rotary pump from running all the time. A simple automatic switch made the pump stop when the lower level of the forevacuum pressure was attained, and start again when the upper forevacuum

Figure 7.6 Furnace and balance under one hat; the original set-up of the vacuum furnace 'Beljara'. Front and top views. **A**: Furnace chamber (bell jar). **B**: High vacuum valve. **C**: Cold trap. **D**: Oil diffusion pump. **E**: Forevacuum tank. **F**: To forevacuum pump. **G**: Bypass line (cf. 'B' on Figure 6.1, p. 180). **H**: Electro-magnetic shut-off valve. **J**: Copper rails for current to furnace. **K**: Pirani head, forevacuum. **L**: Ditto, high vacuum. **M**: Penning head. **P**: Copper tubing (1/4 in.) and valves for inlet of various gases. **Q**: Main inlet of cooling water, with valves leading to the various components. Note the pressure-sensitive switches (a total of four) which prevent current to the furnace in the absence of water pressure.

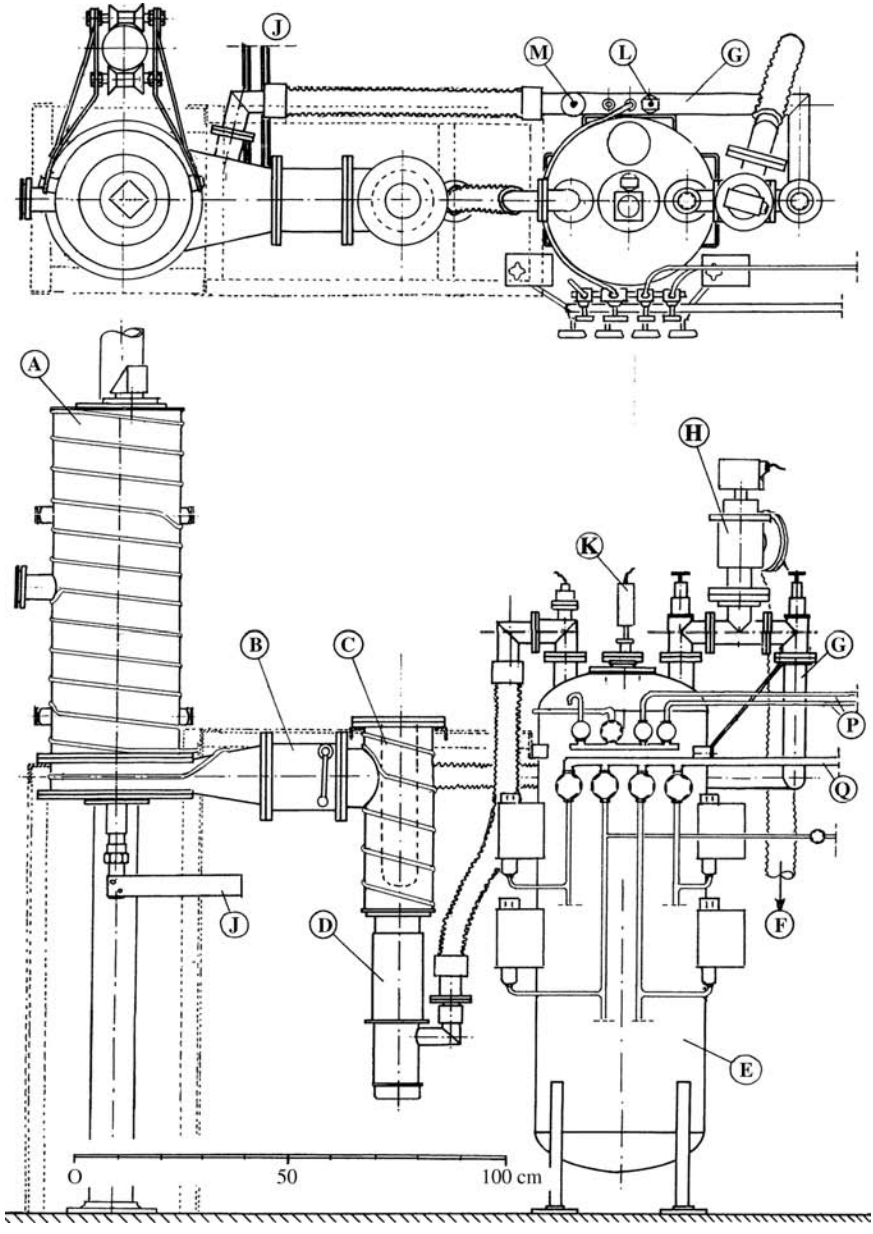
J
M
L
G
A
H
K
B
C
G
P
Q
J
D
F
E
O
50
100 cm

level was reached. In the case of Beljara, an added advantage was the possibility of avoiding vibrations from the pump, which might have adverse effects on the delicate balance.

As it turned out, however, the apparent advantages of a forevacuum tank proved to be of no importance. A modern rotary pump may run continuously for days and weeks with no trouble, and properly mounted it barely transmits any vibration to the system.

The original balance was built from an old-fashioned analytical balance. It was equipped with four levers carrying 10, 20, 20 and 50 mg, and another set of four with 0.1, 0.2, 0.2 and 0.5 g, covering the range 0.01 to 1 g of weight change. Changes between 0.1 and 10 mg were detected by a custom-built electronic balance unit, at a time when such units were not yet commercially available. A drawing of the complete unit is shown in Figure 7.7.

This balance unit is now only of historic interest. Still it may be of value to note the design of the two double concentric rotary lead-throughs, used to handle the two sets of weights, plus a set of windows (see Section 7.4) and an arrest. It is not expected that a similar design will ever be built for the same purpose. Nevertheless, one of the lead-throughs is shown in detail in Figure 7.8, to indicate that such a seemingly complicated design is readily built to vacuum-tight specifications, following the simple rules set forth on pp. 204–206.

Beljara II This second version was considerably simplified, as shown in Figure 7.9. The forevacuum tank was considered superfluous and omitted. Note that the cold-trap (C) of Figure 7.6 is also omitted; the angle valve is considered a sufficient trap for the possible back-streaming of oil from the diffusion pump.

The old-fashioned balance was substituted by a modern 'weighing cell', an electromagnetic device that in principle forms the heart of any modern laboratory balance. The best of weighing cells may have a sensitivity close to 1 part in a million, unthinkable without digital technology. For the purpose of a vacuum thermobalance the weighing cell is placed inside the furnace chamber while the display and most of the electronics are placed on the instrument panel. Note that the instrument panel is placed next to the furnace for the convenience of the operator.

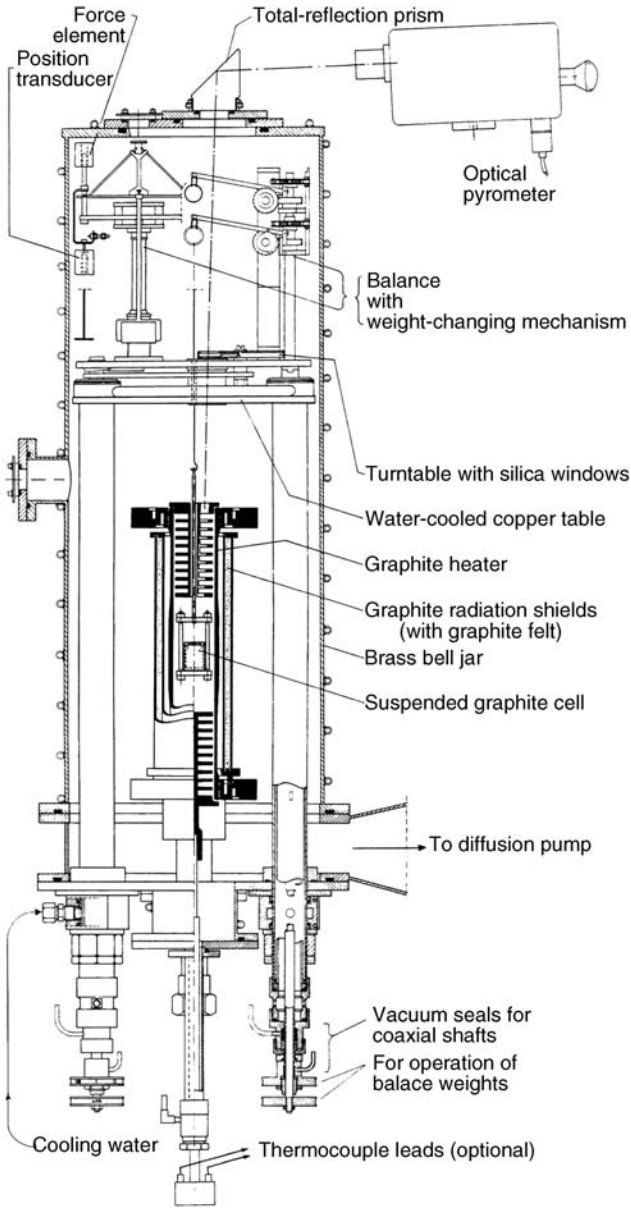

Figure 7.7 The thermobalance 'Beljara', consisting of a graphite tube furnace, and above this, a water-cooled copper table carrying an old-fashioned balance, partly converted to electronic recording. The water to the copper plate enters through one leg, flows across in copper tubing, and leaves through the other leg.

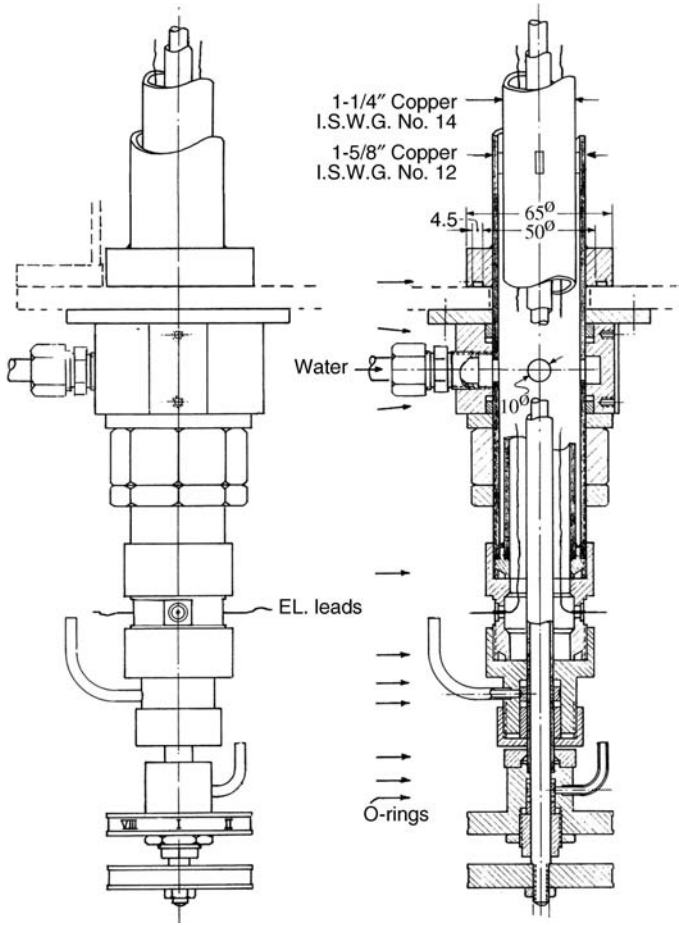

Figure 7.8 Details of one of the two double, concentric leadthroughs. In addition to the concentric rotary axes, the design shows the inlet for cooling water, and the insulated *Kovar* seals for the introduction of the pilot leads to the electronic part of the furnace.

7.3.2 Movable Furnace: *Octopus*

The basic idea, illustrated in Figure 7.5b (p. 235), was that, after the termination of an experiment, the furnace could slide down, giving immediate access to the suspended sample. The actual appearance of the apparatus is shown in Figure 7.10. The furnace chamber with accessories was located in a stand of three 50 mm diameter steel columns,

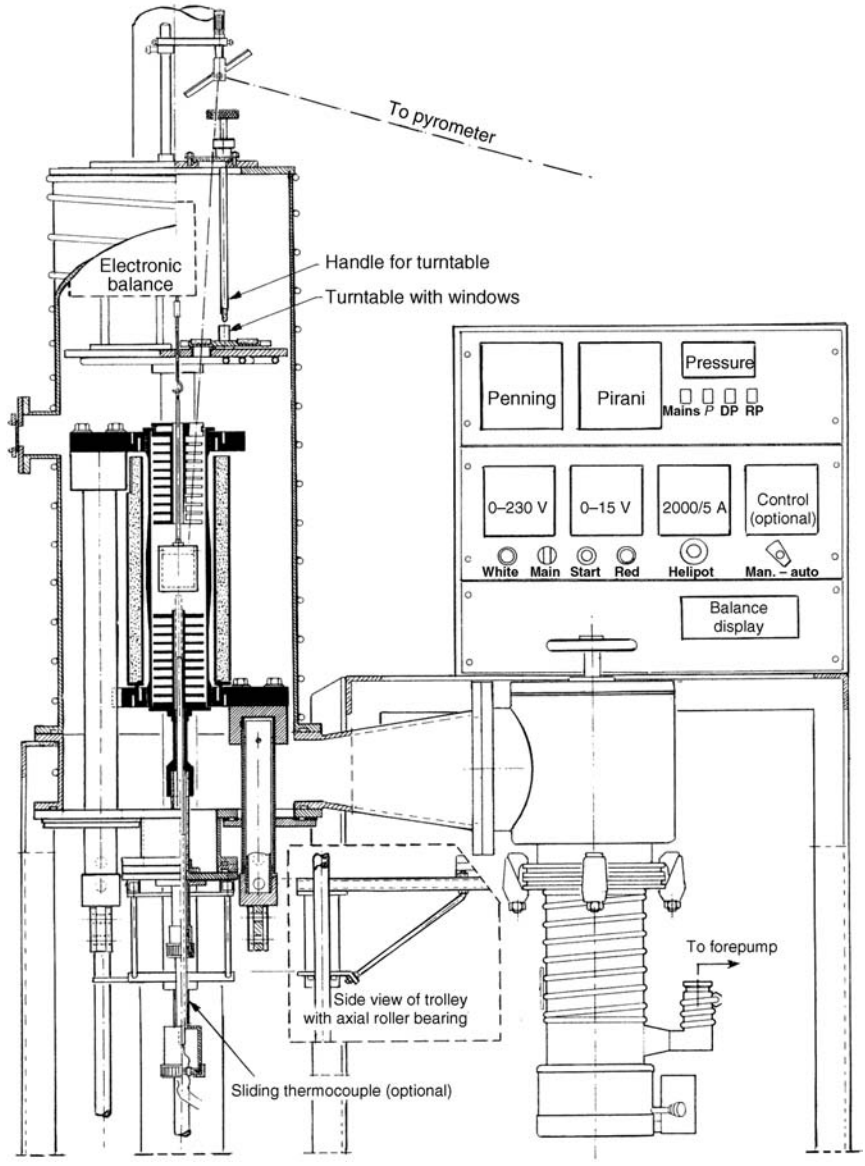

Figure 7.9 'Beljara II'. The furnace and chamber are essentially identical to the first model, but the forevacuum tank and the cold trap have been left out, while the mechanical balance is replaced by an electronic weighing cell.

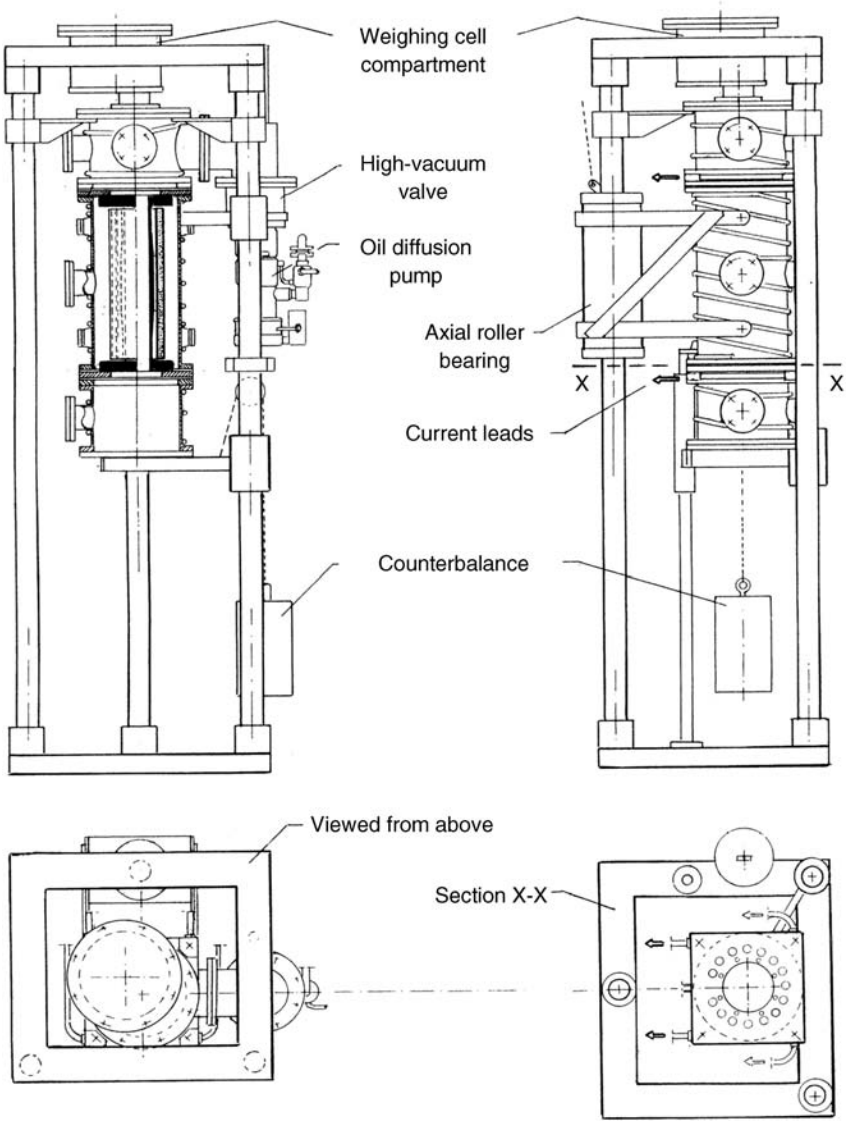

Figure 7.10 The furnace/thermobalance 'Octopus', so named because of its eight flexible leads between the furnace and the low-voltage transformer (indicated by arrows in the right-hand drawings). It is built on a stand of three columns of polished steel supported at both ends by a rectangular frame of channel steel.

connected at the top and bottom by rectangular frames. One of the columns served as a stem for supporting the furnace chamber, with an axial roller bearing as a central component.

The furnace proper is shown in more detail in Figure 7.11. The central idea here is that the brass flanges at each end of the heating element serve both as parts of the vacuum receptacle and as terminals for the furnace power. The current leads in this case must be flexible, and at the same time large currents are required, some 1500 to 2000 A total. The matter was solved by connecting flexible leads to all four corners of each terminal flange; a total of eight leads between the furnace and transformer. To provide electrical insulation and avoid overheating, the

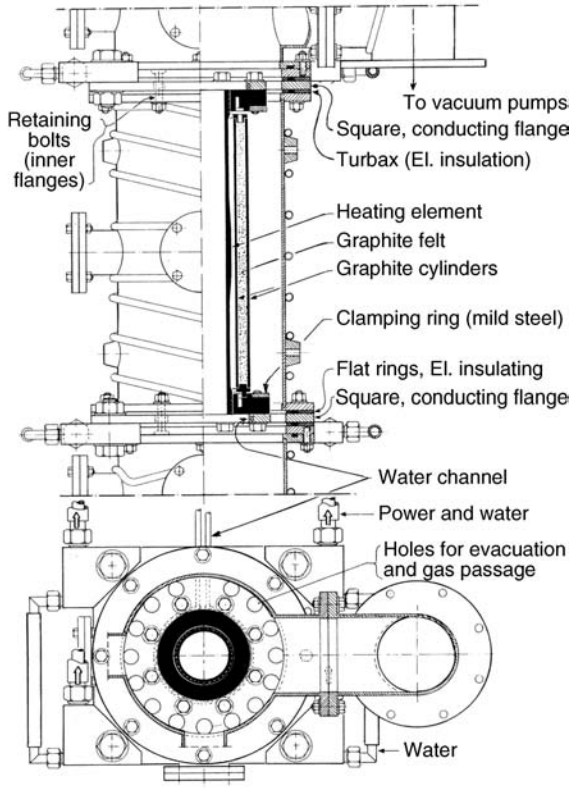

Figure 7.11 'Octopus', a close-up of the furnace proper. When built solely as a low-cost furnace the upper and lower compartments may be omitted, and the vacuum pump attached to one of the 2 in. outlets in the middle.

leads were enclosed in reinforced rubber hose with water cooling. Unfortunately, the multi-strand flexible leads inside the water hose had a tendency to corrode. In consequence the effective cross-section diminished and the resistance increased, with steadily more of the power spent in the leads rather than in the heating element.

Another shortcoming of this design is that the interior of the receptacle is rather inaccessible. The holes in the terminal flanges provide only inadequate access for evacuation, and the whole furnace has to be dismantled for cleaning. Altogether, the design shown in Figure 7.11 (eventually without the framework shown in Figure 7.10) is adequate for stationary use and moderate requirements regarding cleanliness, while it is not to be recommended as part of a thermobalance or for high-vacuum use.

7.3.3 The Jar Upside Down: *Maxine*

The design of Beljara, shown above in Figure 7.5a (p. 235), and in more detail in Figures 7.7 and 7.9, has the entire installation fixed on a base plate. As an alternative, a furnace was conceived with all installations fixed at the upper end, and the chamber free to open downwards as indicated in Figure 7.5c. It was also decided that this design should be suited not only to a vacuum, but also for elevated gas pressures (some 5 or 10 bars). To this end, it is essential to have the smallest possible diameter of the receptacle for a given furnace size. The unsymmetrical design of Beljara (cf. Figure 7.9) is not suited for this purpose.

In addition to the rather large diameter chamber, Beljara also turned out to have another disadvantage: at the highest temperatures the thermal expansion of the graphite heater caused a notable tilt of the heating element; this in turn caused the suspended graphite rod to get stuck at one side of its guide tube, giving trouble for the balance.

Thus it was decided to have a symmetrical design with the smallest possible cross-section compatible with the chosen size of the graphite furnace. The solution is shown in principle in Figure 7.12. The essential parts are an upper and a lower terminal copper plate, with two copper tubes attached to each plate for support, water-cooling and current.

In a furnace according to this design, the graphite heater is fastened to graphite slabs at both ends, the assembly slides into place between the water-cooled copper plates and is secured with bolts and nuts (and mica washers).

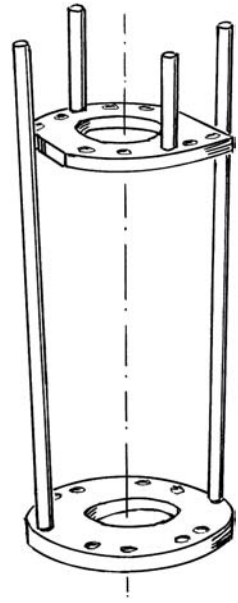

Figure 7.12 The design principle of the 'Maxine' furnace: an upper and a lower terminal in the form of copper plates, each connected to two water-cooled copper tubes (water in, water out) that serve also as current leads. The graphite heating element between the terminals is omitted in the drawing.

The terminal copper plates will be subjected to heavy thermal loads during use, and deserve some consideration. A drawing of the lower terminal is shown in Figure 7.13. The channel for cooling-water is formed by machining a 3×4 mm groove in the copper plate, closed by a somewhat larger, tight-fitting copper ring, which is fastened by means of *electron beam welding*. This method appeared as the only safe one for these critical parts, where water leakage could mean disaster. Electron beam welding requires specialized equipment; the relevant parts on Maxine were welded at the Institute of Energy Technology (at Kjeller, outside Oslo). The connections between water channel and copper tubing was subsequently provided by drilling horizontal holes as indicated by A-A, plugging the ends using hard solder. The upper terminal copper plate is, of course, similar to the lower, differing only in the cut-off segments to allow passage on each side (cf. Figure 7.12).

The complete furnace is shown in Figure 7.14. It will be noted that copper railing has been added to the copper tubes to increase conductance.

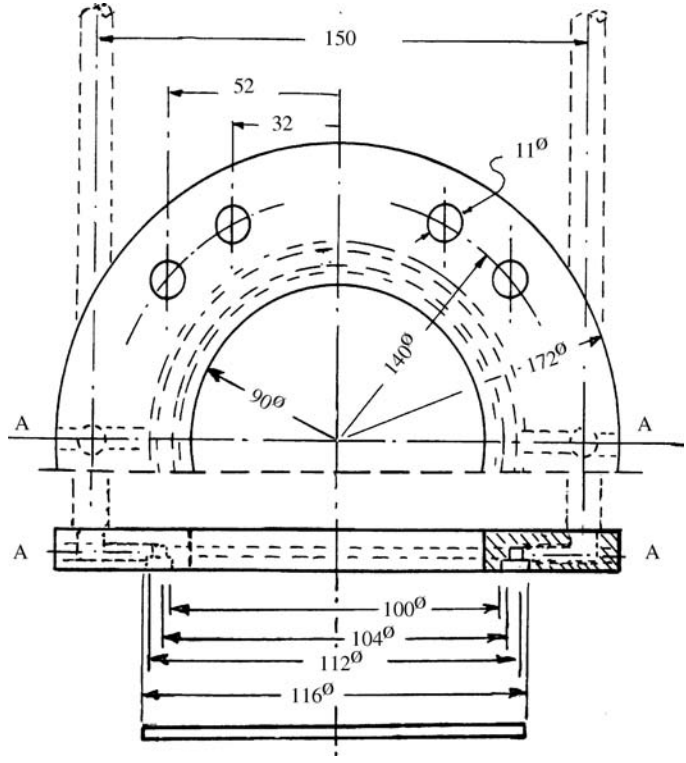

Figure 7.13 Details of the lower terminal copper plate. The water cooling is provided by a circular groove of 3×4 mm cross-section, covered by a tight-fitting copper ring which is fastened by electron beam welding. The connections between the terminal plate and the copper tubes are done with ordinary hard solder.

The upper end connections of this rail-tube combination also deserve some comment. They must be electrically insulated from the main body; they shall carry the current (some 500 A), provide the cooling water and shall be vacuum tight. One of the four upper-end connections is shown in cross-section in Figure 7.15. The electrical insulation is provided by two insulating rings (machined from, e.g., Turbax) that, in combination with a suitable O-ring, at the same time provide vacuum tightness. For this to work properly, the relevant parts must be accurately machined. Suitable dimensions, to the nearest tenth of a millimetre, are given in the drawing. The idea is to provide adequate compression of the O-ring (in this case a ring of

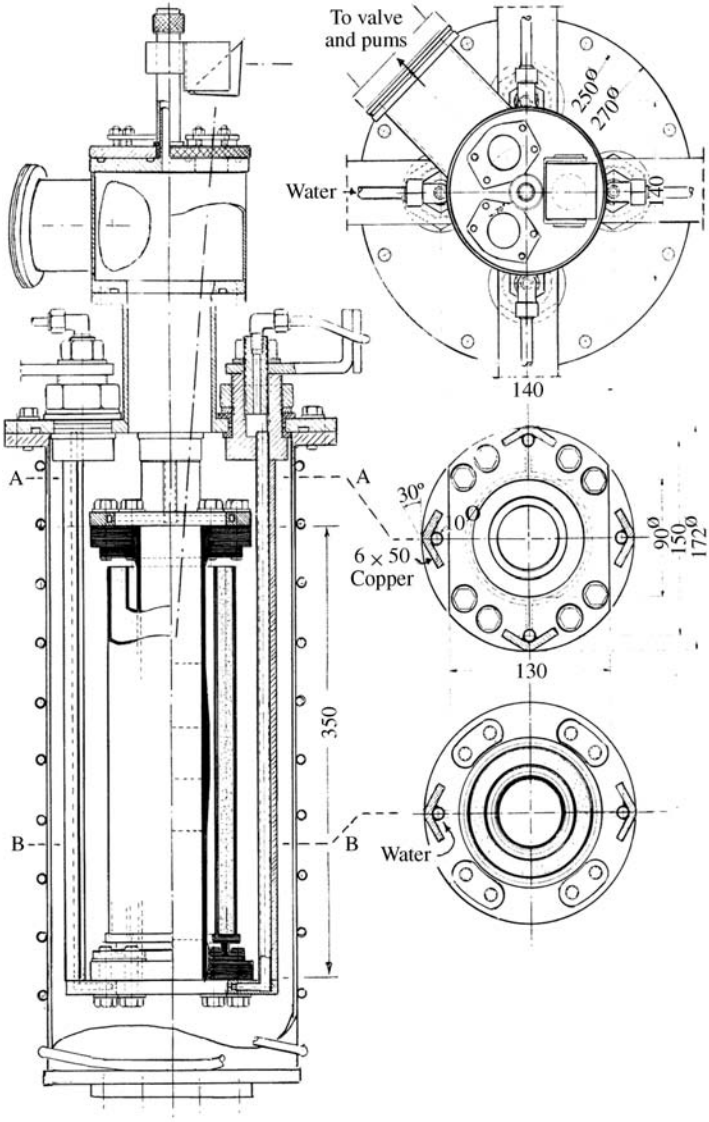

Figure 7.14 The graphite tube furnace 'Maxine', side view in cross-section, and top view plus two cross-sections. Inner diameter of heating element 50 mm, length 350 mm. The water-cooled jar may slide down, leaving the furnace assembly free for inspection.

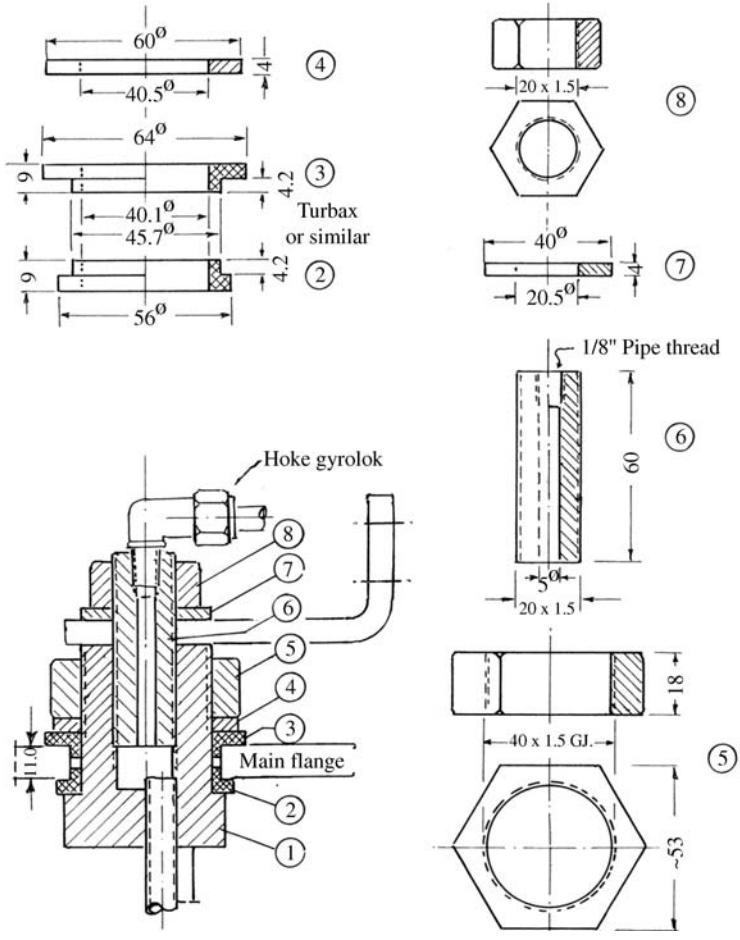

Figure 7.15 Upper connection of one terminal assembled, shown in cross-section, and detailed drawings of the separate parts, with dimensions. All parts except the Turbax rings are made from brass. We will consider in particular the space left for the O-ring. The dimensions given in the drawing leave a 'free space; with cross-section $2.9 \times 2.6 = 7.54\,\text{mm}^2$. An O-ring of diameter 3.0 mm has cross-section area $\pi \times 1.5^2 = 7.07\,\text{mm}^2$, thus the 'free space' left for the O-ring is about 6%, which should be sufficient in this static application. (See also the discussion p. 205.)

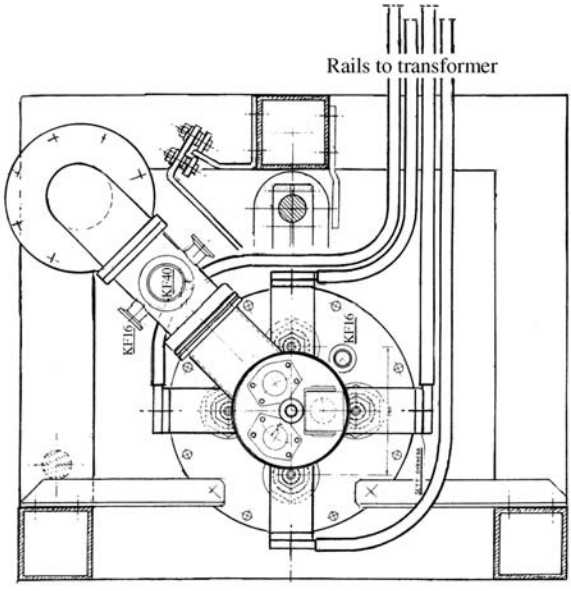

Figure 7.16 'Maxine' seen from above, mounted in its stand with the top frame removed.

3.0 mm thickness) without crushing it. The rest of the drawing should be self-explanatory.

Finally, in Figure 7.16 the complete set-up is seen from above with the top frame removed. Note in particular the layout of the four copper rails from the terminals (Figure 7.15) to the low-voltage transformer.

The furnace 'Maxine', like the rest, was intended for use as a thermobalance (cf. Figure 7.5c) but for various reasons it was never used that way. As a furnace, however, it served quite well. In particular it is believed to represent a sound design for furnaces with high internal pressures, because of its modest outer diameter. A separate high-pressure receptacle, made of thick-walled aluminium, was designed and partly built, but subsequently the project was terminated.

7.3.4 Front Door: *Versatilie*

This design is presented as the last of the four (cf. p. 235), not because it was the last one to be built, but because it is probably the most

convenient one for general use. Entrance through a front door turned out to be quite practical. The three main components, the furnace, the receptacle and the balance, remain stationary. Only the front door, the bottom flange and (eventually) the balance bell jar are movable. An early model of the Versatilie furnace is shown in cross-section in Figure 7.17.

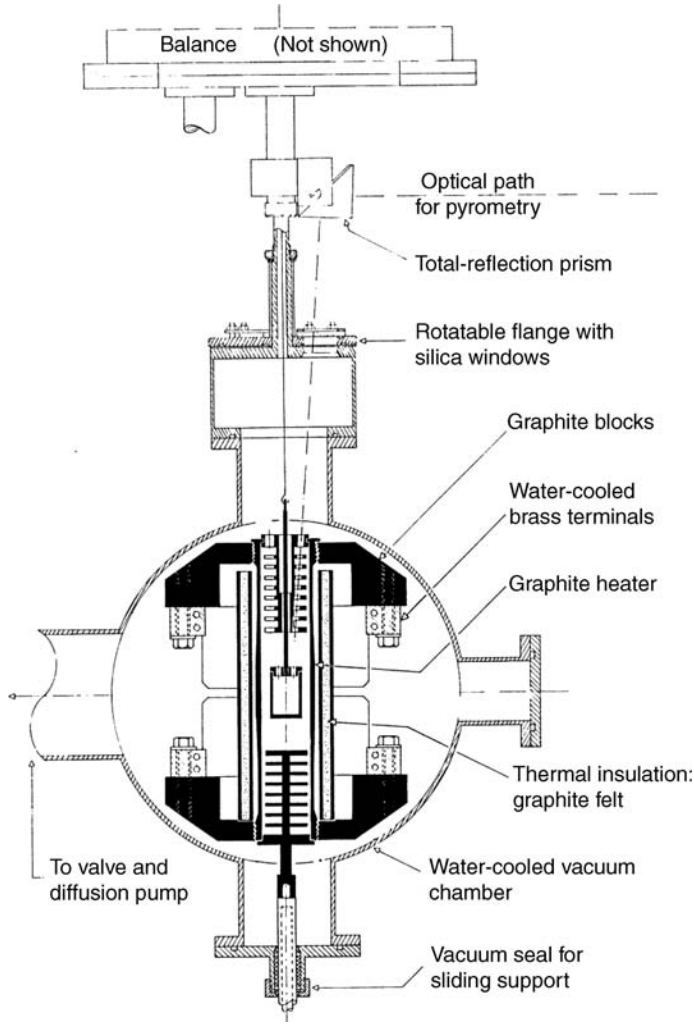

Figure 7.17 An early model of the graphite-tube furnace 'Versatilie' seen in cross-section.

It is seen how a maximum size graphite furnace may be fitted crosswise into a circular receptacle.

The complete set-up is shown in two projections in Figure 7.18, where the various components are described in the figure text. The central part is the circular vacuum chamber containing the furnace (cf. Figure 7.17).

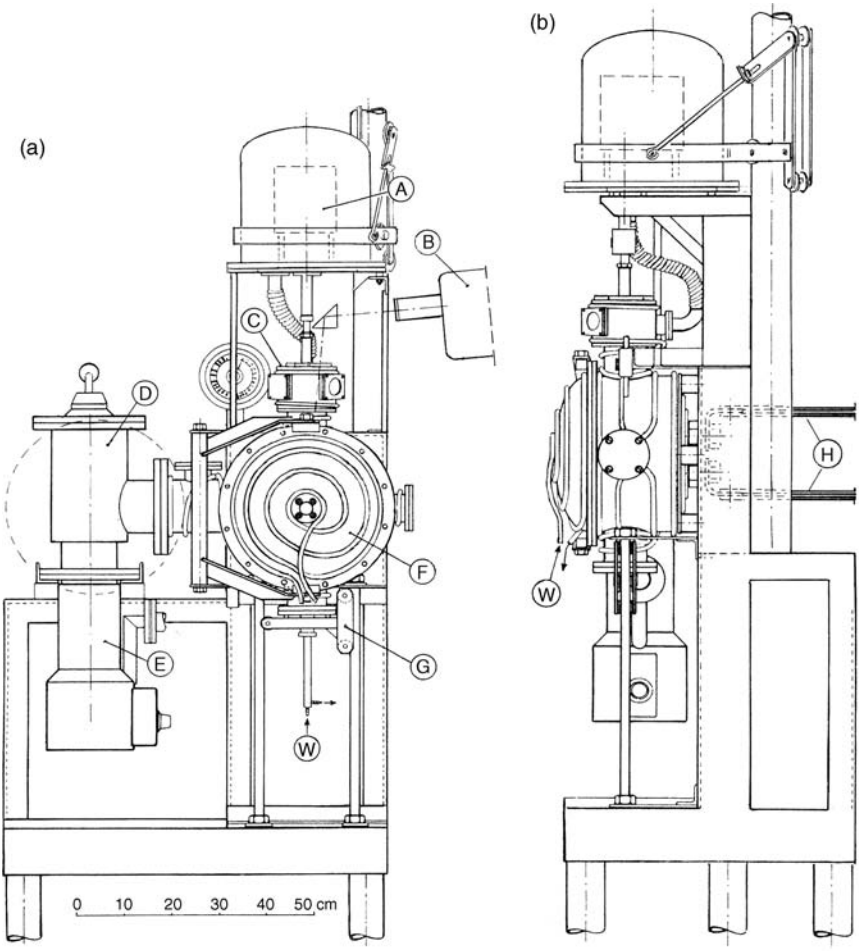

Figure 7.18 (**a**) The vacuum furnace/thermobalance 'Versatilie', front view. **A**: Electronic Balance. **B**: Optical pyrometer. **C**: Rotatable flange with silica windows. **D**: Vacuum valve. **E**: Oil diffusion pump. **F**: Front door. **G**: Trolley for lower flange. **W**: Inlet for cooling water. (**b**) 'Versatilie', side view. **H**: Copper rails for current from low-voltage transformer.

The chamber is essentially a cylinder with horizontal axis. Characteristically the cylinder length is shorter than its diameter. The flat back is stiff and sturdy, providing a base for fastening to the stand, and for the lead-throughs and the furnace inside. The front, which is the door, has a bulb-shaped main area that gives way for an even shorter cylinder wall, and hence improved access to the interior when the door is open.

Note in particular on Figure 7.18a that the front door is hinged by top and bottom pivots, permitting opening and simultaneous turning of the door. Thus, in the open position (dashed circle) the flange with its O-ring may face backwards, protected from incidental dirt or injury.

In principle it is not necessary to remove the bell jar from the balance between each run, and the jar may be lifted off by hand when necessary. In practice, however, the extra column and sliding carriage shown in Figure 7.18 are recommendable. A detailed drawing of these parts is shown in Figure 7.19.

In this furnace design the upper set of radiation shields must be entered from the lower side of the heating element. Once entered, the set of shields are held in place by a pair of flat half-rings, placed from each side into a suitable groove in the top shield. It is evident from Figure 7.17 that this particular design leaves very little room for the necessary manipulations. For this reason an improved design was introduced, as shown in Figure 7.20. The total height of the heating element is reduced from 260 to 230 mm, leaving more free space at the top.

At the same time, the design of the graphite terminal blocks was simplified and improved. While in Figure 7.17 the fastening bolts were threaded into the graphite, in Figure 7.20a the bolts are fastened by threaded holes on a strip of flat steel. Between the steel and the graphite is a thin strip of mica for electrical insulation. This detail was elucidated already in Figure 7.2 (p. 232); the design in Figure 7.20 is somewhat different, but the important point is the same. (This applies also to Figure 7.14, p. 247.)

Figure 7.20b and c show the same design in top and side views. Particularly to be noted are the current-carrying parts (two identical parts, one turned 180° to the other). These parts perform two tasks: bringing the current into the chamber from the outside, and delivering it to the graphite blocks.

As regards the supply of large currents through a vacuum wall, the solution was illustrated already in Figure 7.15 (p. 248). The heavy cylindrical part carrying the current is located between rings of a

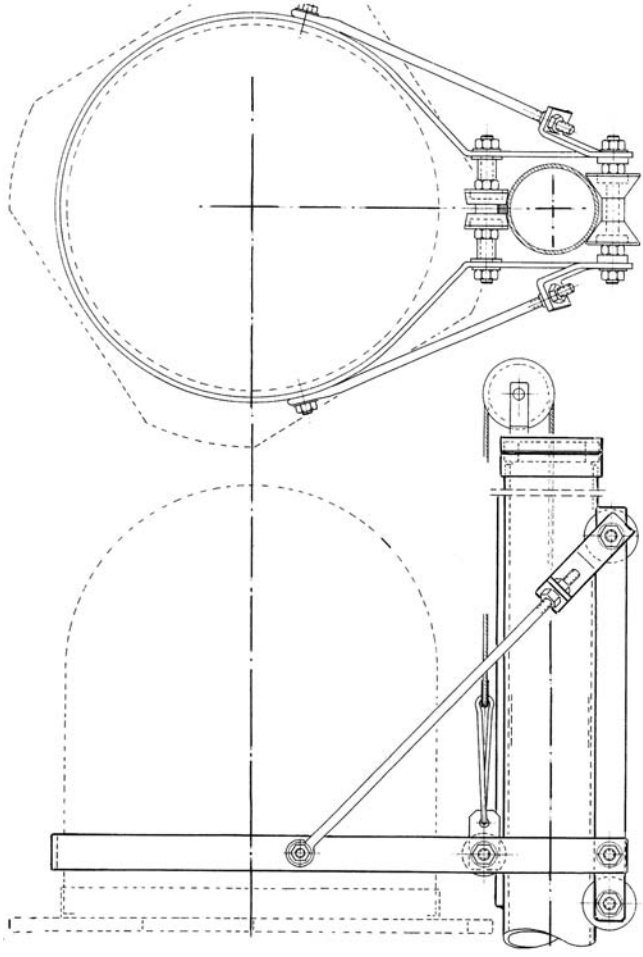

Figure 7.19 Details of the column and the carriage for the bell jar over the balance.

suitable material (e.g., Turbax), dimensioned to give suitable compression for an O-ring.

The second task is more diverse. In Versatilie the current is transferred to the graphite blocks by components whose shape may not be immediately evident from the line drawings. Hence a drawing in perspective is provided in Figure 7.20d, showing the lower of the two terminals.

One important point is that these parts are made from brass. Stainless steel has much too low thermal conductivity, while pure copper is too

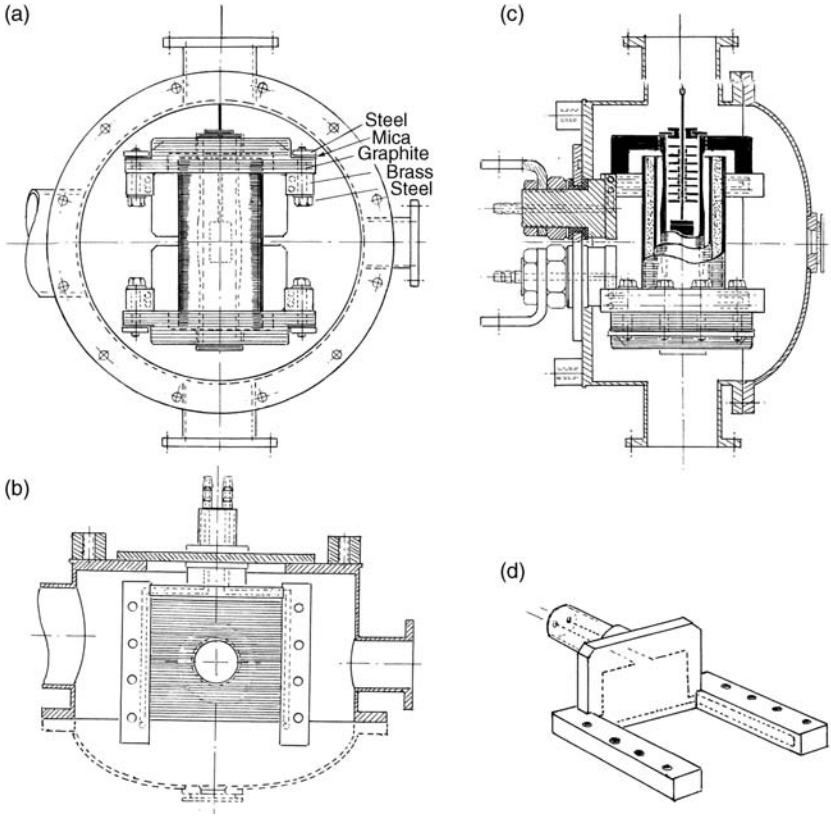

Figure 7.20 (**a**): Front view of the Versatilie furnace, improved model (cf. text). Graphite parts have been horizontally hatched for clarity. (**b**): The same seen in horizontal section, with heating element and thermal insulation omitted. (**c**) Side view of the Versatilie furnace, with the upper half in vertical cross-section. (**d**): Sketch in perspective of the lower of the two terminals conveying electric current to the heating element.

soft for the purpose. The object illustrated in Figure 7.20d may seem a bit complicated, but a skilled mechanic does the job without difficulty. The separate parts after machining are joined by hard solder ('silver solder'). The channels for water cooling (4.5 mm dia.) are drilled straight through (wherever convenient) and the dead ends stoppered by brass plugs and silver solder.

Generally this design has functioned satisfactorily for decades. The stand has also proved suitable for the purpose; a drawing with dimensions is included in Figure 7.21. Rather heavy dimensions of steel are

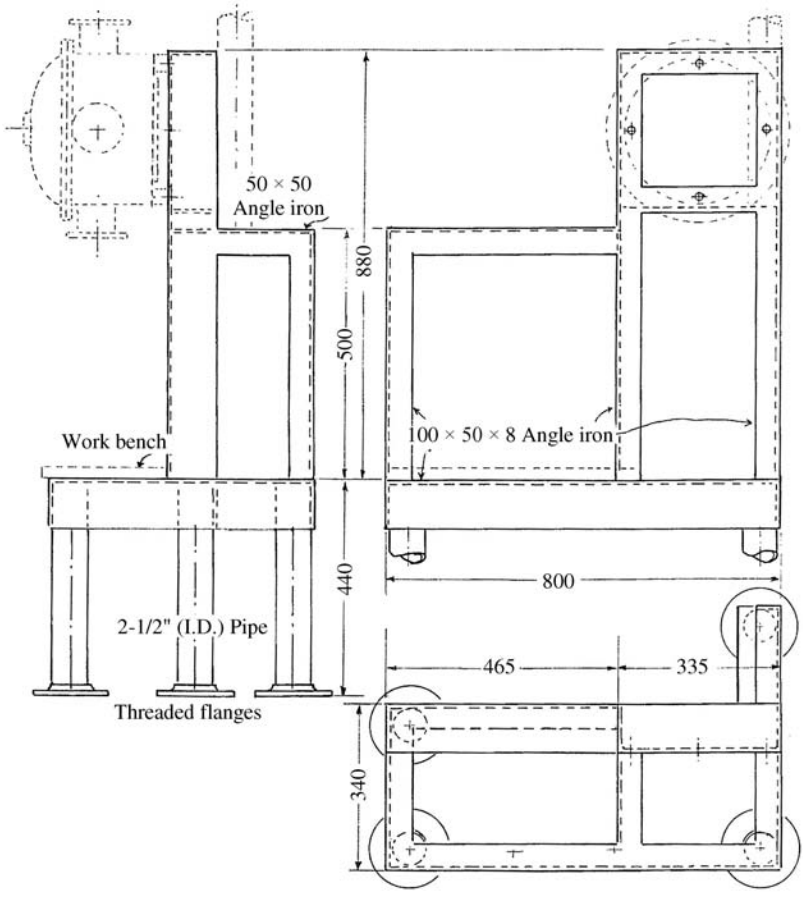

Figure 7.21 Stand for Versatilie, with dimensions. The rather heavy materials are intended to give a sturdy base for the furnace when used as a thermobalance.

specified, with the intent that the whole set-up should be reasonably free of vibrations.

The diameter of the heating elements and the design of graphite parts have varied according to the needs, but the main design, including the current-carrying brass components, has been retained with no problems.

'Thermobalance IV'. The overall size of 300 mm internal diameter of the furnace chamber sets a strict limit to the size of the graphite heating element (mostly 230 mm length and 30 to 45 mm inner dia.). For most

research purposes this is sufficient. A modest size also has the advantage that different parts of the sample will be at (almost) the same temperature.

On the other hand, metallurgical research of a more practical nature may require larger dimensions. For example, when investigating a certain charge material it may be desirable to have lumps of the same size as actually charged to the production furnace.

To this end a larger laboratory furnace was built, essentially the same design as Versatilie, but with the internal diameter increased from 300 to 450 mm, and other dimensions correspondingly increased. After duly considering both stainless steel and aluminium, brass and copper remained the chosen materials.

The front view of this 'Thermobalance IV' is shown in Figure 7.22. The only notable difference in design is that the current is transported by four separate terminals. Each goes straight through the back wall, electrically insulated as shown in principle in Figure 7.15 and paired outside the furnace casing to two sets of copper rails.

7.4 NOTES ON WINDOWS AND BALANCES

7.4.1 Windows for Optical Pyrometry

The use of a window, and the required corrections to the readings, were discussed in Chapter 4 (pp. 116–117). As pointed out there, high temperature experiments often involve fumes (vapours of condensable gases) that lead to coating and thus darkening of the window. Without counter-measures, seriously low temperature readings may result.

The best solution to the problem is to have several windows mounted on a carousel (a rotatable flange). Thus a clean window may be exposed to the radiation and the vapours for only a short time during the measurement, and subsequently withdrawn to remain clean (or *nearly* clean).

The arrangement shown in Figure 7.23 has been used (with minor modifications) on most of the furnaces discussed above. A number of windows (usually three) are mounted vacuum tight on a rotatable flange or disc, with one O-ring inside and one outside the row of windows. Rotation of the disc may require some force when the set-up is under reduced pressure, thus a handle on the disc is required. Furthermore it is

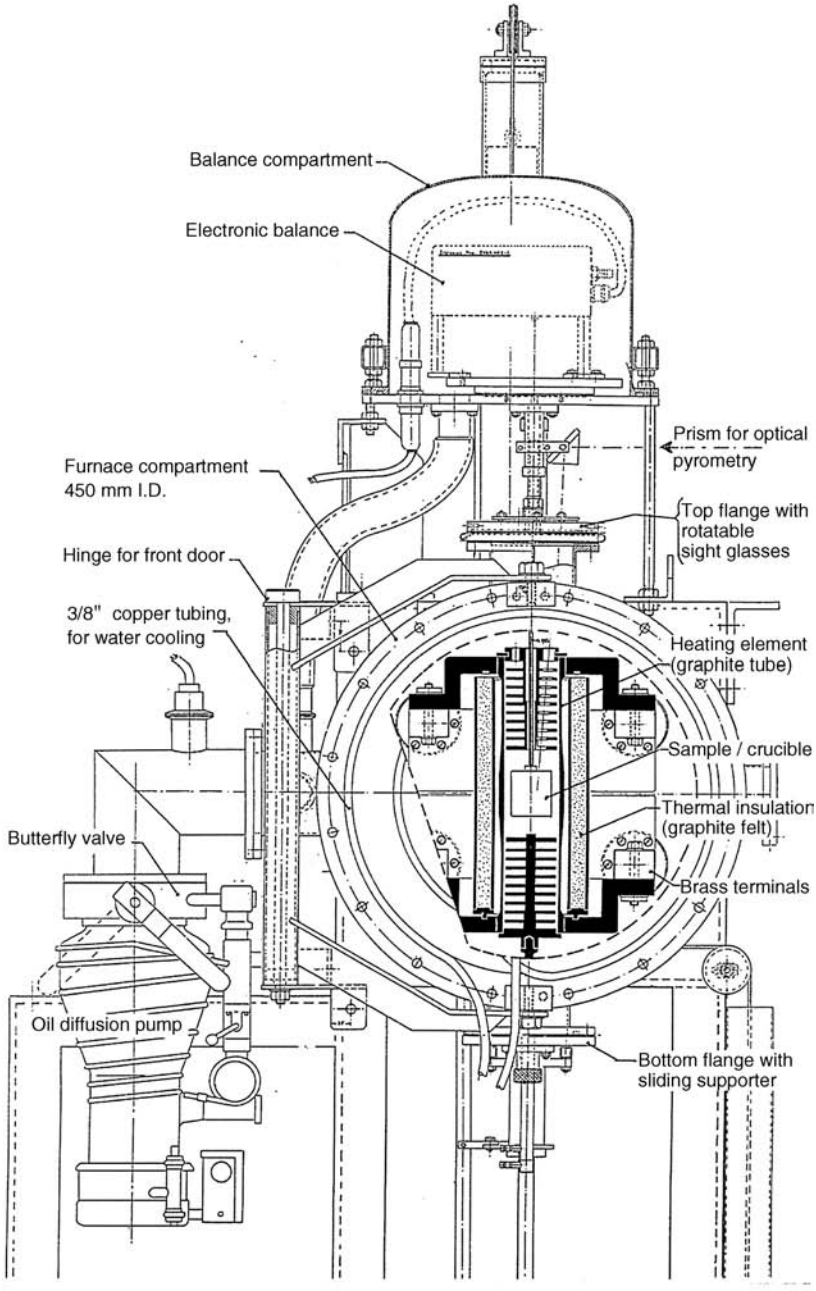

Figure 7.22 Thermobalance IV, front view, partly sectioned to show the interior.

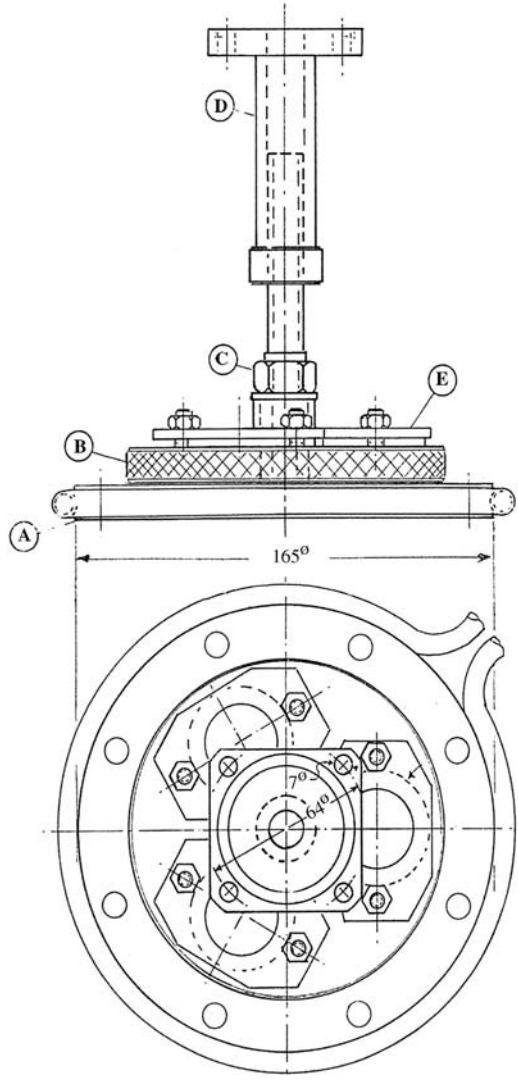

Figure 7.23 (a) Arrangement for changeable windows for optical pyrometry, assembly drawing.

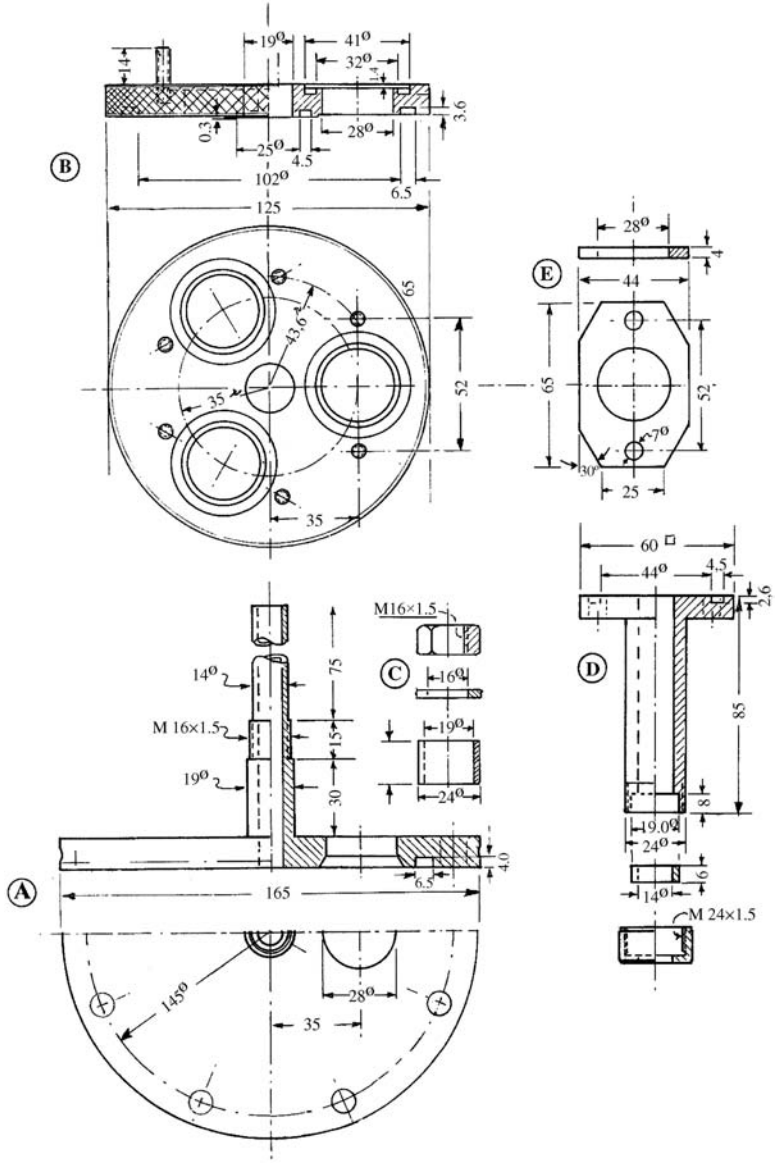

Figure 7.23 *(Continued)* (b) Flanges and changeable windows, details of components. **A:** Lower, stationary flange. It also serves as the central stem for the upper flange. **B:** Upper, rotatable flange with space for windows. **C:** Distance piece with washer and nut. **D:** Connection to the above base of balance. **E:** Plates for securing the silica windows.

an advantage to have only the innermost nave hit the stationary flange below. The rest of the rotatable disc should be reduced a few tenths of a millimetre in thickness on the underside, this makes for easier turning. (On the larger furnace, Figure 7.22, a flat roller bearing was interspaced between the rotatable and the stationary flanges to facilitate turning.)

7.4.2 Balances for Thermogravimetry

Generally, a balance denotes an instrument for determining the mass of an object.

The classical analytical balance had a balance beam resting on a knife edge at the centre, and two pans, one on each side, suspended from knife edges at equal distance from the centre. The three knife edges should be exactly in line. With the centre of gravity slightly below this line, the system will come to rest when the loads on the two pans are (nearly) equal. The weighing is performed by comparing the unknown sample on one pan with known standard weights on the other. Any imbalance shows up as a deviation of the beam from horizontal. The deviation is more clearly shown by a pointer attached at a right angle to the balance beam, usually moving across a suitable scale. By proper adjustment of the centre of gravity of the balance beam, the scale can be applied directly to readings in the miligramme range.

In a vacuum system, the pointer may be replaced by a small mirror attached to the top of the beam, in combination with a window, and another mirror and a spotlight outside the system. This was our first attempt at observing mass changes in real time; the little mirror and the window are seen on top of the balance in Figure 7.7 (p. 239).

An electronic balance must in principle consist of two elements: a sensor to detect the deviation, and a force element to counteract it. As the *sensor* we used a small 'differential transformer', it has one coil at each end wound the same way, and one in the middle wound the opposite way. A probe of soft iron inside will then be very sensitive to displacement from its symmetrical position, and it works as a position transducer. *The force element* in our case consisted of a permanent bar magnet placed halfway into a d.c. coil; not very sophisticated but it works. The current in the coil gives a direct measurement of the force, or more properly the mass change, of the specimen. The differential

transformer and the force element are seen right below and above the balance beam in Figure 7.7.

These two electronic elements were connected to a feedback circuit or 'electronic unit' placed outside the vacuum system. This was produced by the Department of Applied Cybernetics at SINTEF (Trondheim) at a time when no electronic balance was commercially available, and it served us well for a good many years.

The present weighing cell is a product of modern digital technology and bears little similarity to the old-fashioned balance. It appears that the modern device no longer depends on two arms in balance, but on the balance between forces brought about by electromagnetic means. Thanks to digital technology, a modern electronic balance may detect, for example, 0.1 mg in a mass of 100 g. Translating to analogue technology, it is equivalent to measuring 1 mm in a distance of 1 km.

Returning to the question at hand, it is felt that a sensitivity better than ± 1 mg is not necessary because of the unavoidable fluctuations inside a hot furnace.

Today a fair number of companies offer electronic analytical balances or weighing cells of almost any desired capacity and accuracy. It appears, however, that most of them are designed for a load from the top only. The difficulty may be circumvented by making a light and stiff frame surrounding the weighing pan, with the load suspended underneath.

7.4.3 Adjusting to the Pyrometer Target

The load, quite often a graphite crucible as depicted in Figure 7.17 or 7.22, hangs suspended from the thermobalance. Of necessity the suspending wire or rod is in the centre, and the path for pyrometry must then be off to one side. The orifice in the crucible lid, which is the target for temperature measurement, should then be off to the same side. The crucible is freely suspended, but with some patience one may succeed in aligning the hole for pyrometry before closing the system. During the subsequent evacuation and heating, however, the suspended crucible may twist a bit, and the orifice is lost from sight.

Three solutions to this problem are possible. The first is that the whole system of crucible and surroundings is at a uniform temperature, no contours are seen, and temperature may be read as in a black box.

(Or, another alternative, that a few degrees difference in temperature does not matter for this particular experiment.)

The second alternative is that the suspension is stiff, that is, that each part of the suspension from crucible to balance is shaped with hooks and eyes to give a definite direction to the suspended crucible. This is the path we have followed in most of our work.

The third way is to have the possibility of adjusting the position of the pyrometer orifice during the experiment. Adjusting in this context means no more than a slight twist of the suspension. It was realized only in the larger thermobalance shown in Figure 7.22. This detail is not visible from the drawing, but it consists essentially in placing the whole balance on a turntable that permits a turning of some 30° each way. This is sufficient to counteract incidental twisting during the run. The turning is effected by means of a cogged rim on the turntable, mating with a cogwheel on a rotary leadthroughs in the base of the balance.

While this specific application may seem rather special, rotary motion through a vacuum wall is quite often called for. Thus a detailed drawing of this sort of lead-through is given in Figure 7.24.

7.5 NON-GRAPHITE HEATING ELEMENTS

Although graphite is both versatile and non-volatile, its presence is sometimes undesirable for the chemical system in question. In neutral or reducing atmospheres, molybdenum and tungsten are viable alternatives, with molybdenum being the easier to fabricate.

Thus, for specific applications, the graphite heating element of 'Versatilie' was replaced by one of molybdenum as shown in Figure 7.25. The graphite blocks (cf. Figure 7.17, p. 251) were replaced by brackets shaped from 8 mm copper plate.

The heating element is further detailed in Figure 7.26. It is made from 0.2 mm Mo foil, bent to a tube of more or less hexagonal cross-section and spot welded along the seam. At both ends the tube is split and the flaps bent at 90° to serve as terminal connections.

Spot welding of molybdenum was found to be next to impossible, even when using an organic liquid to prevent oxidation. The matter was resolved after consulting the treatise of Espe (1960): with strips of very

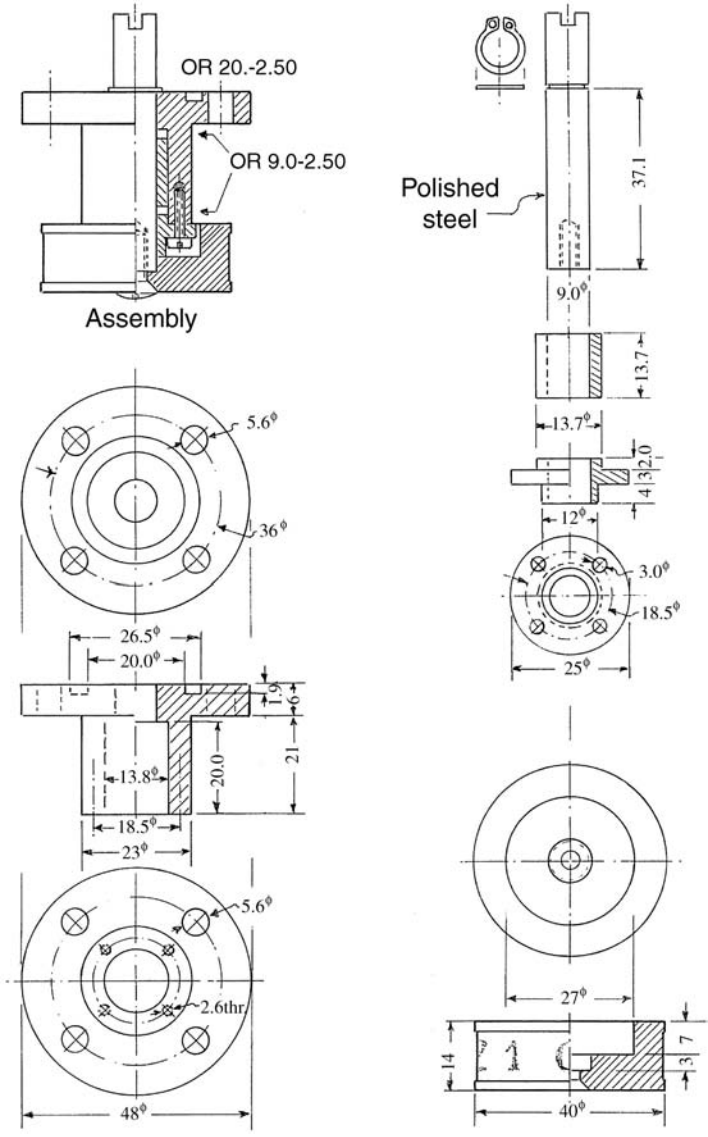

Figure 7.24 A general lead-through for rotary motion: Assembly drawing, and details with suitable dimensions in millimetres.

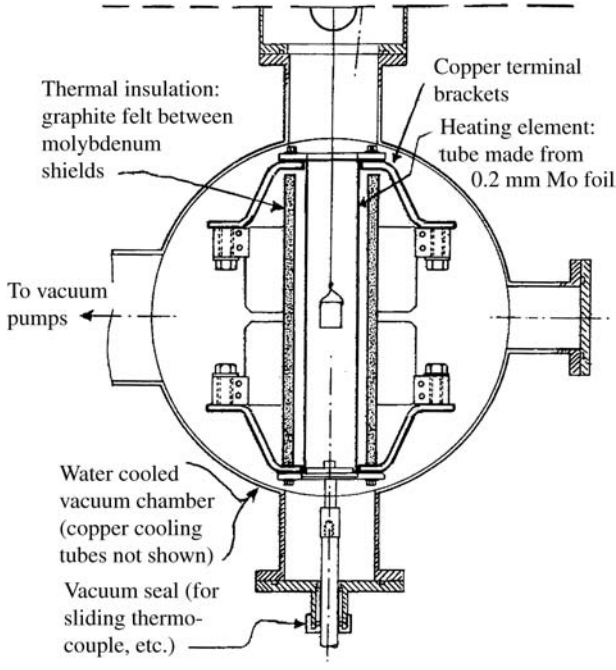

Figure 7.25 The Versatilie furnace with heating element of molybdenum (compare Figure 7.17, p. 251). The graphite blocks are replaced by copper brackets.

thin (0.005 mm) platinum foil between the molybdenum surfaces along the seams, spot welding was readily performed.

A straight tube with uniform wall thickness develops a marked temperature maximum in the middle section (as discussed on p. 18). In the case of molybdenum this effect is enhanced by the fact that the resistivity increases by almost a factor of ten when the temperature is increased from room temperature to 1700 °C (cf. Figure 2.1, p. 16). To counteract this, the molybdenum tube was designed with two, respectively three layers of 0.2 mm Mo sheet in the middle section, spot welded along seams and edges. The resulting temperature distributions at two different temperature levels are shown in Figure 7.26.

The furnace, Figure 7.25, was used without internal radiation shields, but with a closed bottom to prevent excessive draught.

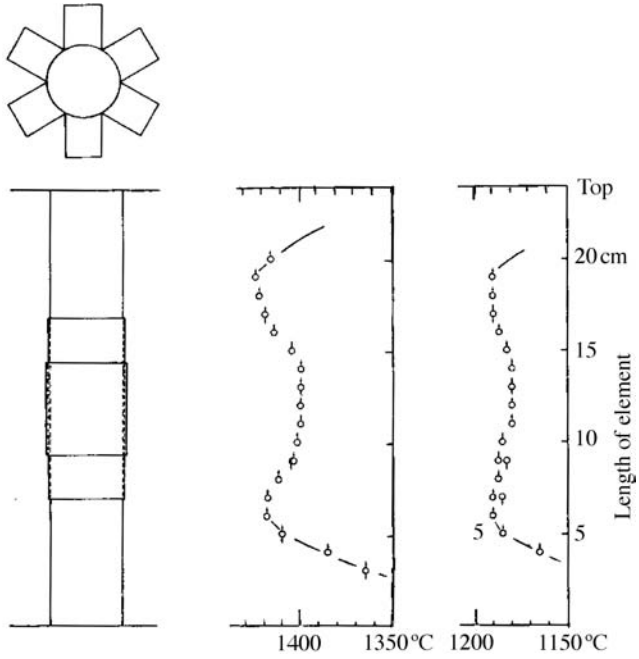

Figure 7.26 *Left*: Heating element made from 0.2 mm Mo foil, spot welded along seams. The centre section has two, respectively three layers of foil to attain a zone of uniform temperature. *Right*: Observed temperature distribution at two different levels of power. Note that the temperature uniformity of the element is somewhat overcompensated; this matches the fact that the furnace was used without horizontal radiation shields, as shown in Figure 7.25. (From Blegen, 1976.)

7.6 CONCLUDING REMARKS

A wealth of experimental work on high temperature chemistry has been published during the last half century. It appears, however, that most of it has been performed using commercially available equipment, or else the equipment is described in rather sketchy terms and drawings. In either case, I have not considered it my duty to review the literature.

Thus, in contrast to preceding chapters, this one has only a few references. The present chapter is essentially the outcome of work done in the workshop and laboratories in Trondheim.

The narrative is not complete, however. Various furnace designs related to heat treatment or qualitative observation have been omitted.

Some equipment for accurate determinations, on the other hand, is described in considerable detail, in the hope that it may be of use to the next generations.

REFERENCES

Blegen, K. (1976) Equilibria and Kinetics in the Systems Si-N, Si-O-N and Si-C-O-N. Dr. Ing. Thesis, NTH, Trondheim, 259 pp. See also Blegen, K. (1975) *Special Ceramics*, **6**, 223–244.

Espe, W. (1960) *Werkstoffkunde der Hochvakuumtechnik, Band I-III*, VEB Deutscher Verlag der Wissenshaften, Berlin, ref. Vol. I, pp. 735–737.

Sandberg, B. (1981) Karbotermisk reduksjon av aluminiumoksyd. Dr. Ing. thesis, NTH, Trondheim, 140 pp.

8

The Summing Up

CONTENTS

High Temperature Experiments in Chemistry and Materials Science, First Edition.
Ketil Motzfeldt.

Preamble

This chapter's title is taken from a book by the British author W. Somerset Maugham, who 'always liked to tell stories'. In a modest way I feel akin to him. So this last chapter is a tale of stories, picked from roughly 60 years' pottering in the lab. Some of them may still be of interest.

8.1 EQUILIBRIUM GAS PRESSURES (I): $\sim 10^{-4}$–10^{-1} MBAR

8.1.1 An Introduction

Determination of the pressure of a gas in equilibrium with condensed phases is amongst the most direct experimental methods for obtaining chemical thermodynamic data. The methods, however, vary with the pressure range. For determination of very low pressures ($\sim 10^{-4}$ to 10^{-1} mbar), the Knudsen effusion method in its various forms is commonly used. At higher pressures ($\sim$1 to 1000 mbar) a number of different methods are available, to be discussed in Section 8.3 (pp. 288–297). For the present we consider the determination of very low equilibrium pressures.

8.1.2 Knudsen Effusion

This method is named after the Danish physicist Martin Knudsen who made fundamental contributions to the kinetic theory of gases 100 years ago (Knudsen, 1909, 1946). 'Knudsen flow' or 'effusion' are terms used

for gas transport in the low pressure range where the mean free path of the molecules is large compared to the cross-section of the conduit (cf. Chapter 6, p. 181).

The effusion method uses a container or cell that is gas tight except for a hole or an orifice of known dimensions. The cell with its charge is placed in a furnace which is then evacuated and heated to the desired temperature. The measurements consist in determining the rate of mass loss of the charge caused by effusion of the sample through the orifice.

An alternative to the mass loss method is the use of a mass spectrometer. It may identify the various evaporating species, and it may eventually also determine the vapour pressure of each. The method is not further treated here, but some results are noted in the next section (pp. 275–285).

The effusion method has been thoroughly discussed by Margrave and coworkers (1967). For the present we will attempt a more limited presentation. The basic ideas were outlined already in Chapter 6, and from p. 183 we reproduce the equation

$$\frac{dn_i}{Adt} = P_i\sqrt{\frac{1}{2\pi RTM_i}} \tag{8.1}$$

where dn_i/Adt represent the number of molecules of species i that pass through an orifice with effective area A in unit time.

Converting from numbers to the mass q_i and rearranging, we have

$$P_i = \frac{dq_i}{Adt}\sqrt{\frac{2\pi RT}{M_i}} \tag{8.2}$$

With all quantities in SI units, Eq. (8.2) gives the vapour pressure in *pascal*. For our purpose we prefer it in *bar* (= 10^5 pascal), and we express the mass q in milligrammes, time t in minutes, area A in mm^2 and M in grammes. This gives

$$P_i = 3.81 \times 10^{-5}\,\frac{dq_i}{Adt}\sqrt{\frac{T}{M_i}} \tag{8.3}$$

8.1.3 The Clausing Factor

The above equations are derived from the expression for collision frequency, and A represents the area of an orifice or opening in a very thin wall, essentially with no thickness. The classical experiments by Knudsen were done in this way, piercing a hole in a very thin platinum foil. For practical use it is preferable to have a lid of definite thickness, thus it was necessary to work out the proper expressions for orifices of defined lengths. This was originally done by Clausing, as explained in Chapter 6. Table 6.1 on p. 194 gives values of the 'transmission probability' W for a circular opening in dependence of the ratio between length and diameter. In the above equations, the area A may be replaced by $A_{eff} = A \times W$, with the area and the Clausing factor determined from accurate measurements of the orifice in question.

Tables have also been worked out for other orifice shapes, such as conical holes, and so on, but a straight, cylindrical orifice is the simplest both to make and to measure.

8.1.4 The Evaporation Coefficient

The above equations, applied to vapour pressures, assume that the substance in question is free to evaporate with no kinetic hindrance. This is the case, for example, for most metals that vaporize to atoms. In other cases the vaporization may be hindered, particularly in cases where the equilibrium form of the vapour has a structure which is different from the structure of the condensed phase. An example is the dissociation/vaporization of molten sodium carbonate, where the trigonal CO_3^{2-} ion in the melt must be reshaped to the linear CO_2 molecule on evaporation (Motzfeldt, 1955). An extreme example is arsenic, it vaporizes to form tetragonal molecules of As_4 which are not present in the structure of the solid (Brewer and Kane, 1955).

Hindered evaporation may be accounted for in experiments by introducing an evaporation coefficient $\alpha < 1$. In a closed cell (no hole) evaporation and condensation must take place at the same rate, from which one may infer that, in an equilibrium situation, the evaporation and the condensation coefficients are identical quantities. (There is no reason, however, to believe that the two coefficients are equal in the general case, more likely they are different.)

8.1.5 Methods of Extrapolation

The basically simple effusion method, based on Eq. (8.3), appears less simple on second glance. An evaporation coefficient less than unity means that the apparent vapour pressure will increase with decreasing orifice size. The true equilibrium vapour pressure must be found by measurements with different orifice sizes and subsequent extrapolation to zero hole. The question, then, is to find a rational form for the extrapolation.

Motzfeldt (1955) attempted a systematic approach to the problem, see Figure 8.1. The treatment takes into account the effective area $A_{eff} = A \times W_A$ of the orifice, the inside cross-section area B and the Clausing factor W_B of the cell itself, and the evaporation coefficient α pertaining to the chemical system in question. We will not go through the reasoning but only give the equilibrium pressure P_{eq} as a function of the measured pressure P_m (as expressed by Eq. (8.3) with A_{eff} inserted):

$$P_{eq} = P_m \left[1 + \frac{A_{eff}}{B} \left(\frac{1}{\alpha} + \frac{1}{W_B} - 2 \right) \right] \tag{8.4}$$

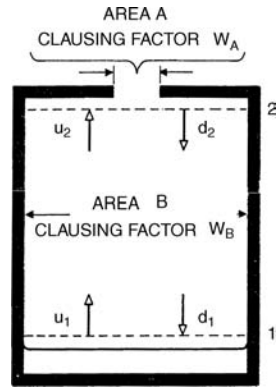

Figure 8.1 The principle of an effusion cell. The orifice has an area ***A*** and a Clausing factor W_A. The cell body has the inside cross-section area ***B*** and a Clausing factor W_B, introduced in an attempt at a theoretical treatment of the method. (Note: The letters ***A*** and ***B*** are exchanged as compared to the original paper.)

Rearrangement of the equation suggests a graphical method for obtaining P_{eq}. For simplicity we write the ratio between the two areas, $A_{eff}/B = f$. By rearrangement we have

$$P_m = P_{eq} - \left(\frac{1}{\alpha} + \frac{1}{W_B} - 2\right) P_m f \tag{8.5}$$

The results for P_m from a number of experiments with different f values (different orifice sizes) may be plotted against $P_m \times f$. A straight line should result, with an intercept for $f = 0$ equal to the equilibrium pressure P_{eq}.

This method gained some acceptance, but in reality the above model is too simple. Rosenblatt (1963) discussed this and other related models, and concluded that none of them are reliable as regards extrapolation to the equilibrium value. He found, however, a simple empirical relationship that appeared promising:

$$P_{eq}/P_m = 1 + (A_{eff}/k)^{2/3} \tag{8.6}$$

The coefficient k is an empirical constant that for our purpose may be set equal to unity. Plotting $1/P_m$ against $(A_{eff})^{2/3}$ and extrapolation to zero orifice should yield $1/P_{eq}$ and hence the equilibrium pressure. This empirical relationship, suggested by Rosenblatt, has since been found useful in a number of cases.

8.1.6 An Example (with Some Difficulties): The System Al – Al_2O_3

At elevated temperatures, aluminium oxide in contact with liquid aluminium forms the gaseous aluminium suboxide:

$$Al_2O_3(s) + 4Al(l) = 3Al_2O(g) \tag{8.7}$$

At the same time aluminium metal also has a vapour pressure of its own:

$$Al(l) = Al(g) \tag{8.8}$$

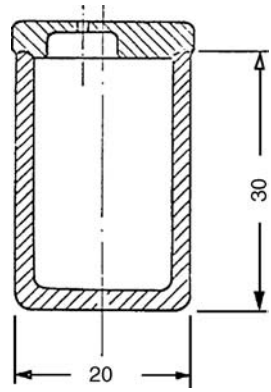

Figure 8.2 Effusion cell of alumina, with the lid ground to a tight fit.

This system has attracted interest, not the least in connection with a possible carbothermal production process for aluminium. Vapour pressures in the system were studied by Herstad and Motzfeldt (1966), using the thermobalance 'Beljara' shown on p. 239. The graphite crucible and suspension shown there was exchanged with an effusion cell of alumina and suspension of molybdenum wire. The effusion cell is shown in Figure 8.2. The centre part of the lid was thinned down (by means of a larger diamond drill) in order to avoid excessive length of the orifice.

For an effusion run the cell was charged with a weighed amount of aluminium plus an excess of powdered alumina, and suspended inside the heating element. The system was evacuated and outgassed as discussed on p. 188, before heating to the desired temperature. Runs were made with four different orifice sizes ranging from 0.8 to 8 mm diameter, to account for the possible effect of a low vaporization coefficient as discussed above. At the end of a run, the remaining amount of aluminium metal was determined by treating the cell and contents with dilute acid, measuring the volume of hydrogen evolved. From Eq. (8.7) it is seen that each mol of alumina lost has consumed 4 mols of metal; metal loss in excess of this must have vaporized as Al(g). Thus the separate vapour pressures of Al and Al_2O were determined.

This method seemed simple in principle. It turned out, however, that the rate of weight loss did not stay constant during a run, it diminished with time. After the run the orifice was partly clogged by a glassy mass. The observation may possibly be explained by reaction Eq. (8.7) running from right to left by the pressure release through the orifice. Anyway,

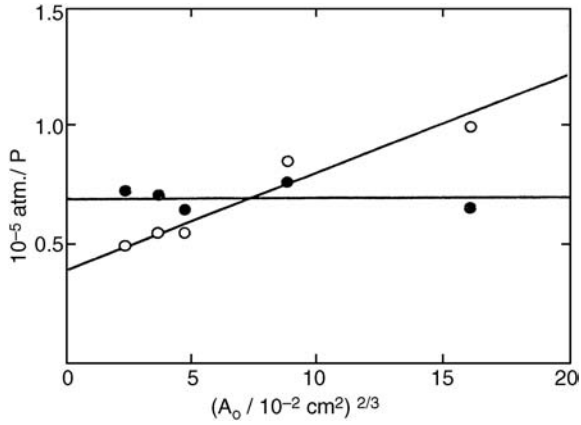

Figure 8.3 Inverse experimental values of the pressures of Al_2O (filled circles) and Al (open circles) versus two-thirds power of the effective initial orifice area A_o. (From Rao and Motzfeldt, 1970.)

it made the experiments and the interpretation more troublesome. Another worry was that the ratio $F = P(Al_2O)/P(Al)$, determined from the analyses, increased excessively with increased orifice size. This effect was presumably caused by some sort of interaction between the alumina cell and the graphite tube.

For this reason, the graphite heater was exchanged for one of molybdenum foil as shown in Chapter 7, p. 264. A tube of dense-sintered alumina was fitted snugly inside this heating element, the effusion cell was thus suspended in an environment of its own material. Experiments were run with five different orifice sizes at one and the same temperature (Rao and Motzfeldt, 1970). The procedure during a run was as described above.

The final observations are plotted in Figure 8.3 in the way suggested by Rosenblatt. The gradual clogging of the orifice was still not completely avoided and may account for the slight irregularity of the points.

It is seen that the observed vapour pressures of Al_2O were almost independent of the orifice size, while those of Al decreased with increasing orifice size. (The difference in behaviour may be correlated with the excess of alumina in the charges.) Extrapolation to zero orifice gave the following values for the equilibrium pressures at 1283 °C:

$$P_{Al_2O} = 1.5 \times 10^{-2}\ \text{mbar}, \quad P_{Al} = 2.5 \times 10^{-2}\ \text{mbar}$$

These values are nearly 50% lower than the results of Herstad and Motzfeldt (1966) adjusted to the same temperature.

On the other hand, the corresponding values calculated from the NIST-JANAF Tables (1998) for the same temperature are considerably higher, $P_{Al2O} = 3.0 \times 10^{-2}$ mbar, $P_{Al} = 3.4 \times 10^{-2}$ mbar. We have to leave it at that.

For a demonstration of the effusion method, we could have chosen a more well-behaved example, such as the vapour pressures over the solid phases in the system NaF – AlF_3 (Grjotheim, Motzfeldt and Rao, 1971). Still the system aluminium oxide–aluminium was chosen because of its interest in connection with a possible carbothermal production process for aluminium. We will return to this towards the end of the chapter.

8.2 THE THERMAL DECOMPOSITION OF SILICON CARBIDE

This is another example of the use of the Knudsen effusion method. Various features of the compound SiC have been discussed already in Chapter 5, pp. 139–145.

8.2.1 Background

Drowart, De Maria and Inghram (1958) studied the vaporization of silicon carbide by means of a high temperature mass spectrometer. Their work is one of the earliest studies of this sort, but probably also one of the most dependable. They showed that the thermal decomposition yields gaseous Si as the main product, with SiC_2 and Si_2C as significant minor species. The question remained, however, whether an investigation done by mass spectrometry also yields correct results for the absolute magnitude of the vapour pressures. This could be checked by an investigation using the weight-loss method. It had to be done very carefully, however, in order to be meaningful.

In anticipation it may be said that the investigation was successfully completed, not the least because of the painstaking work done by my coworker Marit Steinmo. The manuscript was written as a SINTEF[1]

[1] SINTEF: The Foundation for Scientific and Industrial Research at the Norwegian Institute of Techology. Address: N-7465 Trondheim.

report (Motzfeldt and Steinmo, 1989). It was referred to in *Chemical Abstracts*, but for various reasons the full paper never appeared in any journal. Thus it appears justified to report it here in some detail.

8.2.2 Equipment

The vacuum furnace 'Beljara' was again used (Chapter 7, pp. 239–240; the semi-electronic balance shown in Figure 7.7 is also discussed on p. 260.) The balance was connected to a strip chart recorder; the sensitivity as shown on the recorder was 5 mm/1 mg.

Temperature measurements were made by means of an automatic optical pyrometer (Type PB40 AF3 from Keller Spezialtechnik – Pyro-Werk GmbH, Ibbenbüren-Laggenbeck, Germany). The pyrometer was sighted through a quartz prism as seen in Figure 7.7. Counting from the pyrometer end, the sighting path went through the prism, then through a silica window at the base of the balance, down the holes in the radiation shields and on to the lid of the crucible. It took some care and effort, with small adjustments of the position of the pyrometer, to ensure that the pyrometer path was free of obstruction.

The pyrometer was calibrated against the melting points of platinum (1768 °C, cf. p. 63) and alumina (2054 °C, cf. p. 123). The calibrations were made in the same furnace as used for the effusion runs, with the sample crucible in place of the effusion cell. For platinum, an alumina crucible was used, 16 mm ID, 20 mm high. To avoid sighting directly onto the glossy molten Pt, the crucible was equipped with a 5 mm ID, closed bottom sighting tube extending though a hole in the lid. About 28 g of pure Pt was used (obtained in the form of 1 mm Pt thermocouple wire).

For alumina, a molybdenum crucible was turned from solid stock, 40 mm high, about 28 mm ID and slightly conical. The lid had a sighting hole with a diameter of 5.8 mm. Molten alumina is transparent, hence a bundle of short pieces of Mo wire were placed at the bottom of the crucible to avoid reflections. The crucible was charged with about 50 g of Alcoa Tabular Alumina T-60 (99.5% Al_2O_3).

The melting points were observed by heating and cooling curves. The final results were 6.952 mV for platinum at 1768 °C, and 9.59 mV for alumina at 2054 °C. According to the manufacturer the pyrometer is designed to give a strictly linear relationship between the output in mV

and the temperature in °C. With the above data the relationship is:

$$t/°C = 1012 + 108.7\,U/mV \tag{8.9}$$

In this way the separate determination of corrections for absorbtion in the prism and the window were avoided.

Power to the furnace was controlled by a thyristor in the primary circuit of the low-voltage transformer (cf. Chapter 2, p. 53). Automatic temperature control in connection with the optical pyrometer was not used because of the possible coating of the window. However, the thyristor circuit also acts as a power stabilizer, so that the temperature could be kept constant within 1 °C by manual control.

The effusion cell, 25 mm OD, 33 mm high, wall thickness 2.5 mm, with a threaded lid, was made from gas tight graphite (Graph-I-Tite from The Carborundum Co., Specialty Graphite Products, Sanborn, N.Y.) The cell body was tested by attaching it to the vacuum system by means of a rubber gasket, evacuating the system and leaving it closed overnight. From the calculated leak rate the cell was deemed 'gas tight'.

The silicon carbide was obtained from Orkla Exolon a/s & Co. (now Washington Mills a/s), Orkanger, Norway, quality 'Green Crude', grain size 0.71 to 1.00 mm. The grains were not given any cleansing treatment before use. The main impurity was expected to be a thin surface layer of silica which eventually will be volatilized to SiO and CO by reaction with the carbide in the very first part of the heating.

8.2.3 Procedure and Observations

A run consisted of essentially placing the cell in position suspended from the balance, closing and evacuating, and leaving it for several hours at a moderate temperature (some 1000–1200 °C) for degassing. Next, the furnace was brought to the desired temperature. A chosen temperature was kept constant for a sufficient time to get a good straight line on the recorder connected to the balance. The temperature (or strictly speaking, the power) was then changed to another value and the procedure repeated. Periods of between 6 and 60 minutes at each temperature were used, with the longer periods at the lower temperatures with low rates of mass loss.

All of the runs reported here were done with one and the same effusion cell. At first a blank run was made with the empty cell with no orifice.

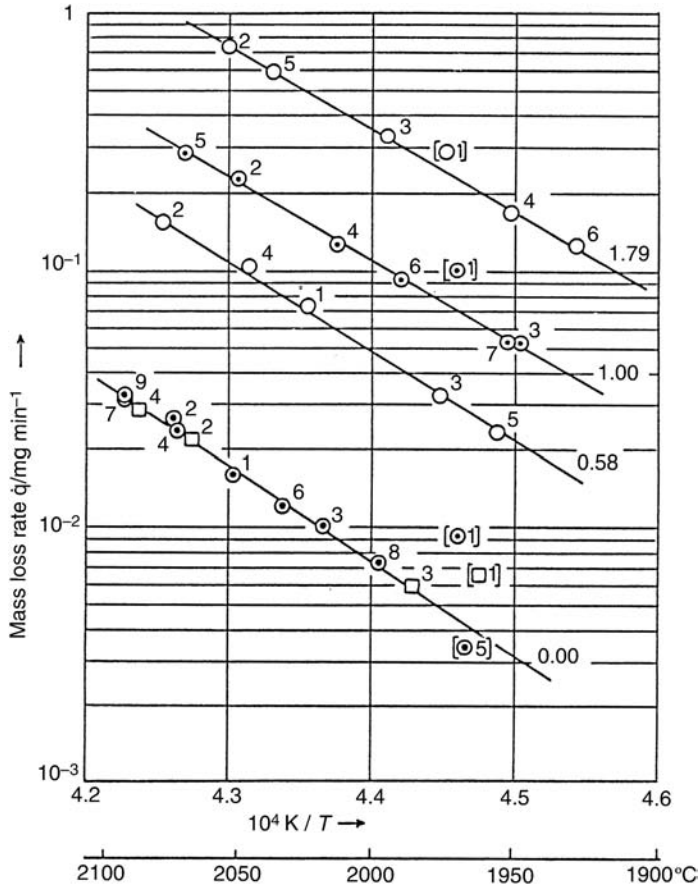

Figure 8.4 Experimental data for mass loss rates as functions of temperature. Numbers to the right of curves are orifice diameters in millimetre; numbers on points represent sequence of observations during a run. The lowest curve represents two blank runs, one with an empty cell (squares), the other with a charge of SiC in the cell, both with no hole in the lid. Curves (straight lines) are obtained by linear regression of the experimental data, with points in brackets omitted. (Filled and open circles are used only to distinguish between different runs.)

Secondly about 4 g of silicon carbide was charged into the cell and the procedure repeated, still without an orifice. The observed mass loss rates with and without the carbide charge were almost indistinguishable, as seen on Figure 8.4's lowest curve. This indicated that the graphite cell was for the present purpose tight, including the fit between the lid and the cell.

The next three runs constituted the effusion experiments. In the first run, a 0.6 mm hole had been drilled in the lid, while the SiC charge was retained. Before the second run the hole was enlarged to 1.0 mm and the SiC charge renewed. The third run was done with a 1.8 mm orifice and once again a new charge. For each run, halts were made at five or six different temperatures, each of sufficient duration to give a reliable value for the rate of mass loss.

The orifice sizes, measured under a microscope, were 0.58, 1.00 and 1.79 mm diameter. The thickness remained constant at 1.36 mm, and hence the effective orifice sizes, including the Clausing factors, were 0.0861, 0.350 and 1.450 mm^2. Results from all of the runs are present in Figure 8.4, in the form of log (mass loss rate) versus inverse absolute temperature.

Two features of these observations deserve mention. First, it is noted that the changes between different temperatures in the same run were made at random, in order to avoid any systematic error due to the progressive vaporization of the carbide or other time-dependent factors. Second, it is seen that the first point in the second and third series lies too high, indicating the volatilization of some surface silica as mentioned above. (This effect is even more marked in the blank run, but absent in the first because the same carbide charge was used.)

For the further treatment, a linear relationship between the log of mass loss rate and the inverse temperature was found by least-squares fitting of the data from each run. Subsequently the expression for the blank run was subtracted from each of the effusion runs. The resulting expressions represent the mass loss rates due to effusion, which we designate $dq/dt = \boldsymbol{r}$:

$$0.6\,\text{mm}\,\text{Ø}: \quad \log\left(\boldsymbol{r}/\text{mg min}^{-1}\right) = -3.390 \times 10^4\,\text{K}/T + 13.516 \quad (8.10)$$

$$1.0\,\text{mm}\,\text{Ø}: \quad \log\left(\boldsymbol{r}/\text{mg min}^{-1}\right) = -3.178 \times 10^4\,\text{K}/T + 12.984 \quad (8.11)$$

$$1.8\,\text{mm}\,\text{Ø}: \quad \log(\boldsymbol{r}/\text{mg min}^{-1}) = -3.206 \times 10^4\,\text{K}/T + 13.636 \quad (8.12)$$

For comparison of results for different orifice sizes at the same temperature, values of the rate of mass loss were calculated from Eqs (8.10) to (8.12) for three temperatures corresponding to $10^4\,\text{K}/T = 4.50$, 4.35 and 4.25 (temperatures 2222, 2299 and 2353 K). For each temperature it

was found that the ratio r/A increases with diminishing orifice size, which is generally taken to indicate kinetic hindrance. The usual procedure, then, is to plot the data in some way that permits extrapolation to zero orifice (as discussed on p. 271 above). But no way of extrapolation was found to be possible for the present data.

On the other hand, a plot of mass loss rate versus effective orifice area gave nice, straight lines, as shown in Figure 8.5. The trouble is that the lines *do not go through the origin*.

8.2.4 Effect of Non-Ideal Effusion

To begin, we suggest that the strict linear relationship shown in Figure 8.5 is in part incidental. A rough evaluation by means of Eq. (8.3) (p. 269) indicates that the higher rates of mass loss in Figures 8.4 and 8.5 correspond to vapour pressures in the transition region where a contribution from viscous flow gives higher mass flow rates than corresponding to pure effusion. Wahlbeck (1971) developed a theoretical treatment for the transport of gases in this region. For practical use, numerical results have been presented in tabular form (Wahlbeck, 1986). The correction factor is dependent upon the 'Knudsen number' $\mathrm{Kn} = \lambda/d$ where λ is the mean free path and d is the diameter of the opening (cf. p. 191). The mean free path depends on the collision diameter δ of the species. The main species in the present case is Si, for which we suggest $\delta = 4 \times 10^{-10}$ m. (In reality the gas consists of SiC_2 and Si_2C in addition to Si, but a more accurate estimation appears unrealistic.) We will abstain from the numerical values (cf. Motzfeldt and Steinmo (1989) p. 12) and only give the results graphically as shown in Figure 8.6 (filled circles). The open circles from Figure 8.5 are retained for comparison.

This refinement of the results does not, however, solve the main problem; a straight line through the filled circles does not go through the origin.

8.2.5 The Effect of Surface Diffusion

Molecular flow through (short) tubes was discussed in Chapter 6, pp. 194–196. The basic assumption for calculations of the rate of flow is that a molecule which hits the wall of the tube, leaves again in a

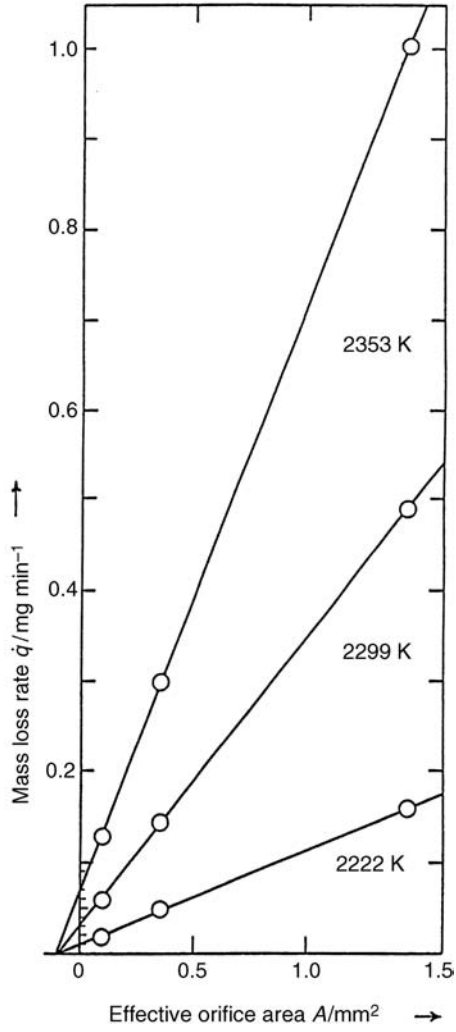

Figure 8.5 Mass loss rates dq/dt at three different temperatures, plotted against the effective orifice area A_{eff}. Numerical values have been obtained from Eqs (8.10) to (8.12).

direction which is independent of the angle of incidence. This implies that the molecule remains adsorbed to the wall for some time. It is concurrently assumed that the molecule is re-emitted from the same spot where it was adsorbed. But this assumption can be valid for very short residence times only, when there is little mutual attraction between the vapour molecule and the material of the wall.

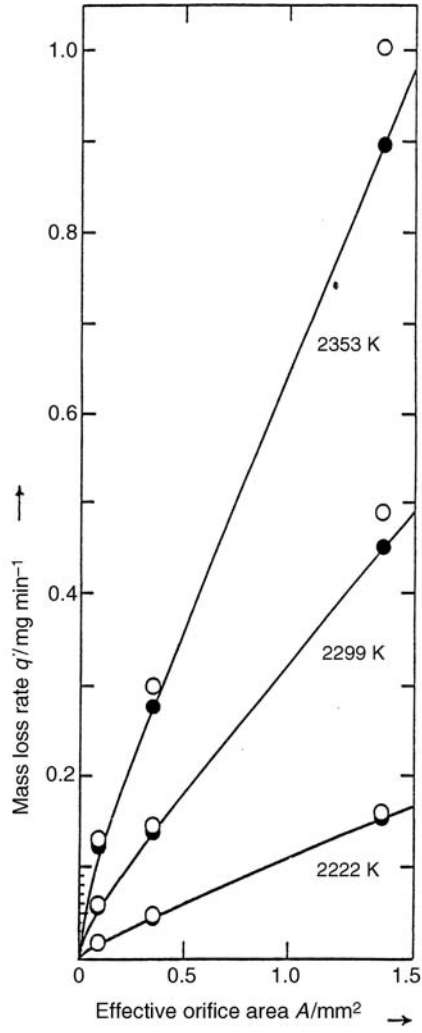

Figure 8.6 Filled circles: Rates of mass loss corrected for contributions from viscous flow, plotted against effective orifice area. Curves calculated from Eq. (8.13) with values of a and b from Table 8.1.

Considering silicon vapour and a graphite wall, there are good reasons to expect strong attraction. Thus, an impinging Si atom is expected to remain for some time. Inside an effusion orifice it is located on a gradient, hence it is quite likely that it will move

while adsorbed at the graphite surface, it will move by *surface diffusion*.

The effect of surface diffusion on vapour pressure measurements by the effusion method was discussed by Freeman and Edwards (1967), but we will adopt a simpler approach. The general analysis would have to take account of the radial gradients in surface concentration on the inside and outside of the lid around the orifice. We will assume, however, that these radial gradients may be neglected, and that the driving force for surface diffusion is the gradient along the orifice wall only.

For the further treatment we will simplify the notation, so that the rate of transport $dq/dt = q$. The rate of transport by surface diffusion, q_s, must be proportional to the circumference of the orifice, which means proportional to its diameter d, and inversely proportional to the orifice length (the thickness of the lid) L. In addition we have the transport rate q_e caused by effusion, which is proportional to the area A of the orifice. The sum is equal to the observed mass loss rate corrected for contributions from viscous flow, that is

$$q_c = q_e + q_s = a \times A + b \times d/L \tag{8.13}$$

where a and b are constants at a given temperature. The dimensions A and d/L are known for the three different orifices, and the observed mass losses q_c after correction for viscous flow are likewise known. Thus for each temperature we get three equations of the form of Eq. (8.13), from which the 'best' values of a and b are obtained by numerical fitting, as seen in Table 8.1. It is also taken into account that $\log a$ and $\log b$ should be linear functions of $1/T$. The resulting curves go through the filled circles in Figure 8.6. The points from Figure 8.5 (open circles) have been retained for comparison.

It is implicit in our interpretation that the observations, including those with the largest orifice, represent equilibrium values. That is, significant hindrance to the evaporation does not occur. Previous reports to the contrary may have been due to surface diffusion since this leads to a significant increase in the apparent vapour pressure for small orifice diameters. According to our interpretation, the coefficient a represents the equilibrium value of mass loss per unit area orifice from effusion alone.

Table 8.1 Values of the parameters a and b in Eq. (8.13), obtained by 'best fit' to the corrected rates of mass loss, compare Figure 8.6.

$10^4\,\mathrm{K}/T$	T/K	a/mg min^{-1} mm^{-2}	b/mg min^{-1} mm^{-1}
4.500	2222	0.087	0.024
4.350	2229	0.245	0.070
4.250	2353	0.490	0.144

8.2.6 Multiple Species

All curves so far represent rates of mass loss. If silicon were the only vaporizing species, conversion to vapour pressure would be straightforward. However, the work of Drowart, De Maria and Inghram (1958) showed that a number of species are formed when silicon carbide volatilizes. All we can do, then, is to convert the total mass loss to vapour pressures of several species, in the same ratio as found by the mass spectrometry. The three most important species are Si, SiC_2 and Si_2C; for simplicity we designate them 1, 2 and 3. For the total mass loss by effusion we have

$$q_e = q_1 + q_2 + q_3 \tag{8.14}$$

From Eq. (8.3) we also have (with f_2 and f_3 introduced for brevity):

$$q_2 = \frac{P_2}{P_1}\left[\frac{M_2}{M_1}\right]^{1/2} q_1 = f_2 q_1; \tag{8.15}$$

$$q_3 = \frac{P_3}{P_1}\left[\frac{M_3}{M_1}\right]^{1/2} q_1 = f_3 q_1 \tag{8.16}$$

Combination of Eqs (8.14)–(8.16) gives

$$q_1 = q_e/(1 + f_2 + f_3); \quad q_2 = f_2 q_1; \quad q_3 = f_3 q_1 \tag{8.17}$$

The ratios P_2/P_1 and P_3/P_1 for various temperatures are found by means of data from JANAF (1985); these are essentially in agreement with the experimental data tabulated by Drowart, De Maria and Inghram (1958). Combined with the molar masses and the value of $a = q_e/A$ from Table 8.1, the resulting vapour pressures are shown graphically in

Figure 8.7. For comparison, the data for Si, Si_2C and SiC_2 from Drowart, De Maria and Inghram (1958, Table II) are also shown.

Focusing on the vapour pressure of silicon, it is seen that the present results are roughly a factor of 2 lower than the results of Drowart *et al.* (and also lower than the results of subsequent investigators). However, effusion measurements for silicon carbide generally have to be done with cells of graphite, and interaction between the charge and the cell is bound to occur. Part of the flow from the effusion orifice must then take place in the form of surface diffusion as indicated above, with increasing

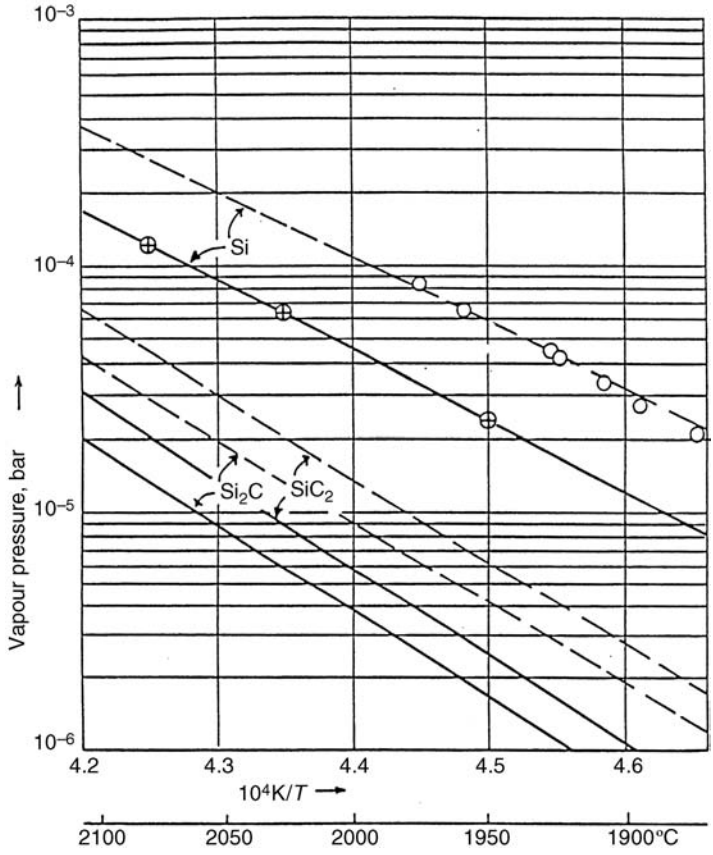

Figure 8.7 Vapour pressure of Si, Si_2C and SiC_2 as functions of temperature. Open points: Experimental data for Si from mass spectrometry by Drowart, De Maria and Inghram (1958). Dashed lines: Calculated from JANAF Thermochemical Data (1985). Crossed points and full-drawn lines: This work (see text).

importance for smaller orifices. According to Drowart and DeMaria (1960), the orifice of their cell had a diameter of 1 mm. Moreover, they believe their vapour pressures are correct within a factor of two (loc. cit., p. 18), that gives room for near-agreement.

Alternatively one may look for sources of error in the present work that would make the results too low. Disregarding weighing errors, the main uncertainty lies in the temperature measurement. To bring our results in line with the others, one would have to assume that our measured temperatures were some 60 to 70 °C *higher* than the true temperature. But errors in the temperature measurement of an optical pyrometer, if any, would be expected to work in the direction of *lower* temperatures, thus we believe that the temperatures are correct.

Finally one may ask, is it very important to know the exact magnitude of the vapour pressures of silicon carbide? The answer is, probably not. On the other hand, an understanding of the concept of surface diffusion may be of importance.

8.2.7 More on Surface Diffusion

It is a commonplace observation amongst workers in silicon carbide plants that, in places where the temperature has been too high, 'skeletons' are left that look almost like coarse SiC crystals. On closer inspection, however, they turn out to consist of graphite only, and fall apart at the touch of a hand.

The same sort of observation may be duplicated in the lab. Heating a sample of coarse SiC crystals in a vacuum thermobalance for a few hours at temperatures increasing to 2100–2200 °C, it is found that not only the silicon, but also a sizable fraction of the carbon is lost (in agreement with the above observations). But strangely, apart from a greyish tint, the sample looks the same as before (cf. Motzfeldt and Steinmo, 1997).

The same phenomenon was reported by Badami (1965) who apparently was the first to go ahead with an X-ray investigation of the residual graphite. It certainly appears strange that the outward appearance is preserved when every second atom in the structure is gone, but we will not pursue this problem. Instead we will look at it as a problem of diffusion.

Ordinary solid-state diffusion is too slow to account for the observations, but then graphite is no ordinary solid. The theoretical density of

2.3 is hardly ever achieved, and graphite may generally be regarded as a porous material. Looking again at the above model of effusion and diffusion, the two modes go as d^2 and d, respectively, where d represents the pore diameter. Reducing the diameter to the order of 1 μm or less, the effusion (flow) becomes insignificant, and *surface diffusion* will be the dominant mechanism.

In this context, some early observations of Volmer and Estermann (1921) are recalled (see also Volmer (1939)). They had an evacuated glass vessel with a pool of mercury at −10 °C and a 'cold finger' at −63 °C. After some time, minute crystals could be observed with a microscope as hexagonal leaves of solid Hg deposited on the cold finger. From the known vapour pressure of mercury and the kinetic theory, the authors calculated the incidence of molecules on the surfaces of the crystal. They found that the rate of growth in the breadth of the crystal was about 1000 times larger than predicted from the rate of arrival of atoms on the edge, while the observed growth in thickness was about 1/10 of that predicted. Volmer concluded that the atoms arriving on the faces of the crystal move towards the edges by 'Oberflächen-wanderung', that is, surface transport.

Admittedly, the above example is far from 'high temperatures'. But we will present yet another cold example: a snow flake. Everybody (in the northern countries at least) have wondered about its minute hexagonal perfection, but how did it get that way? The molecules of water vapour in the air hit the snowflake at random, and its ordered growth can only be explained by surface transport.

More generally, surface diffusion is widely apparent throughout nature. At the same time it appears underrated in the literature. To take a couple of examples: Two recent books on materials science quoted on p. 8 (Askeland and Pulé, respectively Callister and Rethwisch) spend 30–40 pages on diffusion in general, but say hardly a word on surface diffusion!

8.2.8 A Short Account of the Transistor

The more recent development within silicon components and devices is not a part of the present text, and yet it deserves mentioning. In 1956, J. Bardeen, W. Shockley and W. H. Brattain (all from the USA) were awarded the Nobel Prize in Physics for having invented the transistor.

Around 1960 the silicon transistor replaced radio tubes in electronic devices; the first integrated circuits came around 1970. At the turn of the century, the development had led to a complete revolution within communications technology and related areas. It is based on 'VLSI technology' where the four letters stand for Very Large Scale Integration. It concerns transistor units, a million or more on a single silicon chip. Very few of us understand it, but all of us are bound to use it. Such is today's world.

For use in this semiconductor technology, the silicon produced in a metallurgical melting furnace is not nearly pure enough. The silicon is chlorinated, preferably to $SiHCl_3$, subsequently distilled, and converted to pure Si again. Eventually it is also zone-refined by a time-consuming solid–liquid conversion. It all adds to the cost of the final, super-purity silicon, but then it does not take many grammes of silicon to produce a modern integrated circuit.

For use in solar panels, one of the present-day big outlets for silicon, the demands for purity is not as strict. A number of companies are working on methods to produce silicon of sufficient purity by direct metallurgical methods, that is, without intermediate conversion to a gas.

8.3 EQUILIBRIUM GAS PRESSURES (II): ~10–1000 MBAR

8.3.1 Permanent Gases, Direct Measurement

The equilibrium between a condensed phase and a permanent gas may be simply measured by having the sample inside and the manometer outside the furnace. A rather old, but illustrative example is shown in Figure 8.8. It shows the carbon monoxide pressures from a run with reaction between beryllium oxide and carbon. The reaction may be written

$$2\,BeO(s) + 3\,C(s) = Be_2C(s) + 2CO(g) \qquad (8.18)$$

Beryllium oxide in compact form shows good resistance against reaction with carbon, compare Chapter 5, p. 136. On the other hand, when beryllia was finely ground together with graphite and beryllium carbide

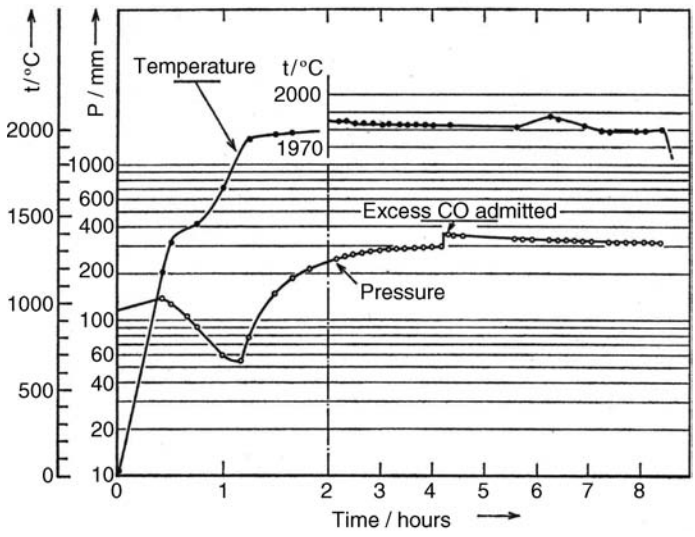

Figure 8.8 The reaction between beryllia and carbon; observed temperature and pressure in dependence of time. Carbon monoxide admitted to a pressure of 115 mm before start of the run. The reverse of reaction (8.18) is seen to take place at temperatures around 1200 to 1500 °C. Equilibrium attained at 2045 ± 5 °C. The hump in temperature after about 3/4 hour is due to the manual increase in power from the transformer. (From Motzfeldt, 1964.)

(separately prepared) it reacted quite readily. The runs were done with the furnace chamber partly filled with CO from a gas cylinder, permitting also the approach to equilibrium from both sides.

It should be noted that Eq. (8.18) is not the only reaction taking place in the system. Gaseous beryllium, Be(g), is also formed, in an amount which (according to thermodynamic data) corresponds to roughly 5% of the total gas pressure. It was assumed that this beryllium gas condensed in the colder parts of the furnace without much effect on the measured CO pressures.

This type of measurement is quite time-consuming, due to the time required for the gas pressure to attain the equilibrium value, and even more so with a large-volume furnace chamber. With the use of a thermobalance, equivalent results may be obtained more quickly, as shown for the reaction between carbon and alumina in a subsequent section.

8.3.2 Condensible Gases; The Ruff-MKW Method

Gases and vapours that condense on cooling, cannot be determined by a direct method as above. An alternative is the classical transpiration method, in which a partial pressure of the vapour is entrained in a flow of inert gas at the elevated temperature, and subsequently condensed by cooling. This method is discussed by Kvande and Wahlbeck (1976) and others. It is a useful method for various purposes, but it will not be further dealt with here.

Another method, more suited to be used with a thermobalance, was introduced by Ruff and coworkers.

Otto Ruff (1871–1939) had a remarkable career. He was educated as a pharmacist at the University of Stuttgart, and later joined Emil Fischer's group in Berlin, working on carbohydrates (sugars). But then, supported by Fischer, he switched field and became head of the new inorganic department in Berlin. In 1904 he became professor at the University of Danzig, and from 1916 he was head of the inorganic department at the University of Breslau. Ruff was the author of nearly 300 papers ranging over wide fields of chemistry and technology. (Biographic data adapted from Wikipedia.)

Of particular interest in the present context is his work within high temperature chemistry. His vacuum furnace (Ruff, 1910) had a carbon tube heating element and could be used to 2650 °C. His first paper in the series 'Investigations at High Temperatures' is dated Ruff (1913), while No. XII in the series (Ruff and Bergdahl, 1919) introduces the method for vapour pressure measurement at high temperatures. Ruff (1929) shows an improved form of his furnace, while Ruff (1935) treats the vaporization of silicon carbide.

In Ruff's method, the substance to be investigated is contained in a cell with a narrow opening in the lid, not unlike an effusion cell except that in the Ruff method the opening should be longer and narrow. The cell is suspended from a balance into a furnace in an inert atmosphere. Initially the inert-gas pressure is higher than the vapour pressure of the sample at the furnace temperature. The inert-gas pressure is then stepwise lowered (or the furnace temperature is increased). For each step the rate of vapour transport out of the cell increases, that is, the weight decreases. The rate of weight loss is particularly marked when the inert-gas pressure falls below the equilibrium vapour pressure of the sample, and this effect may be used to determine the vapour pressure.

Ruff *et al.* followed the mass change of the cell at constant inert-gas pressure and increasing temperature. Fischer and Rahlfs (1932) instead used constant temperature and stepwise decreasing inert-gas pressure, which appears more reasonable. But in either case, the curve for rate of mass loss against temperature (or gas pressure) did not usually give a sharp break. Consequently, some uncertainty remained in the location of the equilibrium point. Even so, Ruff and coworkers made a series of impressive high temperature investigations by means of his method. However, we wanted a firmer theoretical background for the procedure.

At this point, chance came to our assistance. At an Euchem Conference at Schloss Elmau (Ober-Bayern, Germany) in 1965, I met *Dr. W. Moravietz* and chanced to discuss vapour pressure methods with him. He told me that, in connection with aluminium production some 25 years earlier, he wanted to study the vapour pressures of various molten salts by means of the Ruff method. In this context he made contact with *Carl Wagner* (1901–1977) and asked him to develop a theoretical basis for the method. The results, I was told, had been published at some time in the early 1940s. Back in Trondheim it was easy to locate the paper in question (Wagner, 1943).

For a discussion of the method, reference is made to the schematic drawing of a cell in Figure 8.9, equivalent to Figure 1 of Wagner's paper. The outlet has the shape of a capillary with radius r and length l. The cell is suspended from a balance into a furnace at temperature T. The inert gas is denoted with subscript 1 and the vapour with subscript 2, while subscript f denotes furnace space and subscript i denotes the interior of the cell. The symbol c denotes concentration, and P pressure.

A summary of the assumptions made by Wagner is as follows:

1. The system is maintained at a steady state, with a net transport $n_2^\bullet$ (mol/s) of vapour through the capillary, while the net transport of inert gas, $n_1^\bullet = 0$. The flux $J_2 = n_2^\bullet/(\pi r^2)$.
2. At the exit end of the capillary, the vapour dissipates quickly to colder parts of the furnace, so that $P_{1f} = P_f$, $P_{2f} = 0$.

Wagner also made a third assumption, that the total pressure remains uniform throughout the capillary. This assumption, however, cannot be true in the general case. When the total pressure inside the cell exceeds

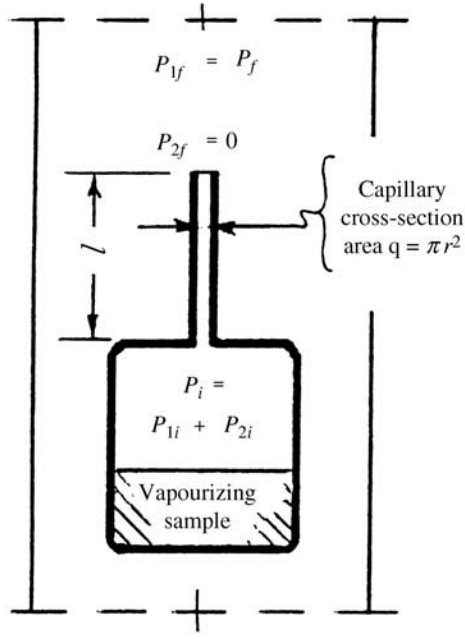

Figure 8.9 Schematic diagram of cell suspended inside the furnace. 1: Inert gas. 2: Vapour. *f*: Furnace space. *i*: Inside of cell.

that in the furnace space, a gas transport through the capillary will result. This transport will occur in part by diffusion, in part by viscous flow with decreasing pressure through the capillary.

In this context the diffusive flow should be written, not in terms of the concentration C_i, but in terms of the total concentration C and the mol fraction X_i. Thus with diffusive transport in the z direction:

$$J_i = -D_i C \frac{dX_i}{dz} \tag{8.19}$$

This form is consistent with the concept of diffusion as transport caused by gradient in composition only. The effect of simultaneous flow may then be taken into account by adding a term $CX_i \times v$ where v is linear velocity.

In the treatment of gaseous diffusion, Graham's law is taken into account, while the transport rate caused by pressure drop through the capillary is treated in terms of laminar flow. The complete treatment has been given by Motzfeldt, Kvande and Wahlbeck (1977). Only the final

expression for the rate $n_2^{\bullet}$ of transport of the vapour is given here:

$$n_2^{\bullet} = C\left[\left(\frac{P_2^0 \exp\left(-\frac{n_2^{\bullet}}{B}\right)}{1-\exp\left(-\frac{n_2^{\bullet}}{A}\right)}\right)^2 - P_f^2\right] - A\ln\left[\gamma + (1-\gamma)\exp\left(-\frac{n_2^{\bullet}}{A}\right)\right] \quad (8.20)$$

Here, $n_2^{\bullet}$ is the rate of weight loss corresponding to a certain value of the inert-gas pressure P_f, while the parameters A, B and C may be regarded at first as unknowns. With a sufficient set of matching values for $n_2^{\bullet}$ and P_f (e.g. eight to ten pairs), it is possible by means of a suitable computer program to obtain the 'best' value for the wanted equilibrium vapour pressure P_2^0 as well as the parameters A, B and C. However, we will first take a closer look at these parameters:

$$A = \frac{\pi r^2 D^*}{RTl}; \quad B = \frac{KRT^2}{\Delta H_V^2}; \quad C = \frac{r^4}{16RTl\eta}; \quad \gamma = \sqrt{\frac{M_2}{M_1}}$$

$D^* = D \times P = \text{const.}$ (D is the interdiffusion coefficient and P total pressure.)
$r =$ capillary radius. $l =$ length. $R =$ gas constant. $T =$ temperature.
$K =$ heat transfer coefficient, a property of the equipment (and unknown).
$\Delta H_v =$ enthalpy of vaporization. $\eta =$ viscosity of the gas mixture.

The complete expression, Eq. (8.20), looks a bit unwieldy, and some simplification may be permitted. We start from the back end, by considering the γ-term in the second part of the equation. M_2 and M_1 are the molar masses of the vapour and the inert gas, respectively. With, for example, argon as an inert gas, $M_1 = 40$, it is found by calculation that the complete second term will be of little significance compared to the first term for all reasonable values of M_2. As a consequence, the complete second term usually may be left out.

Next, we take a suspicious look at the parameter B. In addition to the enthalpy of vaporization, it contains a heat transfer coefficient K which is specific to the furnace in question. It was originally introduced by Wagner, assuming that the heat transfer to the sample

would limit the rate of vaporization, or more explicitly, that the vaporization would cause a significant cooling of the sample. However, for measurements at temperatures of some 3–400 °C and higher, and with reasonable design of the equipment, the temperature difference between furnace space and sample may generally be ignored. This is equivalent to setting the heat transfer coefficient K infinitely large, which in turn makes the exponential term in the numerator of Eq. (8.20) vanish (that is, equal to unity).

With these simplifications, the expression looks more manageable:

$$n_2^{\bullet} = C\left[\left(\frac{P_2^0}{1-\exp\left(-\frac{n_2^{\bullet}}{A}\right)}\right)^2 - P_f^2\right] \tag{8.21}$$

For the further discussion, subscript 2 is omitted as superfluous, and the equilibrium vapour pressure P^0 is placed outside the bracket, introducing the dimensionless parameter $P_f/P^0 = y$. This gives

$$n^{\bullet} = C\left(P^0\right)^2\left[\left(\frac{1}{1-\exp\frac{n^{\bullet}}{A}}\right)^2 - y^2\right] \tag{8.22}$$

The computer fitting is now reduced to determining A, C and P^0. For an initial test of the method, silver was chosen as a suitable material. Molten silver may be conveniently handled in a graphite container, and its vapour pressure is known from a number of previous studies. Figure 8.10 shows the results from the first two runs for silver at 1750 °C. Subsequently a series of measurements with silver were done in the temperature range 1600 to 1850 °C. The results were in perfect agreement with those quoted by Hultgren *et al.* (1973) and need not be quoted here.

Some short notes on the parameters may be in order. The parameter A primarily decides the location of the curve for $P_f \gg P^0$, and it is essentially independent of the total pressure.

The parameter C, on the other hand, is of primary importance in the upper region where $P^0 \gg P_f$. It should be noted first of all that C, and hence the rate $n^{\bullet}$, is proportional to the fourth power of the capillary diameter. This means that the diameter should be chosen with care, using smaller diameter for higher vapour pressures.

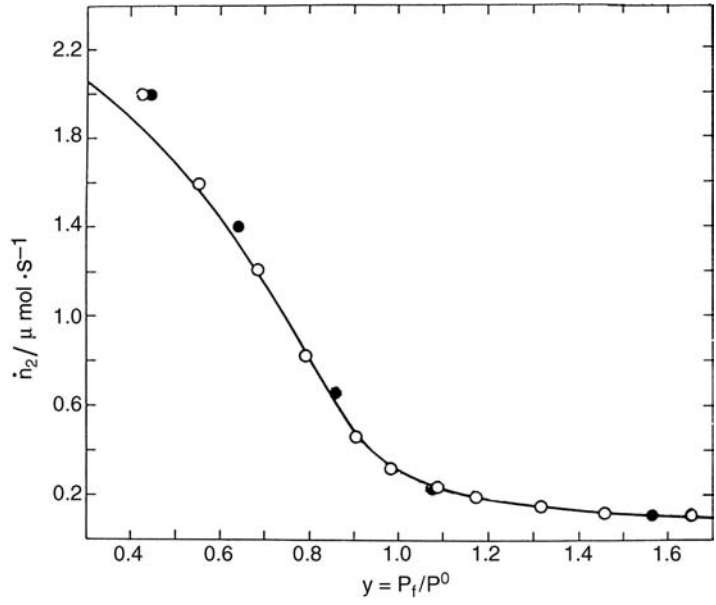

Figure 8.10 Results from two runs with silver in a cell of impervious graphite at 1750 °C. Outlet dia. 0.5 mm, length 9 mm. Observed rates of mass loss $n^{\bullet}$ plotted against $y = P_f/P^0$. Full-drawn line: Best fit obtained by computer program for Eq. (8.22), with the resulting $P^0 = 60$ mbar. (The result is a bit low compared to subsequent runs.).

It is further noted that C is inversely proportional to the viscosity η of the vapour. From kinetic theory we have the expression:

$$\eta = \frac{5}{16}\left(\frac{mkT}{\pi}\right)^{1/2}\frac{1}{d^2} \tag{8.23}$$

The molecular diameter d enters squared in the denominator, which means that large molecules give low viscosity. In this sense the curve in Figure 8.10 is not very typical, since silver vapour is fairly heavy and monatomic.

A different set of experimental data is shown in Figure 8.11, where observations for sodium chloride are shown for three different cell materials at essentially the same temperature. Curve (I) shows the results from measurement with a silica cell, which is definitely gas tight. Curve (II) is obtained with a cell of impervious graphite. It is seen that the rate of mass loss in the diffusion area is somewhat higher, possibly related to some leak in the threads of the lid. (The different slope in the steeper area

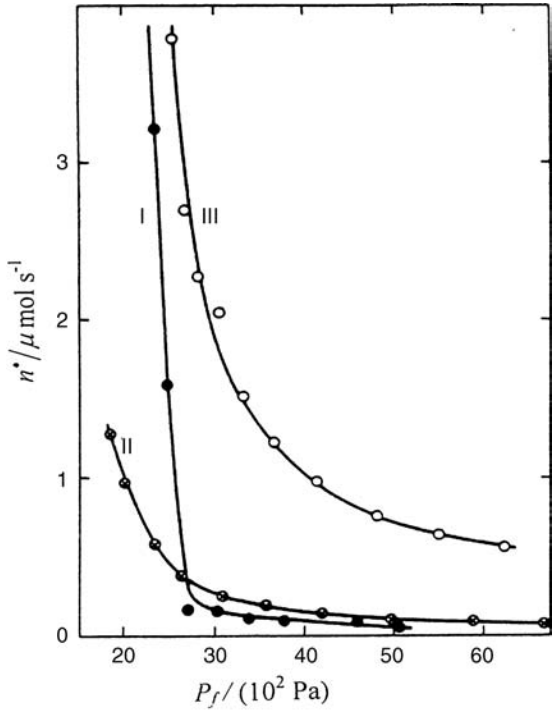

Figure 8.11 Curves for rate of mass loss $n^{\bullet}$ versus the inert-gas pressure P_f; observations for sodium chloride with three different cells at (nearly) the same temperature. (I): Silica cell, $r = 0.25$ mm, $t = 1105\,^{\circ}$C. (II): Cell of impervious graphite, $r = 0.20$ mm, $t = 1107\,^{\circ}$C. (III): Porous graphite cell, $r = 0.25$ mm, $t = 1110\,^{\circ}$C. Curves are shown as resulting from computer fitting. (Reprinted from Kvande, Linga et al. Copyright (1979) Acta Chemica Scandinavica.)

is related to the smaller diameter for this cell, cf. figure text.) Curve (III) shows the results with a cell of porous graphite. It is seen that the A value is increased by a factor of ten, likewise the C value is also higher. Nevertheless, the equilibrium pressures calculated from the three different set of data are in quite good agreement throughout. This indicates that one may indeed obtain reliable measurements of vapour pressures with the present method, even when an impervious cell material is not available.

Kvande *et al.* (1979) went on to calculate the diffusivity and the viscosity of sodium chloride vapour from the data obtained with the silica cell. The data obtained appear quite reasonable, but are beyond the scope of the present text.

The Ruff–MKW method has been thoroughly discussed by Wahlbeck, Myers and Trong (1985), and again by Wahlbeck (1986) in a review paper discussing four different methods of vapour pressure measurement at high temperatures. From the latter paper, the conclusions regarding the present method may be quoted: (1) Vapour pressures greater than 5 torr are reliably determined. (2) The MKW analysis of the Ruff method is correct. (3) The parameters A and C are in agreement with values for the gaseous-interdiffusion and gaseous-viscosity coefficients for the sample using the kinetic theory of gases. (4) Scatter in molecular diameter values based on experimental values of A and C are usually too large to make this a recommended method for determination of molecular size. (5) The temperature criteria for rate determining effects for heat transfer by radiation vs. viscous flow given by MKW are correct.

The method has been used for various systems and purposes, but only one particularly nice paper will be referred to here: The study of molten alkali chloride–aluminium chloride mixtures by Linga, Motzfeldt and Øye (1978).

Finally it should be said that in all likelihood the present authors would not have been able to formulate the problem, or to solve it, if it had not been for Carl Wagner's initial treatment.

8.4 CARBOTHERMAL REDUCTION OF SILICA AND ALUMINA

Silicon 'metal', that is, silicon with a few percent impurities (mostly iron) has been produced for about a hundred years, mostly by carbothermal reduction. Initially it was a difficult process, with some 20% loss of the silica value in the form of smoke out of the stack. Through continuous development the process has been perfected to give low silica losses and efficient use of the energy. The annual production in Norway is at present about 200 000 tons per year, produced by carbothermal reduction. The process has been thoroughly described by Schei, Tuset, and Tveit (1998).

For aluminium, the production in Norway is about 1 million tons, out of a world production of about 40 million tons, but this is all produced by electrolysis. A lot of effort has been spent in developing carbothermal processes for aluminium, but so far none of them have been industrialized. A discussion of the chemistry involved, including a number of the proposed processes, has been given by Motzfeldt *et al.* (1989).

In the present section, we will look at the chemistry of carbothermal reduction for both metals. For each of them we start with a consideration of the incipient reaction as seen in laboratory experiments.

8.4.1 Silica Plus Carbon

If a mixture of coarse grains (1–2 mm) of silica and graphite is heated in a graphite crucible in a thermobalance with continuous evacuation, incipient reaction is seen at about 1450 °C (observed as increased forevacuum pressure and weight loss). The first reaction might be written

$$SiO_2(s) + C(s) = SiO(g) + CO(g) \qquad (8.24)$$

An objection may be raised, however; two solids do not easily react. The incipient reaction under vacuum is mostly due to the thermal decomposition of the silica: $SiO_2(s) = SiO(g) + {}^1/_2O_2(g)$ (with subsequent reaction between oxygen and carbon). According to thermodynamic calculations the vapour pressure of SiO(g) will be about 10^{-7} atm around 1450 °C, just sufficient for a notable reaction.

For a further confirmation of this reaction mechanism, a short length of silica tubing was freely suspended inside the graphite-tube heating element and heated under vacuum. It was found that even in this case, with no physical contact between the reactants, reaction starts at about 1450 °C, with essentially the same mechanism. If the vacuum valve is closed and inert gas is admitted to the system, the reaction stops, as one would expect.

On the other hand, letting in some carbon monoxide causes the rate to increase; the reaction is

$$SiO_2(s) + CO(g) = SiO(g) + CO_2(g) \qquad (8.24a)$$

$$\text{followed by } CO_2(g) + C(s) = 2\,CO(g) \qquad (8.25)$$

In the presence of carbon, the SiO gas will react:

$$SiO(g) + 2\,C(s) = SiC(s) + CO(g) \qquad (8.26)$$

When the experiment is terminated, it is readily seen by inspection that the carbide is formed on the carbon while the silica grains are reduced in size.

The kinetics of these reactions has been studied in detail by Wiik (1990), compare Wiik and Motzfeldt (1996).

In the further progress of the reaction on an industrial scale there are two options: With sufficient carbon present, silicon carbide is the end product, discussed in Chapter 5 pp. 139–140. On the other hand, with a suitable carbon deficit, silicon metal may be produced.

8.4.2 Carbothermal Silicon

Forgetting about the kinetics discussed above, the first step in the process may be written

$$SiO_2(s) + 3\,C(s) = SiC(s) + 2\,CO(g) \tag{8.27}$$

At the same time, some SiO(gas) is formed, but at equilibrium (1 atm at 1510 °C) it amounts to only about 1% of the total gas pressure.

With an initial charge with SiO_2 and C in the ratio 1:2, it is clear from Eq. (8.27) that there is an excess of silica. This will react with the carbide:

$$SiO_2(s) + 2\,SiC(s) = 3\,Si(l) + 2\,CO(g) \tag{8.28}$$

Unfortunately, another reaction proceeds simultaneously:

$$2\,SiO_2(s) + SiC(s) = 3\,SiO(g) + CO(g) \tag{8.29}$$

The equilibrium pressures of SiO and CO over the phase combination SiO_2—SiC—Si are shown in Figure 8.12. It is seen that, at a temperature around 1800 °C when the total pressure is 1 atm, the equilibrium ratio SiO:CO is about 2:1. This means that, if run as an equilibrium process, very little silicon and a lot of white smoke would be produced.

Fortunately, the silicon furnace does not behave like an equilibrium system at all. From the crater (the hottest area right below the three electrodes) the gases emerges upwards through the charge, it is partly cooled, and several reactions take place. The silicon monoxide may disproportionate: $2\,SiO(g) = Si + SiO_2$, with both condensed products following the charge downwards. It may also react according to Eq. (8.29) backwards, this is not desired. Or it may react with the carbon of the charge: $SiO(g) + 2C(s) = SiC(s) + CO(g)$.

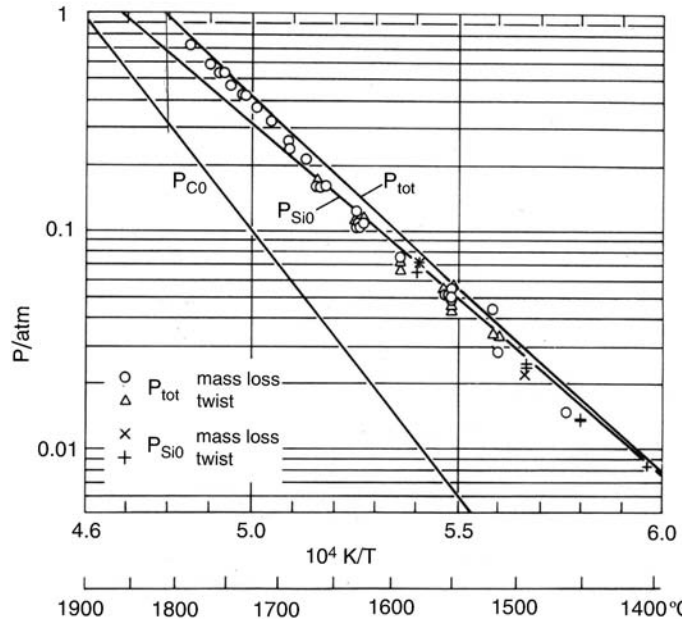

Figure 8.12 Equilibrium pressures for the phase combination SiO_2-SiC-Si. The solid lines are calculated using data from JANAF (1971). Experimental values from Gjerstad (1968). 'Mass loss' essentially means the Ruff method (cf. p. 290 etc.), 'twist' used a sort of torque cell, later abandoned. (Figure from Motzfeldt *et al.*, 1989.)

Whatever happens, under favourable circumstances (that is, with the furnace properly designed and run) nearly all of the SiO(g) emerging from the hottest part of the furnace is retained and follows the charge downwards again. The process may be likened to a reflux condenser for SiO(g). At the same time, some liquid Si steadily drizzles down and collects at the hearth. In spite of the unfavourable SiO/CO ratio, the modern silicon furnace is quite efficient as regards both materials and energy.

Customarily the silicon metal contains a few percent of impurities (mostly iron) and has to go through a costly refining process before it is used for semiconductor purposes. With a rapidly expanding market for solar cells, Norwegian producers have developed processes for the direct production of solar cell silicon. This recent development, however, is beyond the scope of the present text.

8.4.3 Alumina Plus Carbon

Following the same experimental pattern as above, grains of alumina and carbon were heated in a graphite crucible in a vacuum. We first present the 'expected' reaction scheme:

$$2\,Al_2O_3(s) + 3\,C(s) = Al_4O_4C(s) + 2\,CO(g) \qquad (8.30)$$

The tetroxycarbide is the first stable product, as shown by Foster, Long and Hunter (1956). But, once again, we did not believe that this scheme with two solid reactants represented the initial reaction.

The first puzzling observation was that the reaction sometimes started at about the same temperature as observed for silica (some 1450 °C) in spite of the fact that alumina is thermodynamically a lot more stable (cf. Figure 5.1, p. 132). On the other hand the reaction was more unsteady; sometimes it started, sometimes it didn't. But once started, it proceeded with a faster rate than that observed for silica.

In order to clarify the case we did the same type of experiment as described above for silica; a short piece of alumina tubing freely suspended inside the heating element of the thermobalance. In a vacuum and with a fairly slow rate of heating, a temperature of 1700 °C could be reached with no significant weight change. This is in accord with the thermodynamic data for the aluminium suboxides.

When a system shows no perceptible weight loss in a vacuum, it certainly should not react in the presence of an inert gas. Still, with a certain sense of symmetry in the experiments, I admitted argon to the system. And – what a surprise – a rapid weight loss of the alumina began within a few seconds after the admittance of argon!

The experiment was repeated with a different flask of argon, but the same result: a reaction takes place between alumina and graphite without physical contact, in the presence of an inert gas.

It took a few days of wondering before the solution emerged. Let us at Figure 8.13, in particular the metal vapour pressures of the carbides. We note that the vapour pressure of Si(g) over SiC is very low at the temperatures in question. Silicon carbide formed on the surface of graphite by reaction with SiO(g) will remain on the graphite.

The vapour pressure of Al(g) over Al_4C_3, on the other hand, is between two and three powers of ten higher at the same temperature. As

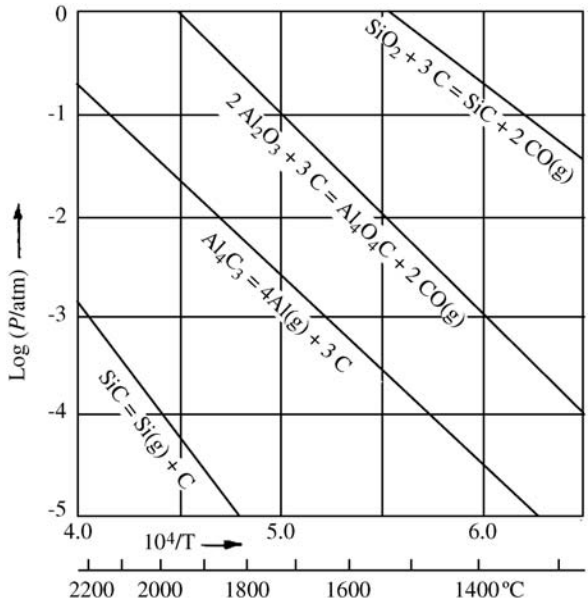

Figure 8.13 Calculated equilibrium gas pressures for some reactions in the systems Si—O—C and Al—O—C. (Diagram modified from Motzfeldt and Steinmo, 1972.)

a consequence, the aluminium vapour from the thermal decomposition of alumina cannot react to form the carbide; the Al atoms hitting the graphite will only rebound. They may then again hit the alumina wherefrom they came. On the alumina surface, the aluminium atoms may react:

$$Al_2O_3(s) + Al(g) = 3\,AlO(g) \tag{8.31}$$

The AlO gas thus formed may hit the graphite and react:

$$AlO(g) + C(s) = Al(g) + CO(g) \tag{8.32}$$

Starting with one aluminium atom, three molecules of AlO are formed by reaction (8.31), and these are converted back to three atoms of aluminium by reaction (8.32). Thus in one 'round trip' between alumina and carbon, the amount of aluminium vapour has been tripled. This multiplication process may be repeated at a high rate (the average speed of an Al atom at 1500 °C is about 1000 m/s),

so that a vapour pressure will be built up in the space between the alumina and graphite surfaces. The limit is reached when the Al pressure equals the saturation pressure of Al over Al_4C_3. According to Figure 8.13 the saturation pressure at 1500 °C is about 10^{-4} atm, sufficient to sustain a reaction once started.

(An alternative scheme goes through the lower suboxide: $Al_2O_3(s) + 4\ Al(g) = 3\ Al_2O(g)$. This reaction, however, seems less likely for kinetic reasons.)

The Verification. The multiplication process presupposes that the Al atoms initially present in low concentration are allowed to alternate between the graphite and alumina surfaces rather than disappearing into the evacuated surroundings. This is precisely the effect of the inert gas: It acts as a 'lid' on both sides of the reaction space. If this explanation is correct, the same effect should be observed with a real lid.

In order to try this experimentally, one should have a graphite crucible filled with alumina grains, suspended under a balance and slowly heated to about 1700 °C. Then a lid should be put on, to see what happens. The arrangement to realize this experiment is shown in Figure 8.14.

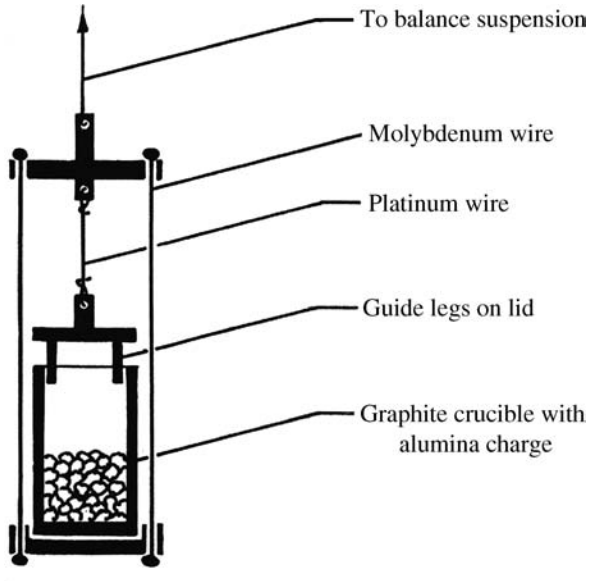

Figure 8.14 Arrangement used for the 'dropping lid' experiment.

The crucible with contents was placed in a small frame with a lid hanging above it in a short length of platinum wire. The frame was suspended in the furnace which was evacuated and left overnight at 950 °C for degassing. The next morning the temperature was increased at a modest rate, about 50 °C per hour. When a temperature of about 1700 °C was attained, oscillations were observed on the balance recorder tracing, and the rate of weight loss changed abruptly from about 0.02 mg/min to 12 mg/min. At the same time, a marked increase was noted in the reading of the forevacuum gauge.

What happened was that the platinum wire broke, the lid closed, and the expected reaction started. (The equilibrium pressure of carbon monoxide from reaction (8.30) at 1700 °C is 50 torr, more than enough to lift the lid for gas escape!) We considered this the conclusive evidence for the correctness of the proposed mechanism.

At the time of this experiment we were still searching for some clue to a successful process for carbothermal production of aluminium. Hence our findings were originally published in a rather modest way, see Motzfeldt and Steinmo (1973).

8.4.4 Carbothermal Aluminium

Forgetting about the kinetics, the first of the equilibrium steps in a carbothermal process for aluminium is represented by Eq. (8.30) above, for convenience repeated here:

$$2\,Al_2O_3(s) + 3\,C(s) = Al_4O_4C(s) + 2\,CO(g) \qquad (8.30)$$

The next step is the conversion to carbide:

$$Al_4O_4C(s) + 6\,C(s) = Al_4C_3(s) + 4\,CO(g) \qquad (8.33)$$

The final step might be written

$$Al_4O_4C(s) + Al_4C_3(s) = 8\,Al(l) + 4\,CO(g) \qquad (8.34)$$

Simultaneously, gaseous Al, Al_2O and AlO are formed, but the partial pressures are significantly lower than that of carbon monoxide at the same temperature, so they are left out at the moment.

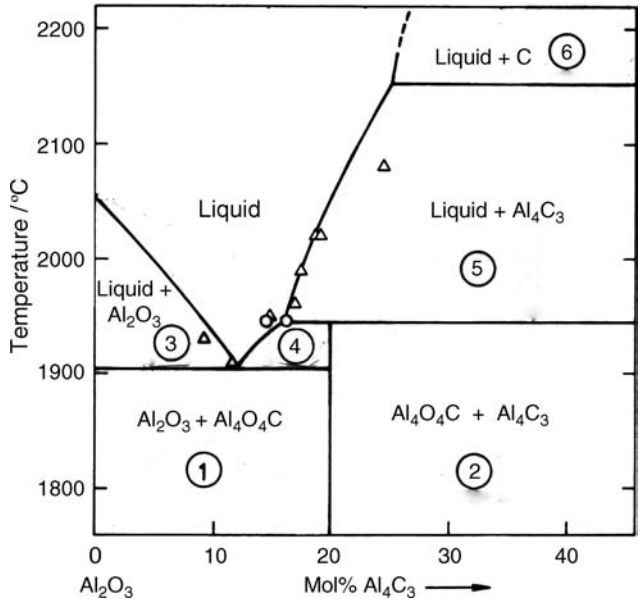

Figure 8.15 Phase diagram for the system Al_2O_3 – Al_4C_3 according to Gjerstad (1968). Circles: Peritectic composition. Triangles: Ginsberg and Sparwald (1965). The numbers are added to identify the different phase areas, compare Figure 8.17.

The above equations look nice on paper, unfortunately they do not give a correct description of the process. At about 1900 °C a molten oxide-carbide mixture starts forming, as seen in the phase diagram Figure 8.15. This alters the whole process.

Equilibrium Pressures. The direct measurement of CO pressures was shown for BeO + C on p. 289. The results were dependable, but it is a fairly slow and tedious method. The same type of measurements were also done for alumina plus carbon, yielding dependable results for the first steps of the reactions (Herstad, 1966).

Subsequently, reaction equilibria in the alumina–carbon system was re-investigated by use of a thermobalance, yielding more accurate results in a fraction of the time (Motzfeldt and Sandberg, 1979; Sandberg, 1981). The thermobalance 'Versatilie' was used (cf. p. 249–255). The

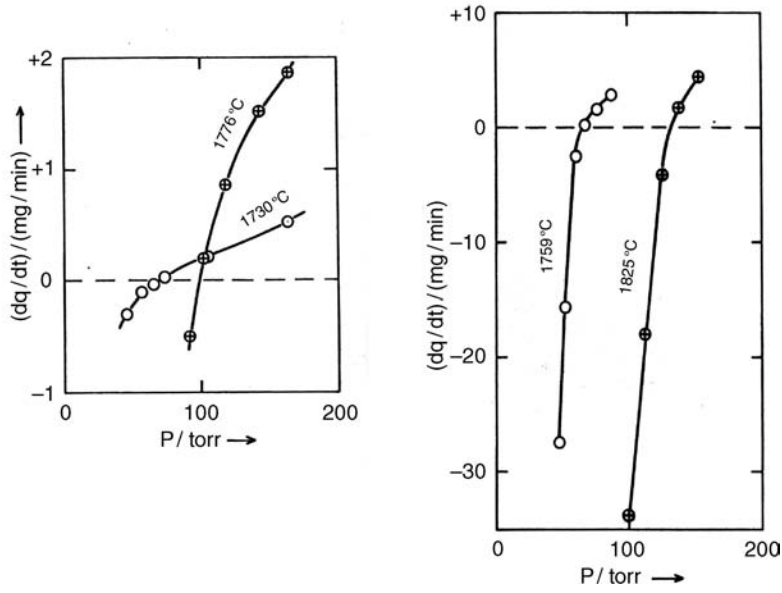

Figure 8.16 Rates of weight change (mg/min) in dependence of applied inert-gas pressure (torr). (**a**): Two runs at different temperatures with composition within phase fileld (1). (**b**): Two runs within (2). (From Sandberg, 1981.)

charges were grains of alumina and graphite, alternatively alumina and separately prepared aluminium carbide. Graphite crucibles were used throughout. Carbon monoxide was added from an external cylinder.

With the CO pressure slightly lower than the equilibrium pressure at a given temperature, the reaction should go forwards with a weight loss; with too high pressure, the reaction should go backwards. This is exactly what was observed, see Figure 8.16a and b.

To comprehend the observations, the phase diagram Al_2O_3-Al_4C_3 is recalled, Figure 8.15. The phase fields are numbered, and each number from (1) to (5) corresponds to a specific combination of two condensed phases, with solid carbon as the third phase throughout.

Each phase field shall consist of two specific phases, solid or liquid, plus solid carbon. Experimentally it was a challenge, but only the results are shown here, Figure 8.17. The numbers correspond to the phase fields shown in Figure 8.15; the two should be compared to comprehend the results.

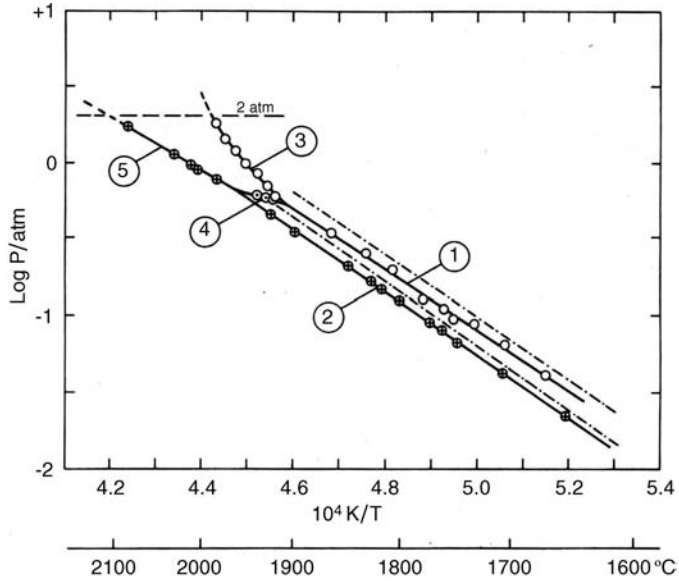

Figure 8.17 Experimentally determined equilibrium pressures of CO(g). The numbers on curves correspond to the phase fields in Figure 8.15 (with carbon as the third phase throughout). Dash-dot lines: Results from Herstad (1966). (From Sandberg, 1981.)

The Metallurgical Process. The final step in a carbothermal process will be notably different from that depicted in Eq. (8.34) (p. 304). At 1 atm the molten oxycarbide phase will eventually react with solid aluminium carbide (or carbon) to give aluminium metal with dissolved carbon, plus the gas phase. The calculated equilibrium pressures are shown in Figure 8.18.

The favourable part seems to be that the partial pressures of suboxide and metal vapours are comparatively lower than in the silicon process. It is less favourable that the aluminium metal phase has a lower density and will float on top of the oxide-carbide melt. As a consequence, in a conventional melting furnace the power from the electrodes would primarily be used to evaporate the metal. A two-stage (or multistage) process seems necessary.

About 50 years ago, a number of the large aluminium companies were working hard to develop one or another carbothermal process for aluminium. With the requirement that it should also be economically attractive

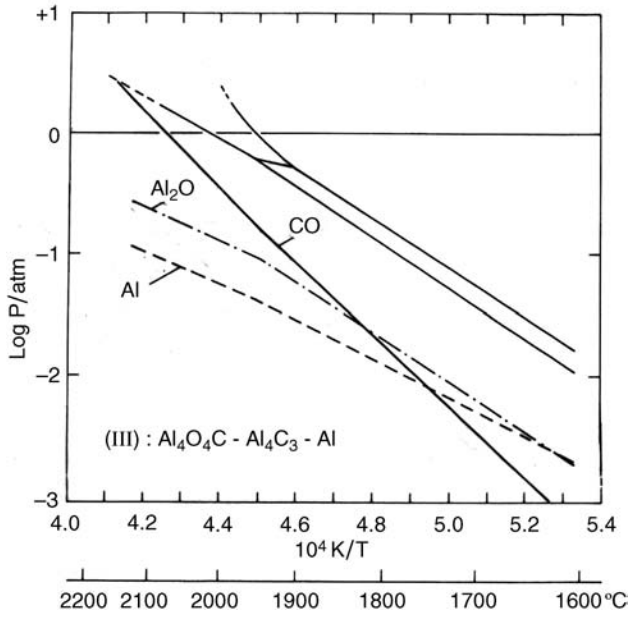

Figure 8.18 Calculated equilibrium pressures for the phase combination Al_4O_4C – Al_4C_3 – Al. The CO pressures from Figure 8.17 are shown for comparison. (From Sandberg, 1981.)

compared to the present electrolytic process, they had to give in (as reviewed by Bruno, 2003). More recently, Alcoa (USA) in a joint effort with Elkem (Norway) resumed working on the carbothermal technology, see Johansen *et al.* (2003). Choate and Green (2006) have made a technoeconomic assessment of the project. A recent update of the Alcoa-Elkem process has been given by White, Mikkelsen and Roha (2012).

8.5 MOLTEN ALUMINIUM OXYCARBIDE AS AN IONIC MELTS

8.5.1 The Treatment of Temkin

It has been known since Arrhenius' time in the late 1870s that salts, when dissolved in water, dissociate into ions and cause electric conductivity in the solution. It was more than half a century, however, before

Temkin (1945) put forth that a similar dissociation occurs when a salt is molten. Furthermore, cations and anions cannot exchange place. In a perfect ionic solution, according to Temkin, the heat of mixing is zero, and the change in entropy is determined by the number of possible permutations amongst different cations, and correspondingly amongst different anions.

As the simplest example we consider a mixture of monovalent salts like NaF and KCl. Assuming that the mixture behaves ideally, the activities of the components are expressed as the products of the ion fractions X_i:

$$a_{NaF} = X_{Na+}X_{F-}; a_{NaCl} = X_{Na+}X_{Cl-}; a_{KF} = X_{K+}X_{F-}; a_{KCl} = X_{K+}X_{Cl-}$$

A similar example is presented by Temkin, except that his example contains the *divalent* ions CaO, FeO, CaS and FeS. It is reasonable, however, to assume that such a charge-symmetric mixture of divalent ions also behaves nearly ideally.

It seems clear, on the other hand, that a mixture of monovalent and divalent ions of the same sign cannot be expected to permute freely or mix ideally. An easy example is that of the mixture KCl – $MgCl_2$; at fairly low ion fractions of Mg^{2+} the anion $MgCl_4^{2-}$ is formed and the mixture is far from ideal. For a further discussion of molten salt mixtures, see, for example, Kleppa (1987).

8.5.2 The Melting of Ionic Compounds

Sodium chloride, with monovalent ions, melts at 800 °C. Magnesium oxide, with two divalent ions, melts at 2800 °C; the difference is striking. Going one step further, to a compound of two trivalent 'ions' like AlN, it does not melt at all.

The melting point of aluminium oxide, consisting of a combination of divalent and trivalent ions, might be expected to be above that of magnesium oxide. In reality it is not; alumina melts at 2054 °C. An explanation is ready at hand, alumina melts to monovalent ions:

$$Al_2O_3(s) = AlO^+ + AlO_2^- = I \qquad (8.35)$$

In general it may be assumed that ionic compounds will melt to species with the lowest possible charge, ±1 if possible. Thus the melting, or

dissociation, of the oxycarbide may take place by the reaction

$$Al_4O_4C(s) = 2\,AlO^+ + AlO_2^- + AlC^- = II \tag{8.36}$$

Aluminium carbide does not melt at all, but it dissolves to some extent in molten alumina. This is assumed to take place by the reaction

$$Al_4C_3(s) + AlO_2^- = 2\,AlO^+ + 3\,AlC^- = III \tag{8.37}$$

The first treatment of the aluminium oxide-carbide system as an ionic liquid was presented by Sandberg (1981), but it included the questionable divalent ion Al_2C^{2+}. The treatment with monovalent ions only was presented by Motzfeldt, Sandberg and Julsrud (2001).

8.5.3 A Model for the Aluminium Oxycarbide Melt

We have an ionic mixture consisting of the three monovalent ions AlO^+, AlO_2^- and AlC^-. Assuming an initial mixture of $(1-x)$ mol of Al_2O_3 and x mol of Al_4C_3, the ion fractions in the molten mixture will be:

$$N_{AlO^+} = 1(\text{always}); \quad N_{AlO_2^-} = \frac{1-2x}{1+x}; \quad N_{AlC^-} = \frac{3x}{1+x} \tag{8.38}$$

According to the Temkin model, the activity of a component in an ideal solution is given by the product of its ion fractions. In the present case this is merely the product of anion fractions:

$$a_{Al_2O_3} = N_{AlO_2^-} = \frac{1-2x}{1+x} \tag{8.39}$$

$$a_{Al_4O_4C} = N_{AlO_2^-} N_{AlC^-} = \frac{3x(1-2x)}{(1+x)^2} \tag{8.40}$$

$$a_{Al_4C_3} = N_{AlC^-}^3 / N_{AlO_2^-} = \frac{27x^3}{(1-2x)(1+x)^2} \tag{8.41}$$

8.5.4 The Phase Diagram

The liquidus line in a phase diagram represents the equilibrium between a given component in the liquid and the same compound in the solid

phase. In the present case the solid phases are pure compounds with unit activity, and thus the general equilibrium condition is very simple:

$$\Delta G^0 = \Delta H^0 - T\Delta S^0 = -\mathrm{RT} \ln a_{\mathrm{comp}} \tag{8.42}$$

where a_{comp} stands for the activity of either alumina, oxycarbide or carbide as given by Eqs (8.39)–(8.41).

In the case of alumina we may use directly the data given by the NIST-JANAF Tables (1998) for solid and liquid alumina. This gives the activity a at various temperatures. By conversion of Eq. (8.39) we have the corresponding compositions

$$x = \frac{(1-a)}{(2+a)} \tag{8.39a}$$

The result is a nearly straight line from the melting point down to the eutectic at 1905 °C (2178 K) with a calculated composition $x = 0.116$.

The liquidus on the oxycarbide side is fixed by noting that we know two points: The eutectic as given above, and the peritectic point which we set at 1945 °C (2218 K) and composition $x = 0.165$. From Eq. (8.42) this gives two equations with two unknowns, and we find

$$\Delta S^0_{II} = 47.1 \text{ J/K mol}; \quad \Delta H^0_{II} = 130.500 \text{ J/mol} \tag{8.43}$$

These values are used with Eq. (8.42) in the form

$$T = \frac{\Delta H^0}{\Delta S^0 - R \ln a} \tag{8.42a}$$

where the activity is calculated from Eq. (8.40) for various values of x. The result is a nicely rounded curve with a hypothetical maximum at 1952 °C as shown in Figure 8.19.

Regarding the liquidus on the carbide side, an observation from Sandberg (1981) should be noted. When samples within the region of primary crystallization of the carbide were cooled, no halt at 1905 °C was observed, but instead a metastable eutectic between carbide and oxide at 1840 °C. Allowing for some undercooling, the eutectic may be set at 1850 °C. The resulting prolonged liquidus for alumina is shown as a dashed line in the phase diagram. It is seen, however, that the

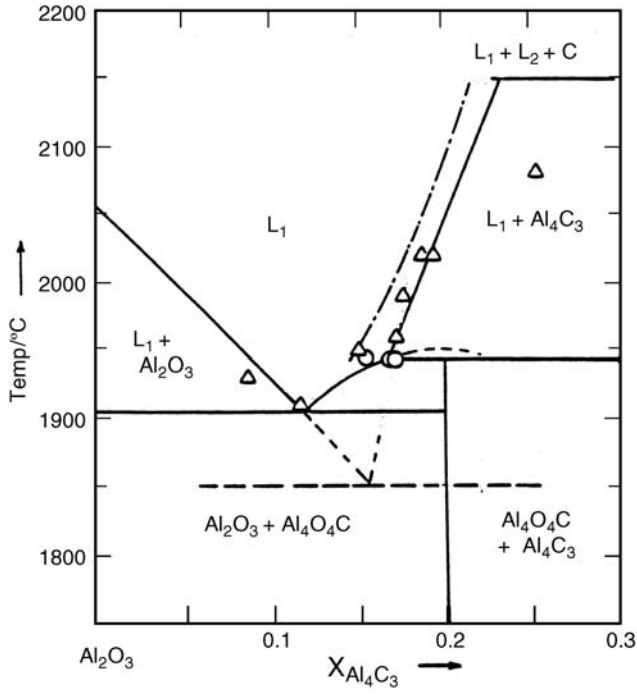

Figure 8.19 Phase diagram for the system Al_2O_3 – Al_4C_3 (left third only shown). *Triangles:* Ginsberg and Sparwald (1965). *Circles:* Gjerstad (1968). Dashed, dotted and full lines: See text.

corresponding carbide liquidus in Figure 8.19 appears exceptionally steep and hence is terminated as unrealistic. Thus another method is called for to fix the liquidus on the carbide side.

As described pp. 305–307, Sandberg (1981) determined the equilibrium pressures of carbon monoxide for reactions within five different regions in this system. For the present we are particularly interested in the reaction above the peritectic temperature:

$$2\,Al_2O_3(\text{in liquid}) + 9\,C(s) = Al_4C_3(s) + 6\,CO(g) \qquad (8.44)$$

The equilibrium constant may be expressed

$$K = \frac{P_{CO}^6}{a_{Al_2O_3}^2}; \quad \text{or rearranged}: \quad a_{Al_2O_3} = \frac{P_{CO}^3}{\sqrt{K}} \qquad (8.45)$$

With K calculated from JANAF data, and P_{CO} at various temperatures taken from Sandberg (1981), $a_{Al_2O_3}$ and hence $x = (1-a)/(2+a)$

(Eq. (8.39a)) is determined. The result, indicated with a dash-dot line in Figure 8.19, shows remarkable agreement when considering that it is obtained by a quite different type of observation.

A still better fit to the phase diagram may be obtained by a slight lowering of the CO pressures from Sandberg. His measured pressures may be slightly high because of the partial pressures of Al_2O and Al produced concurrently with CO in the reaction, Eq. (8.44). A mere 2% reduction of his measured pressures suffices to bring the liquidus to go through the chosen peritectic point.

With this point in combination with a notion of the proper slope from Sandberg's measurements we may also calculate a set of thermodynamic data for the dissolution of the carbide, reaction (8.37):

$$\Delta S^0_{III} = 96\,\text{J/K mol}; \quad \Delta H^0_{III} = 250.000\,\text{J/mol} \tag{8.46}$$

The full line in Figure 8.19 was calculated with these data, using Eqs (8.41) and (8.42a).

The thermodynamic data presented in Eqs (8.43) and (8.46) should be regarded as rather uncertain, while the ionic model of the melt and the ensuing phase diagram appear quite reasonable. It is comforting to note that it has been employed in the further work of Johansen *et al.* (2003).

8.5.5 End of Story

The liquidus line for Al_4C_3 ends at the temperature of peritectic decomposition of the carbide, 2150 °C. Above this temperature the system consists of two liquid phases plus solid carbon, and it cannot be represented as pseudo-binary. The total equilibrium gas pressure will be about 3.0 bar or higher (cf. Figure 8.18), while the maximum pressure in Sandberg's work (with 'Versatilie') was set at 2 bar for safety reasons.

Plans were made to extend the pressure limit, compare Chapter 7, pp. 244–248 ('Maxine'). The combination of high temperatures, elevated pressures and a substantial volume, however, puts severe demands on safety. Even though 'Maxine' had a significantly smaller volume than both 'Beljara' and 'Verstalie', the project was terminated.

And here the book ends.

REFERENCES

Badami, D.V. (1965) X-ray studies of graphite formed by decomposing silicon carbide. *Carbon*, **3**, 53–57.

Brewer, L. and Kane, J. (1955) The importance of complex gaseous molecules in high-temperature systems. *J. Phys. Chem.*, **59**, 105–109.

Bruno, M.J. (2003) Aluminum carbothermic technology comparison to Hall-Héroult process. *Light Metals*, 395–400.

Choate, W. and Green, J. (2006) Technoeconomic assessment of the carbothermic reduction process for aluminum production. *Light Metals*, 445–450.

Drowart, J., DeMaria, G., and Inghram, M.G. (1958) Thermodynamic study of SiC utilizing a mass spectrometer. *J. Chem. Phys.*, **29**, 1015–1021.

Drowart, J. and DeMaria, G. (1960) Thermodynamic study of the binary system carbon – silicon using a mass spectrometer, in *Silicon Carbide* (eds J.R. O'Connor and J. Smiltens), Pergamon Press, New York, pp. 16–23.

Fischer, W. and Rahlfs, O. (1932) Dampfdruck und Dampfdichte von Aluminiumhalogeniden. *Z. anorg. allgem. Chem.*, **205**, 1–41.

Foster, L.M., Long, G., and Hunter, M.S. (1956) Reactions between aluminum oxide and carbon. The Al_2O_3 – Al_4C_3 phase diagram. *J. Am. Ceram. Soc.*, **39**, 1–11.

Freeman, R.D. and Edwards, J.G. (1967) The surface diffusion contribution to effusion through orifices, in *The Characterization of High Temperature Vapors* (ed. J.L. Margrave), John Wiley & Sons, New York, pp. 525–528.

Ginsberg, H. and Sparwald, V. (1965) Beiträge zur Aluminiumgewinnung durch carbothermische Reduction Aluminiumoxids unter besondere Berücksichtung des Systems Aluminium – Kohlenstoff. *Aluminium*, **41**, 181–193.

Gjerstad, S. (1968) *Chemical-Metallurgical Investigations Concerning Carbo-thermal Reduction of Alumina and Silica*, Dr. Ing. Thesis, NTH (now NTNU), Trondheim, 127 pp. (in Norwegian).

Grjotheim, K., Motzfeldt, K., and Rao, D.B. (1971) Vapor pressures over solid phases in the NaF – AlF_3 system studied by the effusion method. *Light Metals* (Proceedings of the 100th AIME Annual Meeting, New York) pp. 223–237.

Herstad, O. (1966) *Reduction of Aluminium Oxide by Carbon. Reaction Equilibria*, Dr. Ing. Thesis, NTH (now NTNU), Trondheim, 135 pp. (in Norwegian).

Herstad, O. and Motzfeldt, K. (1966) Vapour pressures in the system Al – Al_2O_3. The effusion method and pressure compensation methods. *Rev. Hautes Temp. et Réfract.*, **3**, 291–300.

Hultgren, R. *et al.* (1973) *Selected Values of the Thermodynamic Properties of the Elements*, American Soc. for Metals, Metals Park, Ohio, 636 pp.

Johansen, K., Aune, J.A., Bruno, M., and Schei, A. (2003) Aluminum carbothermic technology, Alcoa-Elkem advanced reactor project. *Lights Metals*, 401–406.

Kleppa, O.J. (1987) Thermodynamics of molten salt mixtures, in *Molten Salt Chemistry, NATO ASI Series* (eds G. Mamantov and R. Marassi), D. Reidel Publ. Co., Boston, 79–122.

Knudsen, M. (1909) Die Molekularströmung der Gase durch Öffnungen und die Effusion. *Annalen Der Physik*, **28**, 999–1061.

Knudsen, M. (1946) *Kinetic Theory of Gases*, Methuen & Co., London, 64 pp.
Kvande, H. and Wahlbeck, P.G. (1976) Theory for the determination of vapour pressures by the transpiration method. *Acta Chem. Scand.*, **A30**, 297–302.
Kvande, H., Linga, H., Motzfeldt, K., and Wahlbeck, P.G. (1979) A thermogravimetric method for determination of vapour pressures above 10^{-2} atm. II: Vapour pressures of molten sodium chloride. *Acta Chem. Scand.*, **A33**, 281–288.
Linga, H., Motzfeldt, K., and Øye, H.A. (1978) Vapour pressure of molten alkali chloride – aluminium chloride mixtures. *Ber. Bunsengesellschaft*, **82**, 568–576.
Margrave, J.L. (ed.) (1967) *The Characterization of High Temperature Vapors*, John Wiley & Sons, New York, 555 pp.
Motzfeldt, K. (1955) The thermal decomposition of sodium carbonate by the effusion method. *J. Phys. Chem.*, **59**, 139–147.
Motzfeldt, K. (1964) Equilibrium of the reaction between beryllium oxide and carbon to give beryllium carbide. *Acta Chem. Scand.*, **18**, 495–503.
Motzfeldt, K., Kvande, H., and Wahlbeck, P.G. (1977) A thermogravimetric method for determination of vapour pressures above 10^{-2} atm. I: Theory. *Acta Chem. Scand.*, **A31**, 444–452.
Motzfeldt, K., Kvande, H., Schei, A., and Grjotheim, K. (1989) *Carbothermal Production of Aluminium*, Aluminium-Verlag, Düsseldorf, 218 pp.
Motzfeldt, K. and Sandberg, B. (1979) Chemical investigations concerning carbothermic reduction of alumina. *Light Metals*, 411–428.
Motzfeldt, K., Sandberg, B., and Julsrud, S. (2001) Molten aluminium oxycarbide considered as an ionic mixture. *High Temp. Mater. Proc.*, **20**, 241–245.
Motzfeldt, K. and Steinmo, M. (1973) Kinetics of reactions between carbon and refractory oxides, in *Third Nordic High Temperature Symposium 1972*, vol. 2 (ed. J.G. Rasmussen), Polyteknisk Forlag, pp. 91–109.
Motzfeldt, K. and Steinmo, M. (1989) *SINTEF Report* STF 34-A89061; Vaporization of silicon carbide, studied by mass-loss effusion. 22+33 pp. *Chem. Abstr.*, **111** (1989), 200287w.
Motzfeldt, K. and Steinmo, M. (1997) Transport processes in the thermal decomposition of silicon carbide, in *The Electrochemical Soc. Proceedings*, vol. 39 (ed. K.E. Spear), Ninth International Conference on High Temperature Materials Chemistry, The Pennsylvania State Univ., pp. 523–528.
NIST-JANAF (1998) *Thermochemical Tables*, 4th edn, American Chemical Society/American Institute of Physics, New York, Part I+II, 1950 pp.
Rao, D.B. and Motzfeldt, K. (1970) Vapour pressures in the system Al-Al_2O_3 investigated by the effusion method. *Acta. Chem. Scand.*, **24**, 2796–2802.
Rosenblatt, G.M. (1963) Interpretation of Knudsen vapor-pressure measurements on porous solids. *J. Electrochem. Soc.*, **110**, 563–569.
Ruff, O. (1910) Übere inen elektrischen Vakuumofen. *Berichte deut. chem. Gesellschaft*, **43**, 1564–1574.
Ruff, O. (1913) Arbeiten im Gebiet hoher Temperaturen I: Über das Schmelzen und Verdampfen unserer feuerbeständigsten Oxyden im elektrischen Vakuumofen. *Z. anorg. allgem. Chem.*, **82**, 373–400.

Ruff, O. und Bergdahl, B. (1919) Arbeiten im Gebiet hoher Temperaturen XII: Die Messung von Dampfspannungen bei sehr hoher Temperaturen. *Z. anorg. allgem. Chem.*, **106**, 76–94.

Ruff, O. (1929) Hochtemperaturtechnik und neue Fluoride. *Z. angew. Chem.*, **42**, 807.

Ruff, O. (1935) The formation and dissociation of silicon carbide. *Trans. Electrochem. Soc.*, **68**, 87–109.

Sandberg, B. (1981) *Carbothermal Reduction of Aluminium Oxide* Dr. Ing. Thesis, NTH (now NTNU), Trondheim 140 pp. (in Norwegian).

Schei, A., Tuset, J. Kr., and Tveit, H. (1998) *Production of High Silicon Alloys*, Tapir Forlag, Trondheim, 363 pp.

Temkin, M. (1945) Mixtures of fused salts as ionic solutions. *Acta Physicochimica USSR*, **20**, 411–420.

Volmer, M. and Estermann, I. (1921) Über den Mechanismus der Molekylabscheidung an Kristallen. *Z. Physik*, **7**, 13–17.

Volmer, M. (1939) *Kinetik der Phasenbildung*, Th. Steinkopff, Dresden und Leipzig, 220 pp.

Wagner, C. (1943) Die Ermittlung von Siedetemperaturen und Dampfdrucken durch Bestimmung der Verdampfungsgeschwindigkeit nach der Federwaage-method von *O. Ruff. Z. phys. Chem.*, **192**, 85–100.

Wahlbeck, P.G. (1971) Effusion VII: The failure of isotropy of a gas in an effusion cell and the transition region. *J. Chem. Phys.*, **55**, 1709–1715.

Wahlbeck, P.G. (1986) Comparison and interrelations for four methods of measurement of equilibrium vapor pressures at high temperatures. *High Temp. Sci.*, **21**, 189–232.

Wahlbeck, P.G., Myers, D.L., and Trong, V.V. (1985) Validity of the Ruff-MKW boiling point method: Vapor pressures, diffusion coefficients in argon and helium, and viscosity coefficients for gaseous cadmium and zinc. *J. Chem. Phys.*, **83**, 2447–2456.

White, C.V., Mikkelsen, Ö., and Roha, R. (2012) Status of the Alcoa carbothermic aluminum project, in *International Smelting Technology Symposium* (ed. by J.P. Downey, T.P. Battle and J.F. White), The Minerals, Metals & Materials Soc., pp. 81–88.

Wiik, K. (1990) *Kinetics of Reactions Between Silica and Carbon*, Dr. Ing. Thesis, NTH (now NTNU), Trondheim, 220 pp.

Wiik, K. and Motzfeldt, K. (1996) Kinetics of reactions between silica and carbon and the formation of silicon carbide. *Materials Research Symposium Proceedings*, **410** (Science and Technology of Non-Oxides) 435–440.

Author Index

The index gives surnames only. For multiple authorship, two names are given, followed by "*et al.*". Numbers in *italic* indicate full entries in the reference lists.

High Temperature Experiments in Chemistry and Materials Science, First Edition.
Ketil Motzfeldt.

Subject Index

High Temperature Experiments in Chemistry and Materials Science, First Edition.
Ketil Motzfeldt.